# Mathematical Modelling and Control of a Robotic Manipulator

A THESIS PRESENTED IN PARTIAL FULFILMENT OF THE REQUIREMENTS OF THE DEGREE OF MASTERS OF TECHNOLOGY AT MASSEY UNIVERSITY.

**NIGEL YEE**

**1996**

# Erratum

page 25, line 4

"$T(t)=D(q(t),\ddot{q}(t))+h(q(t),\dot{q}(t))+c(q(t))$"

change to

$T(t)=D(q(t))\ddot{q}(t)+h(q(t),\dot{q}(t))+c(q(t))$

page 26, after line 12

The pseudo inertia matrix is defined by

$$J_i = \begin{bmatrix} \frac{-\hat{I}_{ixx}+\hat{I}_{iyy}+\hat{I}_{izz}}{2} & \hat{H}_{ixy} & \hat{H}_{ixz} & m_i\hat{s}_{ix} \\ \hat{H}_{ixy} & \frac{-\hat{I}_{ixx}+\hat{I}_{iyy}+\hat{I}_{izz}}{2} & \hat{H}_{iyz} & m_i\hat{s}_{iy} \\ \hat{H}_{ixz} & \hat{H}_{iyz} & \frac{-\hat{I}_{ixx}+\hat{I}_{iyy}+\hat{I}_{izz}}{2} & m_i\hat{s}_{iz} \\ m_i\hat{s}_{ix} & m_i\hat{s}_{iy} & m_i\hat{s}_{iz} & m_i \end{bmatrix}$$

*where* $\hat{I}_{ixx}$ *is the moment of inertia about the x axis*

$\hat{I}_{iyy}$ *is the moment of inertia about the y axis*

$\hat{I}_{izz}$ *is the moment of inertia about the z axis*

$\hat{H}_{iyz}$ *is the product of inertia*

$m_i$ *is the mass of link i*

$\hat{s}_{ix}$ *is the centre of mass of link i*

page 31, line 4

"$$\begin{bmatrix} \tau_i \\ \tau_i \\ \tau_i \end{bmatrix} = \begin{bmatrix} A \end{bmatrix} \begin{bmatrix} \ddot{\vartheta}_i \\ \ddot{\vartheta}_i \\ \ddot{\vartheta}_i \end{bmatrix} + \begin{bmatrix} B \end{bmatrix} \begin{bmatrix} \vartheta_{k,m} \\ \vartheta_{k,m} \\ \vartheta_{k,m} \end{bmatrix} + \begin{bmatrix} C \end{bmatrix} \quad i=1,2,\ldots,n$$

Where *A*, *B* and *C* were evaluated"

change to

$$\begin{bmatrix} \tau_i \\ \tau_i \\ \tau_i \end{bmatrix} = \begin{bmatrix} D \end{bmatrix} \begin{bmatrix} \ddot{\vartheta}_i \\ \ddot{\vartheta}_i \\ \ddot{\vartheta}_i \end{bmatrix} + \begin{bmatrix} h \end{bmatrix} \begin{bmatrix} \vartheta_{k,m} \\ \vartheta_{k,m} \\ \vartheta_{k,m} \end{bmatrix} + \begin{bmatrix} c \end{bmatrix} \quad i=1,2,\ldots,n$$

Where *D*, *h* and *c* were evaluated

page 37, line 12

"$dI_i$ is an area change"

change to

$dI_i$ is the change in the inner area radius.

page 42, line 14

"sin a"

change to

sin $\alpha$

page 143, line 7

"A novel pneumatic actuator which provides a rotary action was developed and tested. A model was then developed for this."

change to

A novel pneumatic actuator which provides a rotary action was designed and a model developed for this.

# Abstract

Control system engineering strives to alter a systems performance to suit the objectives of the user. This requires pre-requisite knowledge of the system behaviour. This is often in the form of mathematical models of the system. These models can then be used to simulate the system and obtain a sound understanding of the systems operation, these can then be used in controller design. Every real world physical system has its own unique characteristics. These must be modelled to develop a simulation of the system. The uniqueness of a real world system necessitates the use of experimental practices and procedures to obtain information about the system. This information is then used to form models representing the system. A simulation of the system can then be based on these models. In this project a robotic system comprising of a link structure, a pneumatic driving system and a valve regulating system, is investigated. Mathematical models describing each component of the robotic system are investigated.

Mathematical models describing the dynamic interactions of the link structure are developed and implemented in a fashion to facilitate control of the robot mechanism. The equations are in an explicit form which do not require the use of a numerical method for development of state space equations used in controller development.

The pneumatic muscle used as the desired actuator for the robot structure is analysed. Analytical models obtained from the available literature are examined and new models are developed to describe the characteristics of the pneumatic muscle.

A proto-type valve specially developed for supplying air to the pneumatic muscle is investigated. Experiments are conducted on this valve to characterise the valves behaviour. A model of the valves behaviour is then developed. A selection of controllers are then applied to the valve pneumatic muscle system.

The investigation of alternative actuation systems proposes the a new rotary pneumatic muscle design. Analytical models for the rotary pneumatic muscle are developed, a prototype is constructed as part of a feasibility study.

# Acknowledgements

I would like to thank my supervisor Saied Nahavandi for his help and encouragement and Bob Chaplin my second supervisor for his contribution and technical support. I would like to thank Heather North for the invaluable time she spent editing and reviewing my work, Clive Marsh for organising my seminar as part of the Masters course. Thanks to Professor Don Barnes for his help in mathematical modelling. I would like to thank all the post-graduate students in the Department of the Production Technology for their support and encouragement and a special thanks to my grandmother.

# Table of Contents

# List of figures

# 1. Preliminaries

## 1.1 Objectives

The control aspect of this research is aimed at getting the hand to manipulate and grasp objects. This is not trivial and requires the control of the system components through a series of steps.

- The system must select a grasp type to be used to grasp and/or manipulate the object.
- It must then select points on the object to which the end effectors are moved in order to form the grasp.
- A set of trajectories must be selected for each component in the hand system, which will allow the end effector to move to its desired location.
- The end effectors must then move to these locations in a co-ordinated manner.

Each of these steps are complex.

The method's used to achieve these steps must take into account the inherent properties of the system.

This industrial operating environment is dynamic and may contain other obstacles which operate within the same work-space as the end-effector. This is further complicated if these obstacles move in an unpredictable way.

The object that is to be grasped will contain surfaces. These are suspected to be rigid and will be a volume in the work space where the manipulator cannot pass through but must be navigated around.

The dynamics of the end-effector will change with changes in inertia of the object being grasped.

When the manipulator moves, the individual links will have accelerations and torque's; these will change the torque's applied to the other links in the manipulator. This is known as a coupled system [26].

The manipulator must be modelled and designed to follow a set trajectory robustly enough to cope with this dynamic operating environment.

## 1.2 Introduction

This report is a discussion of the theoretical aspects involved in the design of a robotic manipulator. Chapter one contains an introduction to the problem with a description of the system and a the list of steps involved in solving the control problem. Chapter two describes mathematical modelling techniques used to model link structures. Chapter three outlines types of actuation systems available and then describes the development of a novel pneumatic actuator. Chapter four is on the modelling of the braided pneumatic muscle. Chapter five investigates the characteristics of the air supply system delivering the air to the pneumatic muscle. Different control strategies are investigated for the muscle, valve control problem and finally Chapter six outlines conclusions and future work to be undertaken.

### 1.2.1 Description of the Robot Structure

The robotic hand design under consideration in this thesis is a system incorporating two fingers and two thumbs. Each finger will comprise three links with a total of four degrees of freedom. There will be two degrees of freedom about the base of the system (link number 1) with one degree of freedom in each of the other links. The thumb is similar with four degrees of freedom associated with a serial three link structure. This incorporates two degrees of freedom about the base link with one degree of freedom in each of the other links as shown in Figure 1-1.

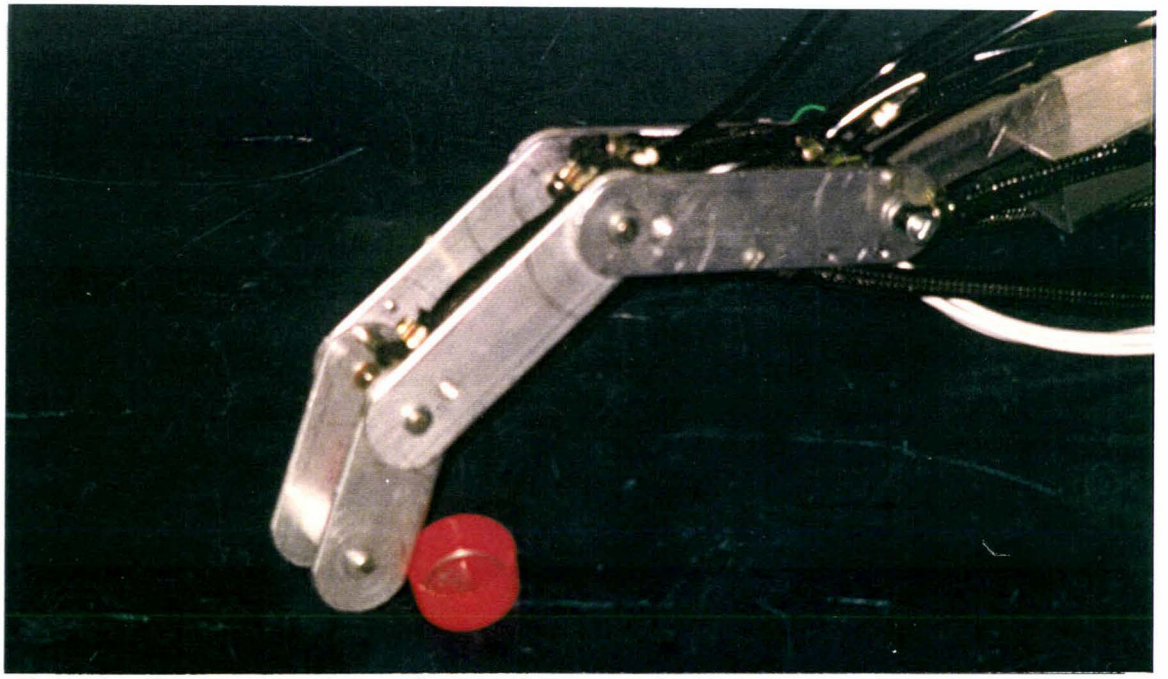

**Figure 1-1 diagrammatic picture of a three link mechanism.**

## 1.3 Background

The mechanical development of an intelligent robotic end effector at Massey University, initiated more research into robotic control [1]. An investigation was undertaken to source suitable controllers. It was quickly identified that a variety of control techniques have been applied to similar problems, many of these controllers require models to make them operational and to evaluate their performance [2]. This meant that it was necessary to model the robotic end effector in order to design the controller. The investigation then focused on the development of models for a controller for the robot end effector.

This was not a straight-forward task, involving the identification of existing models for the robotic end effector and adaptation of these to the particular robotic end effector under-development.

A design decision was made to use a new pneumatic technology for the actuation mechanism known as *The Pneumatic Muscle* [54]. Models describing this new technology are still in development. This necessitated the evaluation of existing models, to identify how well they applied to these Pneumatic Muscle's and the development of further models which better described the behaviour of the Pneumatic Muscle.

Models of the static and dynamic characteristics of the link structures were developed. These were obtained from available literature and applied to the design specifications of the structure being developed.

A valve was also designed to supply air to the pneumatic muscle. As the valve was specifically designed for the air supply application, no data was available on the valve characteristics for a model. Data was thus collected from the valve and a model of its characteristics was formed. This concluded the modelling of the robotic end effector, resulting in models of the three sub-systems of the robotic end effector;

- The model of the robotic structure.
- The model of the pneumatic muscle providing the actuating force for the link mechanism.
- The model of the valve providing the air to drive the pneumatic muscle.

Whilst looking at the existing actuation technology, an investigations into alternative actuation systems was undertaken. This resulted in the development of a novel pneumatic muscle design. This new muscle design provides a rotary action. An analytical model describing its behaviour was produced.

## 1.4 Background and Literature Review of the Mathematical Modelling of a Robotic Hand

### 1.4.1 Automatic Control

Automatic control has played a vital role in the advancement of engineering and science. In addition to its extreme importance in space-vehicle systems, missile-guidance systems, aircraft-autopiloting systems, robotic systems and the like, automatic control has become an integral part of modern manufacturing and industrial processes [3]. For example, automatic control is essential in the numerical control of machine tools in the manufacturing industries. It is also essential in such industrial operations as controlling pressure, temperature, humidity, viscosity, and flow in process industries [4].

Since advances in the theory and practice of automatic control provide the means for attaining optimal performance of dynamic systems, improving productivity of many routine repetitive manual operations, engineers and scientists must have a good understanding of this field.

### 1.4.2 Historical Review

The first significant work in automation and automatic control was James Watt's centrifugal governor for the speed of a steam engine in the eighteenth century. Other significant works in the early stages of development of control theory were due to Minorsky, Hazen, and Nyquist, amongst many others. In 1922 Minorsky worked on automatic controllers for steering ships and showed how stability could be determined from the differential equations describing the system. In 1932 Nyquist developed a relatively simple procedure for determining the stability of closed loop systems on the basis of open-loop response to steady-state sinusoidal inputs. In 1934 Hazen, who introduced the term *servomechanisms* for position control systems, discussed the design of relay servomechanisms capable of closely following a changing input.

During the decade of the 1940s, frequency-response methods made it possible for engineers to design a linear closed-loop control system that satisfied performance requirements. From the end of the 1940s to the early 1950s, the root locus method due to Evans was fully developed.

The frequency-response and root-locus methods, which are the core of classical control theory, lead to systems that are stable and satisfy a set of more of less arbitrary

performance requirements. Such systems are, in general, acceptable but not optimal in any meaningful sense. Since the late 1950s, the emphasis in control design problems has been shifted from the design of one of many systems that works, to the design of one optimal system in some meaningful sense.

As modern plants with many inputs and outputs become more and more complex, the description of a modern control system requires a large number of equations, Classical control theory, which deals only with single-input, single output systems, becomes powerless for multiple-input, multiple-output systems [5]. Since the 1960s the availability of digital computers made possible time-domain analysis of complex systems, modern control theory based on time-domain analysis and synthesis using state variables, has been developed to cope with the increased complexity of modern plants and the stringent requirements on accuracy, weight, and cost in military, space and industrial applications.

Recent developments in modern control theory include optimal control of both deterministic and stochastic systems, as well as the adaptive and learning control of complex systems. Now that digital computers have become cheaper and more compact, they are used as integral parts in these control systems. Recent applications of modern control theory include such non-engineering systems as biological, biomedical, economic, and socio-economic systems.

### 1.4.3 An Overview of Robotic Control Systems

Industrial robots are frequently used in industry to improve productivity and quality. The robot can handle monotonous jobs as well as complex jobs without error in operation. The robot can work in an environment intolerable to human operators. For example, it can work in extreme temperatures (both high and low), high- or low- pressure environments, under water or in space exploration [6].

The industrial robot must handle mechanical parts that may have particular shapes and weights. Hence, it must have at least an arm, a wrist and maybe a hand. It must have sufficient power to perform the task and the capability for at least limited mobility. In fact, some of today's robots are able to move freely by themselves in a limited space in a factory [7].

The industrial robot must have some sensory devices. In some more primitive robots, microswitches are installed in the arms as sensory devices. The robot first touches an object and then, through the microswitches, confirms the existence of the object in space and proceeds in the next step to grasp it.

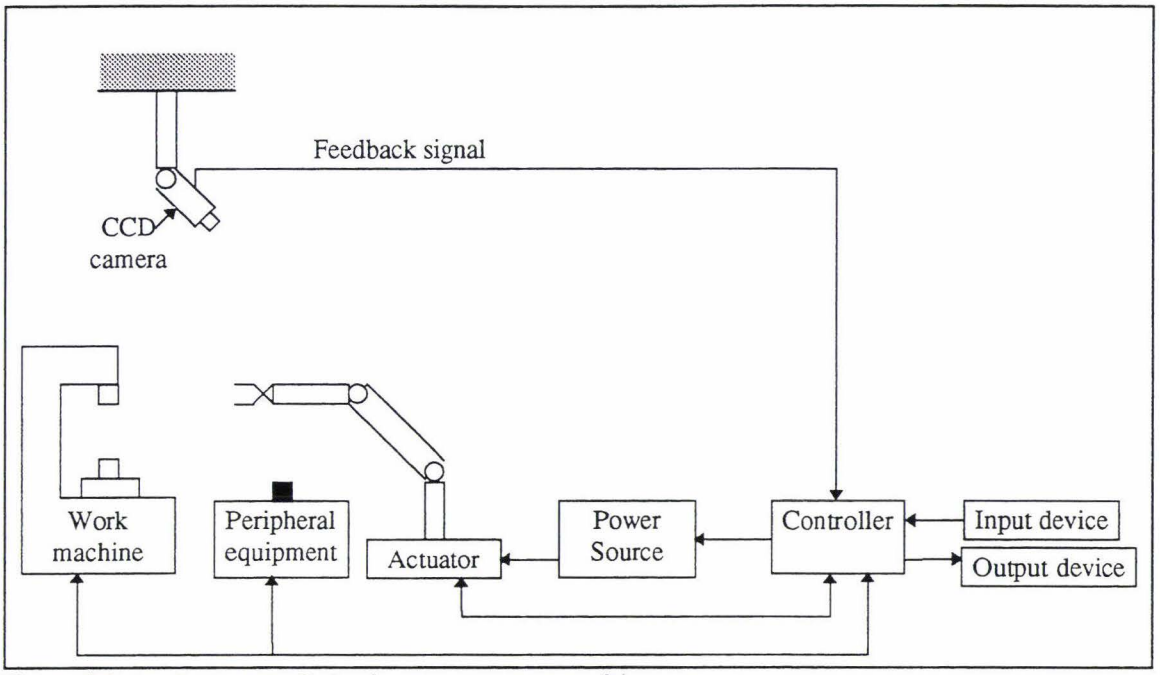


**Figure 1-2 A robot controlled using a pattern recognition process.**

In a high-level robot, an optical means (such as a CCD camera system) may be used to scan the background of the object. It recognises the pattern and determines the presence and orientation of the object. A computer is necessary to process signals in the pattern-recognition process (see Figure 1-2). In some applications, the computerised robot's control system recognises the presence and orientation of each mechanical part by a pattern recognition process that consists of reading the code numbers attached to it. Then the robot picks up the part and moves it to an appropriate place for assembling, and there it assembles several parts into a component. Normally a well-programmed digital computer acts as a controller.

### 1.4.4 The Arrangement for a One Arm Controlled Robot

Figure 1-3 shows a schematic diagram for a simplified version of a robot arm control system. The diagram shows a straight-line motion controlled version of the robot arm. A straight line motion is a 1 degree of freedom motion. The actual robot arm has 3 degrees of freedom, that is up-and-down motion, forward-and-backward motion and left-and-right motion. The wrist attached to the end of the arm also has 3 degrees of freedom and the hand has 1 degree of freedom (grasp motion). Altogether the robot arm system has 7 degrees of freedom. Additional degrees of freedom are required if the robot body must move on a plane. In general, robot hands may be interchangable parts: a different type of grasping device can be attached to the wrist to serve as a hand to handle each different type of object.

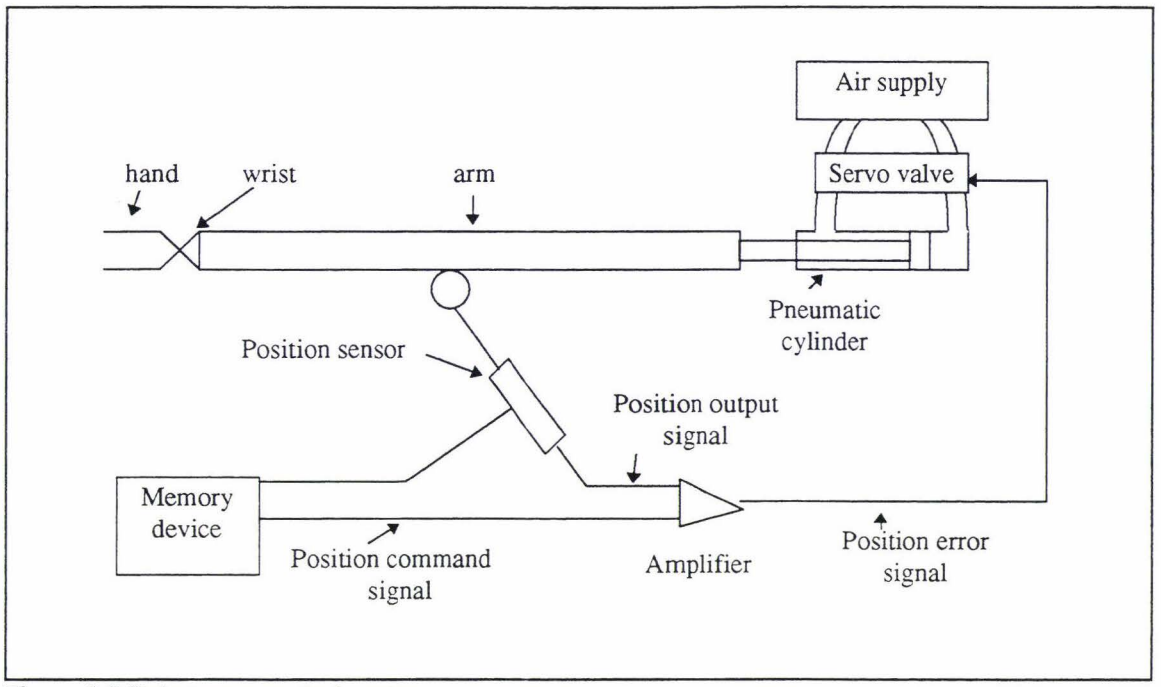


**Figure 1-3 Robot arm control system.**

A servo system may be used to position the arm and wrist. Since the robot arm motion frequently requires speed and power, hydraulic pressure or pneumatic pressure is used as the source of power. For medium power requirements dc motors may be used, and for small power requirements stepper motors may be used.

## *1.5 A Review of some Control Schemes used in Robotic Manipulators*

### 1.5.1 Classically Based Controllers

Classical controllers are those which involve PID, PI, P or PD control.

For a classical controller with a classical control action, the controller produces signals based on the difference between the reference inputs R(s) and the output C(s). The output of the controller U(s), is determined from the error signal E(s), by one of the four schemes, shown in Equation 1-1 to Equation 1-4.

$$u(t) = k_p\, e(t)$$ **Equation 1-1**

**Proportional action**

$$u(t) = k_p\, e(t) + k_p\, T_d \frac{de(t)}{dt}$$ **Equation 1-2**

**Proportional Derivative action**

$$u(t) = k_p\, e(t) + k_p \int_0^t e(t)\, dt$$ **Equation 1-3**

**Proportional Integral action**

$$u(t) = k_p e(t) + k_p \int_0^t e(t)\, dt + k_p\, T_d \frac{de(t)}{dt}$$ **Equation 1-4**

**Proportional Integral and Derivative action (PID)**

The control action can be shown in Figure 1-4.

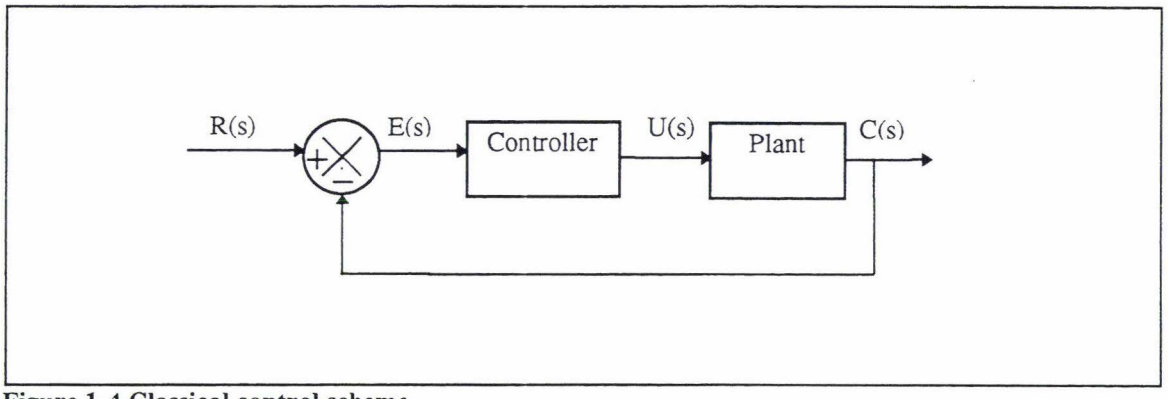


**Figure 1-4 Classical control scheme.**
R(s) is the reference input, U(s) is the controller output, C(s) is the output variable, E(s) is the error signal.

The conventional way of tuning a classical controller is known as the Ziegler Nichols criteria [5]. This requires the development of a system, with a proportional only controller incorporated into the system. Then the gain on the proportional controller ($k_p$) is increased until the system begins to exhibit sustained oscillations. The controller parameters are then based on this proportional controller value, known as the critical gain ($k_{cr}$), which causes the sustained oscillations.

It should be noted that this technique usually employ's simulations of the system [8,9,10].

## 1.6 Model Based Control

This technique provides a useful method of specifying system performance by means of a model that will produce the desired output for a given input. The model is often a mathematical model simulated on a computer. In a model based control system, the output of the model and that of the plant are compared and the difference is used to generate the control signals. The basic layout for model based control schemes is shown in Figure 1-5.

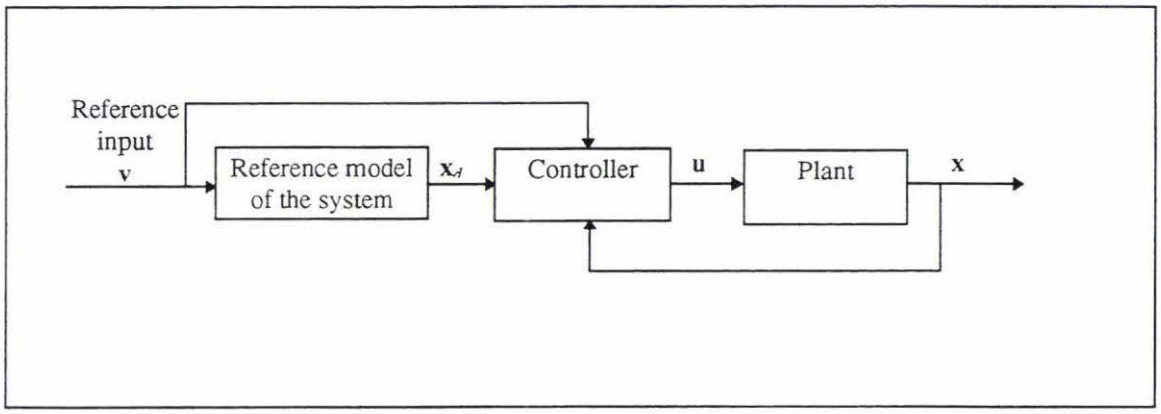


**Figure 1-5 Model based control schematic.**

$X_d$ is the output of the model, u is the output from the controller, x is the output from the plant, v is the reference input.

### 1.6.1 Pole Placement Controller Design

Pole placement control uses a mathematical model of the plant to be controlled. Controller values are assigned according to desired pole locations [5]. Pole placement requires the feedback of all state variables as shown in Figure 1-6, therefore it becomes necessary for all state variables be available for feedback.

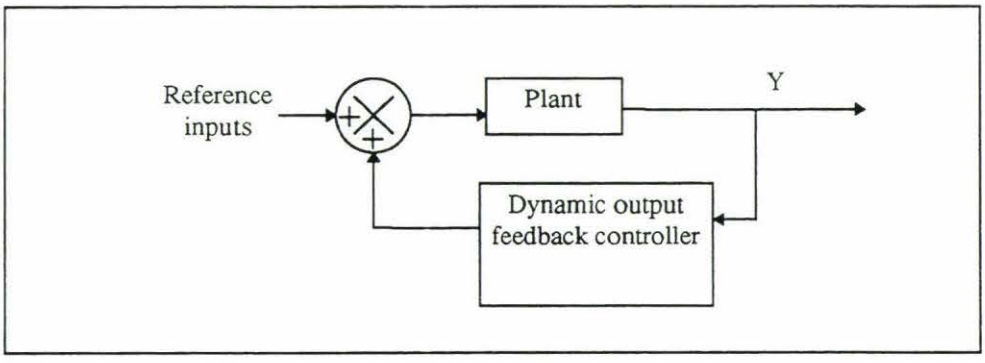


**Figure 1-6 Diagram of closed loop control system using pole placement.**

In the above diagram it was assumed that all the states were directly measurable. If this is not the case then an observer must be incorporated into the control diagram. A state observer estimates the state variables based on measurements of the output and control variables. The design of a state observer requires a model of how the plant operates. Using this model and outputs from the plant, estimates of the states are made without being able to physically measure them as shown in Figure 1-7.

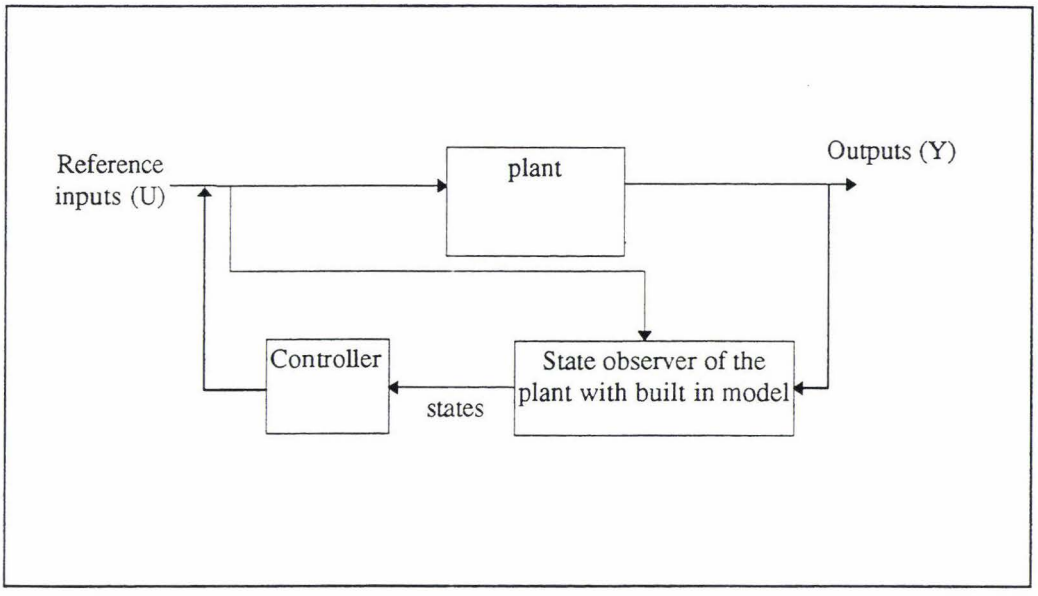


**Figure 1-7 Observer schematic for a model based controller.**

This is the schematic used to estimate the value of the states which are otherwise unmeasurable.

Model based control algorithms have been applied to robot applications by various researchers [11,12,13].

### 1.6.2 Feed Forward Control

Feed forward control is a method of dealing with the effects of disturbances in a control scheme.

If disturbances are measurable, for example the increase in air flow from a valve, then feedforward control is a useful method of concealing their effects on the system output. Feed forward control is defined in Ogata [14] as *'Control of undesirable effects of measurable disturbances by approximately compensating for them before they*

*materialise'*. This is advantageous because generally in a usual feedback control system the corrective action starts only after the output has been affected.

Feed forward control can minimise the transient error, but since feed forward control is open-loop control, there are limitations to its functional accuracy. Feed forward control will not cancel the effects of unmeasurable disturbances under normal operating conditions. It is therefore necessary that a feed forward control system include a feedback loop.

Feed forward control minimises the transient error caused by measurable disturbances while feedback control compensates for any imperfections in the functioning of the feed forward control and provides corrections for measurable disturbances, Figure 1-8 shows a feed forward schematic.

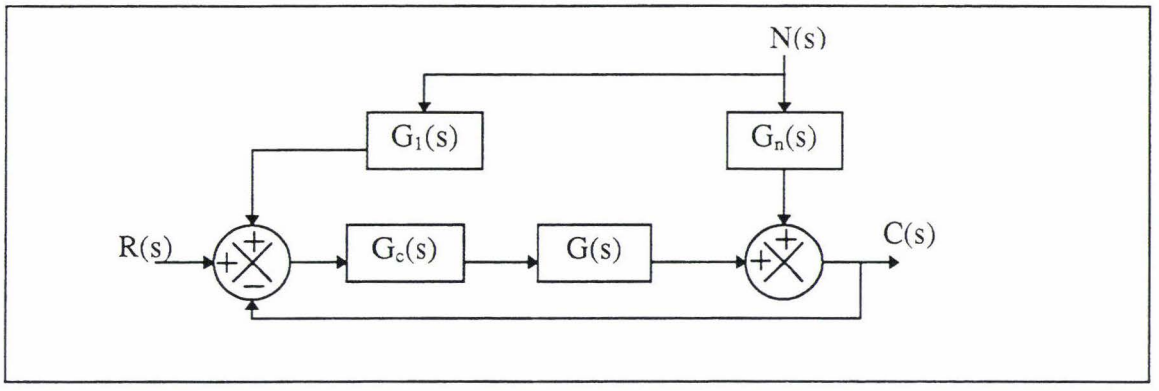


**Figure 1-8 Generalised feed forward controller.**

R(s) is the reference signal, N(s) is the noise term, C(s) is the output of the system.
The controller transfer function $G_c(s)$ is designed to satisfy the required system specifications in the absence of the disturbances. The disturbance feed forward transfer function $G_1(s)$ is determined such that the effects of N(s) are eliminated in the output C(s).

$G_1(s)$ is determined in general by.

$$G_1(s) = \frac{-G_n(S)}{G_c(S)\,G(S)} \qquad \textbf{Equation 1-5}$$

The procedure for determining $G_c(s)$ requires the use of a system model for the design of the controller and for simulation. Likewise a model of the system is used for determining $G_1(s)$ and simulating the performance of the system with the feed forward controller $G_1(s)$, incorporated into the system. The feed forward technique has been utilised by numerous researchers [15,16].

### 1.6.3 Adaptive Position Control

An adaptive control system is one that continuously and automatically measures the dynamic characteristics (such as the transfer function or state equations) of the plant, compares them with the desired dynamic characteristics, and uses the difference to vary adjustable system parameters (usually controller characteristics) or to generate an actuating signal so that optimal performance can be maintained regardless of the environmental changes. Alternatively, such a system may continuously measure its own performance according to a given performance index and modify, if necessary, its own parameters so as to maintain optimal performance regardless of the environmental changes.

An adaptive controller consists of the following three functions;

- Identification of dynamic characteristics of the plant.
- Decision making based on the identification of the plant.
- Modification or actuation based on the decision made.

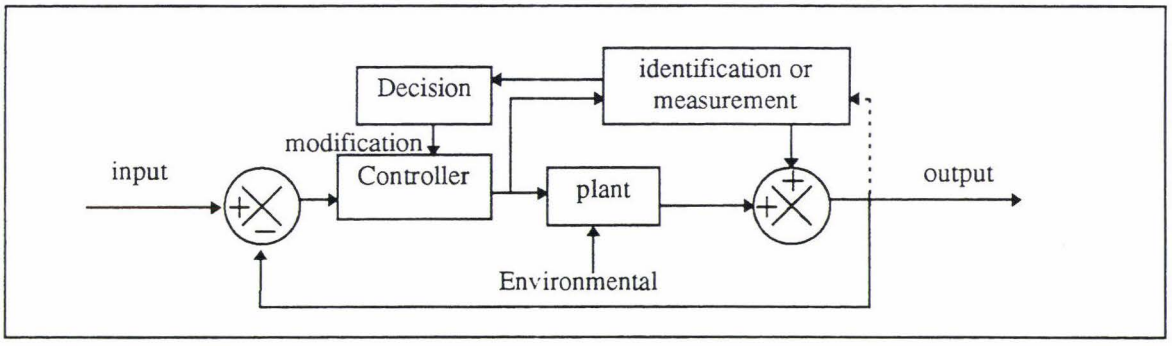


**Figure 1-9 Adaptive control scheme.**

A block diagram of an adaptive control system is shown in Figure 1-9. In this system the plant characteristics are identified and compared with the optimal then a decision is made on the findings as to how the actuating signal should be modified. Since the plant is identified within the system itself, adjustment of the parameters is a closed-loop operation.

Adaptive control provides an intelligent method of controlling a robot manipulator. It can successfully deal with changes in the robot system and operating environment while still maintaining a reasonable operating performance. There are many different adaptive control algorithms available.

Design of adaptive controllers requires knowledge of the plant dynamics. The general procedure for obtaining these dynamics is by the use of a model. This model is used in the

design of a controller to set the initial controller parameters. This model is then implemented in the plant and the controller parameters are updated in order to obtain optimal performance of the plant [17,18,19].

## 1.7 Modelling Process

There is a broad spectrum of components which are used in control. These may be electromechanical, hydraulic, pneumatic, electronic and so on. In control engineering we replace such devices or components by their mathematical models, rather than dealing with hardware devices.

To obtain such adequate mathematical models of a physical component is one of the most important problems in control engineering.

A mathematical model must represent the essential aspects of a physical component. The predictions of the system behaviour based on the mathematical model must be reasonably accurate, as they will be used to design the controller.

### 1.7.1 Controller Design Steps

Given a system (in most cases its dynamics are unalterable), we must first choose appropriate actuators and sensors. Then using the previously developed mathematical models, we design a controller such that the closed-loop system will satisfy the given specifications. The controller designed is the solution to the mathematical version of the design problem.

After a mathematical design has been completed, the control engineer simulates the model on a computer to test the behaviour of the resulting system in its response to various signals and disturbances. The system is then modified and analysed until satisfactory responses are obtained. This process of design and analysis is repeated until a satisfactory system is obtained. Then a prototype physical system can be constructed [5].

Note that this process of constructing a prototype is the reverse process to modelling. The prototype is a physical system that represents the mathematical model with reasonable accuracy. Once the prototype has been built, the engineer tests it to see whether or not it is satisfactory. If it is, the design is complete. If not, the prototype must be modified and tested. This process continues until the prototype is completely satisfactory.

## 1.8 Development of Mathematical Models of the System

Mathematical modelling is used in the development of control systems to;

1. Simulate the system and then analyse the performance of the control system investigated.

2. Obtain models which are incorporation directly into certain control system schematics that is, model based control.

The modelling process used for a model based control in robot manipulators as suggested by An, Atkinson et al [20] is;

- Motor models for joint torque control.

- Kinematic models of link lengths and of locations of joints and axes.

- Inertial models of mass, centre of mass, and moment of inertia for loads and links.

This author's strategy also cites the need for separate modelling of motor characteristics, kinematic parameters and inertial parameters.

Motion control consists of ;

- Obtaining dynamic models of the manipulator.

- Using these models to determine control laws or strategies to achieve the desired system response and performance [21].

## 1.9 Overview of Models Describing the Robotic System

The actual modelling of the robotic mechanism will contains three parts. These will be models which describe the main parts of the physical system. These are;

1. The robotic structure must be modelled. The robotic structure is that which moves and carries out the operations of the robot.

2. The actuation mechanism must be modelled. This is the part of the system which supplies the force to the structure. As the pneumatic muscle was chosen as the actuation mechanism this must be modelled.

3. The power supply to the actuation mechanism must be modelled. As a pneumatic mechanism was chosen, and this employed valves to regulate the actuation force to the structure the valves must be modelled.

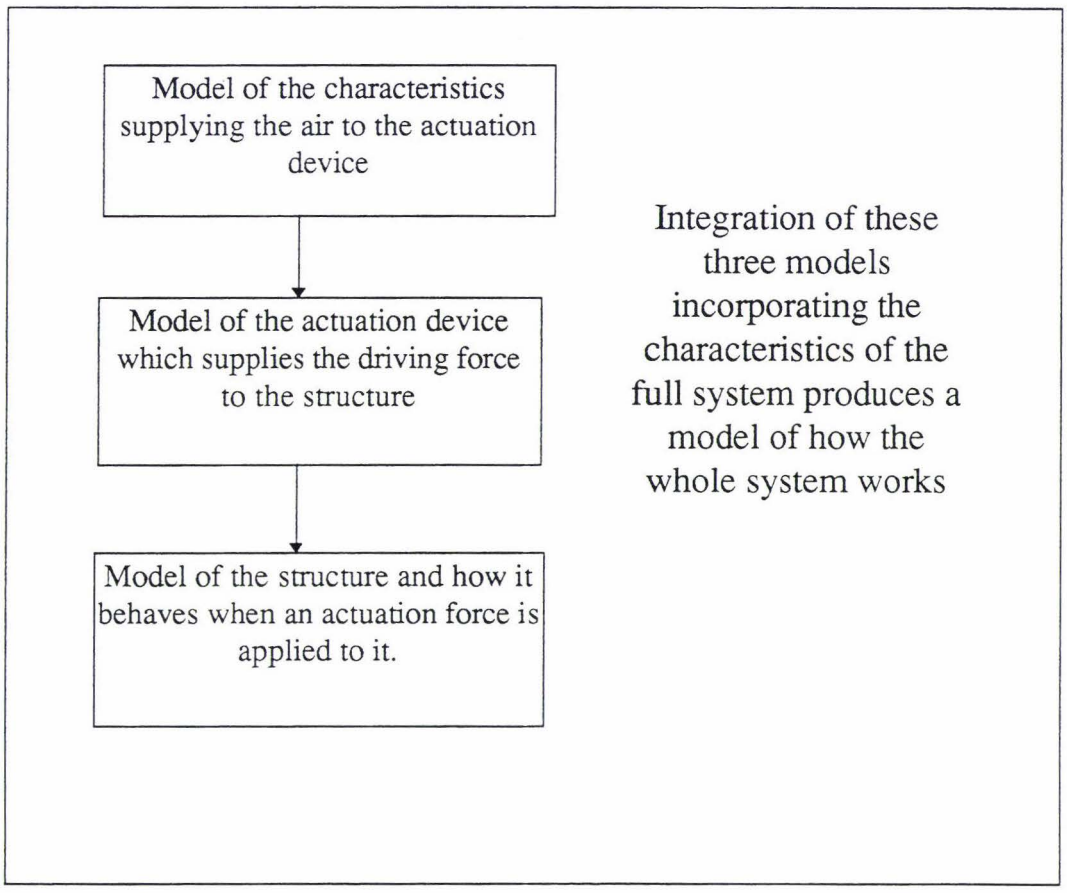


**Figure 1-10 Overview of system modelling.**

Once the full system has been modelled, the system can then be simulated and different control strategies investigated.

# 2. Modelling of the Robot Structure

## 2.1 Background of Modelling Robot Structures

The robotic structure was built and designed in the Department of Production Technology [1] as part of the development of a robotic hand. The robotic hand will have two fingers and two thumbs. Each finger will comprise of three links with a total of four degrees of freedom. There will be two degrees of freedom about the base of the system (link number 1) with one degree of freedom in each of the other links. The thumb is similar with four degrees of freedom associated with a serial three link structure. This incorporates two degrees of freedom about the base link with one degree of freedom in each of the other links (refer Figure 2-1). At present the design aspect of the project has seen the construction of a proto-type finger unit.

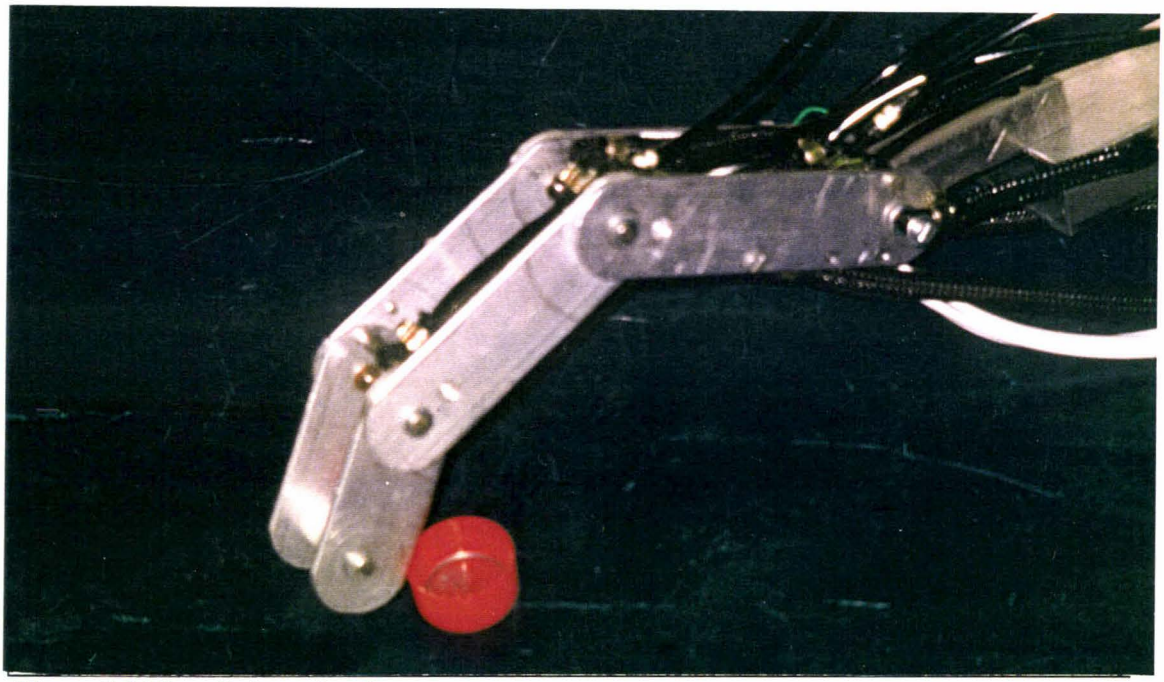

**Figure 2-1 Three link mechanism.**

### 2.1.1 The Need for Modelling of the Link Structure

The aim of the modelling aspects of this work is to develop a set of dynamic equations describing the motion of the robot arm and manipulator.

Such equations of motion are needed for computer simulation of the robot arm motion, the design of suitable control equations for the robot mechanism, and the evaluation of the kinematic design and structure of the robot mechanism.

It is stated in Foo et al [21] that the purpose of manipulator control is to maintain dynamic response of a computer-based manipulator in accordance with some pre-specified performance and goals.

In general the dynamic performance of a manipulator depends directly on the efficiency of the control algorithms and on the dynamic model of the manipulator. The control problem consists of obtaining dynamic models of the robot arm and specifying corresponding laws or strategies to achieve the desired system response and performance.

The dynamic model of the robot arm can be obtained from known physical laws such as the laws of Newtonian mechanics and Lagrangian mechanics [22,23,24]. This leads to the development of dynamic equations of motion for the various articulated joints of the manipulator in terms of specified geometric and inertial parameters, of the links. Conventional approaches like the Lagrange-Euler (L-E) and Newton-Euler (N-E) formulations can be applied systematically to develop the robot arm motion equations. It should be noted that all these formulations are equivalent to each other in the sense that they describe the dynamic behaviour of the same physical robot manipulator [21].

The structure of these equations may differ for various reasons however, some emphasise fast computation time in evaluating the nominal joint torques for servoing a manipulator, others are aimed at facilitating control analysis and synthesis and still others at improving computer simulation of robot motion.

### 2.1.2 Review of Different Approaches to Link Structure Modelling

In order to undertake any form of control on the three link mechanism a mathematical description of the system is required. This generally involves the mathematical modelling of the inter-relations of links.

There are several different techniques used for modelling multiple link structures. The modelling techniques shown below are concerned with the more specific case of modelling the forces which act on the joints of the structure.

The first and simplest approach is to model each joint independently and assume all the other joints to be static thus ignoring the coupling effects of the system (Figure 2-2). This approach is advocated by N-Nagy and Siegler [26].

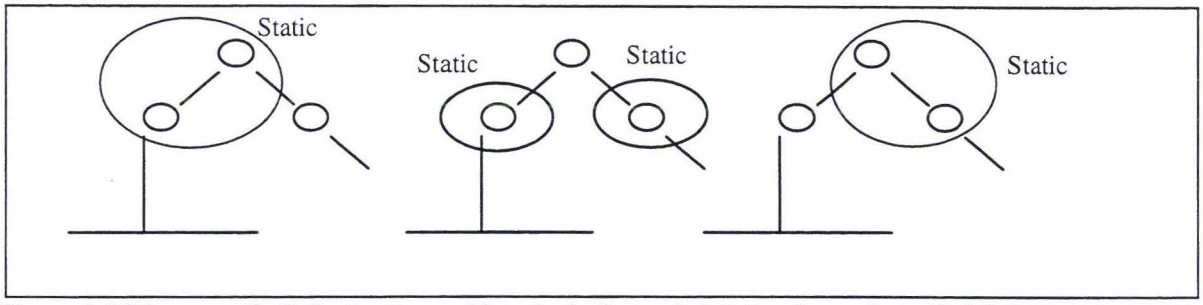


**Figure 2-2 Diagram of a link structure with a single dynamic joint and puesdo static joints.**

This technique models a robotic manipulator at low speed as a series of loosely coupled servo-systems, each servo controlling a single joint-link segment. This greatly simplifies the mathematical modelling of the robot system.

The robot is thus reduced to a mechanical chain decomposed into independent joint link segments, on which both first- and second-order effects can easily be dealt with. The first and second order effects can easily be identified, but higher order effects inherently present in the robotic arm will be disregarded.

The more complex method of modelling involves considering all of the joints in the structure to be part of a dynamic system, with all single joints as dynamic entities. Two common methods of doing this are the Lagrange-Euler and Newton-Euler methods.

The Lagrange-Euler method is widely documented in a variety of texts [22,23,24] and has been practically applied in many cases [4,5,6]. The Lagrange-Euler method involves evaluating the energies associated with each link. Then Lagrange's equation Equation 2-1, is applied to that particular link, this involves an energy balance for all objects in the system.

$$L = K - P \qquad \textbf{Equation 2-1}$$

$$T_i = \frac{d}{dt}\left(\frac{dL}{dq_i}\right) - \frac{dL}{dq_i} \qquad \textbf{Equation 2-2}$$

where K is the kinetic energy, P is the potential energy and $q_i$ is the generalised co-ordinates of the robot arm.

### 2.1.3 Theoretical Background to the Lagrange-Euler Formulation

The derivation of the dynamic model of a manipulator based on the L-E formulation is simple and systematic. Assuming rigid body motion and excluding the dynamics of

electronic control devices, backlash, and gear friction, the resulting equations of motion, are a set of second-order coupled non-linear differential equations.

The L-E equations of motion provide explicit state equations for the robot arm dynamics [21]. These can be used to analyse and design advanced joint-variable space control strategies [27].

The computation of the L-E requires a significant number of arithmetic operations and thus these equations are very difficult to utilise for real time control purposes.

Many applications of L-E use the Denavit-Hartenberg matrix representation, to describe the spatial displacements between neighbouring link co-ordinate frames and to obtain the kinematic information and they employ the Lagrangian dynamics technique to derive dynamic equations of a manipulator. The direct application of the Lagrangian formulation, together with the Denavit-Hartenberg link co-ordinate representation, results in a convenient and compact algorithmic description of the manipulator equations of motion. The algorithm is expressed by matrix operations which facilitates both analysis and computer implementation.

The evaluation of the dynamic and control equations in functionally explicit terms will be based on the compact matrix algorithm derived in this section.

The derivation of the dynamic equations of an *n-degrees* of freedom manipulator is based on the understanding of:

1. The 4×4 homogeneous co-ordinate transformation matrix ${}^{i-1}A_i$, which describes the spatial relationship between $i^{th}$ and $(i-1)^{th}$ links. The co-ordinate reference frame is shown in Figure 2-3.

2. The Lagrange-Euler equation, Equation 2-3.

$$\frac{d}{dt}\left[\frac{\partial L}{\partial q_i}\right] - \frac{\partial L}{\partial q_i} = \tau_i \qquad i = 1,2,\ldots,n \qquad \textbf{Equation 2-3}$$

where $L$ = Lagrangian function
= K - P
= kinematic energy (K)-potential energy(P).

K = total kinetic energy of the robot arm.
P = total potential energy of the robot arm.
$q_i$ = generalised co-ordinates of the robot arm.
$\tau_i$ = generalised force or torque applied to the system at joint $i$.

The Lagrangian-Euler formulation requires knowledge of the kinetic energy of the physical system which in turn requires knowledge of the velocity of each joint.

### 2.1.4 Theoretical Background to the Newton-Euler Formulation

As an alternative to deriving more efficient equations of motion several investigators turned to Newton's second law and developed various forms of Newton-Euler equations for an open link kinematic chain [28,29]. These formulations when applied to a robot arm result in a set of forward and backward recursive equations with "messy" vector cross-product terms. The most significant aspect of this formulation is that the computational time is reduced for real-time control [21].

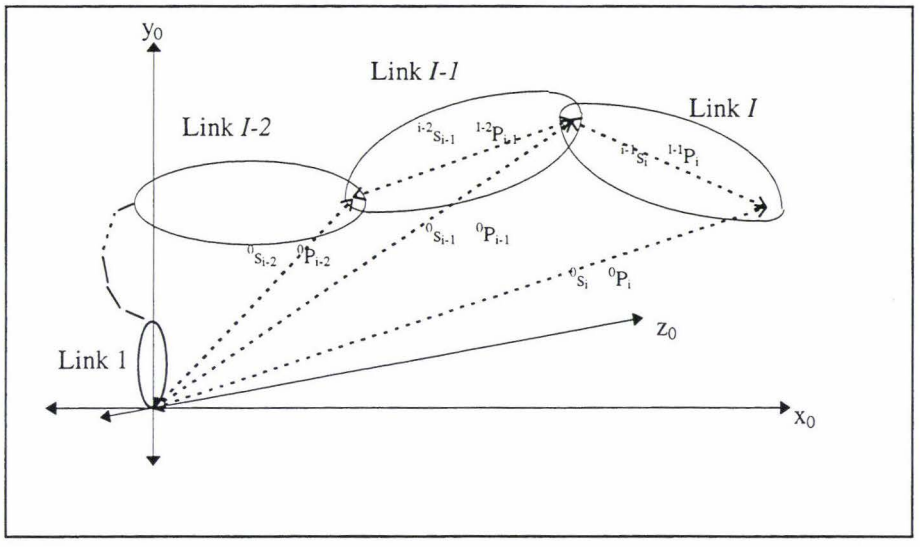


**Figure 2-3 Co-ordinate reference frame for robot structure.**

Given that there is movement about joint $I$ as shown in Figure 2-3 and the using notation ${}^{A}R_{B}$ to describe the translation matrix, the rotational vector is ${}^{0}w_{i}$ is given by,

$$ {}^{0}w_{i} = \begin{cases} {}^{0}w_{i-1} + {}^{0}R_{i} e_{z} \dot{q}_{i} & \text{if Revolute} \\ {}^{0}w_{i-1} & \text{if Prismatic,} \end{cases} \qquad \textbf{Equation 2-4} $$

where

$${}^{0}R_{i} = \left[ {}^{0}x_{i}\ {}^{0}y_{i}\ {}^{0}z_{i} \right] \quad \text{and} \quad e_{z} = [0,0,1]^{T}$$

and the accelerations are

$$ {}^{0}\dot{w}_i = \begin{cases} {}^{0}w_{i-1} + {}^{0}R_i e_z \ddot{q}_i + {}^{0}w_{i-1} \times \left( {}^{0}R_i e_z \dot{q}_i \right) & \text{if R,} \\ {}^{0}w_{i-1} & \text{if P,} \end{cases} $$ **Equation 2-5**

and ${}^{0}\ddot{P}_i$ is the translational acceleration of link $i$ with respect to link 0

$$ {}^{0}\ddot{P}_i = \begin{cases} {}^{0}\ddot{P}_{i-1} + {}^{0}\dot{w}_{i-1} \times \left( {}^{0}R_i \, {}^{i-1}\hat{P}_i \right) + {}^{0}w_{i-1} \times \left[ {}^{0}w_{i-1} \times \left( {}^{0}R_{i-1} \, {}^{i-1}\hat{P}_i \right) \right] & \text{if R} \end{cases} $$ **Equation 2-6**

To find the acceleration vector ${}^{0}\ddot{s}_i$

$$ {}^{0}\ddot{s}_i = {}^{0}\ddot{P}_i + {}^{0}\dot{w}_i + \left( {}^{0}R_i \, {}^{i-1}\hat{s}_i \right) + {}^{0}w_i \times \left[ {}^{0}w_i \times \left( {}^{0}R_i \, {}^{i-1}\hat{s}_i \right) \right] $$ **Equation 2-7**

If $m_i$ is the mass of link $i$ and ${}^{0}I_i$ is the inertia tensor with respect to the frame with the origin located at the centre of mass and $s_i$ is the translation vector then the total external force ${}^{0}f_i$ and total external moment ${}^{0}n_i$ is given by

$$ {}^{0}f_i = m_i \, {}^{0}\ddot{s}_i $$ **Equation 2-8**

and

$$ {}^{0}n_i = {}^{0}I_i \, {}^{0}\dot{w}_i + {}^{0}w_i \times \left( {}^{0}I_i \, {}^{0}w_i \right). $$ **Equation 2-9**

Let ${}^{o}f_i$ and ${}^{o}n_i$ be the force and moment exerted by link $i$-$1$ on link $i$. Also let

$$ {}^{0}s_i = {}^{0}R_i \, {}^{i-1}s_i $$ **Equation 2-10**

and

${}^{0}P_i = {}^{0}R_i \, {}^{i}P_{i+1}$ then

$$ {}^{0}f_i - {}^{0}f_{i-1} = {}^{i-1}f_i $$ **Equation 2-11**

and

$$ {}^{0}n_i - {}^{0}n_{i-1} = {}^{i}\hat{P}_{i+1} \times {}^{i-1}n_i + {}^{0}s_i + {}^{i-1}f_i. $$ **Equation 2-12**

Finally the relation between the joint driving force $\tau_i$ and $\{{}^0f_i, {}^0n_i\}$ is obtained from Equation 2-4 to Equation 2-12.

$$\tau_i = \left\{ {}^0z_i^T \, {}^0n_i \qquad (if \ \ R) \right\} \qquad \textbf{Equation 2-13}$$

## 2.2 Algorithm Implementation

The mathematical package 'Maple' was chosen for the implementation. It is specifically designed for equation manipulations and has powerful algebraic commands which allow the simplification of formulae.

The derivation for the Lagrange Euler algorithm will now be presented.

The Lagrangian funcion $L = K - P$ is given by

$$L = \frac{1}{2}\sum_{i=1}^{n}\sum_{j=1}^{i}\sum_{k=1}^{i}\left[\mathrm{Tr}\left(U_{ij}J_iU_{ik}^T\right)\dot{q}_j\dot{q}_k\right] + \sum_{i=1}^{n} m_i g\left({}^oA_i\,{}^i\bar{r}_i\right) \qquad \textbf{Equation 2-14}$$

note that Tr denotes the trace of a matrix

Applying the Lagrange - Euler formulation to a function of a robot arm yields the necesary generalised torque $\tau_i$ for a joint $i$ actuator to drive the $i^{th}$ link of the manipulator.

$$\tau_i = \frac{d}{dt}\left[\frac{\partial L}{\partial \dot{q}_i}\right] - \frac{\partial L}{\partial q_i}$$

$$= \sum_{j=1}^{n}\sum_{k=1}^{j}\mathrm{Tr}\left(U_{jk}J_jU_{ji}^{\mathrm{T}}\right)\ddot{q}_k + \sum_{j=1}^{n}\sum_{k=1}^{j}\sum_{m=1}^{j}\mathrm{Tr}\left(U_{jkm}J_jU_{ji}^{\mathrm{T}}\right)\dot{q}_k\dot{q}_m - \sum_{j=1}^{n} m_j g U_{ji}\,{}^j\bar{r}_j \qquad \textbf{Equation 2-15}$$

for $i = 1,2,\ldots,n$.

Equation 2-15 can be expressed in much simpler form as

$$\tau_i = \sum_{k=1}^{n} D_{ik} \ddot{q}_k + \sum_{k=1}^{n}\sum_{m=1}^{n} h_{ikm} \dot{q}_k \dot{q}_m + c_i \qquad \textbf{Equation 2-16}$$

for $i = 1,2,....,n.$
or in matrix form as

$$T(t)=D\left(q(t),\ddot{q}(t)\right)+h\left(q(t),\dot{q}(t)\right)+c\left(q(t)\right) \qquad \textbf{Equation 2-17}$$

$T(t)$ = torques
$q(t)$ = joint variables
$\dot{q}(t)$ = velocity joint variable
$\ddot{q}(t)$ = acceleration joint variable
$D(q)$ = an $n \times n$ inertial acceleration - realated symmetric matrix whose elements are.

$$D_{ik} = \sum_{j=\max(i,k)}^{n} \mathrm{Tr}\left(U_{jk} J_k U_{ji}^{\mathrm{T}}\right) \quad i,k = 1,2,....,n. \qquad \textbf{Equation 2-18}$$

$h(q,\dot{q}) =$ an $n \times 1$ non - linear coriolis and centrifugal force vector whose elements are.

$h(q,\dot{q}) = (h_1, h_2, ..., h_n)^{\mathrm{T}}$

where $h_i = \sum_{k=1}^{n}\sum_{m=1}^{n} h_{ikm} \dot{q}_k \dot{q}_m \qquad i = 1,2,....,n.$ **Equation 2-19**

and $h_{ikm} = \sum_{j=\max(i,k,m)}^{n} \mathrm{Tr}\left(U_{jkm} J_j U_{ji}^{\mathrm{T}}\right) \qquad i,k,m = 1,2,....,n.$ **Equation 2-20**

$c(q) =$ an $n \times 1$ gravity loading force vector whose elements are
$c(q) = (c_1, c_2, ....., c_n)^{\mathrm{T}}$

where $c_i = \sum_{j=1}^{n} \left(-m_j g U_{ij}\, {}^{j}\bar{r}_j\right) \qquad i = 1,2,....,n.$

Note that

$$U_{ij} = \begin{pmatrix} {}^{0}A_{j-1} Q_j\, {}^{j-1}A_i & \text{for } j \le i \\ 0 & \text{for } j > i \end{pmatrix}$$

and

$$U_{ijk} = \begin{pmatrix} {}^{0}A_{j-1}Q_j{}^{j-1}A_{k-1}Q_k{}^{k-1}A_i & i \geq k \geq j \\ {}^{0}A_{k-1}Q_k{}^{k-1}A_{j-1}Q_j{}^{j-1}A_i & i \geq j \geq i \\ 0 & i < j \text{ and } i < k \end{pmatrix}$$

where $Q_i$ is defined for a revolute joint as

$$Q_i = \begin{bmatrix} 0 & -1 & 0 & 0 \\ 1 & 0 & 0 & 0 \\ 0 & 0 & 0 & 0 \\ 0 & 0 & 0 & 0 \end{bmatrix}$$

and ${}^{0}A_i$ is the co - ordinate transformation matrix which relates the $i^{th}$ co - ordinate frame to the base co - ordinate frame

$${}^{0}A_i = {}^{0}A_1\,{}^{1}A_2 \ldots\ldots {}^{i-1}A_i$$

for a revolute joint the general form of ${}^{i-1}A_i$ is given by

$${}^{i-1}A_i = \begin{bmatrix} \cos\vartheta_i & -\cos\alpha_i \sin\vartheta_i & \sin\alpha_i \sin\vartheta_i & a_i \cos\vartheta_i \\ \sin\vartheta_i & \cos\alpha_i \cos\vartheta_i & -\sin\alpha_i \cos\vartheta_i & a_i \sin\vartheta_i \\ 0 & \sin\alpha_i & \cos\alpha_i & d_i \\ 0 & 0 & 0 & 1 \end{bmatrix}$$

where $a_i$ and $d_i$ are known parameters from the kinematic structure.

These equations were then implemented in *Maple* [47]. The algorithms used to do this are presented below in flow chart diagram form, the program listings are given in appendix A-1.

# Algorithm for the determination of the coriolis terms

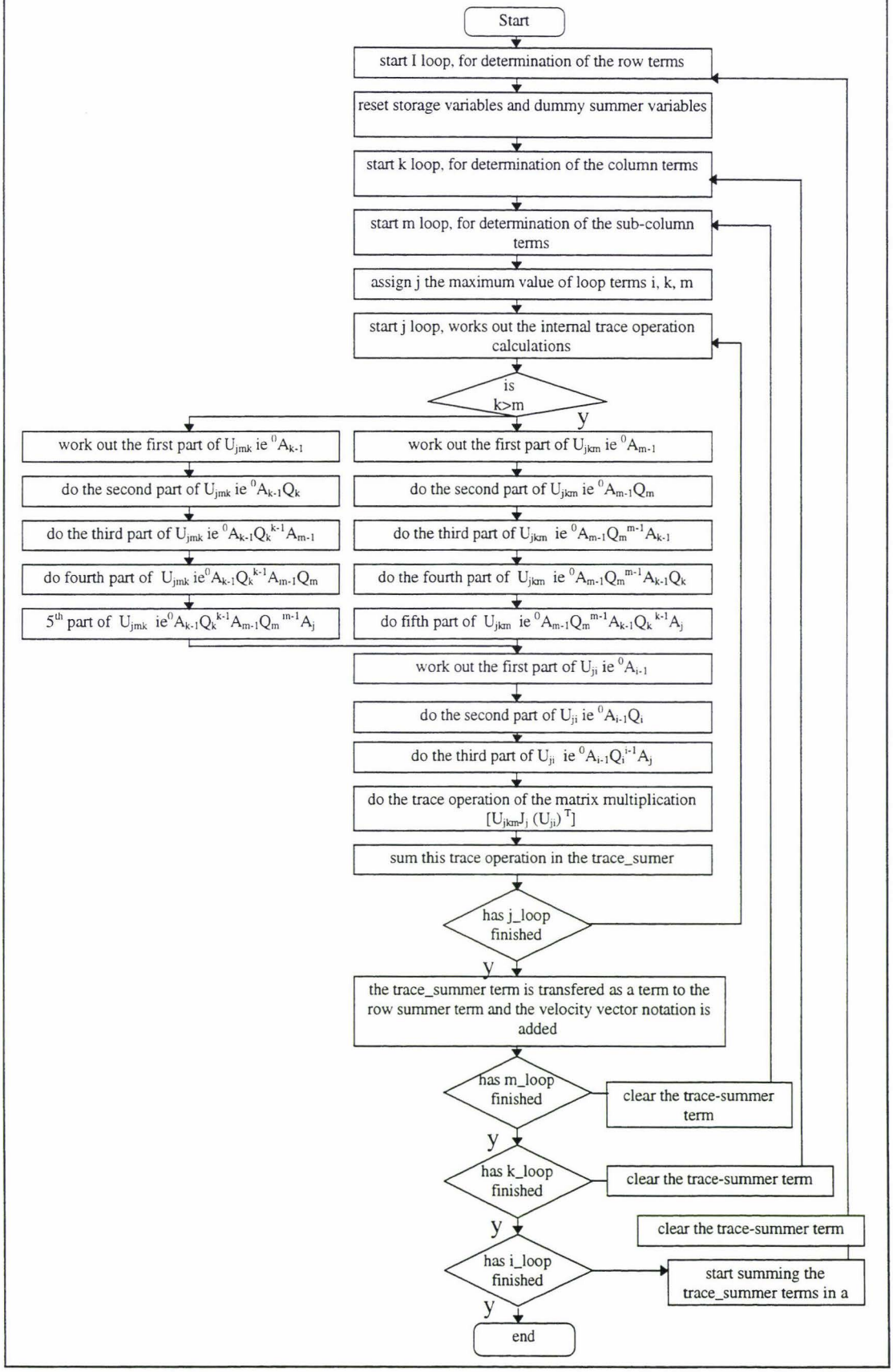

## Algorithm for the determination of the pseudo inertia matrix terms

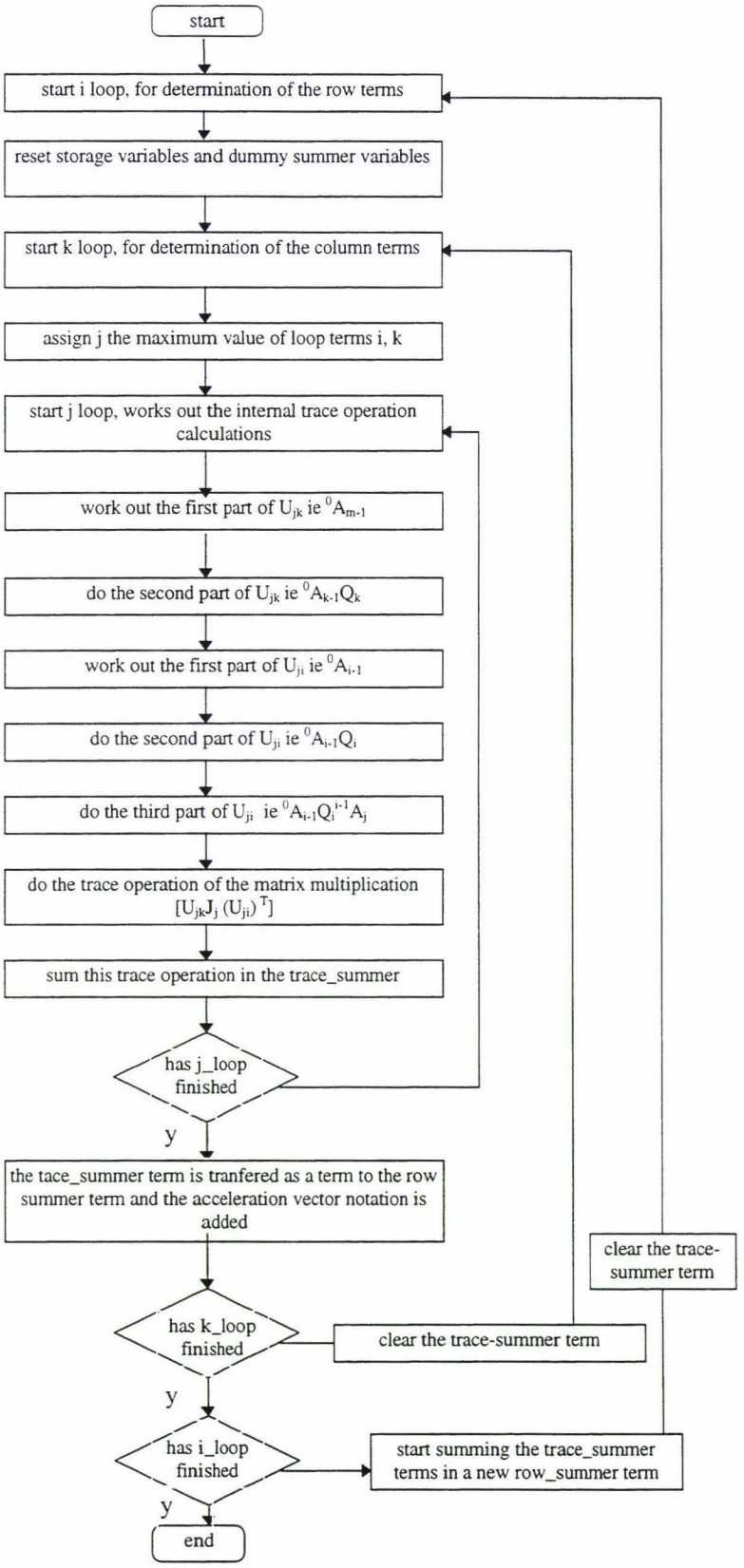

## Algorithm for the determination of the gravity terms

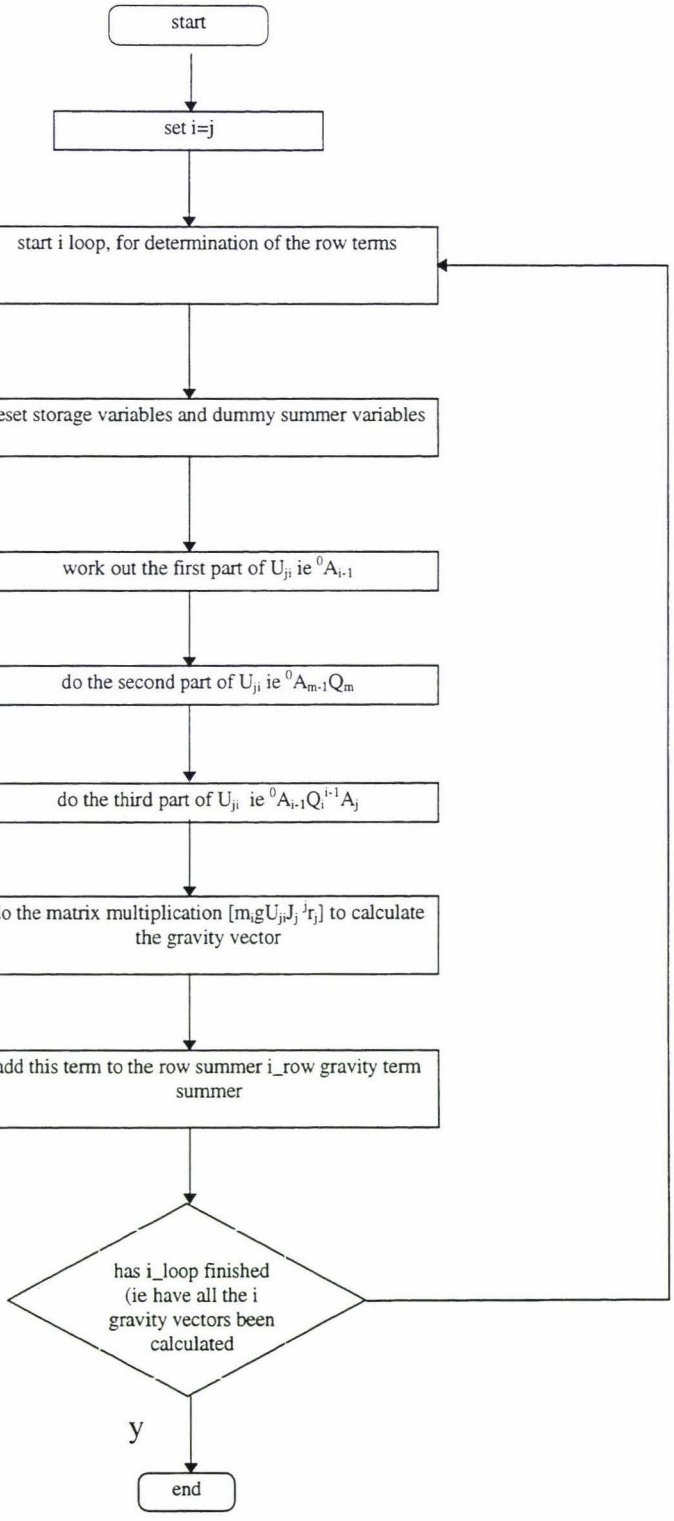

## 2.3 Limitations of the Implementation

The development package ran on the Apple Macintosh computer, (Quatra), this machine had insufficient computational power to effectively run the program in one simulation. The computational deficiencies encountered were lack of memory and low processing speed. This resulted in long computational times for the calculations and frequent machine crashes. This limitation necessitated segmentation of the program. Segmentation of the program enabled equations for the three link manipulator to be obtained. Future work, in generating dynamic equations of the link structure, would be benefited by the use of a more powerful machine with more memory.

## 2.4 Verification of the Algorithm Implementation

The equations for a two-link manipulator were obtained from Foo et al [21] and are presented in appendix A-2. When the program was run with two links instead of three, the equations produced by the package were the same as those from the available literature.

For the three link equations, verification of the implementation was achieved by setting the mass and length of one of the three links to zero, thus reducing equations to those of a two link manipulator.

The three link equations could now be used to develop a controller. The input requirements for the equations are the masses and moments of inertia of the links. These would be used to fill in the equation constants.

## 2.5 Discussion of the Implementation using Matlab

The L-E algorithm was implemented using *Matlab* [53] as well as *Maple*. This was required as at this stage it was expected that Matlab would be used to undertake the on-line control of the manipulator, the program listings are shown in Appendix B-1.

The equations generated by Matlab were not in a desirable form for algebraic manipulation, ie partial differentiation and then arrangement into state-space form.

Matlab is an analytical package which evaluates the matrices and does not carry constants through the calculations. Hence the resulting equations obtained from Matlab were in the form;

$$\begin{bmatrix} \tau_i \\ \tau_i \\ \tau_i \end{bmatrix} = \begin{bmatrix} \quad A \quad \end{bmatrix} \begin{bmatrix} \ddot{\vartheta}_i \\ \ddot{\vartheta}_i \\ \ddot{\vartheta}_i \end{bmatrix} + \begin{bmatrix} \quad B \quad \end{bmatrix} \begin{bmatrix} \vartheta_{k,m} \\ \vartheta_{k,m} \\ \vartheta_{k,m} \end{bmatrix} + \begin{bmatrix} C \end{bmatrix} \qquad i = 1,2,\ldots,n.$$

Where $A$, $B$ and $C$ were evaluated

The equations in this form could only be used if they were solved at each time step using a numerical technique.

The symbolically manipulated equations produced by 'Maple' were in a form requiring less computation. It was therefore decided to implement the equations generated by *Maple* in *Matlab*.

The Matlab equations in this form did provide an alternative for estimation of the dynamics outside of the controller.

The Lagrange-Euler technique [22,23,24] is noted for its computational in-efficiency so it was decided that the equations for the simulation of the arm dynamics be the Newton-Euler implementation. This was already available for Matlab in the form of a robotic simulation package called Robo-sim [52]. The Newton-Euler implementation in the Robo-sim package, had the same problems as the Lagrange-Euler implementation; specifically the requirement of a numerical technique to put the equations in the state space form.

## 2.6 Summary and Conclusions

The equations for the dynamic interactions on the link structure were developed. There were produced in the *Maple* mathematical package. This implementation provides explicit equations for the dynamics of the robot structure. The equations are in a form where they can be algebraically manipulated, partially differentiated and then arranged into state space form without the use of a numerical technique.

The equations generated by Maple can be transferred to Matlab for use in the controller as a model of the behaviour of the link structure. They form the first part of the robot system model.

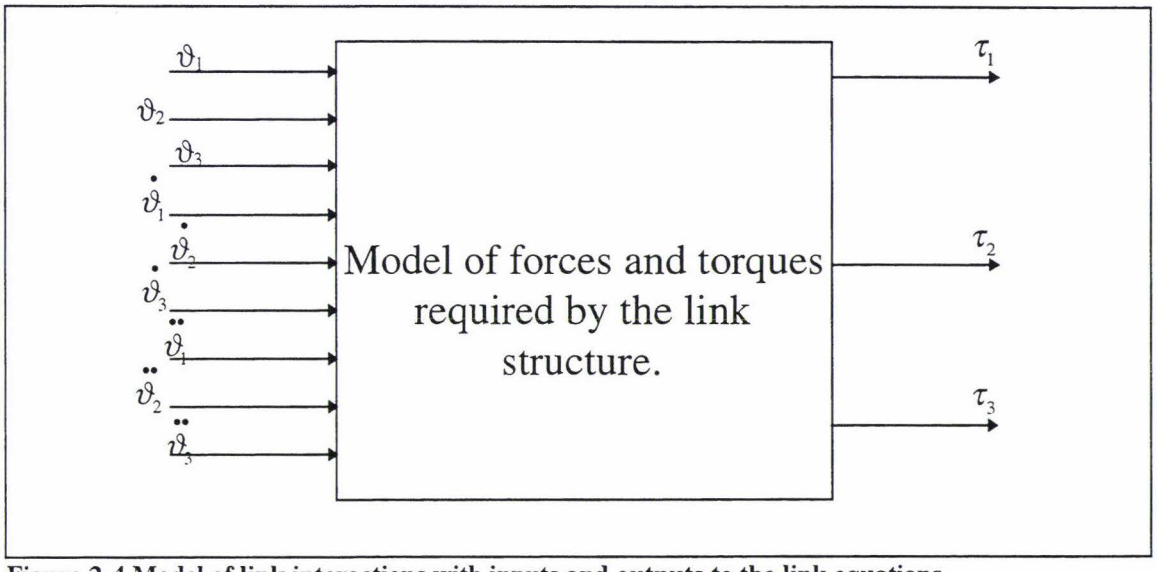


**Figure 2-4 Model of link interactions with inputs and outputs to the link equations.**

The equations describing the link structure give the relationship between the input joint variables and the output torque's as shown in Figure 2-4.

These algebraic equations can then be integrated into a model for the system containing the link structure, the pneumatic muscle's and the valves supplying air to the pneumatic muscles as shown in Figure 2-5.

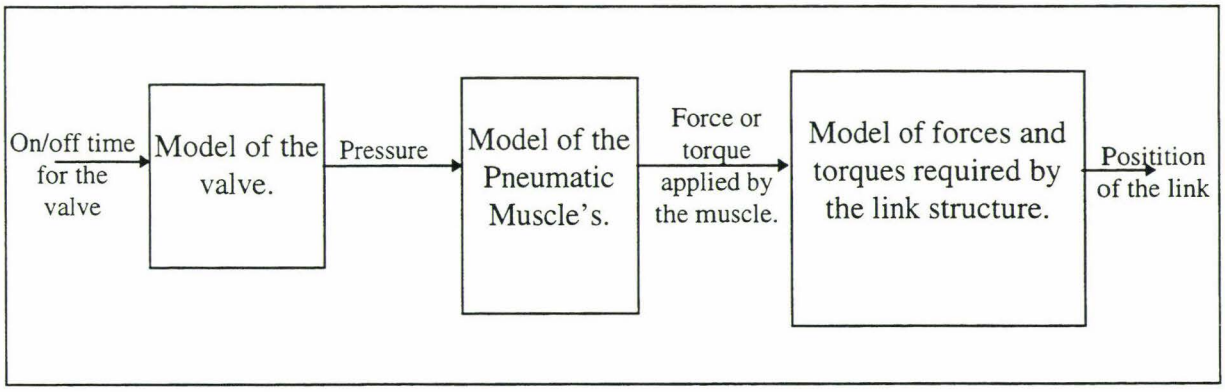


**Figure 2-5 Model of the link equations integrated into the model of the muscle, valve, link structure system.**

The Lagrange-Euler algorithm was also implemented in Matlab. This was done so that Matlab would be capable of undertaking online control.

The resulting equations from the algorithm implemented in Matlab did not facilitate partial differentiation and then implementation into state space form, without the use of a numerical technique.

A package Robo-sim had an implementation of the Newton-Euler algorithm. This implementation produced equations in a similar form to those produced from the Lagrange-Euler algorithm in Matlab. The Maple equations had advantages over both these implementations and in future work will provide the means for future controller design.

# 3. Development of a Rotary Pneumatic Muscle

## 3.1 Introduction

The actuation system is an essential feature of a robotic mechanism. This provides the forces, torque's and mechanical motions needed to move the joints, limbs or body. Whatever actuator is used, there are certain general requirements. The actuator should have a high ratio of power output to weight. In addition it should provide flexible control of the movement.

It is important in robotic applications that the weights of all components should be minimised. These components include the actuator and the energy store [30]. The actuator should be as quiet as possible if it is to be used as a general purpose robot. Above all, safety must be considered, if the robot is to be generally acceptable.

When designing actuators, it is important to consider how the power is transmitted to the link mechanism. Systems where the power is transmitted by belts, cables, straps and chains tend to suffer from friction related problems such as hysteresis, and backlash. Use of direct drive actuators can overcome this. The important issues for direct drive actuators are that they must be light so as not to adversely affect the weight of the manipulator and they must be small in size so the manipulator does not become unwieldy [31].

### 3.1.1 Literature Review

The quest to improve performance has seen research in different fields, stepper motors have been used because they are reasonably accurate in systems with open loop control and provide greater torque relative to other types of motors [32]. Thermal actuators make use of the fact that materials expand when heated. Thermal actuators are simple and capable of high output forces for the size of the actuator. Unfortunately, they are slow and have a very short stroke [33,34]. Shape memory alloys (SMA) are metals which return to a "memorised shape". Most of these applications of SMA have produced actuators which are reliable with high force for the size of the actuator. The disadvantages are long cycle times and low efficiency (<10%). Piezo-electric actuators use materials such as quartz [35]. When subjected to an electric current the shape of this material changes. These actuators are compact, accurate and have a fast response time. They are also very easily controlled [36]. The disadvantage of these actuators is that the stroke is very small. This has seen their use mainly in micro-robotic applications. Artificial polymeric muscles take advantage of the energy stored in chemical substances. This type of actuator has been used in proto-type robotic devices developed by the Massachusetts Institute of Technology [37]. The McKibben based muscle has been used by in a number of applications and is discussed extensively in Chapter four [38]-[41].

This muscle uses a rubber inner bladder with a braided outer sheathing to produce a linear contraction or elongation.

### 3.1.2 The need for a rotary pneumatic muscle

A new variant on the McKibben muscle has been developed in this research. This produces a rotary action. As most joints are rotary, the advantages of a rotary pneumatic muscle is that it can be used directly as the joint of a robot to act as a direct drive mechanism. In addition the use of pneumatics also enables the use of a cheap power source, with high output power and low weight actuators so that a high power to weight ratio is obtained.

## 3.2 Construction of Rotary pneumatic muscle

The pneumatic muscle is constructed from two metal cylinder's held together with a bearing in the middle as shown in Figure 3-1. This forms a single cylinder where each end is able to rotate in opposite directions about the longitudinal axis. A rubber bladder is attached at each end of the composite cylinder. Nylon fibres at a predetermined angle to the longitudinal axis are bound at each end to the cylinder to form an outer sheath. The sheathing is located on the outside of the rubber bladder. When the muscle inner bladder is inflated, the angle of the nylon fibres to the longitudinal axis changes as the fibres are pushed outwards thus causing the rotation.

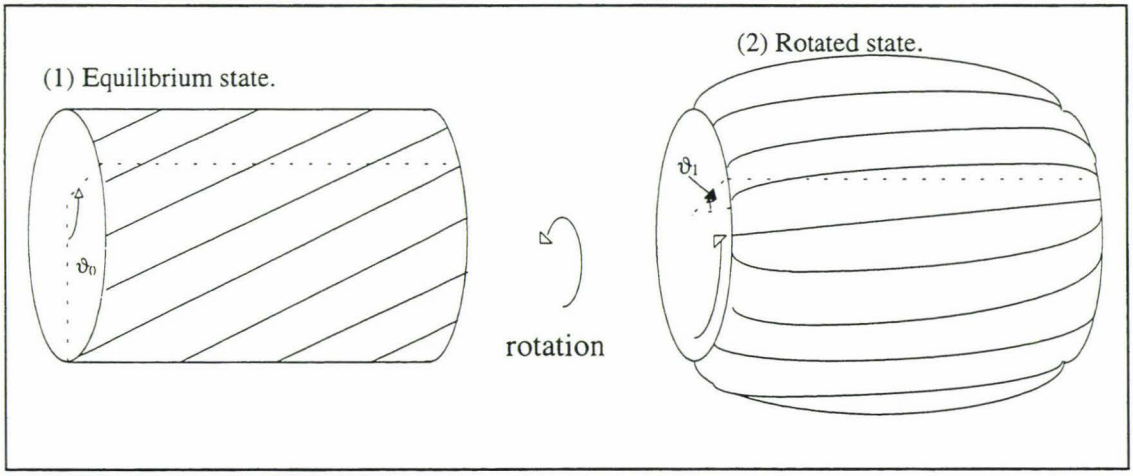


**Figure 3-1 Diagram of the rotary pneumatic cylinder**
(1) Is the rotary muscle in the uninflated state.
(2) The muscle after it has been inflated.

## 3.3 Modelling of the Rotary Pneumatic Muscle

The rotary pneumatic muscle converts pneumatic energy into mechanical energy by transferring the pressure applied on the inner surface of the bladder to radial tension. In order to find the tension as a function of pressure and actuator rotation without considering the geometric structure, a theoretic approach using the principle of energy conservation is described as follows:

1. Input work is done when the inner surfaces of the bladder is inflated by gas.

$$\begin{aligned} dW_{in} &= \int_{si} (P - P_0) dI_i dS_i \\ &= (P - P_0) \int_{si} dI_i dS_i \\ &= P' dV \end{aligned}$$

**Equation 3-1**

*where*
$S_i$ is the surface area.
$dI_i$ is the inner area change.
$dV$ is the volume change.

The output work ($W_{out}$) is the work done when the actuator rotates with changes in the volume

$$dW_{out} = -F d\vartheta$$

**Equation 3-2**

where $F$ is the axial tension and $d\vartheta$ is axial displacement. From the view of energy conservation, the input work should equal the output work if a system is lossless and without energy storage. Assuming this ideal state, the virtual work argument is

$dW_{out}=dW_{in}$,

equating Equation 3-1 and Equation 3-2 gives

$-Fd\vartheta=P'dV$

$$F = -P'\frac{dV}{d\vartheta}$$ **Equation 3-3**

The estimation of $dV/d\vartheta$, the change in volume of the bladder with respect to axial displacement requires some geometric assumptions.

It is assumed that when there is no pressure in the muscle and the muscle is uninflated, the fibres lie in a certain orientation ($\vartheta_0$). If the muscle were not constrained about its length and was lying in a flat two dimensional plane this would appear as

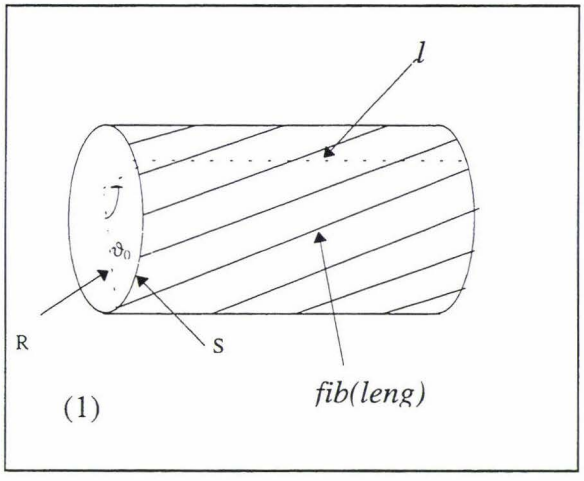


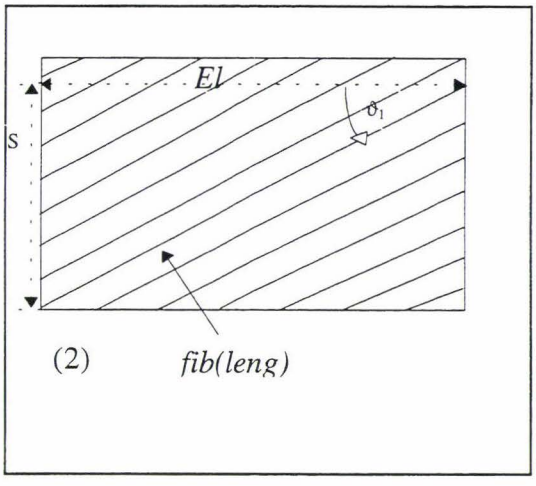


**Figure 3-2 Muscle uninflated.** **Figure3-3 2D representation of the muscle.**

Figure 3-2 is the muscle at angle $\vartheta_0$, where $\vartheta_0$ is the angle when the muscle is un-inflated.
Figure 3-3 is the geometric view of the muscle in the two dimensional plane.
$\vartheta_1$ is the angle between the fibre and the effective length of the two dimensional representation.
R is the radius of the rotary pneumatic muscle.
S is the arc length of the angle of rotation of the rotary pneumatic muscle with radius R.
*fib(leng)* is the fibre length.
*l* is the length of the cylinder.
*El* is the effective length. In this case it is the same as the cylinder length.

Next an assumption is made about the two dimensional representation of the rotary pneumatic cylinder. Given that the length of the cylinder is fixed, then if an increase in the pressure occurs, a change in $\vartheta_0$ must occur. The assumption is that if these changes in the real cylinder were applied to the two dimensional representation where the length was not constrained, the change in $\vartheta_0$ would increase the effective length of the two dimensional representation and cause a change in the angle $\vartheta_1$, as shown in Figure 3-4.

A rotation about the longitudinal axis produces a change in $\vartheta_0$ and $\vartheta_1$.

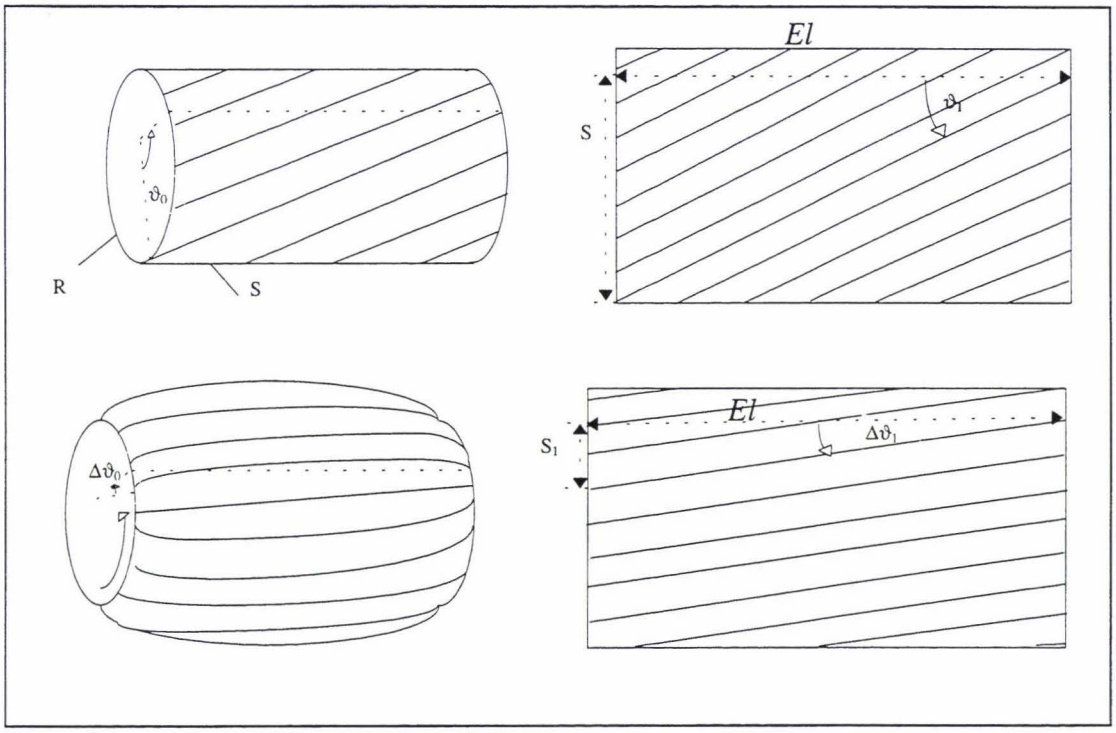


**Figure 3-4 Rotation of 2D pneumatic cylinder.**

Using these geometrical approximations the effective length and angle the fibre makes with the longitudinal axis can be found if the rotation of the cylinder is known. The equations describing this are given below.

$$r\vartheta_1 = S$$ **Equation 3-4**

Assuming the fibre length is known and $\vartheta$ is the angle to the datum position, then by basic trigonometry, this trigonometry is shown diagrammatically in Figure 3-5.

$$\vartheta_2 = \cos^{-1}\frac{El}{fib(leng)}$$ **Equation 3-5**

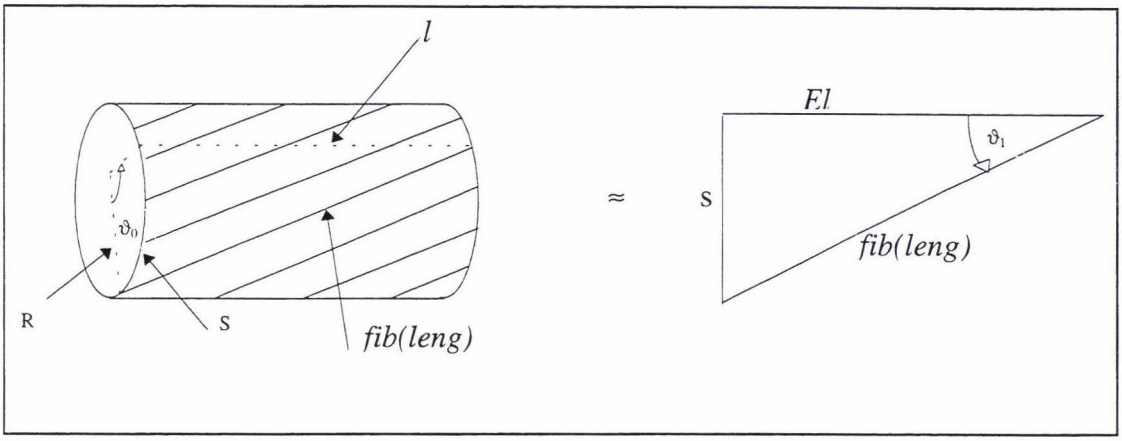


**Figure 3-5 fibre angle changes with rotation.**

$\vartheta_1$ results from the angle of the fibre and is related to $\vartheta_0$ by

$$\frac{s}{fib(leng)}\sin^{-1} = \vartheta_2$$

$\Rightarrow$ relation is

$$\frac{r\vartheta_1}{fib(leng)}\sin^{-1} = \vartheta_2 \qquad \textbf{Equation 3-6}$$

We now make a geometric assumption about the cross sectional view of the muscle as shown in Figure 3-6 and Figure 3-7.

If a cross sectional view of the rotary pneumatic muscle were taken, the muscle surface from one end of the cylinder to the other takes the shape of an arc. This is termed the arc length *(Al)*. Furthermore the assumption is made that the arc length is approximated by the effective length of the two dimensional representation of the muscle.

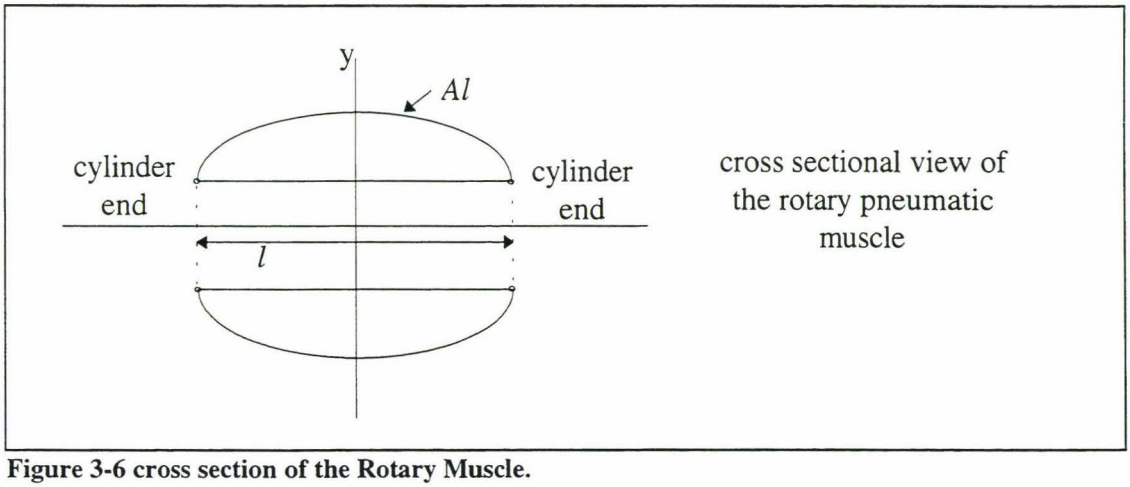


**Figure 3-6 cross section of the Rotary Muscle.**

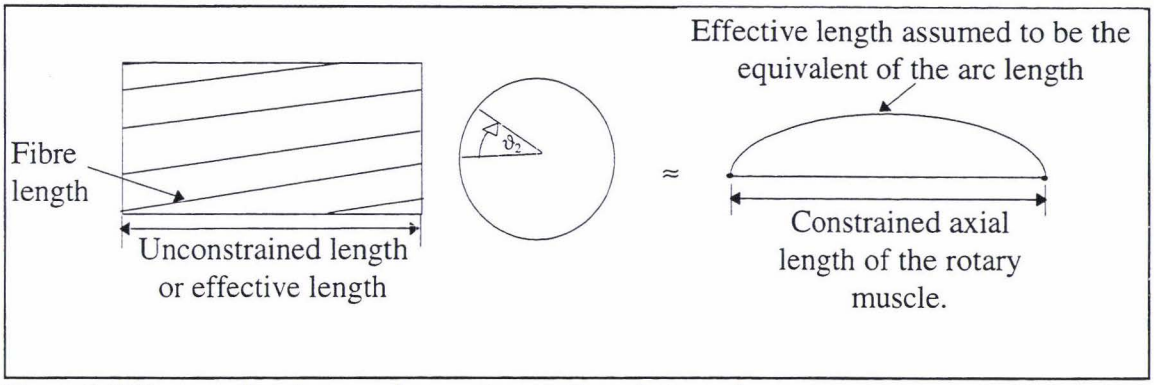


**Figure 3-7 Diagram showing muscle curvature with angle turned.**

Hence if we know the rotation undergone by the rotary pneumatic muscle we know the effective length and the arc length of the rotary pneumatic muscle.

From this we next attempt to find the volume of the muscle. This is found by revolving the shape about the x-axis.

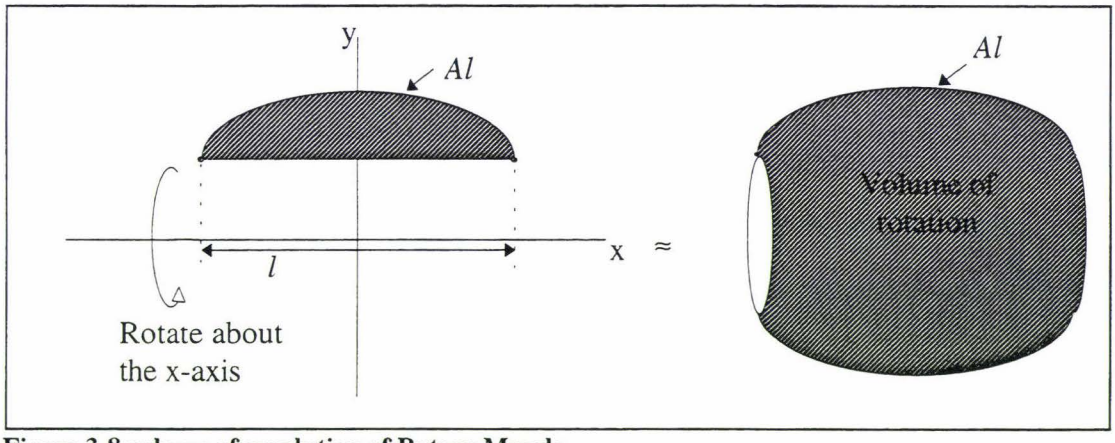


**Figure 3-8 volume of revolution of Rotary Muscle.**

The problem then reduces to finding the equations describing the curve of the arc.

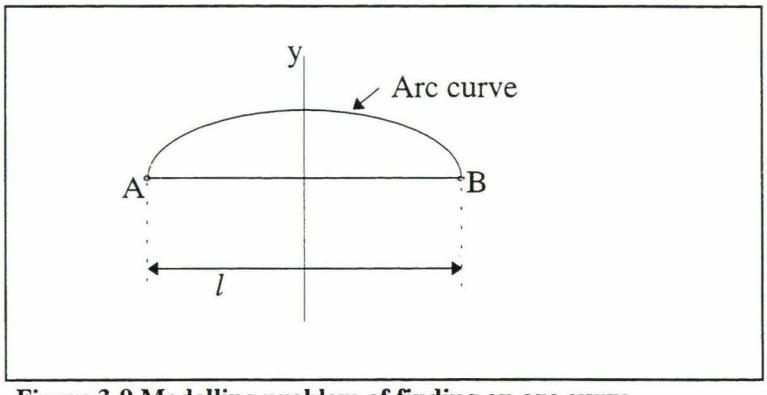


**Figure 3-9 Modelling problem of finding an arc curve.**

We know points, A and B and the arc length, but the problem cannot be solved directly and requires a numerical solution or a further approximation. If we assume that the radius is large and changes very little with $l$ we can treat the radius R as a constant.

We then obtain the volume of revolution by

$$V = 4\pi \int_0^y y^2 dx \qquad \textbf{Equation 3-7}$$

once we find V we then find $\frac{dV}{d\vartheta}$

$$F = P\frac{dV}{d\vartheta}$$

The equations to find the volume V are given below.

The terminology used below is illustrated in Figure 3-10.

$h, k$ fixed

$l$, $a$, $\alpha$, variable

$$\text{radius of circle} = \sqrt{(a+h)^2 + \left(\frac{k}{2}\right)^2}$$

$$= R \qquad \text{say (1)}$$

$$\frac{l}{2} = R\alpha \qquad (2)$$

$$\sin a = \frac{k}{2R} \qquad (3)$$

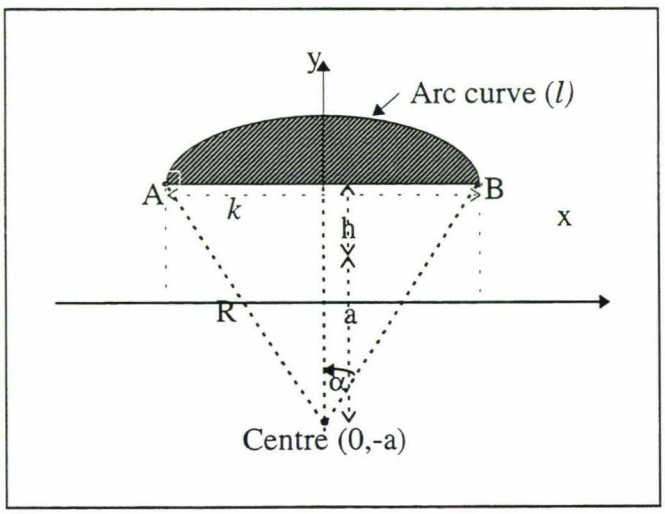


**Figure 3-10 terminology for the volume calculations.**

Equation of a circle function is: $x^2+(y+a)^2=R^2$

ie $y+a=\pm\sqrt{R^2-x^2}$

Equation of upper semi - circle is thus: $y=\sqrt{R^2-x^2}-a$

Let volume of revolution of shaded area be $V$

h is radius of the cylinder, k is the length of the cylinder, R = radius of arc formed from the arc length $l$ is the arc length

$$V=2\pi\int_0^{k/2}y^2dx-\pi kh^2$$

$$=2\pi\int_0^{k/2}\left[R^2-x^2-a^2-2a\sqrt{R^2-x^2}\right]dx-\pi kh^2$$

$$=2\pi\left[\frac{k}{2}(R^2+a^2)-\frac{k^3}{24}-2a\left[\frac{x}{2}\sqrt{R^2-x^2}+\frac{R^2}{2}\arcsin\frac{x}{R}\right]_0^{k/2}\right]-\pi kh^2$$

$$=2\pi\left[\frac{kR^2}{2}+\frac{ka^2}{2}-\frac{k^3}{24}-2a\left[\frac{x}{2}\sqrt{R^2-x^2}+\frac{R^2}{2}\arcsin\frac{k}{R}\right]_0^{k/2}\right]-\pi kh^2$$

from (1) we obtain $a=\pm\sqrt{R^2-\frac{k^2}{4}}-h$, and substituting this gives:

$$V=2\pi\left[\frac{kR^2}{2}+\frac{k}{2}\left\{R^2-\frac{k^2}{4}+h^2-2h\sqrt{R^2-\frac{k^2}{4}}\right\}-\frac{k^3}{24}-\frac{k}{2}\left(R^2-\frac{k^2}{4}\right)-R^2\sqrt{R^2-\frac{k^2}{4}}\arcsin\frac{k}{2R}+\frac{kh}{2}\sqrt{R^2-\frac{k^2}{4}}+R^2h\arcsin\frac{k}{2R}\right]-\pi kh^2$$

$$=2\pi\left[\frac{kR^2}{2}-kh\sqrt{R^2-\frac{k^2}{4}}-\frac{k^3}{24}-R^2\sqrt{R^2-\frac{k^2}{4}}\arcsin\frac{k}{2R}+\frac{kh}{2}\sqrt{R^2-\frac{k^2}{4}}+R^2h\arcsin\frac{k}{2R}\right]$$

$$=2\pi\left[\frac{kR^2}{2}-\frac{k^3}{24}-R^2\sqrt{R^2-\frac{k^2}{4}}\arcsin\frac{k}{2R}+R^2h\arcsin\frac{k}{2R}-\frac{kh}{2}\sqrt{R^2-\frac{k^2}{4}}\right]$$

$$=2\pi\left[\frac{kR^2}{2}-\frac{k^3}{24}-\left(\frac{Rl}{2}+\frac{kh}{2}\right)\sqrt{R^2-\frac{k^2}{4}}+\frac{Rlh}{2}\right]\quad\text{since } R\arcsin\frac{k}{2R}=\frac{l}{2}\text{ by (2) and (3)}$$

Also by (2) and (3), $\sin\left(\frac{l}{2R}\right) = \frac{k}{2R}$.

Differentiating with respect to $l$ gives:

$$\cos\left(\frac{l}{2R}\right)\left[\frac{2R - 2l\,dR/dl}{4R^2}\right] = -\frac{k}{2R^2}\frac{dR}{dl}$$

i.e. $$\frac{1}{2R}\cos\left(\frac{l}{2R}\right) - \frac{l}{2R^2}\frac{dR}{dl}\cos\left(\frac{l}{2R}\right) = -\frac{k}{2R^2}\frac{dR}{dl}$$

i.e. $$\frac{dR}{dl} = \frac{\frac{1}{2R}\cos\left(\frac{l}{2R}\right)}{\frac{1}{2R}\cos\left(\frac{l}{2R}\right) - \frac{k}{2R^2}}$$

$$= \frac{R\cos\left(\frac{l}{2R}\right)}{l\cos\left(\frac{l}{2R}\right) - k}$$

$$= \frac{R\sqrt{1 - \frac{k^2}{4R^2}}}{l\sqrt{1 - \frac{k^2}{4R^2}} - k}$$

$$= \frac{R\sqrt{R^2 - \frac{k^2}{4}}}{l\sqrt{R^2 - \frac{k^2}{4}} - kR}$$

now we know $V = \pi\left\{kR^2 - \frac{k^3}{12} - (Rl + kh)\sqrt{R^2 - \frac{k^2}{4}} + Rlh\right\}$ and so

$$\frac{\partial V}{\partial l} = \frac{\partial V}{\partial R}\frac{dR}{dl} + \frac{\partial V}{\partial l} = \pi\left\{2kR - l\sqrt{R^2 - \frac{k^2}{4}} - (Rl + kh)\frac{R}{\sqrt{R^2 - \frac{k^2}{4}}} + lh\right\}\frac{R\sqrt{R^2 - \frac{k^2}{4}}}{l\sqrt{R^2 - \frac{k^2}{4}} - kR} + \pi\left\{-R\sqrt{R^2 - \frac{k^2}{4}} + Rh\right\}$$

$$= \frac{\pi R}{l\sqrt{R^2 - \frac{k^2}{4}} - kR}\left\{2kR\sqrt{R^2 - \frac{k^2}{4}} - l\left(R^2 - \frac{k^2}{4}\right) - R(Rl + kh) + lh\sqrt{R^2 - \frac{k^2}{4}} - l\left(R^2 - \frac{k^2}{4}\right) + lh\sqrt{R^2 - \frac{k^2}{4}} + kR\sqrt{R^2 - \frac{k^2}{4}} -\right.$$

i.e. $$\frac{\partial V}{\partial l} = \frac{\pi R}{l\sqrt{R^2 - \frac{k^2}{4}} - kR}\left\{3kR\sqrt{R^2 - \frac{k^2}{4}} + 2lh\sqrt{R^2 - \frac{k^2}{4}} - 3lR^2 + \frac{lk^2}{2} - 2khR\right\}$$

From equation3 - 6

$l^2 - fib(len)^2 = h^2\vartheta_1^2$

so $l = \sqrt{h^2\vartheta_1^2 - fib(len)}$

so $$\frac{dl}{d\vartheta_1} = h^2\vartheta_1\left(h^2\vartheta_1^2 + fib(len)^2\right)^{\frac{-1}{2}}$$

and using the chain rule

$$\frac{dV}{d\vartheta_1} = \frac{dV}{dl}\frac{dl}{d\vartheta_1}$$

$$= \frac{\pi R h^2\vartheta_1\left(h^2\vartheta_1^2 + fib(len)^2\right)^{\frac{-1}{2}}}{l\sqrt{R^2 - \frac{k^2}{4}} - kR}\left\{3kR\sqrt{R^2 - \frac{k^2}{4}} + 2lh\sqrt{R^2 - \frac{k^2}{4}} - 3lR^2 + \frac{lk^2}{2} - 2khR\right\}$$

using equation 3 - 3

$$F = -P'\frac{dV}{d\vartheta_1}$$

$$= -P'\frac{\pi R h^2\vartheta_1\left(h^2\vartheta_1^2 + fib(len)^2\right)^{\frac{-1}{2}}}{l\sqrt{R^2 - \frac{k^2}{4}} - kR}\left\{3kR\sqrt{R^2 - \frac{k^2}{4}} + 2lh\sqrt{R^2 - \frac{k^2}{4}} - 3lR^2 + \frac{lk^2}{2} - 2khR\right\}$$

## 3.4 Summary and Conclusion

An investigation into alternative robotic actuation systems resulted in the design and development of a novel pneumatic muscle. This muscle provides a rotary action. This rotary action is useful in the design of robotic devices because often robotic joints are revolute and the rotary actuator can be used directly as a revolute joint thus creating a direct drive robot. Direct drive robots do not have the problems of friction within the power transmission system that non direct drive robots have.

Models describing the behaviour of the rotary pneumatic muscle were investigated. An analytical model describing the relationship between torque produced, muscle pressure and amount of rotation of the muscle, was developed. This model was developed using the laws of energy conservation, a diagram of the inputs and outputs required by the model is shown in Figure 3-11.

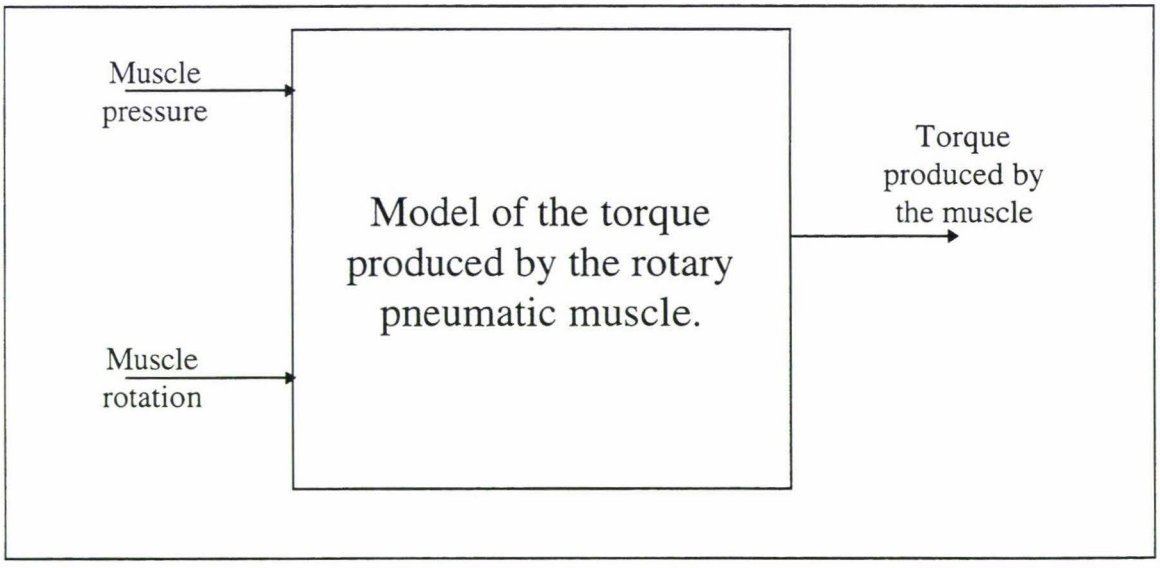


**Figure 3-11 Model of the rotary pneumatic muscle.**

This model of the muscle can be used in a model based simulation of a robot system, incorporating the rotary muscle as shown in Figure 3-12. The model of the system can be used to design a controller.

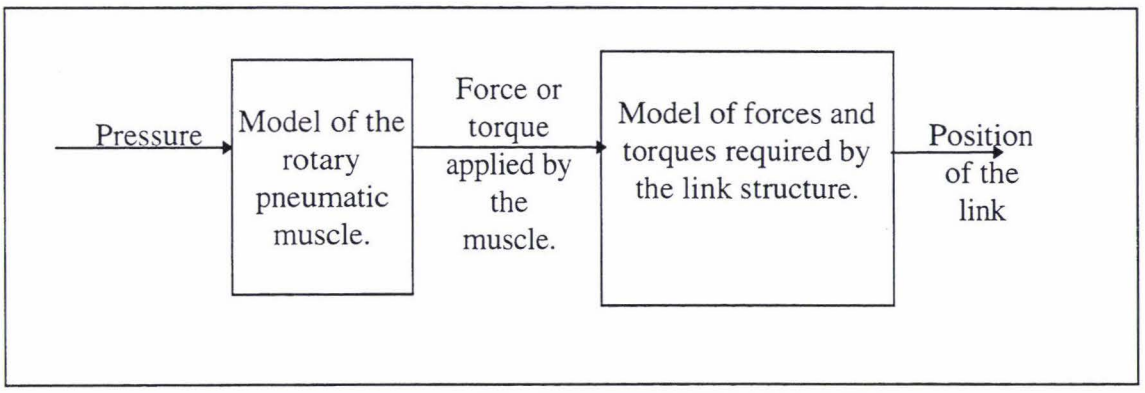


**Figure 3-12 Model of the rotary pneumatic muscle incorporated into robot system.**

# 4. Modelling of the Pneumatic Muscle

## 4.1 Objectives of this Chapter

- To develop new models for the pneumatic muscle.
- To compare the presently available models for the pneumatic muscle with the new models developed.
- To investigate the effects of temperature on the pneumatic muscle.
- To develop models of the pneumatic muscle incorporating temperature as a factor.
- To investigate the effects of hysteresis.

## 4.2 Background to the Choice of Actuation

Actuators and actuation systems are essential features of all robots, providing the forces, torques and mechanical motions needed to move the joints and limbs in robotic manipulators.

The performance of actuators is critical in determining the strength, speed of motion, power, (in particular the power/weight and power volume ratios), response rate, reliability, controllability, compactness and in many cases the compliance exhibited by robots. Unfortunately current drive systems (usually electric, hydraulic or pneumatic), seldom achieve these demands due to well known and well documented drawbacks that place constraints on their application in future generations of dextrous manipulators. With this in mind the pneumatic muscle was selected as the actuation mechanism in the direct drive system powering the dextrous manipulator [1]. The motivation for this was its relatively small size and high power to weight ratio.

## 4.3 Review of Actuators

The McKibben pneumatic muscle's were developed in artificial limb research in the 1950's and 1960's (Schulte 1961) [45]. They have recently been commercialised by the Bridgestone Rubber Company of Japan for robotic applications [46]. These actuators can be physically described as comprising a rubber tube, surrounded by a braided outer sheathing (made of flexible yet non-extensible threads). The rubber inner tube is sealed at one end with a plastic plug and the other end has an air supply hose attached to it. When the internal bladder is pressurised, the high pressure gas pushes against its inner surface and the external shell, and tends to increase its volume. Due to the non-extensibility of the threads in the nylon braided shell, the actuator shortens according to its volume increase and/or produces tension if it is coupled to a mechanical load.

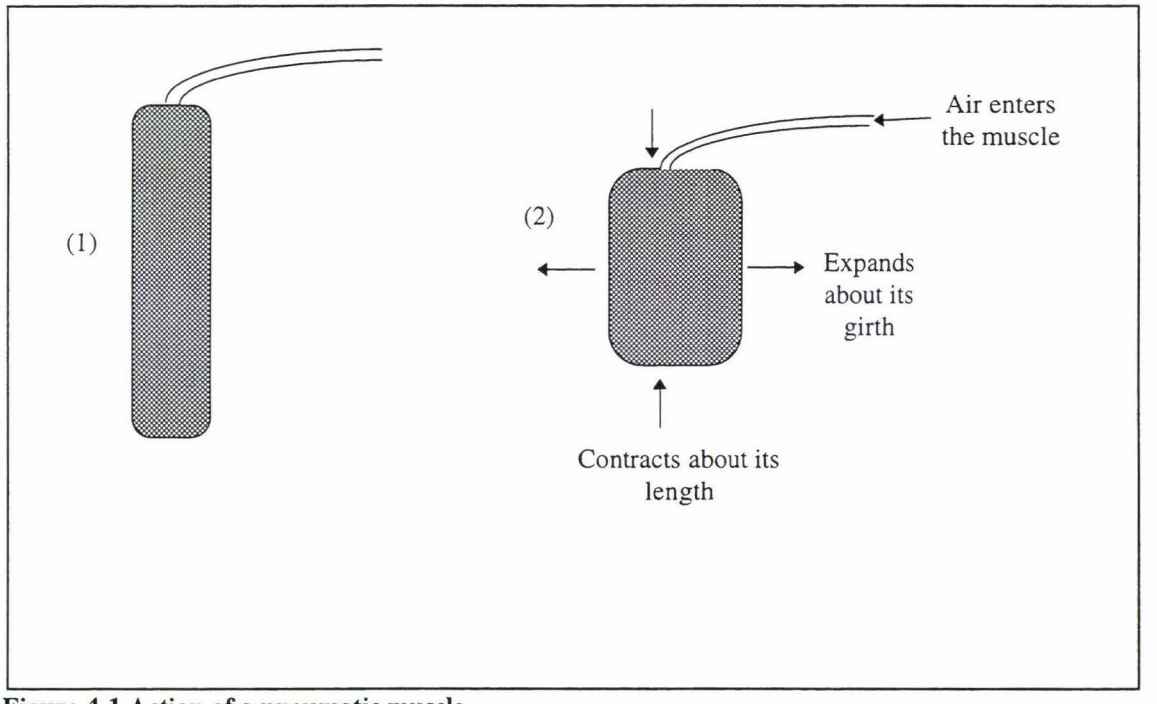


**Figure 4-1 Action of a pneumatic muscle.**
(1) The muscle at its original length.
(2) The muscle contracts in length when air enters the muscle.

The modelling of the pneumatic muscle's static properties is an area of research that has seen renewed interest with the need for control when they are incorporated into robotic devices. Finding adequate models for the pneumatic muscle has proved a challenging problem. One approach to the modelling problem uses the laws of energy conservation in the development of theoretical models. Work by Chou and Hannaford [40], Schulte [45], Winters [48] developed theoretical models from the view of energy conservation. The derivation is given below.

The input work (Win) when the gas pushes the inner surface of the bladder, which is:

$$dW_{in} = \int_{si} (P - P_0) dI . dS_i$$

$$= (P - P_0) \int_{si} dI . dS_i = P' dV \qquad \textbf{Equation 4-1}$$

where $P$ is absolute internal gas pressure, $P_o$, is the environment pressure (1 atm). $P'$ is the relative pressure ($P$-$P_o$), $S_i$ is the total inner surface, $dS_i$ is the area vector, $dI$ inner surface displacement and $dV$ the volume change. The output work ($W_{out}$) is done when the actuator shortens in response to the pressure changes,

$$dW_{out} = -FdL \qquad \textbf{Equation 4-2}$$

where $F$ is axial tension and $dL$ is axial displacement.

From the view of energy conservation, the input work should equal the output work if a system is lossless and without energy storage. Assume the actuator is in this ideal condition.

$$dW_{out} = dW_{in}$$

from Equation 4-1 and Equation 4-2,

$$-FdL = P' dV$$

$$\Rightarrow F = -P' \frac{dV}{dL} \qquad \textbf{Equation 4-3}$$

To estimate $dV/dL$ the middle portion of the actuator is modelled as a perfect cylinder, where $L$ is the length of the cylinder, $\vartheta$ is the angle between a braided thread and the cylinder long axis, $D$ the diameter of the cylinder, $n$ the number of turns of the thread, and $b$ the thread length. $L$ and $D$ can be expressed as functions of $\vartheta$ with constant parameters $n$ and $b$,

$$L = b\cos(\vartheta), \qquad \textbf{Equation 4-4}$$

$$D = \frac{b\sin(\vartheta)}{n\pi} \qquad \textbf{Equation 4-5}$$

The volume of the cylinder is then

$$V = \frac{1}{4}\pi D^2 L = \frac{b^3}{4\pi n^2}\sin^2(\vartheta)\cos(\vartheta) \qquad \textbf{Equation 4-6}$$

so from, Equation 4-6 $F$ can be expressed as a function of $P'$ and $\vartheta$

$$F=-P\frac{dV}{dL}=-P\frac{dV/d\vartheta}{dL/d\vartheta}=P\frac{b^2\left(3\cos^2\vartheta-1\right)}{4\pi n^2}$$ **Equation 4-7**

which is equivalent to

$$F=\frac{p\ D_0^{\ 2}P}{4}\left(3\cos^2(\vartheta)-1\right)$$ **Equation 4-8**

where $D_0=\frac{b}{n\pi}$ is the diameter.

The tension is thus linearly proportional to the pressure and is a monotonic function of the braid angle. The maximal shortening will be reached when $F$=0, that is, $\vartheta$ = 54.7°.

Other approaches have used the basic gas laws with the idea of minimum energy states[38]. Work by Caldwell et al [39], gives the best description of this approach. Their derivation of a theoretical model is given below.

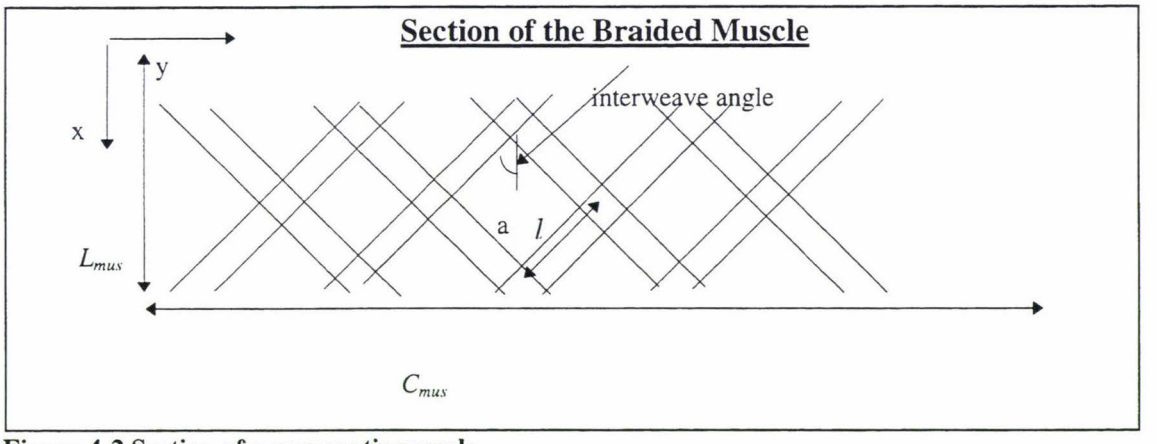


**Figure 4-2 Section of a pneumatic muscle.**

First the cylindrical muscle is opened up to expose the two-dimensional nature of the muscle. The derivation is based on this two dimensional view of the muscle.

If $l$ is the length of the trapezoid, the overall length of the muscle is:

$$L_{mus}=2\,A\,l\cos\,a_{mus}=h\,\cos\,a_{mus}$$ **Equation 4-9**

where $A$ is the number of trapezoids in the x plane, h is helical fibre length ($h$=2$Al$), and $a_{mus}$ is the interweave angle. Similarly in the y direction the circumference is:

$$C_{mus}=2\,B\,l\sin(a_{mus}) \qquad \textbf{Equation 4-10}$$

where $B$ is the number of trapezoids in the y plane (around the muscle body). Since the circumference is proportional to the diameter this becomes:

$$D_{mus}=f\,\sin\,a_{mus} \qquad \textbf{Equation 4-11}$$

where $f$ is the distance parameter and equals $2B/\pi$. Constants were then developed,

$$h=(L_{\max})/\cos\,a_{\max}=(L_{\min})/\cos\,(a_{\min}) \qquad \textbf{Equation 4-12}$$

$$f=(D_{\max})/\sin\,a_{\max}=(D_{\min})/\sin\,(a_{\min}) \qquad \textbf{Equation 4-13}$$

using Equation 4-9 to Equation 4-13, the surface area is determined by

$$S_a=\pi\,D_{mus}\,L_{mus}=\pi\,(f\sin(a_{mus}))\,(h\cos(a_{mus})) \qquad \textbf{Equation 4-14}$$

From the basic gas laws, pressure is known to be inversely proportional to volume. The volume is given by

$$Vol=(D_{mus}/4)^2\,\pi\,L_{mus}=K(\sin(a_{mus}))^2\,(\cos(a_{mus})) \qquad \textbf{Equation 4-15}$$

where $K=(\pi/4)f^2\,h$

Volume is maximised at 54.5°, hence minimum force occurs at this interweave angle. When the actuator is in this position it is said to be in its minimum energy state. Any change from this state causes an increase in pressure and induces a force to return to the minimum energy state. The drive (restoring) force is produced to maintain the minimum energy/force state. In this minimum energy/force state the internal force is given by

$$F_{\min}=S_a\,P+2\,E_a\,P=P(S_a+2E_a) \qquad \textbf{Equation 4-16}$$

where $E_a$ is the area of the end plates, and $P$ is the internal pressure.

When elongated or compressed from this point the drive force is produced.

$$F=S_a\,P_{new}+2\,E_a\,P_{new}=P_{new}(S_a+2E_a) \qquad \textbf{Equation 4-17}$$

where $P_{new}$ is the new internal pressure caused by a reduction in the system volume.

As the pneumatic muscle is a practical system, it is not 100% efficient, and the force output is typically only 50% of the theoretical value. To take account of this an efficiency factor is used in the final equation, Equation 4-18.

$$F_d=Eff\,(F-F_{\min}) \qquad \textbf{Equation 4-18}$$

Hasselroth et al [42] developed a static model using a statistical approach. The model they developed uses the following equation.

$$F_j=P_j D_j 2(a((1-\epsilon_j)^2-b) \qquad \textbf{Equation 4-19}$$

Where $P_j$ is the supply pressure, $a$ and $b$ are constants depending on the particular tube, $0<\epsilon_j<0.2$ is the contraction ratio which is directly related to the length of the pneumatic muscle, $l_j$ and $D_j$ is the effective diameter before displacement.

Although there have been attempts to describe the behaviour of the muscle from different points of view, there has been no attempt to compare the accuracy of these models. It also appears that there is still scope for improvement of the presently available models of the pneumatic muscle.

All of the models presented identify relationships between force, pressure, length of the actuator and diameter of the actuator. Another factor which affects performance is temperature. This is not included in any of these models as a parameter.

Hasselroth et al [42], investigated the effects of temperature on the muscle. Their research involved showing that the pressure position relationship changes when the muscle was used for long periods of time. They concluded this was due to the effect of temperature. They then decided that 'a precise model for the pneumatic actuator could not easily be constructed'. They decided to deal with the effects of temperature by using a self tuning neural network controller avoiding the need to formally model the effects of temperature.

Temperature was also identified as a factor by Caldwell et al [42]. They showed that the properties of the muscle changed when the muscle was heated. Their method of dealing with the effects of temperature was to implement a self tuning adaptive controller.

Although temperature has been investigated by some researchers, there has been no formal model developed to describe the effects of temperature.

## 4.4 Model Development Strategy

When looking at model development for a pneumatic muscle, it was decided that statistical models would be developed . The model development strategy known as the top down approach was then chosen as the desired technique. The top down methodology firstly requires the development of a basic model which takes into account just the main characteristics of the system. This initial model can be conceptualised as being at the top of a ladder. Other more complex effects such as temperature changes and hysteresis effects on the system can be dealt with after a basic model has been developed. These effects are further down the ladder. When the bottom of the ladder is reached, a final model incorporating all the factors and effects thought to be important is produced.

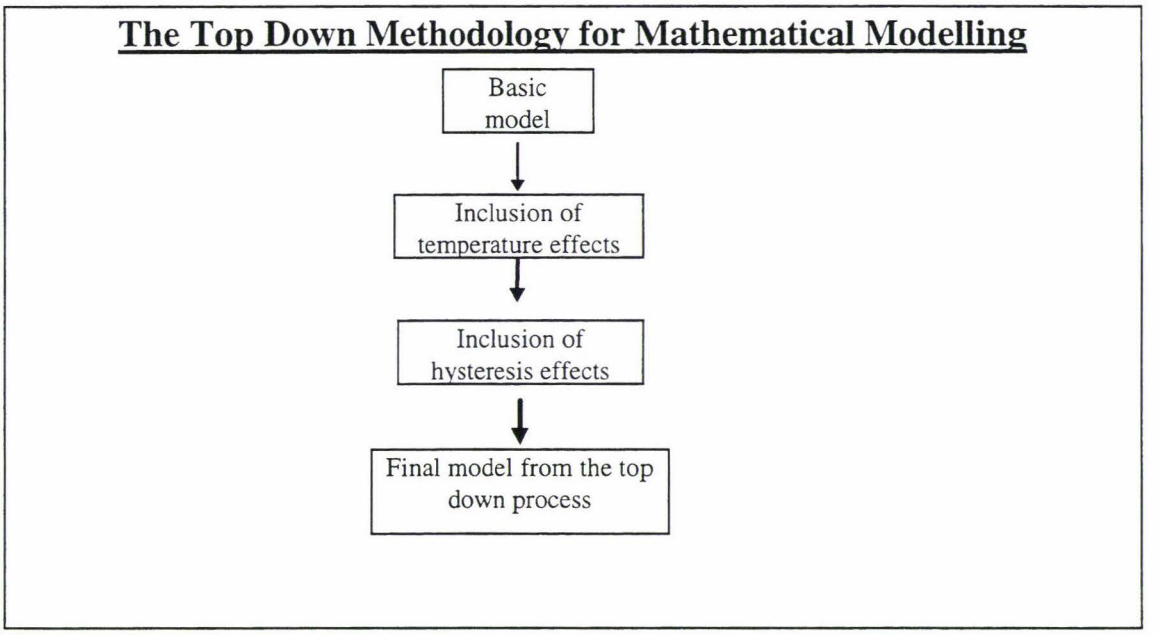


**Figure 4-3 Model development process.**

## 4.5 Selection of a Modelling Technique

There were six options under consideration for the development of a model for the pneumatic muscle

- Use of models found in the literature search. For example the Caldwell model. Use of the Caldwell model has the advantage that the equations describing their pneumatic muscle are already available. The problem is that the applicability of these equations are to our muscle is not known.

- Developing a new empirical model. The approach of developing a new empirical model would produce some novel research but there is no guarantee that an accurate model would be developed in time.

- Development of a black box type model, a process which would require taking more measurements and using a statistical package to find a mathematical relationship in the data. The black box approach would provide a result but there is no guarantee that the model will be an accurate tool for extrapolation of results. This method will require lots of measurements. The model may become very complex and unwieldy depending on what accuracy is required.

- Development of quasi static models, a process which involves making observations and assumptions about the physical system. Predictors thought to be important are then devised from the assumptions on the physical system and these are optimised by statistical means using data obtained from the system.

- Use of a neural network type model which would require obtaining data and programming a neural network to imitate the behaviour of the pneumatic muscle. The neural network approach would need large quantities of data to train the net. There is also the question of how applicable a neural network is to a simulation given the computationally intensive nature of the neural net.

- Use of a Finite Element Analysis approach which would require developing a model of the muscle on a finite elements package, then using the results to generalise the muscle's behaviour. The Finite Element approach is the most technically difficult option. Retrieval of results from a finite element model would be too slow for a simulation. The results could however be used to assist in the development of an empirical model.

### 4.5.1 The Modelling Approach Taken

A decision was made to develop a black box type of model, and a quasi static model.

An experimental design approach was taken and experimental measurements were collected in the formation of the black box and quasi static model. Results and outputs from the black box and quasi static models can then be compared to other models from available literature, and the best used as the final model.

It was decided to use one factorial experimental design to obtain the data on the pneumatic muscle. This methodology requires that one experimental design parameter is varied one at a time while the others are held constant. Each of the mass, pressure and length were kept constant, while the relationship between the two varying parameters was investigated. The effect of temperature were then also considered.

## 4.6 Types of Tests Conducted

There were four types of tests conducted in order to develop the static model. In each of these tests one factor was held constant and the others were allowed to vary. The isometric tests were conducted first. These required that the length of the muscle and temperature be constrained and the pressure and mass allowed to vary.

The apparatus for this experiment is shown in Figure 4-4. The muscle was suspended on a bar and air was passed in via a pressure regulator. A load cell was used to measure the resulting force exerted by the muscle.

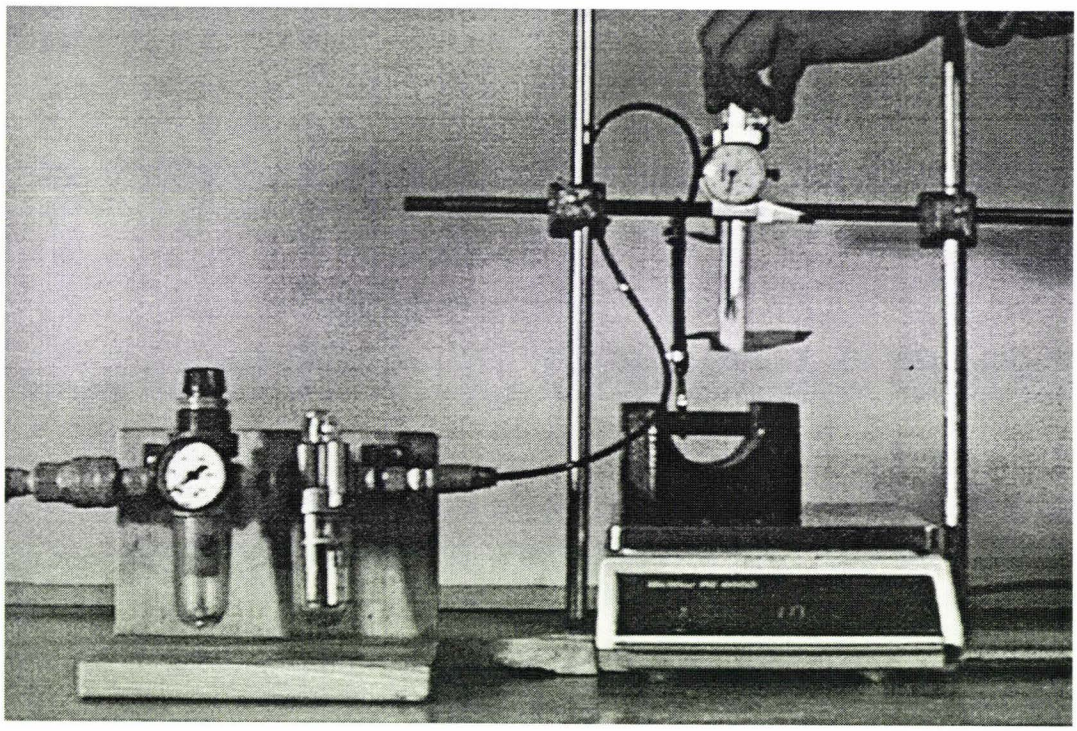

**Figure 4-4 Isometric and isobaric test arrangement.**

The second set of tests were the constant pressure, or isobaric, tests.

These required that the pressure be held constant while the force and muscle length are allowed to vary. The apparatus in Figure 4-4 was used for these tests.

The third set of tests were the constant mass/force tests, or isotonic tests. A fixed mass was placed on the end of the muscle and the pressure and length of the muscle were allowed to vary. An isotonic test arrangement is shown in Figure 4-5.

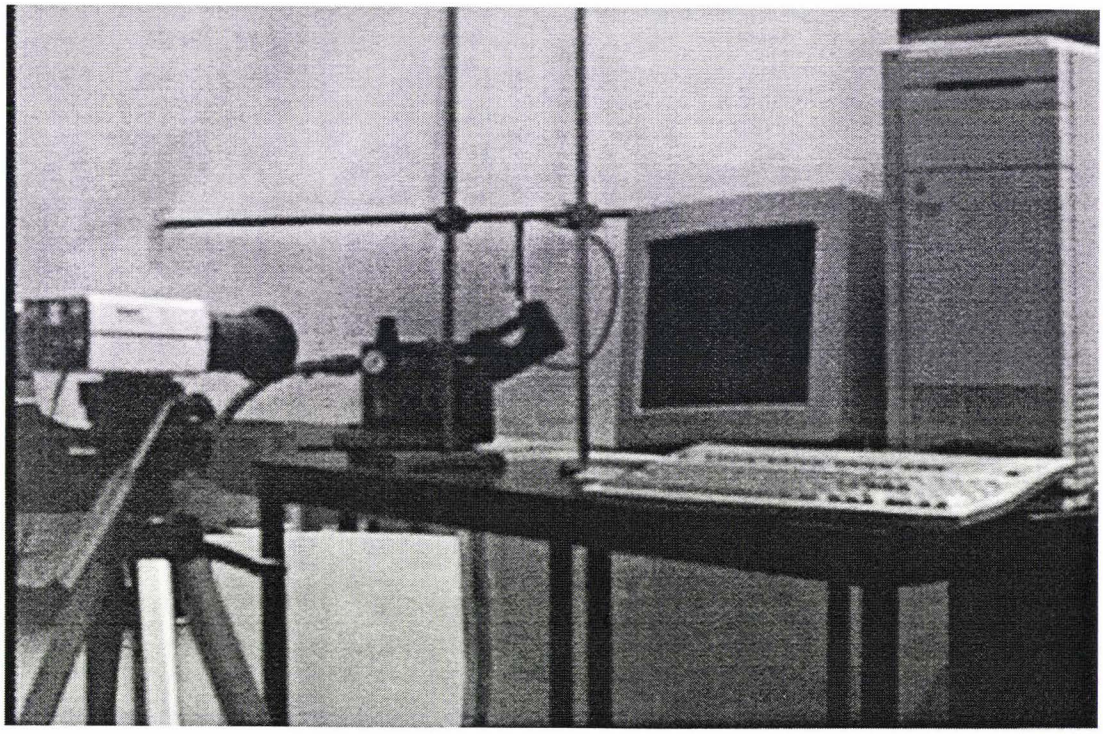

**Figure 4-5 Isotonic test arrangement.**

### 4.6.1 Experimental Arrangement for Isobaric and Isometric Tests

The isobaric and isometric tests were conducted on a rig specifically built for the test, a bar was held in place between two tripod stands. The muscle was then attached to this.

The bottom of the muscle was then attached with a large mass which was placed on a scale.

As the full scale deflection movement of the scale is only 0.2mm the bottom of the muscle is effectively held in a fixed position, and the upward force exerted by the muscle could be measured by the subtraction of the weight of the mass from the reading on the scale.

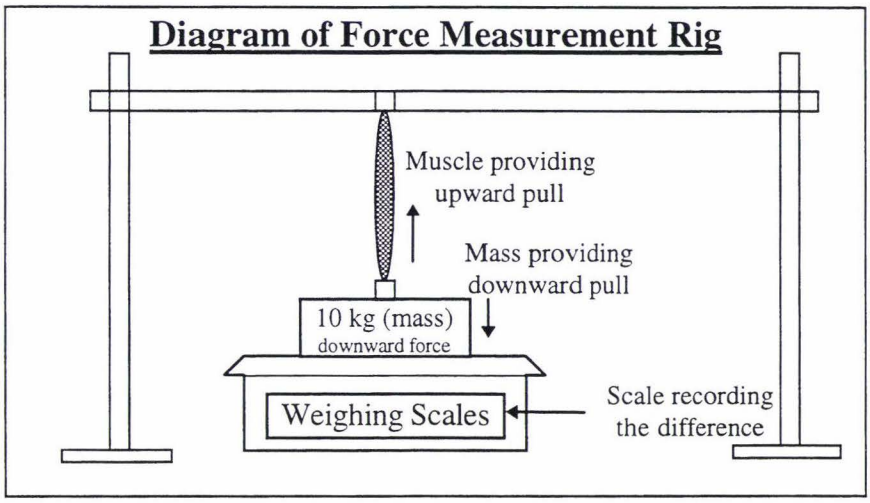


**Figure 4-6 Force measurement rig.**

### 4.6.2 Experimental Arrangement for the Isotonic tests

When the isotonic tests were conducted several methods were considered for measuring the length of the muscle, such as fixing an attachment on the bottom of the muscle and having the other end operate a potentiometer, a laser measuring device, manual use of vernier callipers and making use of an image processing technique. The image processing technique was chosen. This is illustrated in Figure 4-7.

The muscle was suspended from a stand at a fixed height. A pressure regulator was connected to the muscle and masses of known weights were then attached to the muscle. A marker was attached at the bottom end of the muscle whose position was viewed and measured via a video camera image.

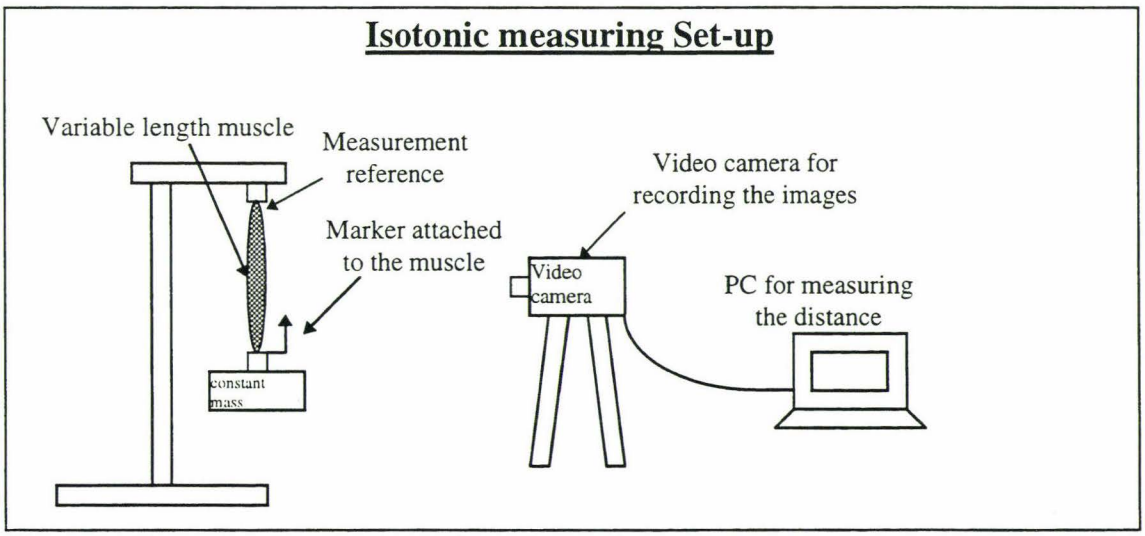


**Figure 4-7 diagrammatic set up for the isotonic experiments.**

The image processing package *NIH Image* [56] was used to capture the images, remove the unwanted background and find the length of the muscle.

### 4.6.3 The Distance Measuring Algorithm for the Isotonic Tests

A program to measure the length of the muscle was written for use in NIH Image. This required capturing images containing both a marker, marking the end of the muscle and a measurement reference point. The interval between the marker and the measurement reference point had been arranged to be lighter than any other part in the scene. Then when the image is thresholded and binarized, only these two features remain in the region of interest. A single scan can then be used to determine the number of pixels between them, and this measurement is displayed. The algorithm used is shown in Figure 4-8 and the Appendix C-5.

The length /pixel calibration was carried out by setting the marker to reference a known measurement and then determining the number of pixels in the image to milli-meters in the scene.

The muscle length with no pressure was taken as the datum for each suspended weight. The measurements are made to a precision of +/-0.05 mm.

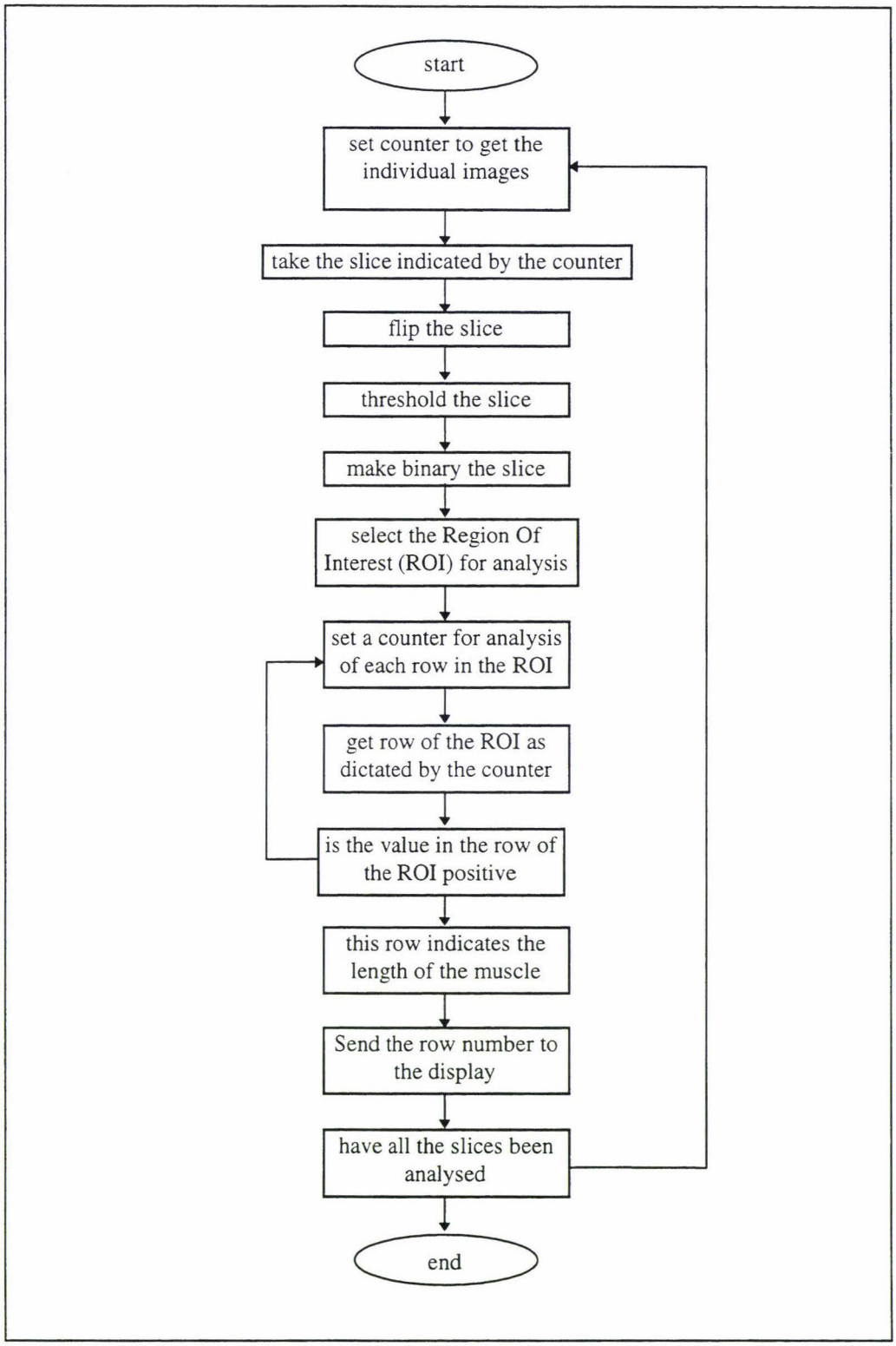


**Figure 4-8 Length measuring algorithm.**

### 4.6.4 Experimental Errors

The errors associated with the experimental setup were of two types;

- Equipment errors due to the precision of the experimental equipment.
- Human errors resulting from incorrect reading being taken by the human operator.

All of the measurement equipment had a limited precision. The errors associated with the measurement of length of the pneumatic muscle were +/- 0.05mm for the video camera measurement algorithm and +/-0.1mm for the venier callipers. The temperature could be measured to +/-0.01°C with the temperature measuring device. The mass on the scale could be measured to +/-0.001 gramme. The pressure was measured by the use of an analogue pressure gauge on a pressure regulator. This had a range from 0kpa to 1000kpa with scale increments at 50kpa, readings could be taken between the scale increments, so the actual experimental error was of the order of +/-5kpa.

## *4.7 Advantages and Disadvantages of Statistical and Black Box Methods*

A black box model is obtained empirically by use of the results from a number of experiments. Obtaining the necessary experimental results poses significant problems in many situations, and the model may not perform well for physical behaviours which fall outside the experimental results incorporated in the model. A black box model can be made very accurate if the results from large numbers of experiments are used, but then the model may become excessively large and unusable due to computational limitations. There is thus a trade off between the accuracy and usability of the model.

Statistical or black box models have the advantage that they do not require intimate knowledge of the physical process; only a knowledge of the prediction variables is required.

## 4.8 Results

### 4.8.1 Isometric Tests

The first set of tests conducted were isometric tests. These required the muscle length to be fixed and the pressure to be increased from 0kpa to 600kpa. The results are shown in Figure 4-9, experimental results are presented in Appendix C-1, Table C-1. Each curve represents the force versus pressure results or a particular muscle length.

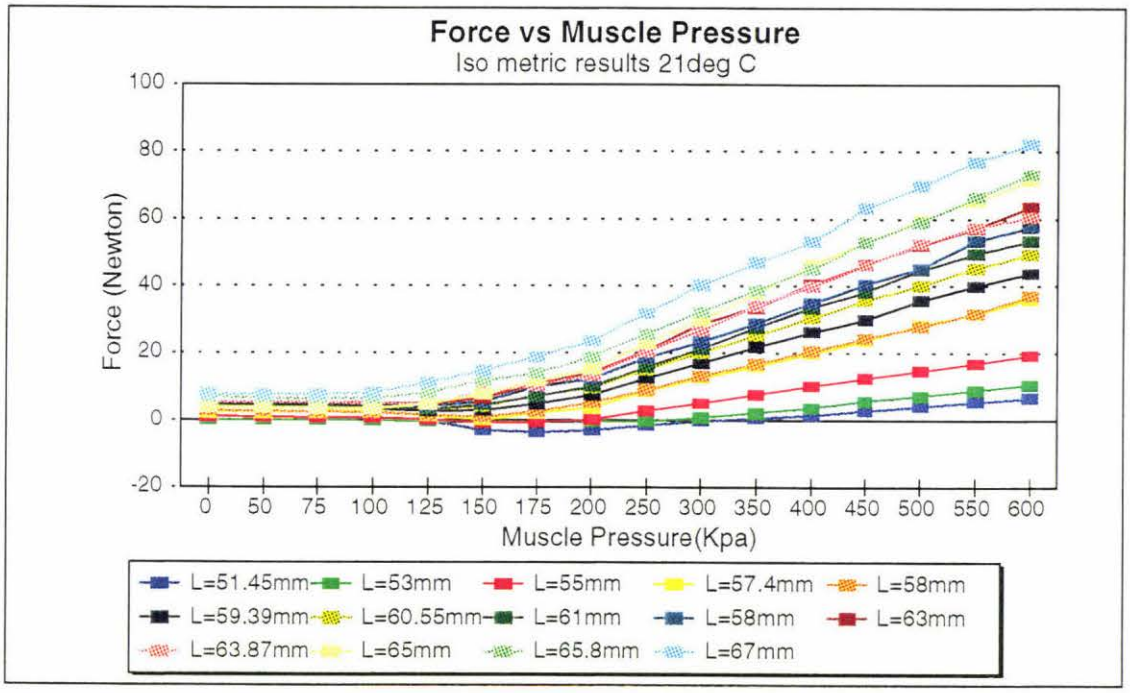


**Figure 4-9 Isometric results.**

From a visual inspection of the graphical results, it can be seen that there are two regions.

The first region from 0kpa to 125kpa contains curves which have the same gradient and lie parallel to each other. These curves all appear to have a zero gradient which indicates that the gradient coefficient, $K_{P1}$ is unaffected by pressure and muscle length in this region. The intercept coefficient, $c$ for these curves appears to increase with muscle length thus indicating a relationship between force and muscle length. These results are generalised by Equation 4-20 and Equation 4-21.

**Generalised equation of the isometric curves in the pressure range 0-125kpa from inspection of the graph**

$$Force = K_{P1}P + c \qquad \textbf{Equation 4-20}$$

$$c \approx f(L) \qquad \textbf{Equation 4-21}$$

*where* $P$ is the muscle pressure
$K_{P1}$ is the pressure gradient coefficient
$c$ is the intercept coefficient
$f(L)$ is the function relating muscle length ($L$) to the intercept coefficient $c$

The second region between 150kpa and 600kpa appears to have a linear or quadratic relationship between pressure and force. When we look at these curves as a set, it appears that the gradient of the force/pressure curve, $K_{P2}$ is different for each muscle length. This indicates that the gradient is somehow related to the muscle length. These generalisations are expressed in Equation 4-22 and Equation 4-23.

**Generalised equation of the isometric curves in the pressure range 150-600kpa from inspection**

$$Force = K_{P2}P^{a} + c_2 \qquad \textbf{Equation 4-22}$$

$$K_{P2} \approx f(L) \qquad \textbf{Equation 4-23}$$

*where* $P$ is the pressure within the muscle
$c_2$ is the intercept coefficient
$a$ is the constant indicating the linear ($a=1$) or quadratic ($a=2$) nature of the relationship
$K_{P2}$ is the pressure gradient coefficient and is dependent on muscle length ($L$)
$f(L)$ is the function relating muscle length $L$ to $K_{P2}$

Another feature of these curves is that there are negative force values. A negative force value indicates that the muscle is applying an elongation force rather than a contraction force. This occurs in the region where the pressure is less than 250kpa and the muscle length is less than 58mm. These generalised trends are shown in Figure 4-10.

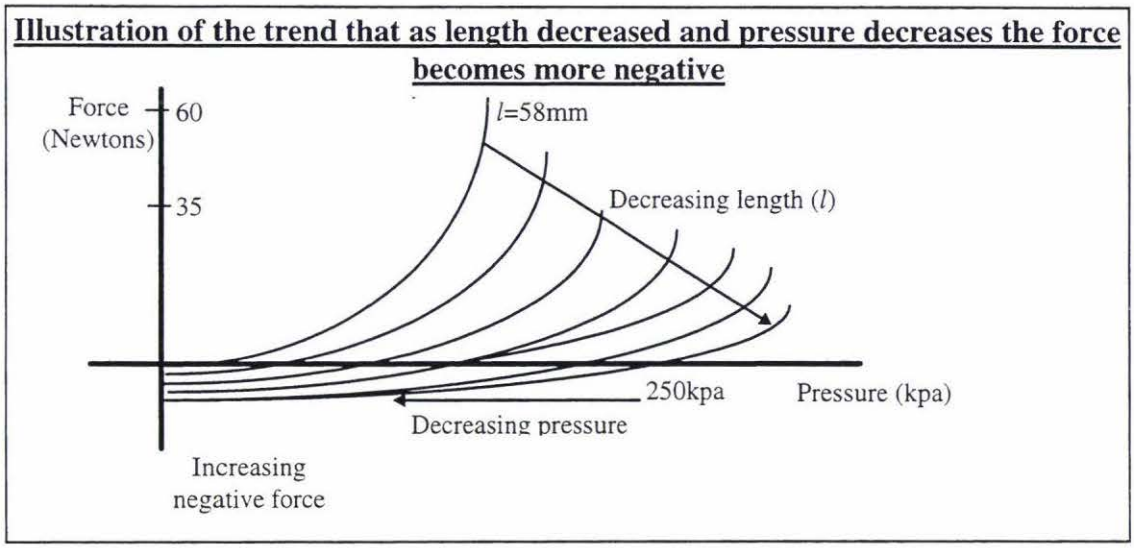


**Figure 4-10 Decreasing pressure/force trend.**

In this diagram the trend is for decreases in muscle length and muscle pressure to be associated with the curves exhibiting negative values for force.

### 4.8.2 Isobaric Tests

These required that the pressure was fixed while the distance was increased through the whole extension range of the muscle.

The isobaric results are shown in Figure 4-11 and Appendix C-1 Table C-2, where each curve is a representation of the force exerted by the muscle responding to a change in muscle length while the pressure is held constant.

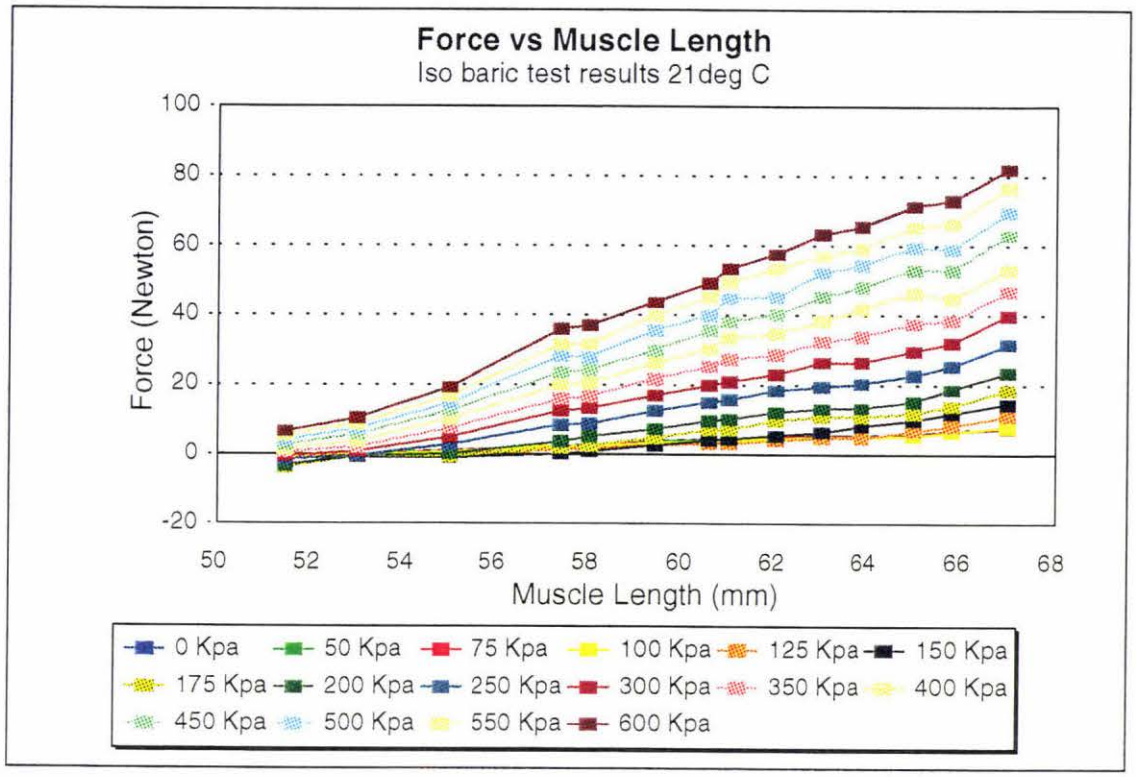


**Figure 4-11 Isobaric test results.**

From a visual inspection of the results, it can be seen that there are two types of curves. Those associated with pressures from 0kpa to 125kpa appear all to have the same gradient, and lie vertically on top of each other. These curves have a non zero gradient and intercept. These curves indicate a relationship between force and muscle length which is unaffected by pressure.

**Generalised equation of the isobaric curves in the pressure range 0-125Kpa from inspection**

$$Force = K_{L1} L^{a} + c_3$$ **Equation 4-24**

*where* $L$ is muscle length
a could be 1 for a linear relationship or 2 for a quadratic relationship
$c_3$ is the intercept coefficient
$K_{L1}$ is the muscle length gradient coefficient

The higher pressure set of curves appear to have a linear or quadratic relationship between muscle length and force. When we look at these curves as a group, it appears that the gradient coefficient, $K_{L2}$ of the force vs muscle length curve is dependent on pressure, $P$.

**Generalised equation of the isobaric curves in the pressure range 150-600kpa from inspection**

$$Force = K_{L2} L^{a} + c_4 \qquad \textbf{Equation 4-25}$$

$$K_{L2} \approx f(P) \qquad \textbf{Equation 4-26}$$

*where* $K_{L2}$ is muscle length gradient coefficient
$L$ is the length
a could be 1 for a linear relationship or 2 for a quadratic relationship
$f(P)$ is the function relating pressure $P$ to $K_{L2}$
$c_4$ is the intercept coefficient

At small muscle lengths all the curves appear to converge towards a single value. This indicates that there exists a critical length beyond which the nature of the force muscle length relationship changes. If the muscle length contracts past this length, the force being exerted by the muscle remains constant regardless of the pressure applied to it. This occurs because when the muscle is highly contracted, the inner lining of the muscle is slack inside the sheath. This is illustrated in Figure 4-12.

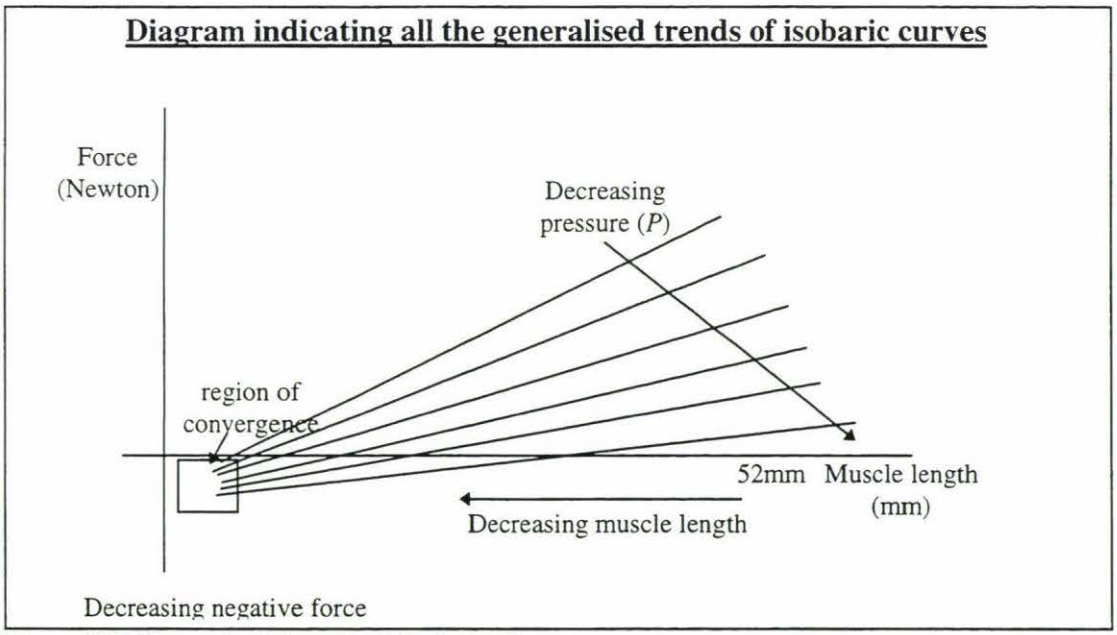


**Figure 4-12 Generalised trends of the isobaric curves.**

### 4.8.3 The Isotonic Tests

The isotonic tests required that the mass that is, the force, was kept constant and the pressure was varied between 0kpa and 600kpa, while the resulting muscle length was recorded. The results for these curves are shown in Figure 4-13, with the experimental data in Appendix C-1 Table C-3.

Again there appears to be two regions. One where there is a logarithmic, quadratic or linear relationship which occurs at pressures between 150kpa and 600kpa. In this region the effect of changing the mass is only to add an offset between curves. It appears that this offset decreases with increasing mass.

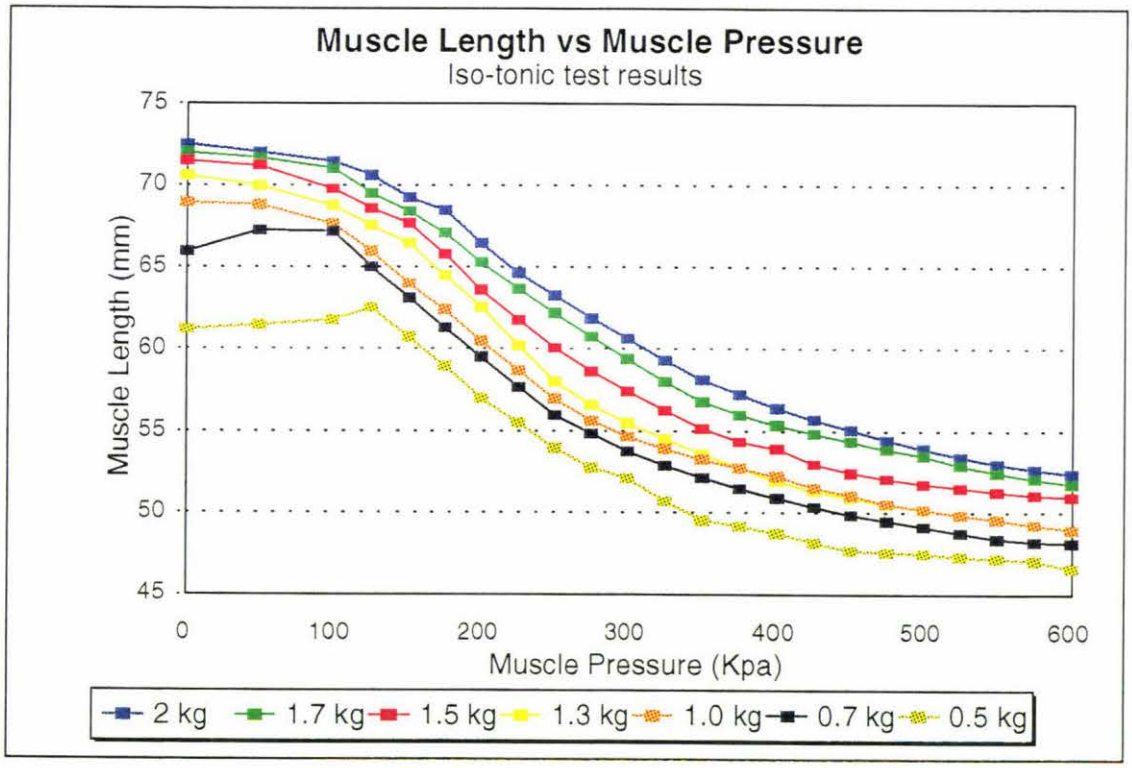


**Figure 4-13 Isotonic results.**

It would appear that in this region of curves, the relationship between pressure and muscle length is linear or quadratic or logarithmic and dependent on mass. These curves can be described as pressure, $P$ being a logarithmic or power function of muscle length, $L$ with a gradient coefficient, $K_P$ where the gradient coefficient is related to mass by a function $f(m)$.

**Generalised equations for the isotonic tests for pressures between 150kpa and 600kpa**

$$L \approx K_P \log(P) + c_5 \qquad \textbf{Equation 4-27}$$

$$L \approx K_P P^a + c \qquad \textbf{Equation 4-28}$$

$$K_P \approx f(m) \qquad \textbf{Equation 4-29}$$

where $L$ is muscle length
muscle pressure is $P$
$a$ could be 1 indicating a linear relationship or 2 indicating a quadratic relationship
$K_p$ is the gradient coefficient
$f(m)$ is a function relating mass ($m$) to $K_p$

In the 0-125kpa region it appears that for the two curves with the smallest masses, the muscle length increases with pressure. Three curves are shown in Figure 4-14. From inspection this region appears to be linear.

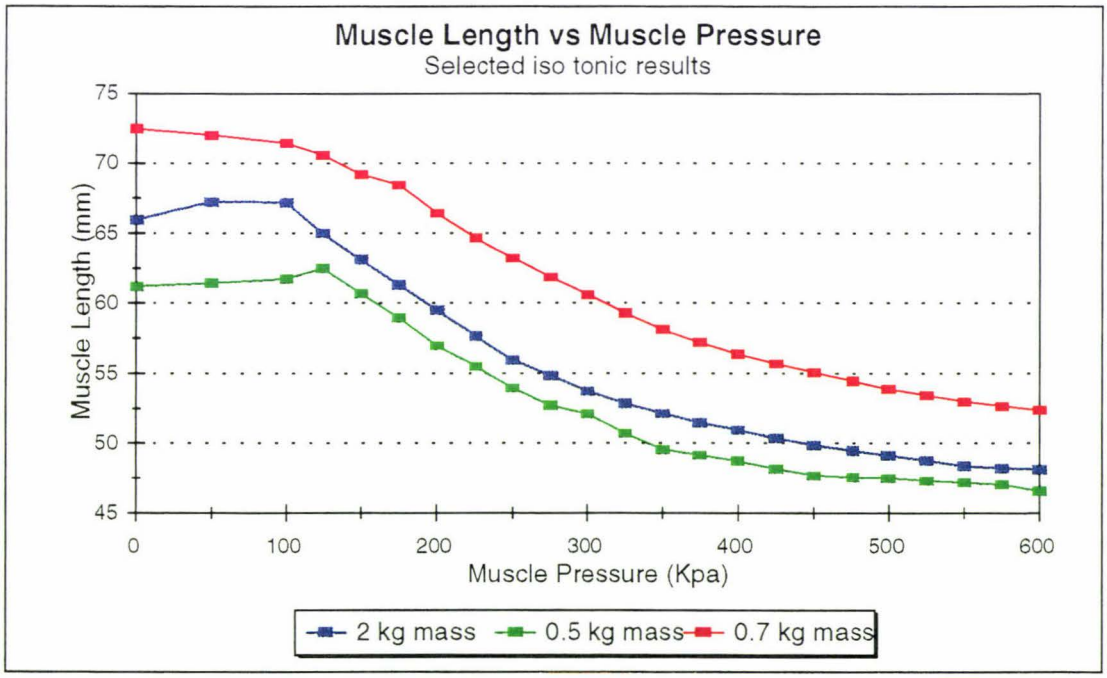


**Figure 4-14 Isotonic muscle length increase.**

### 4.8.4 Temperature Tests

The isothermal tests required the temperature to be kept constant while the isometric and isobaric tests were repeated.

The results of the isometric tests are shown in Figure 4-15 with the experimental data in Appendix C-1, Tables C1 and C2.

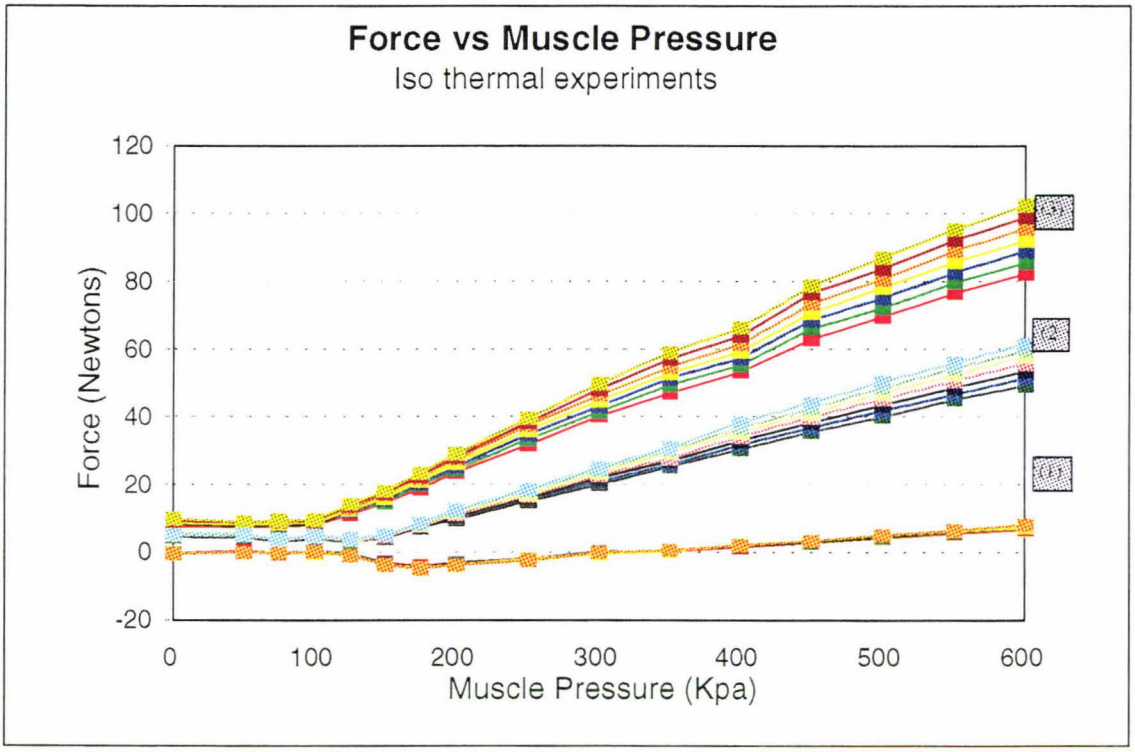


**Figure 4-15 Isothermal test results.**
(1) correspond to a temperature of 21°C and distances 53-59mm
(2) correspond to a temperature of 30°C and distances 53-59mm
(3) correspond to a temperature of 39°C and distances 53-59mm.

Each curve is representative of how the force changes when the pressure is increased while the distance is fixed (isometric) so variation within a group of curves is caused by the changes in distance. A new group of curves indicates the experiment repeated with a change in temperature. An increase in temperature causes the gradient of the force/pressure curve to increase. It is also noted, as before, the gradient increases with increasing muscle length.

**Generalised equation of the isothermal curves in the pressure range 150-600kpa from inspection**

$$Force = K_{P2}P^{a} + c_6 \qquad \textbf{Equation 4-30}$$

$$K_{P2} \approx f(L,T) \qquad \textbf{Equation 4-31}$$

*where* $K_{P2}$ is the pressure gradient coefficient
$P$ is the muscle pressure
$c_6$ is the intercept coefficient
$a$ is the constant indicating the linear (a=1) or quadratic (a=2) nature of the relationship.
$f(L,T)$ is the function relating muscle length $L$ and temperature $T$ to the pressure gradient coefficient $K_{P2}$

## 4.9 Black box Isometric Results

The next stage in the model construction using the black box approach was to analyse the results from the factorial experiment.

The force vs pressure tests were analysed to determine the type of relationship between pressure and force with the possibilities being $P$, $P^2$, $P^3$, $sin(P)$ and $cos(P)$. The numerical analysis was done using a regression analysis in the statistics package *Mini-tab* [57]. The most likely relationship was found to be linear for all the muscle length curves, Appendix C-2 Table C-8 shows the summarised best fits results.

This confirms the result in Equation 4-22 which was previously hypothesised.

**Generalised equation of the isometric curves in the pressure range 150-600kpa from inspection**

$$Force = K_{P2}P^{1} + c_2 \qquad \textbf{Equation 4-32}$$

$$K_{P2} \approx f(L) \qquad \textbf{Equation 4-33}$$

*where* $P$ is the pressure within the muscle
$c_2$ is the intercept coefficient
$K_{P2}$ is the pressure gradient coefficient and is dependent on muscle length ($L$)
$f(L)$ is the function relating muscle length $L$ to $K_{P2}$

### 4.9.1 Identification of the Relationship Between Muscle Length and the Pressure Gradient Coefficient

For each of the force pressure curves a regression was performed to see quantify the gradient and intercept coefficients ($K_{P2}$, $c_2$) for the functions specified in Equation 4-32

and Equation 4-33. The gradient and intercept coefficients are given in Appendix C-2 Table C-9.

The pressure gradient coefficient values were then plotted against the muscle length. This was done to investigate the nature of the relationship between the gradient coefficients and the muscle length, as suggested from inspection of the isometric graph, Figure 4-9, Equation 4-24.

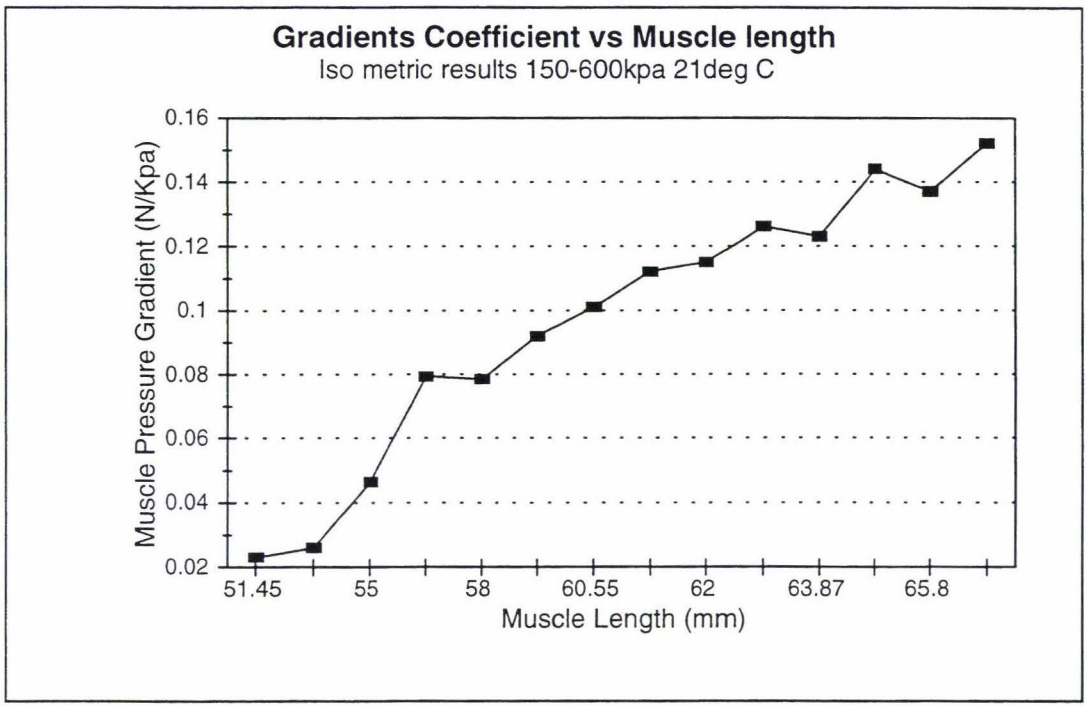


**Figure 4-16 Gradient coefficients vs distance.**

A best fit regression analysis was then done to identify the relationship between the pressure gradient coefficients and the distance. The relationships tested were $L$, $L^2$, $L^3$, and $\log(L)$. The results are shown in Appendix C-2 Table C-16 and C-17.

This numerical analysis indicates that the distance is linearly related to the pressure gradient coefficient in the isometric tests.

A full regression then was done to determine the parameters of this linear relationship. This quantifies Equation 4-33 as

**Quantified Pressure Gradient Coefficient Relationship**

$$K_{P2} = 0.0087\,L - 0.426 \qquad \textbf{Equation 4-34}$$

*where* $K_{P2}$ is the pressure gradient coefficient
$L$ is the muscle length

### 4.9.2 Identification of the Relationship Between Muscle Length and the Intercept Coefficient

The intercept coefficients of the regression equations for the isometric tests were then analysed using a bests sub-sets regression function; log and quadratic and linear relationships were tested. The intercepts were found to be linearly related to the muscle length.

The intercept coefficients were plotted against pressure, to visually express the relationship between pressure and the intercept coefficient, as shown in Figure 4-17.

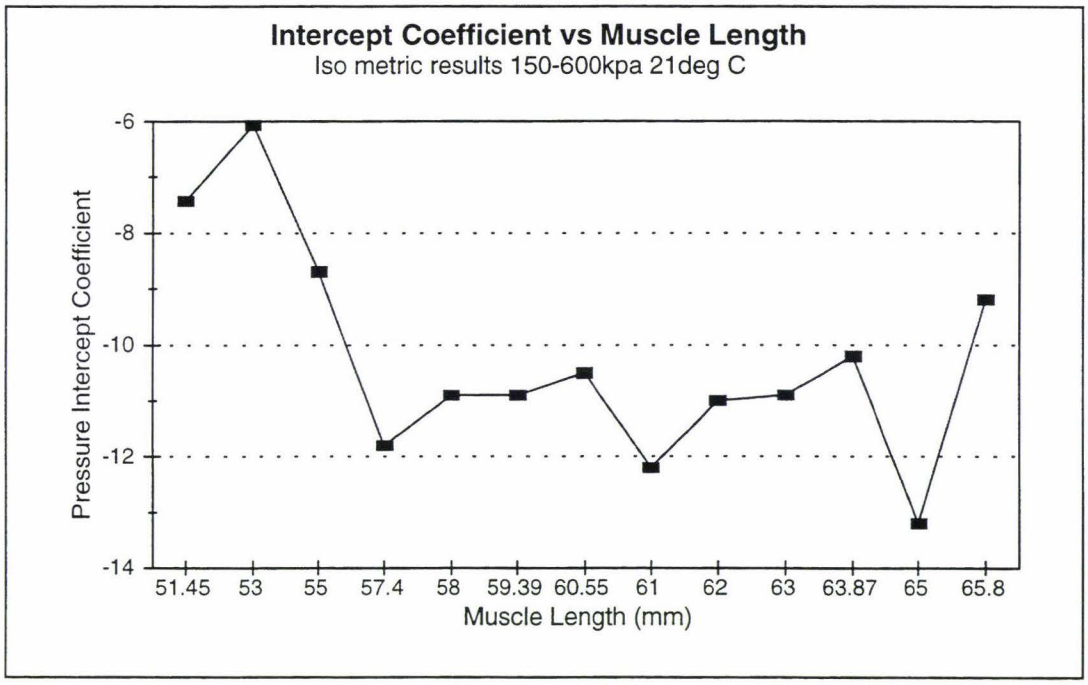


**Figure 4-17 Intercept coefficient vs muscle length.**

A full regression was then done to determine the parameters of the linear relationship between pressure and the distance intercept coefficient. This was found to be

**Quantified Muscle Length Coefficient**

$$c_2 = - 0.043 - 0..159\ L \qquad \textbf{Equation 4-35}$$

*where* $c_2$ is the pressure intercept coefficient
$L$ is the muscle length

Combining, Equation 4-32, Equation 4-34 and Equation 4-35 to produce an equation describing force, the final equation is

**Equation For Force Produced by Muscle 150-600kpa**

$$Force = 0.0087\,P\,L - 0.426\,P - 0.043\,L - 0.159 \qquad \textbf{Equation 4-36}$$

*where* $P$ is the pressure of the muscle
$L$ is the muscle length

### 4.9.3 0-125kpa Isometric Analysis

The analysis in sections 4.9 to 4.9.2 was then repeated for the 0-150kpa pressure region.

This required the analysis of the isometric tests. First the possible relationships between force and pressure were tested. The relationships tested were $P$, $P^2$, $sin(P)$ and $cos(P)$, the data is shown in Appendix C-2 Table C-19.

The most likely relationship was found to be linear. This confirms the result previously hypothesised in Equation 4-20.

**Generalised equation of the isometric curves in the pressure range 0-125kpa from inspection of the graph**

$$Force = K_{P1}P^1 + c \qquad \textbf{Equation 4-37}$$

$$c \approx f(L) \qquad \textbf{Equation 4-38}$$

*where* $P$ is the muscle pressure
$K_{P1}$ is the pressure gradient coefficient
$c$ is the intercept coefficient
$f(L)$ is the function relating muscle length $(L)$ to the intercept coefficient $c$

A regression using pressure as the predictor was then done for each muscle length curve. The pressure gradient coefficients and pressure intercept coefficients obtained from the least squares regression are shown in Appendix C-2 Table C-26.

Graphs of the pressure gradient and intercept coefficients vs muscle length are shown in Figure 4-18 and Figure 4-19 respectively. These indicate that the gradient coefficient is related to muscle length by a non-linear function, and the intercept coefficient appears to be linearly related to muscle length as seen in Figure 4-18.

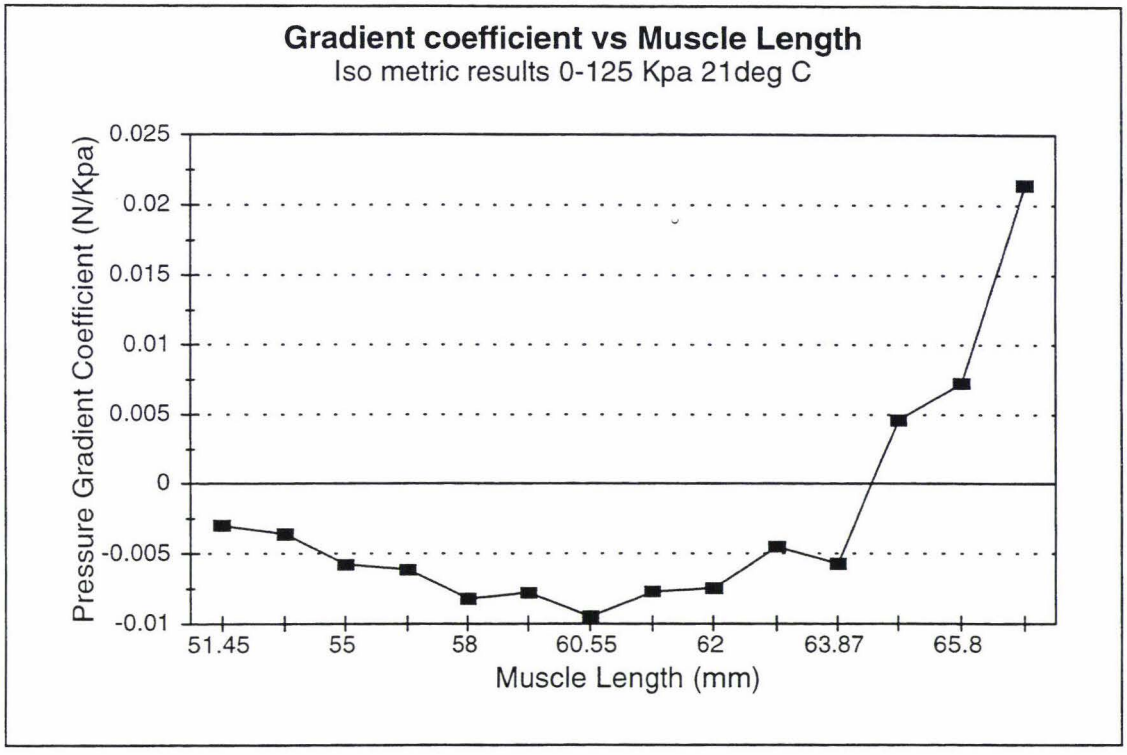


**Figure 4-18 Isometric pressure gradient coefficient vs distance, 0-125kpa.**

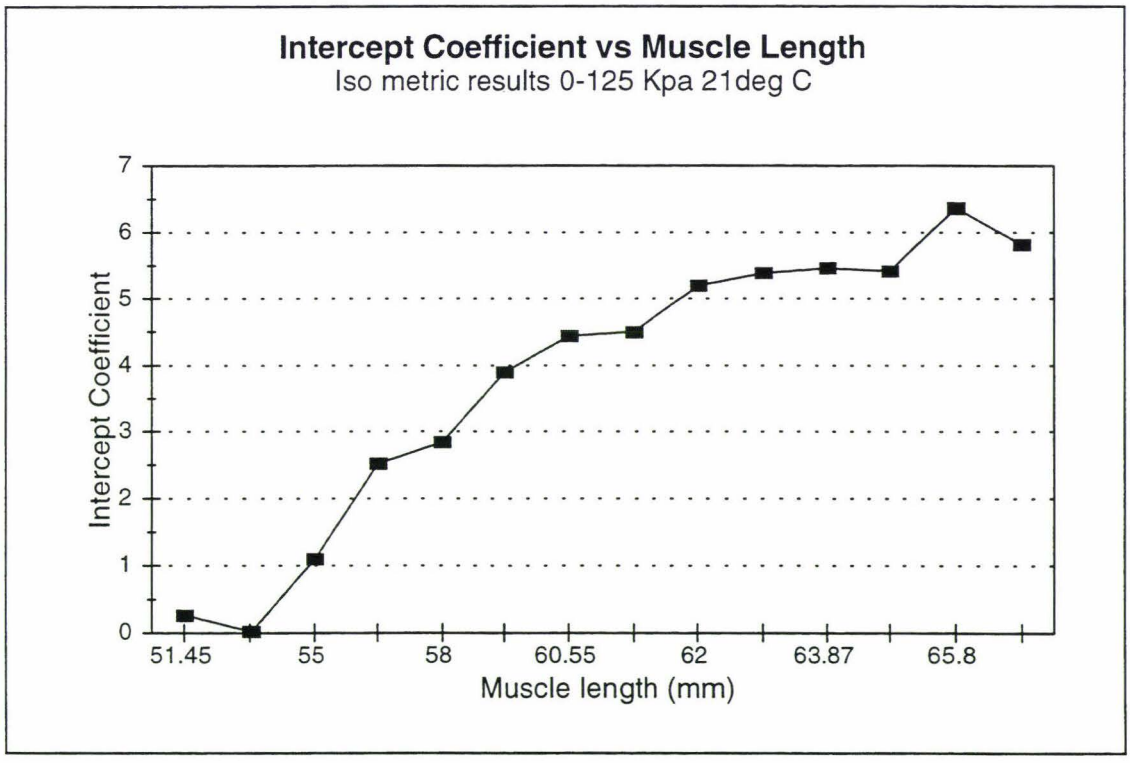


**Figure 4-19 Isometric pressure intercept coefficient vs distance, 0-125kpa.**

A best fits regression was done to identify a relationship between intercept coefficients and the muscle length. It was confirmed that the intercept was linearly related to the length, and the gradient was related to both the length and the length cubed. The best fit regression results are shown in Appendix C-2 Table C-33 and C-34.

A full regression was done to determine the parameters in the pressure intercept relationship. This was found to be

**Pressure Intercept Coefficient Equation 0-125kpa**

$$c = -20.4 + 0.400\,L$$ **Equation 4-39**

*where* $c$ is the pressure intercept coefficient
$L$ is the muscle length

Using distance and distance cubed as predictors, a full regression was done. The parameters in the pressure gradient equation were determined to be

**Pressure Gradient Coefficient Equation 0-125kpa**

$$K_{PI} = 0.625 - 0.0165\,L + 0.000002\,L^3$$ **Equation 4-40**

*where* $K_{PI}$ is the pressure gradient coefficient
$L$ is the muscle length

Combining Equation 4-37, Equation 4-39 and Equation 4-40 to produce an equation describing force, the final equation is

**Force Equation 0-125kpa**

$$Force = (0.62 - 0.0165\,L + 0.000002\,(L)^3)\,P + 0.400\,L - 20.4$$ **Equation 4-41**

*where* $L$ is the muscle length
$P$ is the muscle pressure

## 4.10 Black Box Isobaric Results

The next stage was the evaluation of the isobaric tests. For this each individual curve was analysed to determine which of the possible muscle length relationships, $L$, $L^2$, $\sin(L)$ and $\cos(L)$, best described it. The isobaric test results are shown in Figure 4-11.

Using the best subsets regression function it was found that for the higher pressure curves the most likely relationship between force and muscle length was linear, and for the lower pressure curves the relationship was quadratic. The best subsets regression results are shown in Appendix C-3 Table C-36.

From this it is not clear if the relation is $L$ or $L^2$, but $L$ was chosen as the most likely variable, as the majority of the curves had linear relationships. This confirms the equations obtained from inspection, Equation 4-35, Equation 4-36.

**Generalised Equation of the Isobaric Curves in the Pressure Range 150-600kpa from Inspection**

$$Force = K_{L2} L^1 + c_4 \qquad \textbf{Equation 4-42}$$

$$K_{L2} \approx f(P) \qquad \textbf{Equation 4-43}$$

*where* $K_{d2}$ is muscle length gradient coefficient
$L$ is the length
$f(P)$ is the function relating pressure $P$ to $K_{d2}$
$c_4$ is the intercept coefficient

### 4.10.1 Identification of the Relationship Between Pressure and the Distance Gradient Coefficient

A regression analysis was then performed to identify the muscle length gradient and intercept coefficients ($K_{L2}$,$c_4$) for the function specified in Equation 4-42 and Equation 4-43. The muscle length gradient and intercept coefficients are shown in Appendix C-3 Table C-37. The muscle length gradient coefficient values were plotted against the pressure, shown in Figure 4-20.

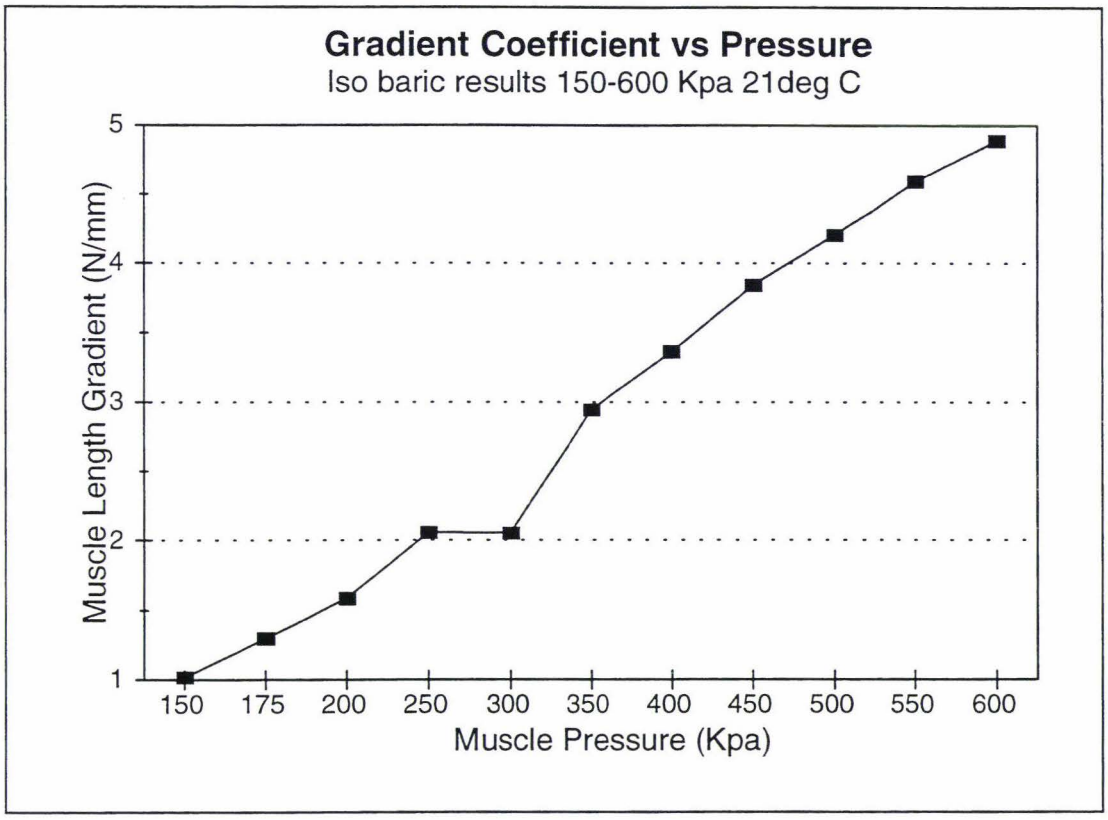


**Figure 4-20 Distance gradient vs pressure.**

From inspection there appears to be a linear relationship between the muscle length gradient coefficient and pressure. A best fits regression analysis was then done to identify the relationship between the gradient coefficient and pressure. The functions which were used were in this analysis were a $P$, $P^2$ and $\log(P)$.

This numerical analysis shown in Appendix C-3 Best-fit C-10, indicates that the pressure is linearly related to the muscle length gradient.

A full regression then was done to determine the parameters of this linear relationship. This was found to be

**Quantified Muscle Length Gradient Coefficient**

$$K_{L2} = 0.00878\,P - 0.231 \qquad \textbf{Equation 4-44}$$

*where* $K_{L2}$ is the pressure gradient coefficient
$P$ is the muscle pressure

### 4.10.2 Intercept Coefficient Identification

The intercept coefficients of the regression equations for the isobaric tests were then analysed using a bests sub-sets regression function; log and quadratic and linear relationships were tested. The intercepts were found to be linearly related to pressure as shown in Appendix C-3 Best-fit C-11.

The distance intercept coefficients were plotted against pressure, to visually express the relationship between pressure and the distance intercept coefficient.

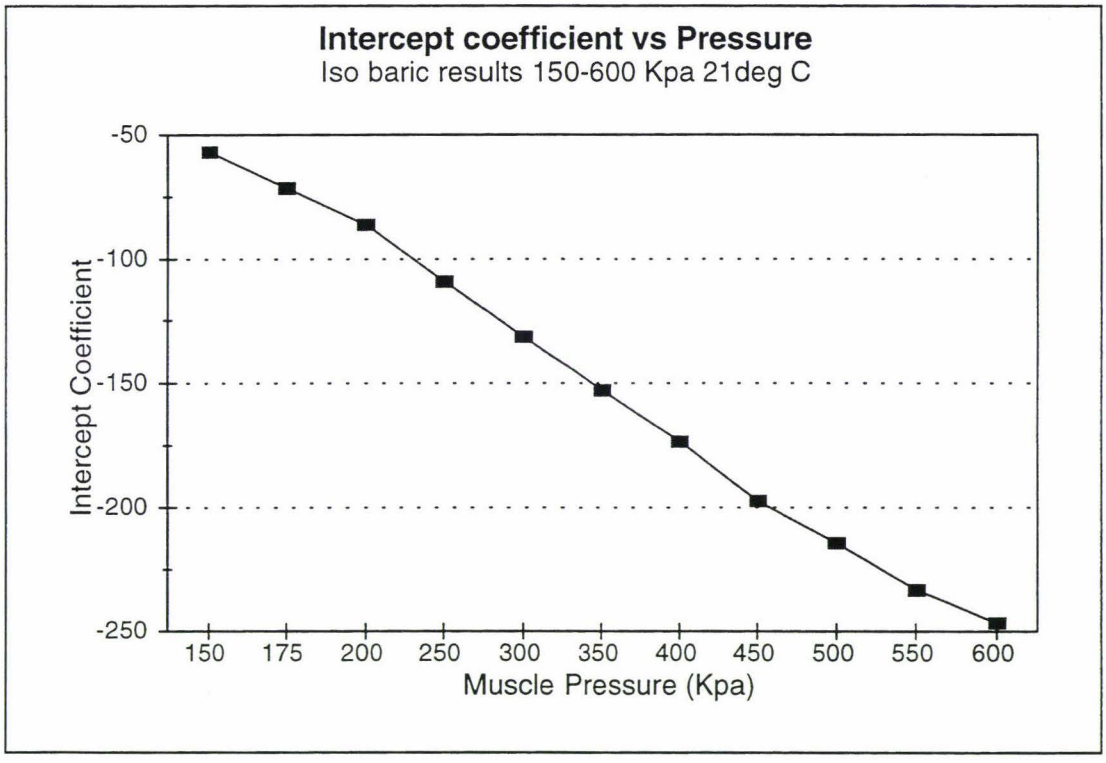


**Figure 4-21 Intercept coefficient vs pressure.**

A full regression was then done to determine the parameters of the linear relationship between pressure and the distance intercept coefficient. This was found to be

**Quantified Muscle Length Coefficient**

$$c_4 = -0.38 - 0.425\,P \qquad \textbf{Equation 4-45}$$

*where* $c_4$ is the muscle length intercept coefficient
$P$ is the pressure

### 4.10.3 Black Box Model of the Muscles Behaviour 0-600kpa

Regression analysis was not undertaken on the data from the isotonic test data as the models produced from the isobaric and isometric test data provided reasonable accounts of the pneumatic muscles behaviour.

The results of the black box approach were used to produce Equation 4-36 and Equation 4-41 given below. The use of the isobaric test results Equation 4-42, Equation 4-44 and Equation 4-45 produced equations with similar parameters to the equations obtained from the isometric test results. It was decided that the results obtained from the isometric tests would be used to form the model of the muscles behaviour with the isobaric tests used as a replicate set of measurements.

**Equations describing the muscles behaviour over 0-600kpa**

$Force = 0.0087\,P\,L - 0.426\,P - 0.159\,L - 0.043$ **Equation 4-36**
if 125>Pressure>600

$Force = (0.62 - 0.0165\,L + 0.000002\,(L)^3)\,P + 0.400\,L - 20.4$ **Equation 4-41**
if Pressure<125

## 4.11 Temperature Effects

### 4.11.1 Regression Analysis 150kpa to 600kpa

These isometric and isobaric experiments were then repeated at fixed temperatures. A set of isometric and isobaric results pertaining to a unique temperature were produced. At each temperature a regression analysis was undertaken, following the procedures used in section 4.9, an equation relating force to pressure and muscle length, for each temperature was produced. Each equation had four terms and was of the form specified in Equation 4-46, which contained gradient and intercept coefficients, the regression results used are shown in Appendix C-2 Tables C-9 to C-18.

**Form of the Force Equation**

$$Force = K_1 L^3 P + K_2 LP + K_3 P + K_4 L + c$$ **Equation 4-46**

*where* $K_1$ is the pressure muscle length gradient coefficient
$K_2$ is the pressure gradient coefficient
$K_3$ is the muscle length gradient coefficient
$c$ is the intercept coefficient

The gradient and intercept coefficients for Equation 4-46, are presented in Table 4-1, with the temperature the tests were conducted at.

| Temp\Coefficient type | muscle length pressure gradient ($K_1$) | muscle length gradient ($K_2$) | pressure gradient ($K_3$) | intercept (c) |
|---|---|---|---|---|
| 21 | 0.0086 | -0.159 | -0.426 | -0.43 |
| 24 | 0.0089 | -0.143 | -0.439 | -1.78 |
| 27 | 0.0093 | -0.176 | -0.461 | -0.09 |
| 30 | 0.0102 | -0.221 | -0.501 | 1.86 |
| 33 | 0.0101 | -0.177 | -0.494 | -0.95 |
| 36 | 0.0105 | -0.211 | -0.513 | 0.54 |
| 39 | 0.0108 | -0.203 | -0.531 | -0.29 |

**Table 4-1 Isothermal gradient and intercept coefficients 150-600kpa**

The pressure muscle length gradient coefficient is plotted against temperature in Figure 4-22. This graph indicates a linear relationship between temperature and gradient coefficient.

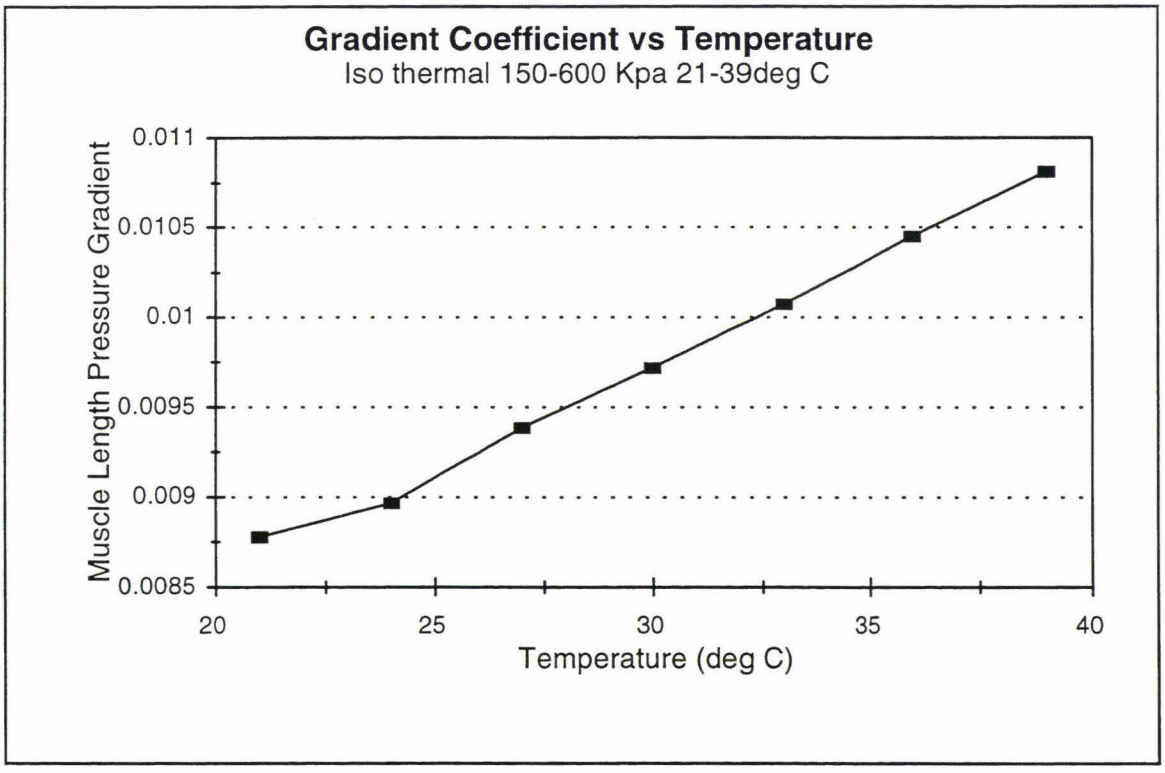


**Figure 4-22 Muscle length pressure gradient coefficient vs temperature.**

It was confirmed using a best fits regression analysis, shown in Appendix C-2 Best-fit C-1, that the temperature was linearly related to the muscle length pressure gradient. A full regression was to determine the parameters in the linear relationship. This was found to be

**Relationship Between Muscle Length Pressure Gradient and Temperature**

$$K_1 = 0.00012T + 0.0062 \qquad \textbf{Equation 4-47}$$

*where* $K_1$ is the muscle length pressure gradient coefficient
$T$ is the temperature

The muscle length gradient coefficient is plotted against temperature, Figure 4-23. This graph indicated that there was little relationship between temperature and the muscle length gradient coefficient. The best fits regression also indicated that there was little relationship in the data. The best fits regression results are shown in Appendix C-2 Best-fits C-2. A mean value was used to describe changes in the muscle length gradient coefficients. This is shown in Equation 4-48.

**Muscle Length Gradient Coefficients**

$$K_2 = -0.18429 \qquad \textbf{Equation 4-48}$$

*where* $K_2$ is the muscle length gradient coefficient.

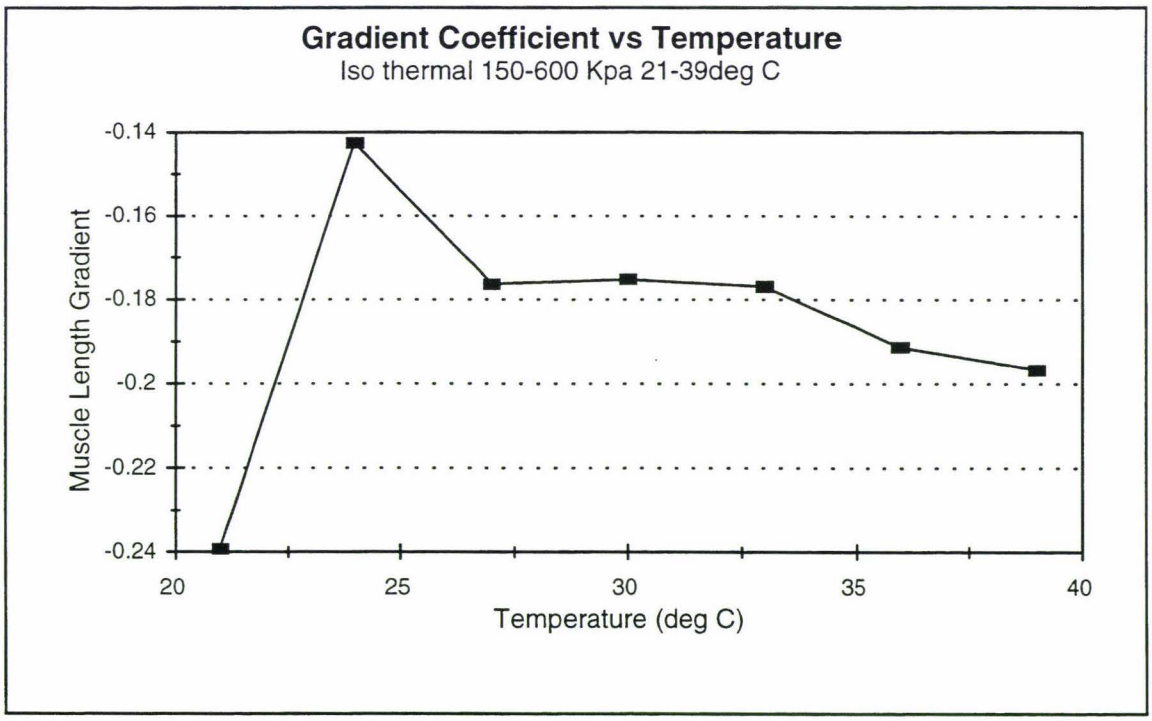


**Figure 4-23 Muscle length gradient coefficient vs temperature.**

The muscle length gradient coefficient is plotted against temperature, Figure 4-24. This graph indicated a linear relationship between temperature and the pressure gradient coefficient. The best fits regression confirmed the linear relationship. The best fits regression results are shown in Appendix C-2 Best-fits C-3. A full regression was to determine the parameters in the linear relationship. This was found to be

**Relationship Between Muscle Pressure Gradient and Temperature**

$$K_3 = -0.0058T - 0.3 \qquad \textbf{Equation 4-49}$$

*where* $K_3$ is the pressure gradient coefficient
$T$ is the temperature

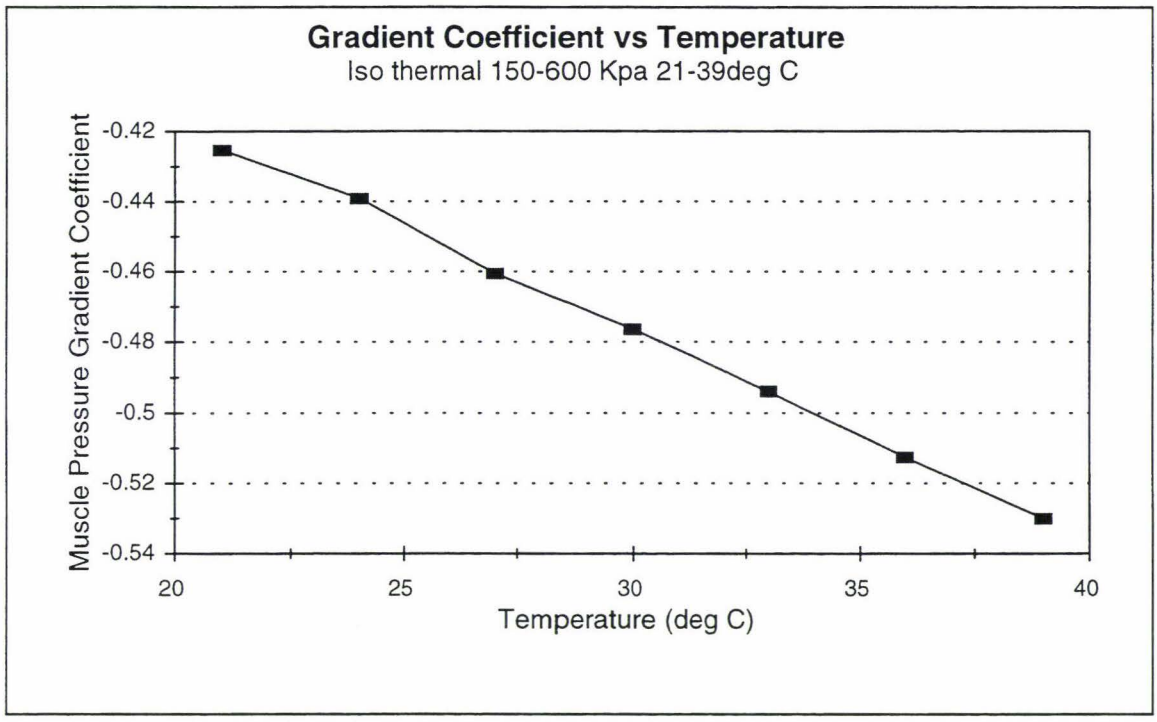


**Figure 4-24 Intercept gradient coefficient vs temperature.**

The intercept coefficient is plotted against temperature, Figure 4-25. This graph indicated that there was little relationship between temperature and the intercept coefficient. The best fits regression also indicated that there was little relationship in the data. The best fits regression results are shown in Appendix C-2 Best-fits C-4. A mean value was used to describe changes in the muscle length gradient coefficients. This is shown in Equation 4-50.

**Intercept Coefficient**

$c = -0.16286$ **Equation 4-50**

*where* $c$ is the intercept coefficient.

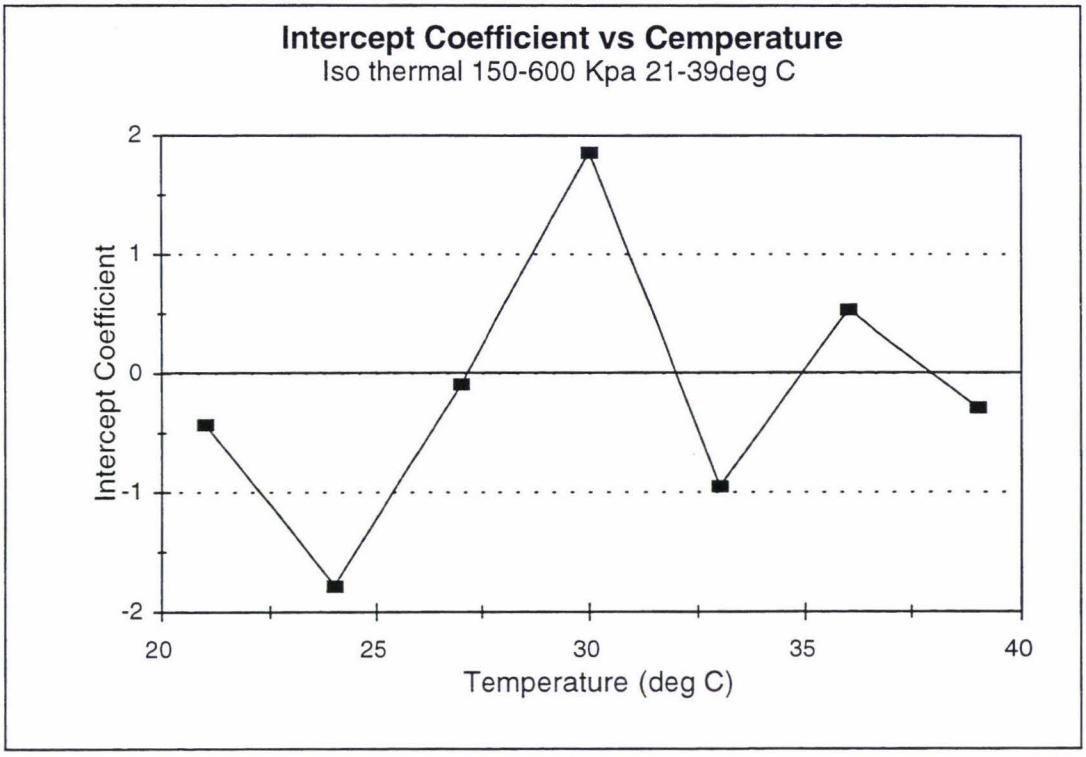


**Figure 4-25 intercept coefficient vs temperature.**

Combining Equation 4-46 to Equation 4-50, an equation describing force is produced, this is

**Force Equation with Pressure, Muscle Length and Temperature as Predictors**

$$Force = [0.00012(T) + 0.0062]\,PL - 0.18429\,L + [-0.0058(T) - 0.300]P - 0.16286$$ **Equation 4-51**

*where* $P$ is the muscle pressure
$L$ is the muscle length
$T$ is the temperature

### 4.11.2 Temperature Effects 0-125kpa Region

The linear region was analysed, isometric and isobaric tests were repeated at fixed temperatures. At each temperature a regression analysis was undertaken, following the procedures used in section 4.10.4, an equation relating force to pressure and muscle length, for each temperature was produced. Each equation had six terms and was of the form specified in Equation 4-52, which contains gradient and intercept coefficients, the regression results used are shown in Appendix C-2 Tables C-19 to C-35.

**Force Equation Form 0-125kpa**

$$Force = K_1 L^3 P + K_2 LP + K_3 P + K_4 L + c \qquad \textbf{Equation 4-52}$$

*where* $K_1$ is the pressure muscle length cubed gradient coefficient
is the muscle length pressure gradient coefficient
$K_3$ is the pressure gradient coefficient
$K_4$ is the muscle length gradient coefficient
$c$ is the intercept coefficient

The gradient and intercept coefficients for Equation 4-52, are presented Table 4-2, with the temperature the tests were conducted at.

| Temp\ Coefficient type | Pressure muscle length cubed gradient coefficient ($K_1$) | Pressure muscle length gradient coefficient ($K_2$) | Pressure gradient coefficient ($K_3$) | Muscle length gradient coefficient ($K_4$) | intercept coefficient ($c$) |
|---|---|---|---|---|---|
| 21 | 0.00000164 | -0.016488 | 0.6250 | 0.40029 | -20.429 |
| 24 | 0.00000158 | -0.016100 | 0.6151 | 0.46120 | -23.891 |
| 27 | 0.00000161 | -0.016175 | 0.6147 | 0.47898 | -24.797 |
| 30 | 0.00000193 | -0.019331 | 0.7331 | 0.47788 | -24.671 |
| 33 | 0.00000196 | -0.019707 | 0.7492 | 0.51017 | -26.384 |
| 36 | 0.00000203 | -0.020492 | 0.7804 | 0.52730 | -27.321 |
| 39 | 0.00000197 | -0.019754 | 0.7499 | 0.55010 | -28.506 |

**Table 4-2 Isothermal gradient and intercept coefficients 0-125kpa.**

A plot of the pressure muscle length cubed coefficient vs temperature reveals a linear relationship as shown in Figure 4-26.

It was confirmed using a best fits regression analysis, shown in Appendix C-2 Best-fit C-5, that the temperature was linearly related to the pressure muscle length cubed gradient coefficient. A full regression was to determine the parameters in the linear relationship. This was found to be

**Pressure Muscle Length Cubed Gradient Coefficient**

$$K_1 = 0.00000003T + 0.000001$$ **Equation 4-53**

*where* $K_1$ is the pressure muscle length cubed gradient coefficient
$T$ is the temperature

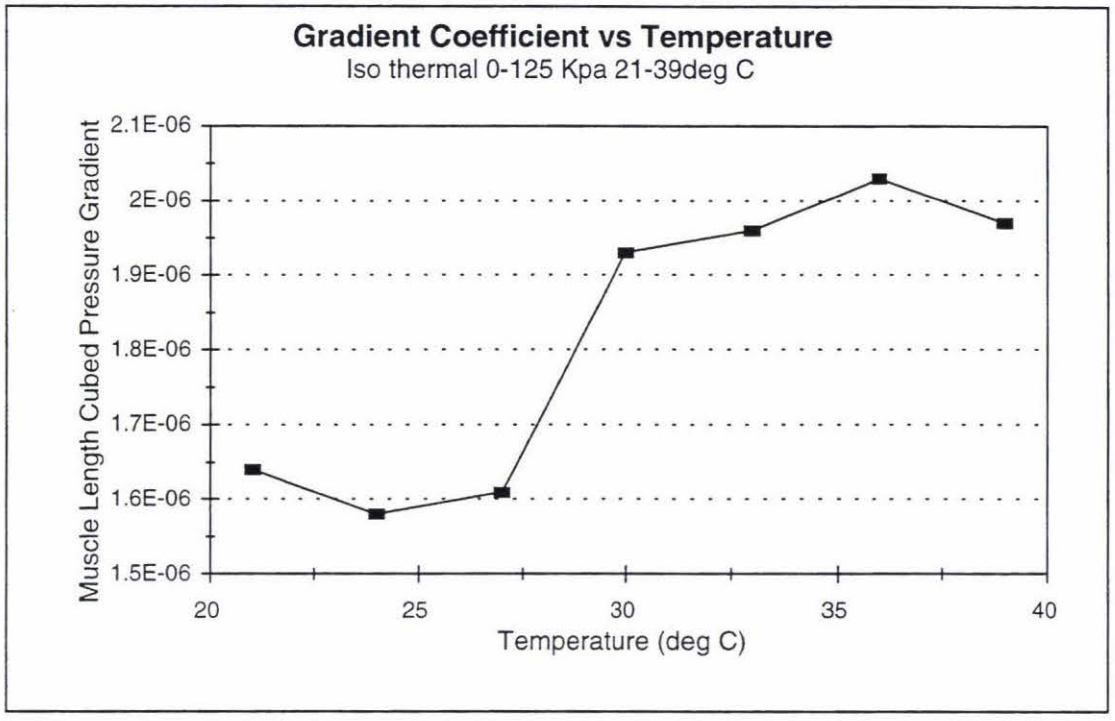


**Figure 4-26 Distance cubed gradient coefficient vs temperature.**

A plot of the pressure muscle length gradient coefficient vs temperature reveals a linear relationship, Figure 4-27.

It was confirmed using a best fits regression analysis, shown in Appendix C-2 Best-fit C-6, that the temperature was linearly related to the pressure muscle length gradient coefficient. A full regression was to determine the parameters in the linear relationship. This was found to be

**Pressure Muscle Length Gradient Coefficient**

$$K_2 = -0.000263\,T - 0.01041$$ **Equation 4-54**

*where* $K_2$ is the pressure muscle length gradient coefficient
$T$ is the temperature

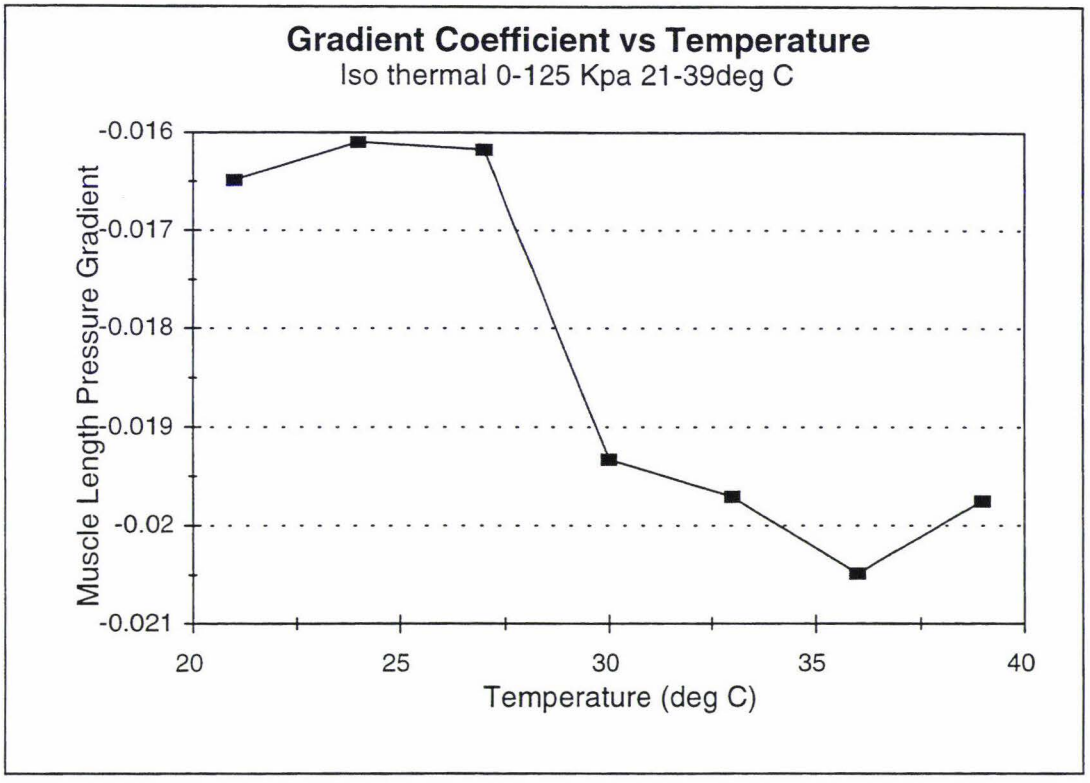


**Figure 4-27 Pressure muscle length gradient coefficient vs temperature.**

A plot of the pressure gradient coefficient vs temperature reveals a linear relationship, Figure 4-28.

It was confirmed using a best fits regression analysis, shown in Appendix C-2 Best-fit C-7, that the temperature was linearly related to the pressure gradient. A full regression was to determine the parameters in the linear relationship. This was found to be

**Pressure Gradient Coefficient**

$$K_3 = 0.395T + 0.01 \qquad \textbf{Equation 4-55}$$

*where* $K_3$ is the pressure gradient coefficient
$T$ is the temperature

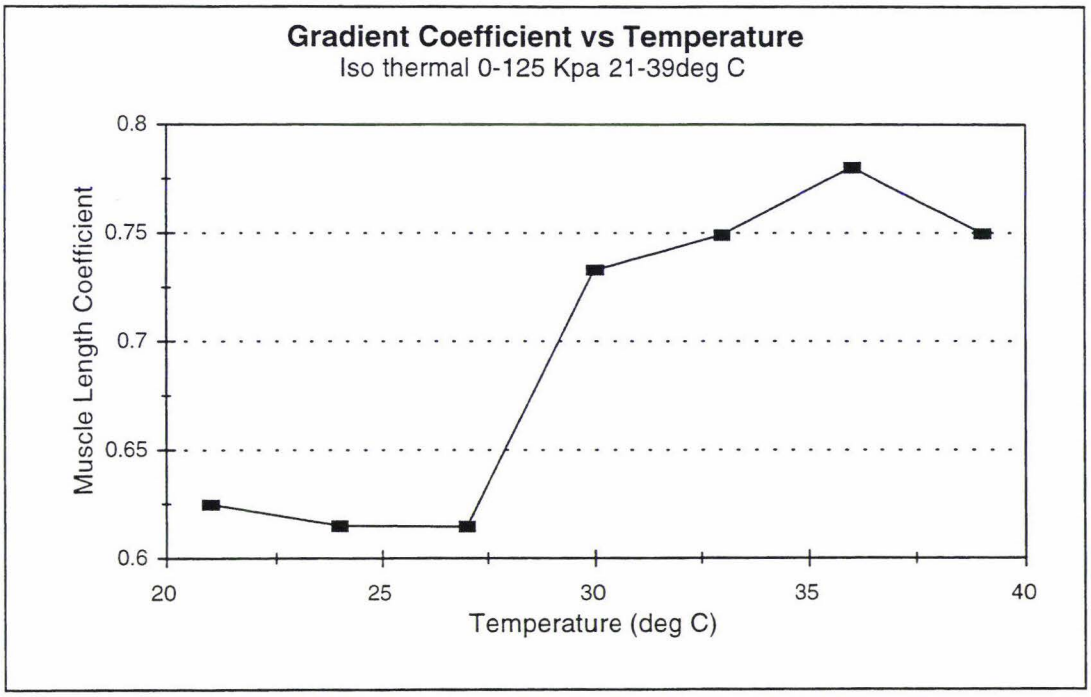


**Figure 4-28 Pressure gradient coefficient vs temperature.**

A plot of the muscle length gradient coefficient vs temperature reveals a linear relationship, Figure 4-29.

It was confirmed using a best fits regression analysis, shown in Appendix C-2 Best-fit C-8, that the temperature was linearly related to the muscle length gradient. A full regression was to determine the parameters in the linear relationship. This was found to be

**Muscle Length Gradient Coefficient**

$$K_2 = 0.00730T + 0.268 \qquad \textbf{Equation 4-56}$$

*where* $K_4$ is the muscle length gradient coefficient
$T$ is the temperature

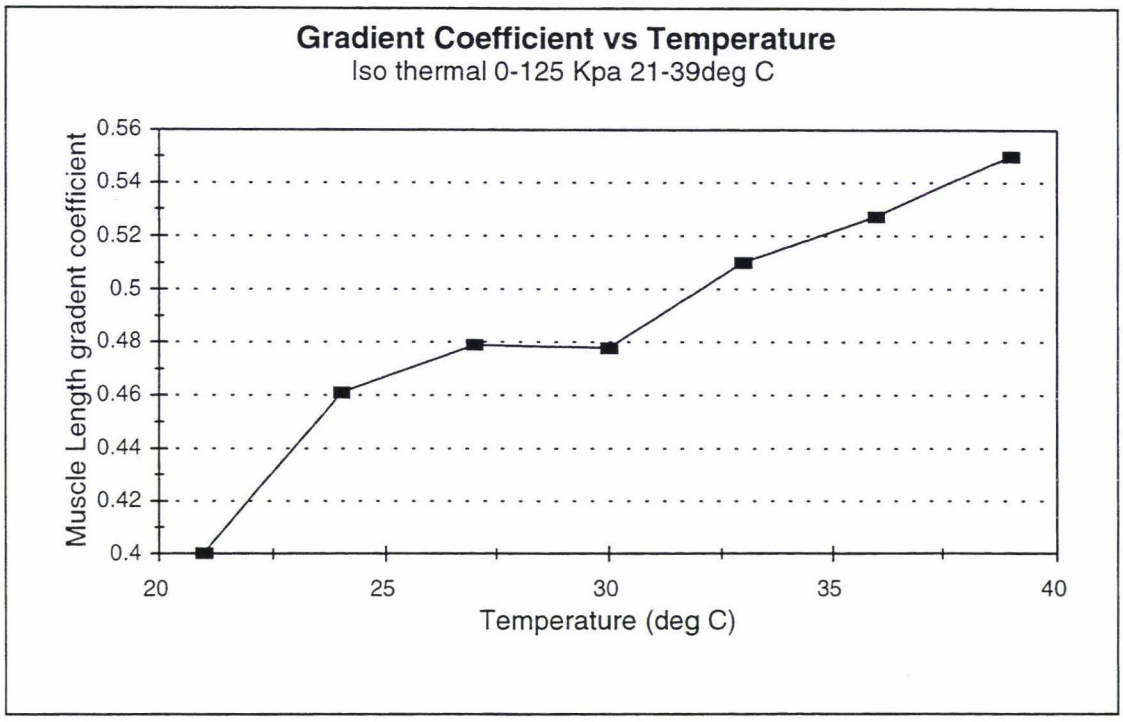


**Figure 4-29 Muscle length gradient coefficient vs temperature.**

A plot of the intercept coefficient vs temperature reveals a linear relationship, Figure 4-30.

It was confirmed using a best fits regression analysis, shown in Appendix C-2 Best-fit C-9, that the temperature was linearly related to the intercept coefficient. A full regression was to determine the parameters in the linear relationship. This was found to be

**Intercept Coefficient**

$$c = -0.389T - 13.5$$ **Equation 4-57**

*where* $c$ is the intercept coefficient
$T$ is the temperature

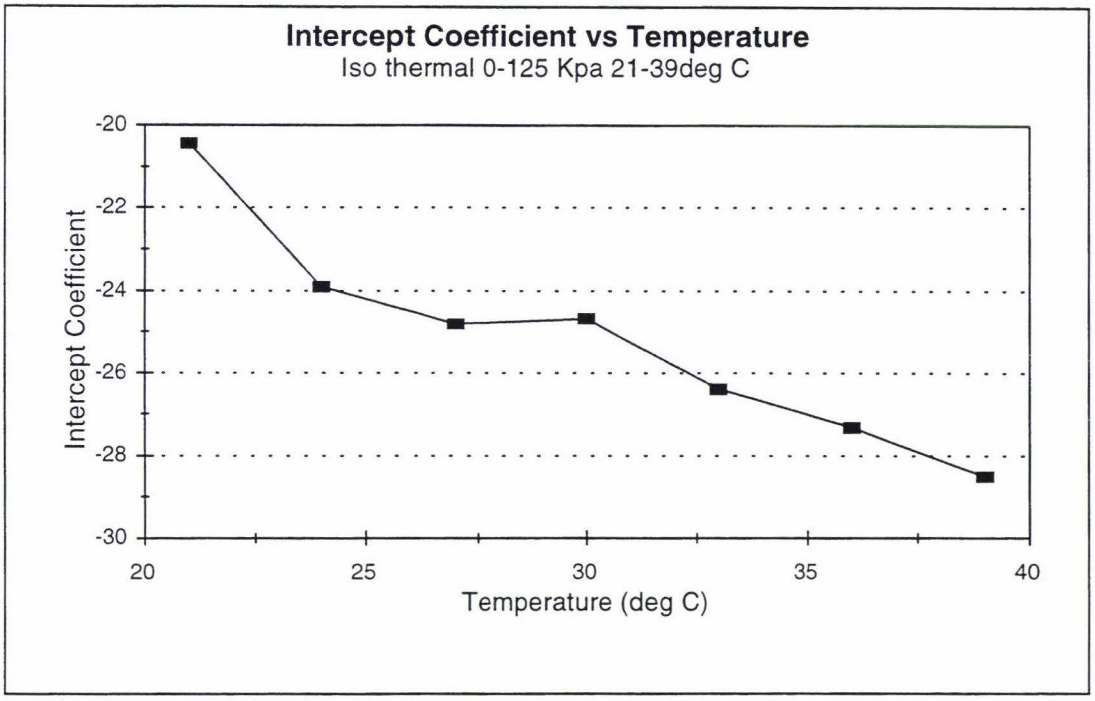


**Figure 4-30 intercept coefficient vs temperature.**

The results in Equation 4-52 to Equation 4-57 were then used to form the final equation, shown below

**Force Equation Using Pressure, Muscle Length and Temperature as Predictors for 0-125kpa**

$$Force = \left[(0.000001 + 0.00000003\,T)\,L^3 + (-0.01 - 0.00026\,T)\,L + 0.39 + 0.01\,T\right] P + \left[0.268 + 0.0073\,T\right] L - 0.38\,T - 13.5 \qquad \textbf{Equation 4-58}$$

*where* $P$ is the muscle pressure
$L$ is the muscle length
$T$ is the temperature

# 4.12 Observations of Factors Affecting the Muscle for Quasi-static Model Development

## 4.12.1 Expansion of the Inner Liner

It was noted that there were two distinct operating regions refer section 4-8.

Under close observation, this was found to be due to a space between the inner liner and the outside tubing. It was found that the muscle does not contract until the inner tubing fully expands to remove the vacant space between the inner and outside liner, Figure 4-31.

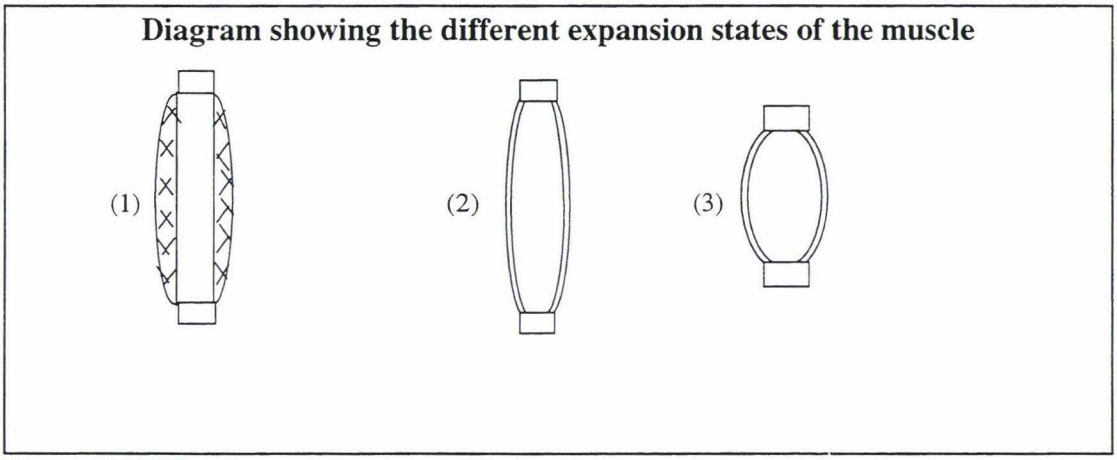


**Figure 4-31 Different expansion states of the muscle.**
The transition form state (1) to state (2) is in the 0-150kpa region. Here the inner liner is expanding to remove vacant space between itself and the outer sheath. There is very little force applied by the muscle. State (3) is in the 150-600kpa region where any expansion of the inner liner results in a contraction.

## 4.12.2 Non-linearity's Reaching a Point where it will No-longer Expand or Contract

The physical properties of the material from which the muscle is constructed from place limitations on the amount of expansion or contraction that can take place.

Once the elastic limit of the muscle has been reached, it can no longer be stretched any further.

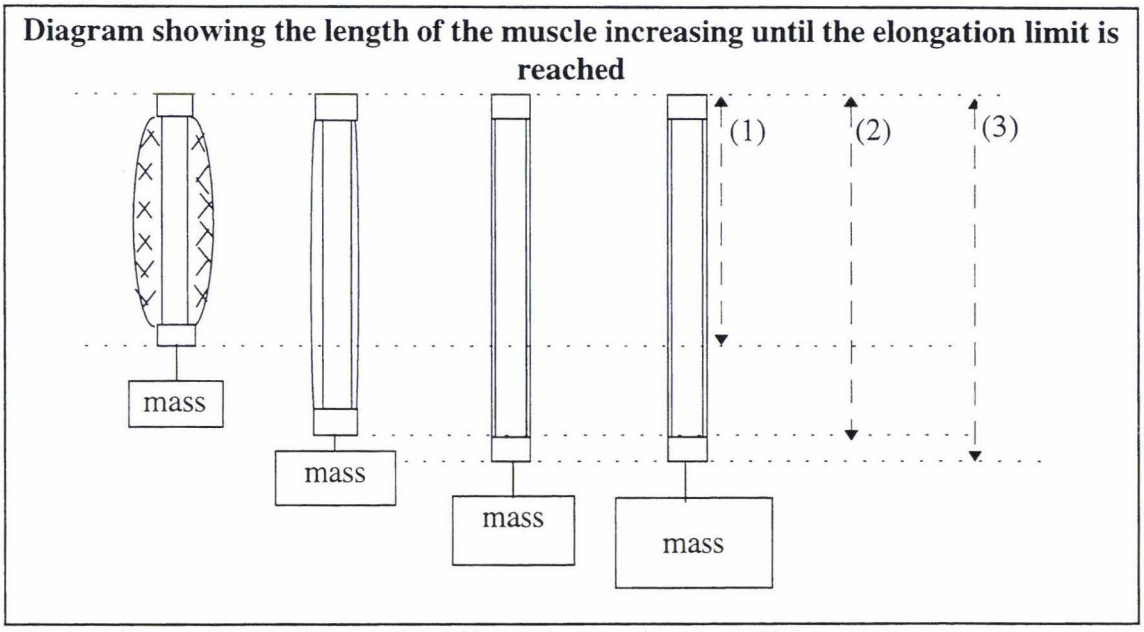


**Figure 4-32 muscle elongation with small mass and contraction with larger masses.**

1. Insufficient mass is applied to the muscle to reach the elongation limit
2. More mass is applied to the muscle but this is still insufficient to reach the elongation limit
3. Sufficient mass is applied to the muscle to cause the muscle to reach the elongation limit. Further increases in mass cause little or no elongation.

At this point the muscle will not act as an elastic system but will act like a piece of string. Any increases in mass will result in no further elongation. This region is characterised by excessive amounts of downward force being required to produce small amounts of elongation as the elastic limit is approached. The elastic limit is characterised as an asymptote where no further elongation can take place in response to increases in force as shown in Figure 4-33.

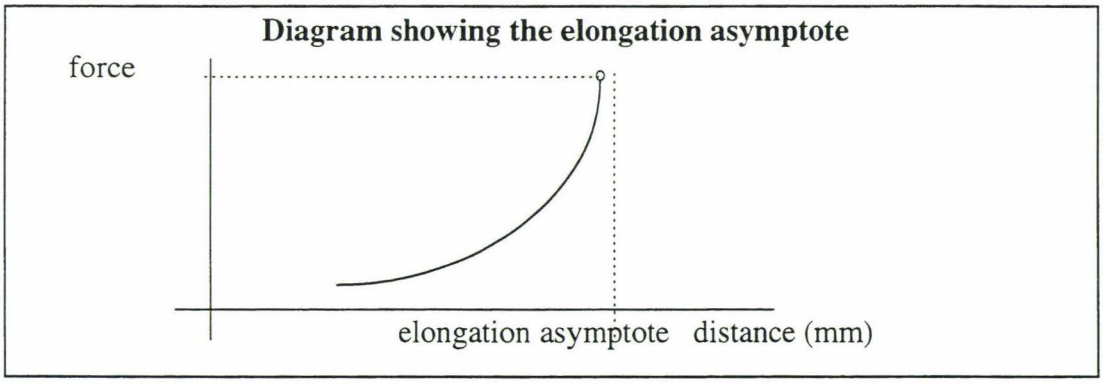


**Figure 4-33 Muscle elongation asymptote.**

Further increases in force from this point will eventually break the muscle as its yield point is reached.

At the other extreme, a compression force applied to the pneumatic muscle will cause a contraction to take place. The length of the muscle shortens until a minimum distance is reached. At this point the muscle will not contract any further.

The muscle will no longer behave like an elastic system but will behave like a piece of solid material. The limit is characterised as an asymptote where no further contraction can take place with increases in contraction force. As the elastic limit is approached excessive amounts of compressive force are required to produce small amounts of length reduction in the muscle as seen in Figure 4-34.

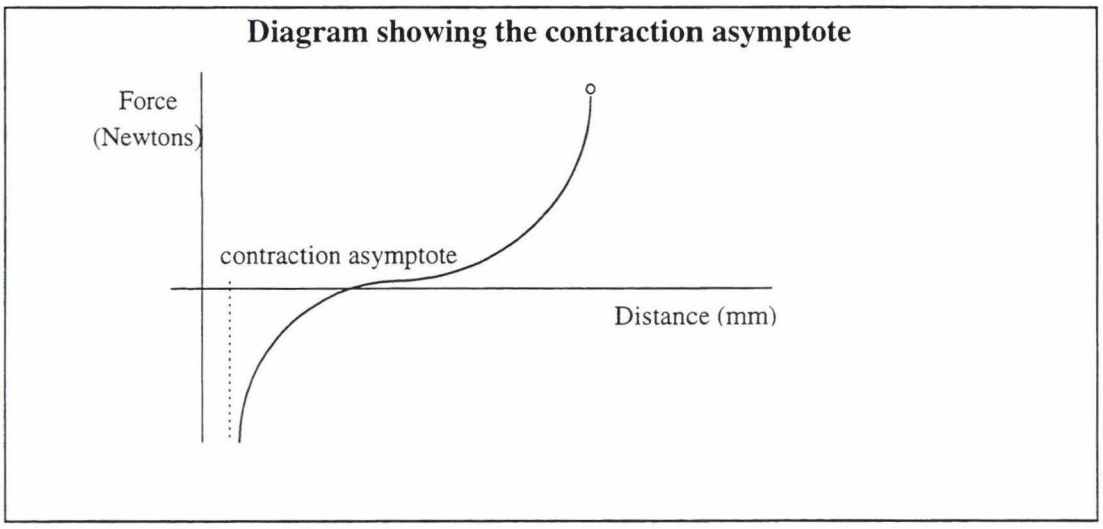


**Figure 4-34 Muscle contraction asymptote.**

### 4.12.3 Weaknesses in Empirical Model with Non-linearity's

The empirical models derived do not take the above non-linearity's into account. Fortunately these non-linearity's are outside the usual region of operation and will not be encountered. Attempts to model these non-linearity's by statistical methods also proved difficult as this required destructive testing. Only a limited number of muscles were available and these were considered too valuable to be used for destructive testing.

# 4.13 Development of a New Quasi-Static Model

### 4.13.1 Behaviour within the 0-125kpa Region

Before the inner liner expands and reaches the outer liner, the pneumatic muscle is thought to behave in a fashion similar to a rubber bladder being expanded. When a rubber bladder is pressurised it expands and elongates about its length, this was observed in the muscle. In a rubber bladder the force exerted is thought to be linearly related to the pressure and the muscle length. In a system where there is no length changes, the force exerted by a rubber bladder can be described by

**Force exerted by a rubber bladder with no length change**

$$Force = K_B P \qquad \textbf{Equation 4-59}$$

*where* $K_B$ is the force constant
$P$ is the muscle pressure.

As the rubber bladder is an elastic system increases in length are known to be proportional to the increase in contraction force exerted by the elastic. This can be described by

**Force exerted by a rubber bladder with no pressure change**

$$Force = -K_E L \qquad \textbf{Equation 4-60}$$

*where* $K_E$ is the force constant
$L$ is the muscle length.

The non-linearity's due to the muscle reaching a point where it will no longer contract are described by a non linear function.

**Behaviour in the non-linear contraction region**

$$Force = -nl(L,P) \qquad \textbf{Equation 4-61}$$

*where nl* is a non-linear function.

Combining Equation 4-59 to Equation 4-61 we produce the quasi-static model for the muscles operation in the 0-125kpa region, this model was optimised using the isometric

**Quasi-static model for pressure 0-125kpa**

$$Force = K_B(P) - K_E(L) + nl(L,P) \qquad \textbf{Equation 4-62}$$

test data Appendix C-1 Table C1, Appendix C-4 Full-regression C-8.

### 4.13.2 Behaviour within the 150-600kpa Region

The quasi-static model for the behaviour in the 150-600kpa region comprises of three separate sub-models. The first is an active model which describes the main operating region, an assumption is made that the muscle will operate in a manner similar to that of a pneumatic cylinder. The second is a passive model which acts as an offset and accounts for the behaviour of the inner liner. The final part is the non-linear model. This model is included to describe the muscles behaviour at its elastic limits. These three models are illustrated in Figure 4-35. This model was optimised using the isometric test data Appendix C-1 Table C1, Appendix C-4 Full-regression C-9.

1. $F = K_d P L$ — This is the form of the equation for a pneumatic cylinder, where $K_d$ is an equality constant.

2. $F = K_p (P\text{-}Pth)$ — This is the intercept term is included as cylinder assumption is only valid at pressures above 175kpa.

3. $F = nl(P)$ — A non-linear term is added to account for the asymptotic behaviour at the muscles operational limits

4. $F = K_d P L + K_p(P\text{-}Pth) + nl(P)$ — Combination of the three models

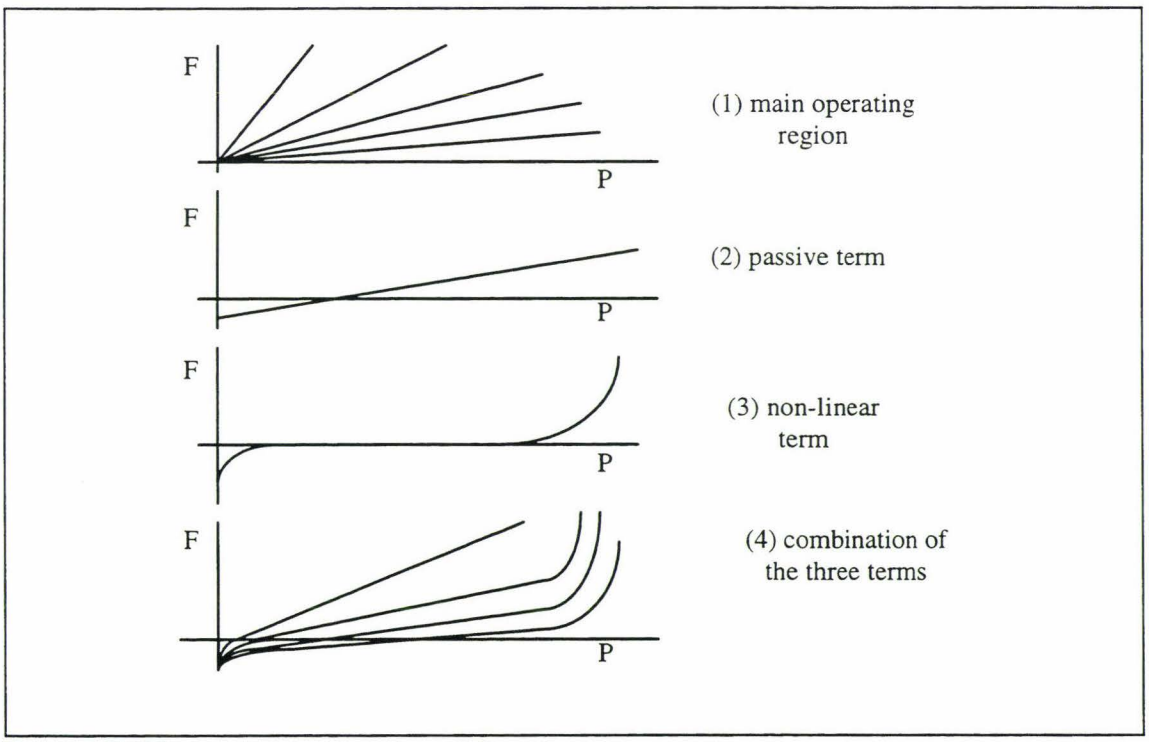


**Figure 4-35 Diagrams of quasi-static models.**

## 4.14 Comparison of the Different Models Used

From inspection of the experimental data, it was clear that the pneumatic muscle had two regions of operation. Neither the Caldwell model [39] nor the deterministic model [40] took into account these different regions of operation or any changes in temperature. In order to compare the models under consideration, the experimental data was split into different regimes where each regime was representative of the system performing under certain conditions. The conditions assumed that there was a constant temperature (21°C) and the data was split up into three groups. The first group was for data in the 0-125kpa region which was where the inner liner of the muscle did not touch the outer sheathing. The second group of data was for the 125-600kpa region, which is where the inner liner is in contact with the outer liner and the muscle contracts as a result. The third set of data was for the 0-600kpa regions combining both of the previous regions.

The analysis was then extended to data where the temperature varied between 21 & 39°C. This was also split up into the three regions described above. The experimental data used for these tests was the isobaric data, this was not used to form any of the models tested below and is used in the capacity as a set of near perfect replicates, the data can be found in Appendix C-1 Table C-2.

The different models tested using this data were

- The deterministic model.
- The Caldwell model.
- The black box regression model for the 0-125kpa region where the temperature was held constant(4.9-3).
- The black box regression model developed using data from the 125-600kpa region where the temperature was held constant (4.9-2).
- The black box regression model where the temperature was allowed to vary for pressures between 0-125kpa (4.11-2).
- The black box regression model where the temperature was allowed to vary and the pressures were between 125-600kpa (4.11-1).
- The quasi-static model where there are no temperature changes and the pressure varies between 0-125kpa (4-13-1)
- The quasi-static model where there are no temperature changes and the pressure varies between 0-125kpa (4-13-2)

The results of the tests are listed in Table 4-3, with regression and standard deviation of models in Appendix C-4 Tables C-39 to C-44.

| Model type \ Data range | 0-125kpa 21°C | 125-600kpa 21°C | 0-600kpa 21°C | 0-125kpa 21-39°C | 125-600kpa 21-39°C | 0-600kpa 21-39°C |
|---|---|---|---|---|---|---|
| 1. deterministic | 3.414 | 7.047 | 6.156 | 4.213 | 9.352 | 8.28 |
| 2. Caldwell model | 3.210 | 5.924 | 4.265 | 3.892 | 8.265 | 7.549 |
| 3. quasi static model (0-125) 21 | 2.891 | × | × | 3.769 | × | × |
| 4. quasi static model (125-600) 21 | × | 2.45 | × | × | 5.951 | × |
| 5. full quasi static model | × | × | 2.532 | × | × | 5.696 |
| 6. regressed (0-125) 21°C | 1.012 | × | × | 2.32 | × | × |
| 7. regressed (125-600) 21°C | × | 1.922 | × | × | 4.490 | × |
| 8. piecewise combination of 6 & 7 (0-600) 21°C | × | × | 2.041 | × | × | 4.584 |
| 9. regressed (0-125) 21-39°C | 0.986 | × | × | 2.0071 | × | × |
| 10. regressed (125-600) 21-39°C | × | 1.693 | × | × | 3.292 | × |
| 11. piecewise combination of 9 & 10 (0-600) 21-39°C | × | × | 1.671 | × | × | 3.0561 |

**Table 4-3 Comparison of models developed. Standard deviations of the models against the data sets they were tested against.**

## 4.15 Reasons for the Performance Differences

Over all the data ranges, the deterministic model performed the worst out of the models tested. This is because this model had no provision for the first region where the inner liner of the muscle has yet to come into contact with the outer sheathing. The deterministic model also does not fare well when used with the variable temperature data. This is because the deterministic model does not use temperature as a predictor. It is thus concluded that the deterministic model, while qualitatively describing the muscles behaviour, does not work well with real world data.

The Caldwell model performed better than the deterministic model but still was not an accurate predictor of the muscles behaviour. When this model was tested against the data in the linear region it did not predict the data well. This is because the Caldwell model does not take into account the inner sheathing of the muscle coming into contact with the

outer sheathing. When the variable temperature data was used, the Caldwell model did not predict this behaviour well because this model also does not use temperature as a predictor.

The quasi-static model did manage to predict the behaviour of linear region of the pneumatic muscle. This is because the model was based on the assumption that the system behaved like an elastic balloon being inflated. In 125-600kpa region the performance of the quasi-static model was quite reasonable.

When the temperature effects were taken into account the quasi-static model, while being better than the Caldwell and deterministic models, still had a high standard deviation, this is because the quasi static model does not use temperature as a predictor. This indicate that the model was still not a very reliable predictor of the data when the temperature changes.

The statistical model when compared to data in the linear region at constant temperature, proved a better predictor than the other models mentioned so-far, probably because similar data was used to determine its parameters. However when the statistical model for the 0-125kpa region with no temperature changes was applied to the data in the 0-125kpa region with temperature changes the model performed better than all the other models mentioned. This is because the statistical approach included more predictors which were more significant in predicting the data's behaviour.

The statistically based model for the 125-600kpa region with no temperature change was tested on similar data used to determine its parameters. This produced better results than the Caldwell model, the deterministic model and the quasi-static model. When the model was applied to data where the temperature was allowed to vary, the model again produced better results than the other models used. This is because this model had more predictors than the other models mentioned.

The statistical model which used data in the 0-125kpa region with temperature changes, provided the best predictor of the muscles behaviour in the 0-125kpa region with no temperature changes. This is because it had more predictors in it than the other models. These predictors appeared to improve the models performance. This model performed better than the other models when applied to data where the temperature was allowed to vary.

The statistical model which used data in the 150-600kpa region with temperature changes, provided the best predictor of the muscles behaviour in the 150-600kpa region with no temperature changes. This is because it had more predictors in it than the other models. These predictors appeared to improve the models performance. This model performed better than the other models when applied to data where the temperature was allowed to vary.

### 4.15.1 Non-linearity's due to Uncertainty of Shape

In all the empirical models so far we have made an assumption, that muscle takes on the shape of a cylinder or an oval, depending on its pressure. This does not happen in the physical system. In reality the muscle is probably always a combination of the two. Because there is an offset between the outer sheath and the inner liner at the ends of the muscle the inner liner places less pressure on the outer sheath in this area. This effect causes the muscle to tend towards a cylinder shape.

In the middle of the muscle the cylinder model is not appropriate. There is no off-set between the inner liner and the outer sheath. Hence the outer sheath can take on more of the shape of the inner liner, and it consequently has more pressure applied to it. As a result it will take on more of an oval shape.

At lower pressures the outer liner conforms more closely to the inner liner, hence it resembles an expanding oval. At higher pressures as the inner liner is fully expanded removing all the dead space, the muscle is constrained about it length and girth by the outer liner. As a result it takes on a more of a cylinder shape.

This has not been accounted for our empirical models and may be a source of inaccuracy in our experimental results.

### 4.15.2 Other non-linearity's

Because both the Salford and deterministic models required a measure of the interweave angle to measure the force exerted, the accuracy with which the interweave can be measured affects the final result. In the pneumatic muscle, because the shape is not cylindrical and the pressure is not evenly distributed over the whole muscle, the result is that the interweave angle is also variable.

When the muscle is inflated the middle portion of the muscle has the largest diameter. The largest interweave angle is therefore to be found in this area. At the base of the muscle however, the diameter of the muscle is much smaller due to the diameter being fixed by the clip which holds the muscle in place as shown in Figure 4-36, so the interweave angle is smaller here.

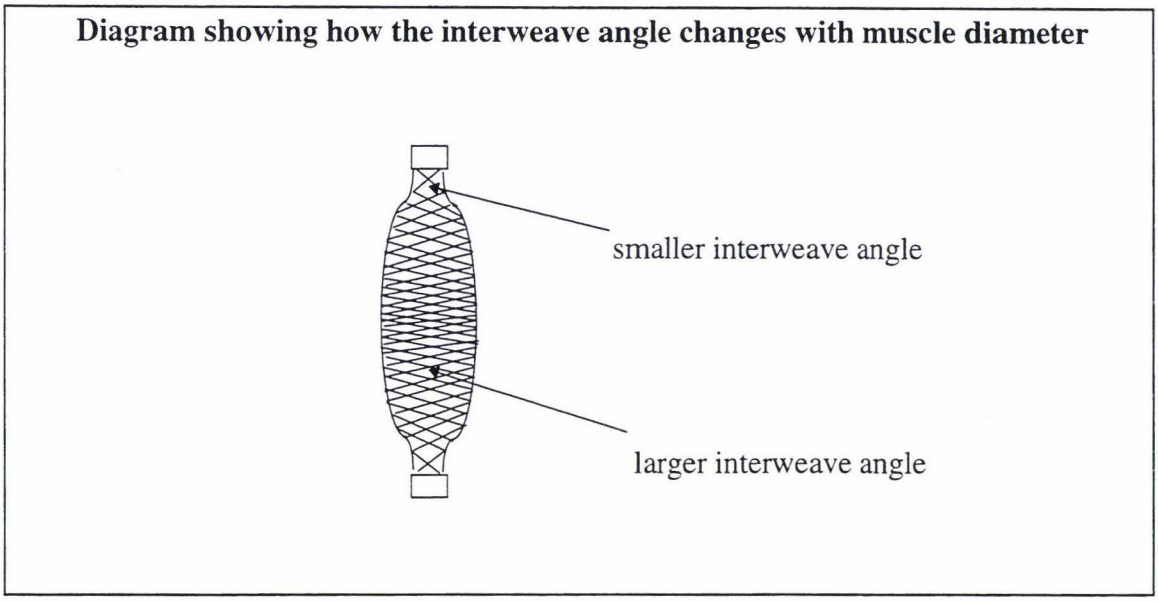


**Figure 4-36 Interweave angle.**

Hence the interweave angle will not be constant for the cylinder and will be highly dependent on where it is measured. The interweave angle is therefore not a good indicator of the length of the cylinder.

### 4.15.3 The Effects of Temperature

Temperature appears to significantly affect the muscles behaviour, particularly at higher temperatures. A deterministic attempt at evaluating the effect of temperature appears to be very difficult. Increases in temperature do not increase the pressure in the muscle. The higher force exerted by the muscle at higher temperatures as shown by the isobaric tests appears not to be due to an increase in pressure. Instead it appears that the mechanism creating the increase in force produced by the muscle is the result of changes in the structure of the pneumatic muscle. Given that the shape of the outside sheathing constrains the shape of the muscle and hence the force applied by the muscle, changes in the properties of the outer sheathing produce changes in the force applied by the muscle. Increasing the temperature of nylons, along with most other material, is known to increase ductile properties. It is also known that greater contraction is obtained when a larger volume is occupied by the cylinder. If the cylinder becomes more rounded due to the more ductile sheathing, it occupies more volume giving greater contraction as shown in Figure 4-37.

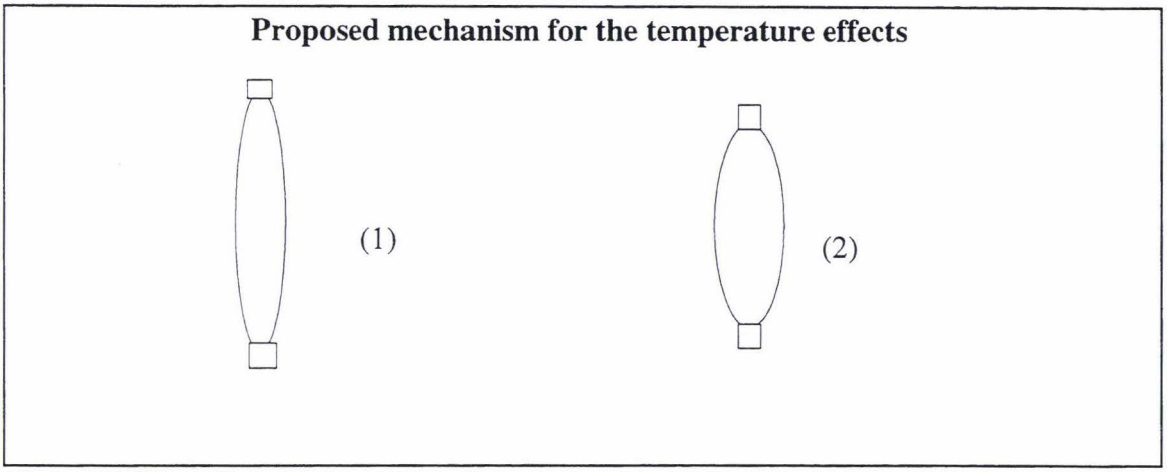


**Figure 4-37 The effect of temperature.**

1. The muscle is at a lower temperature, this causes the fibres to be stiffer and as a result the muscle is more cylindrical. This produces less contraction/force.
2. At higher temperatures the ductility of the muscle fibres increases. This results in a more oval shaped muscle. This produces more contraction/force.

The exact shape the muscle takes on due to changes in temperature is not known, as the change is gradual and is quite hard to determine analytically. These results do confirm that temperature is a factor in the force applied by the muscle but more analysis is required to confirm the mechanism.

## 4.16 Hysteresis Background

There has been little modelling and analysis work done on the effects of hysteresis.

The work of Chow and Hannaford [40] is the most searching analysis of the effects of hysteresis of the literature reviewed. They looked at the amount of hysteresis present in McKibben muscles with different materials used for the fibres. They showed that hysteresis was significant and recorded changes in force of the order of 25% associated with changes in direction. They also showed that hysteresis was velocity independent, but dependent on the material used and the cycle length. Their attempt at modelling hysteresis was to introduce a correction constant which was added on to take account of the effects of hysteresis.

The effects of hysteresis are also noted to be significant in the modelling of pneumatic muscles in the research conducted by Caldwell et al [39]. In their investigations into the effects of hysteresis, no attempt was made to quantify these effects or mathematically model them.

The work by Hasselroth et al [42] indicates that hysteresis is significant. They did not attempt to quantify or model the effects of hysteresis, but conjectured that the hysteresis was present because the force exerted by the muscle depended on the pressure of the muscle at its previous position.

What is clear from research into hysteresis effects on the pneumatic muscle is that the amount of hysteresis is dependent on the muscle design. There is very little work done on the modelling of hysteresis in the literature. This section investigates the effect of hysteresis on this particular muscle design.

## 4.17 Hysteresis Experiments

In the hysteresis experiments the system was moved in one direction over a range of values then moved back in the opposite direction over the same range of values. If there was a discrepancy in the recorded values this is said to be due to hysteresis. This means that the direction the system moves in is a variable which affects the results.

## 4.18 The Methodology Used

In trying to model the hysteresis it was decided to use a top down approach. First experiments would be conducted to ascertain whether hysteresis was present and if so the next stage would be to quantify the hysteresis and the effect it was having on the results. If hysteresis was found to be significant; investigations of the factors which contributed to the hysteresis would be undertaken. This involves conducting experiments to try to quantify the contribution of each of the factors to the hysteresis. A model would then be developed based on this. These experimental steps are shown diagrammatically in Figure 4-38.

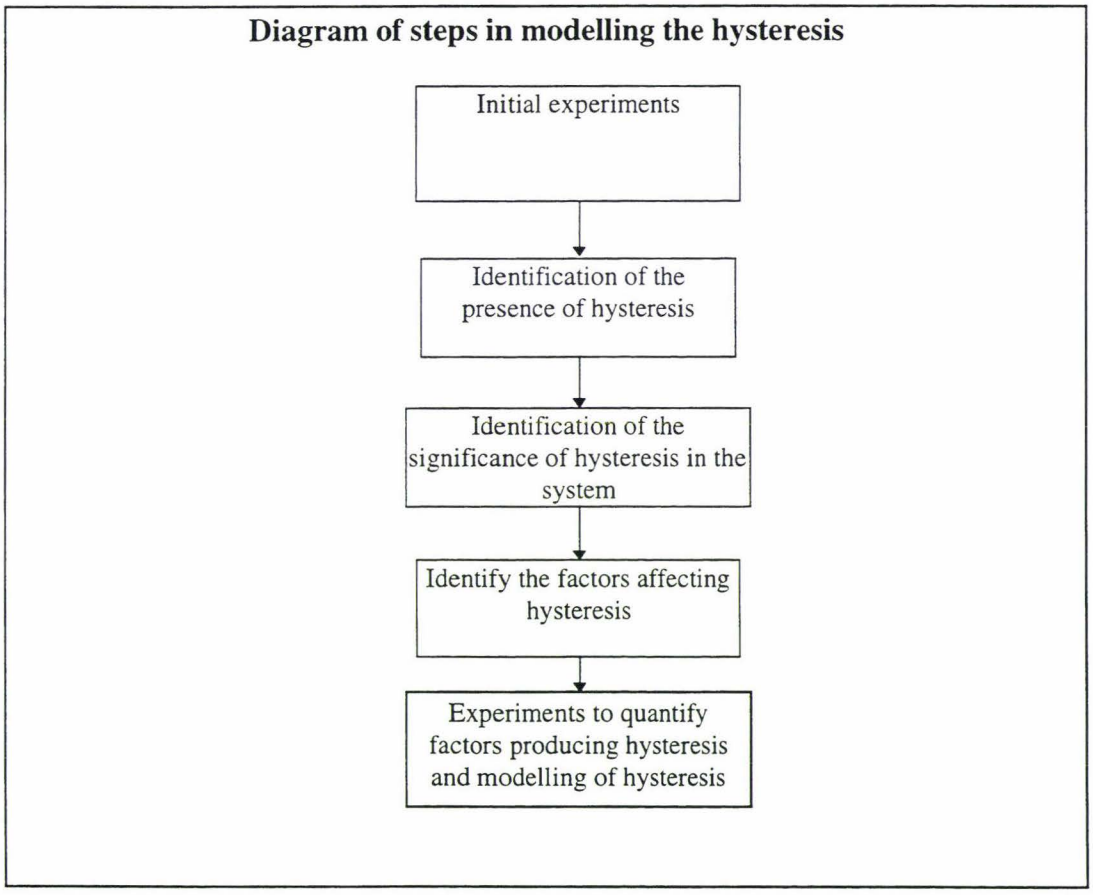


**Figure 4-38 Hysteresis experiment methodology.**

## 4.19 Types of Hysteresis Experiments

There were two types of hysteresis tests done, as follows.

1. A constant length (isometric) test.

This was done by setting the muscle at a fixed length using the rig in section 4.9. Pressure was then increased at 50kpa intervals from 0kpa to 600kpa, and then decreased over the same range. At each increment in both the forward and backward directions the force produced by the muscle was recorded.

A second test was also conducted at this length where the pressure was increased from 0kpa to 400kpa and then brought back down. This was done to see if the maximum pressure, the muscle was raised to, would affect the amount of hysteresis.

2. The constant force (isotonic) tests.

These required that the force applied to the muscle was kept constant using the rig in section 4.10, pressure was then varied. The pressure was increased from 0kpa to 600kpa in 50kpa increments and then decreased over this range with the distance recorded at each increment.

A second test was conducted with the same force where the pressure was increased from 0kpa to 400kpa and then brought back down. This was done to see if the maximum pressure, the muscle was raised to, would affect the amount of hysteresis.

## 4.20 Analysis of the Isometric Hysteresis Results

The isometric tests showed only a small amount of hysteresis in the 0-600kpa range. In general higher force values were recorded while the pressure was increasing than when the pressure was decreasing. The trend observed was that the amount of hysteresis was smallest for the shortest length of muscle tested (59 mm). The largest hysteresis measurement was obtained when the muscle was at its largest length tested (64 mm). Hence it is concluded that the amount of hysteresis is related to the length of the muscle. It was also noted that the amount of hysteresis was lower for the 400kpa cycle. This indicates that the amount of hysteresis is dependant on the position of the change of direction. The results are shown in Figure 4-39 and Appendix C-1, Table C-4.

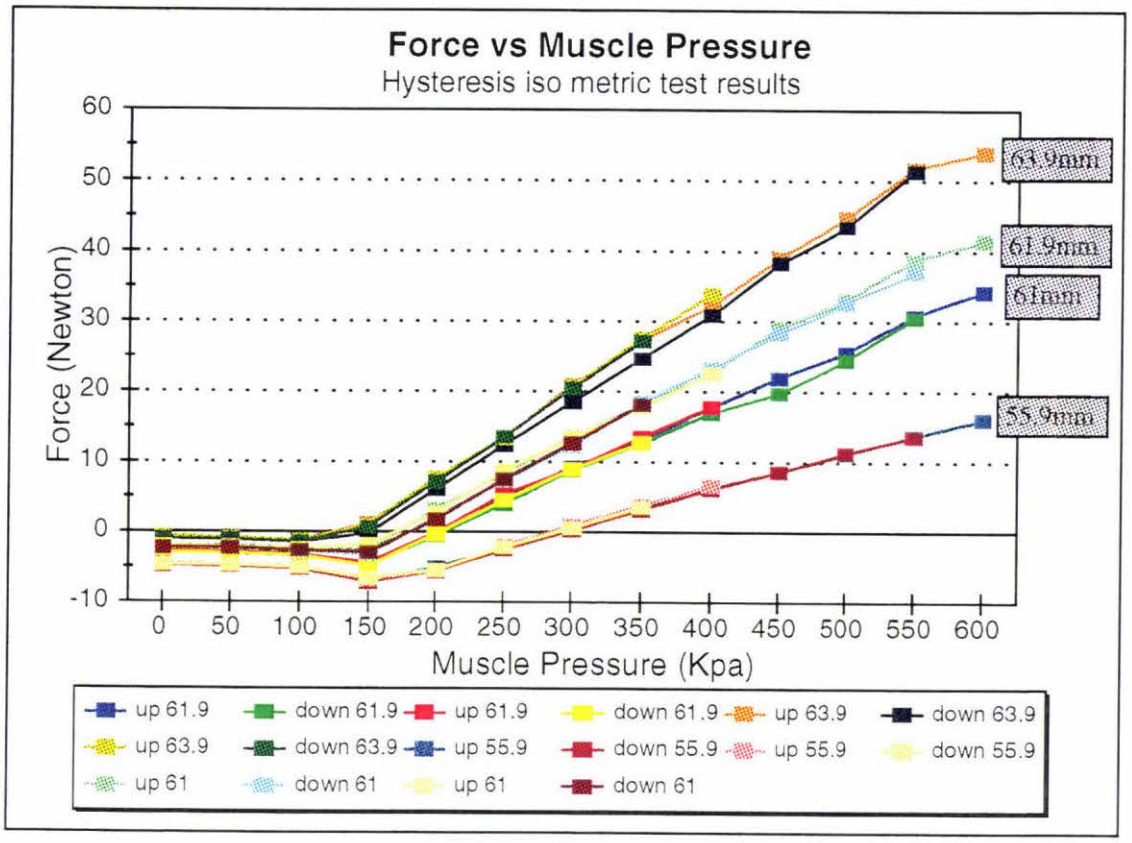


**Figure 4-39** Isometric hysteresis results.

## *4.21 Isotonic Hysteresis Tests*

It was pointed out that in the real world situation the pressure and distance would be changing and the mass would change very little, which is essentially an isotonic situation.

The results from this test indicated there was very little hysteresis. This could be due to the lack of precision in our video camera measuring system which had an accuracy of +/- 0.05 mm. It appears that the hysteresis decreases as the pressure cycle is reduced from 600kpa to 400kpa. This is in agreement with the results obtained from the isometric hysteresis tests, Figure 4-40 and Appendix C-1, Table C-6 show the results.

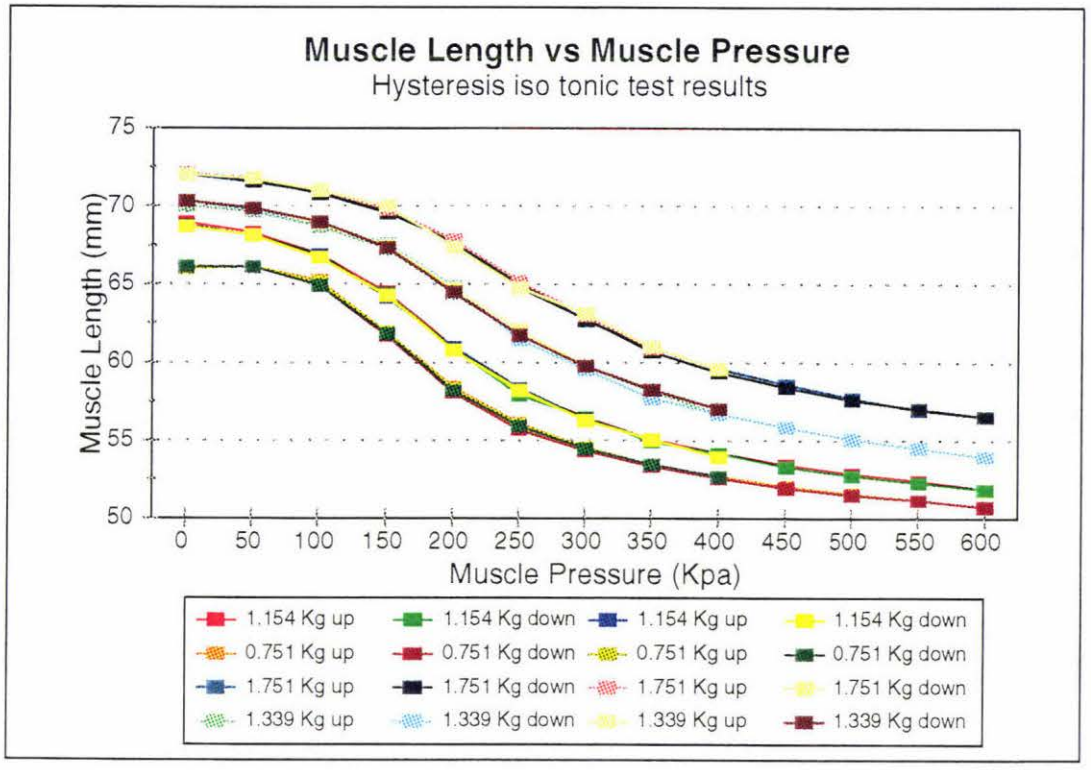


**Figure 4-40 Isotonic hysteresis results.**

## *4.22 Hysteresis Conclusions*

From looking at the isometric tests the amount of hysteresis present is about 1% of the total force which is extremely small. At 1% it is comparable to the experimental error so it can be ignored. For the isotonic tests the hysteresis is also about 1% of the muscle length which is so small it too can be ignored, Table 4-4 and Appendix C-1, Table C-5 and C-7 present experimental results.

| Length and cycle size | 61.9mm (600 kpa cycle) | 61.9 mm (400 kpa cycle) | 63.9mm (600 kpa cycle) | 63.9mm (400 kpa cycle) | 55.9mm (600 kpa cycle) | 55.9mm (400 kpa cycle) | 61mm (600 kpa cycle) | 61mm (400 kpa cycle) |
|---|---|---|---|---|---|---|---|---|
| difference between directions (Newton) | 0.79 | 0.46 | 1.40 | 0.26 | 0.17 | 0.14 | 0.64 | 0.62 |

**Table 4-4 Average difference in force recorded between the upward and downward cycles in the isometric hysteresis tests.**

| length difference \ Pressure | 1.154Kg (600 kpa cycle) | 1.154Kg (400 kpa cycle) | 0.751Kg (600 kpa cycle) | 0.751Kg (400 kpa cycle) | 1.751Kg (600 kpa cycle) | 1.751Kg (400 kpa cycle) | 1.339Kg (600 kpa cycle) | 1.339Kg (400 kpa cycle) |
|---|---|---|---|---|---|---|---|---|
| difference between directions (mm) | 0.79 | 0.46 | 1.40 | 0.26 | 0.17 | 0.14 | 0.64 | 0.62 |

**Table 4-5 Average difference in length recorded between the upward and downward cycles in the isotonic hysteresis tests.**

The general trend in the hysteresis tests is that the upward values are larger than the downward values. Increases in the length of the muscle increase the amount of hysteresis present. Hysteresis increases with an increasing cycle length.

## 4.23 Physical Reasons for Hysteresis

Coulomb friction is given as the main cause of hysteresis in the paper by Chow and Hannaford [40]. Coulomb friction is caused by nylon fibres rubbing against each other. This increases with increasing force being applied to the nylon fibre to fibre interface. We can assume that the increasing force associated with the increases in length would increase hysteresis. This is verified in the isometric and isotonic tests. Increases in either pressure or force lead to more coulomb friction and larger hysteresis. This is also indicated by our results. It is therefore concluded that coulomb friction is indeed causing the hysteresis.

## 4.24 Summary and Conclusions

A series of models describing the behaviour of the pneumatic muscle were investigated. Two analytical models were obtained from available literature, they were based on the work of Caldwell et al and the Chow and Hannaford. The Chow and Hannaford model uses an energy conservation approach to model the muscles behaviour, and the Caldwell et al model which uses the idea of minimum energy states. Both of these models describe the effects of pressure and muscle length on the force produced by the muscle.

Statistical models based on tests on the pneumatic muscle were developed. These were a black box model, where regression was used to optimise a set of predictors to the test results, and a quasi-static model, where observations and assumptions on which

parameters within the system were made. The parameters thought to be important were used to form a model of the pneumatic muscle. These parameters were then optimised using a data set obtained from the physical system to form a model of the pneumatic muscle.

The analytical models were compared against experimental results obtained from the muscle and it was found that these models do not adequately describe the muscles behaviour. This was concluded to be due to these models not taking into account dead space with in the system and temperature effects. The quasi static model was designed to take into account dead space within the system and provided a better description of the system than the analytical models. The black box regression model took into account dead space and temperature effects and provided the most accurate description of the system.

The effects of hysteresis were investigated, these proved to be small. This is because the muscle has been made by a new process. This produces significantly less hysteresis than in other muscles reviewed. It was found that hysteresis under the conditions tested was not a significant factor affecting the muscles behaviour. It is thus left out of the model of the muscles behaviour.

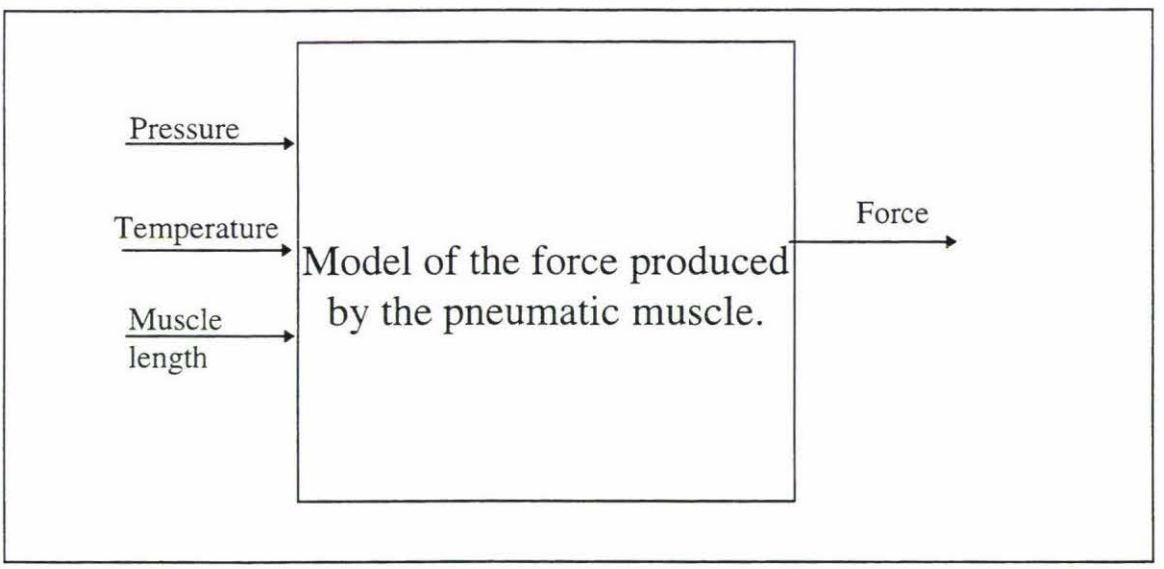


**Figure 4-41 Model of the pneumatic muscle.**

The equations describing the pneumatic muscle give the relationship between the force produced by the muscle, muscle pressure and muscle length as shown in Figure 4-41. These models are incorporated into a model of the whole system as shown in Figure 4-42, which can be used to simulate the systems performance and used in controller design.

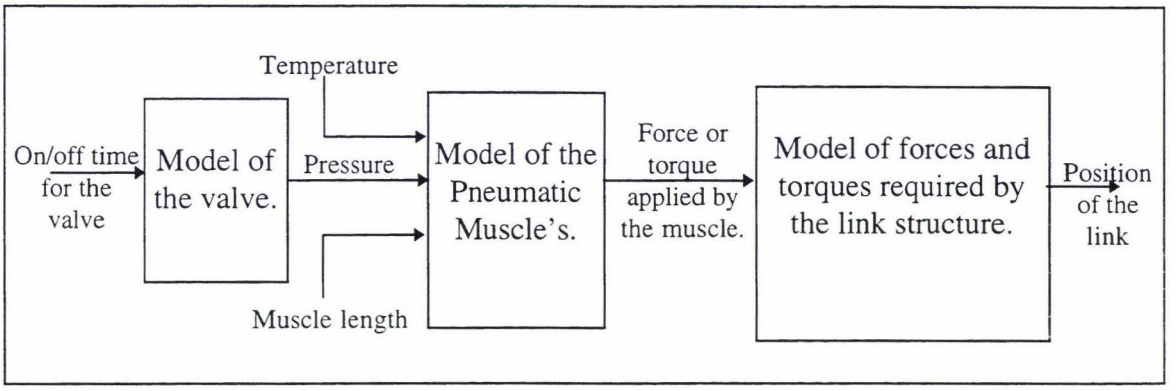


**Figure 4-42 Model of the pneumatic muscle integrated into a model of the whole system.**

# 5. Valve design

## 5.1 Background to the Valve

The braided muscle actuator required a regulated air supply, so a valve was used to regulate the supply of air to the system.

A valve was designed by Spellman [49] for use in the robotic hand. The valve is a double acting solenoid valve for supplying air to the actuation system.

### 5.1.1 Literature Review

Valve technology has been in development for a long time. The Greek and Roman periods saw the development of many mechanical and hydraulic machines and the first use of many sophisticated designs [50].

Development has continued in this field and is still continuing to this present day. Over the past 60 years a plethora of valve designs has emerged. This has been brought about by the need to design valves to cater for new processes and technological innovations. The valves that are available today are split into five main families-

1. Linear valves such as gate valves, diaphragm valves, globe valves and pinch valves.
2. Rotary valves such as plug valves, ball valves, general purpose butterfly valves and high performance butterfly valves.
3. Safety and relief valves.
4. Pressure control valves including pressure reducing valves, pressure retaining valves and automatic control valves.
5. Solenoid valves.

The selection of valves used to control pneumatic muscles in the reviewed literature includes the use of electric solenoid valves in the system developed by Hasselroth et al [42]. This uses what is known as a double acting solenoid valve. It is composed of two valves used; one for letting pressure into the system and the other for letting pressure out.

The approach taken by Caldwell et al [39] was to use pulse width modulation of low-powered piezoelectric valves. The choice of piezo-electric valves was made to facilitate control purposes.

The approach taken by Chou and Hannaford [40] was to use a manual pressure regulator to set the pressure. The pressure regulator was connected to a reservoir to increase the volume of the system which helps to reduce pressure variation. This arrangement was

specifically designed to conduct static tests where an accurate unvarying pressure was required. This certainly gave the set-up the advantage of accuracy but there was no analysis as to how quickly the system was able to respond. Fast response is desirable in robotics applications.

### 5.1.2 Review of Valve Modelling

Development of a simulation for a robotic mechanism which uses a pneumatic actuator controlled by valves requires a model of the valve system. This model is then used to assess the design of the system and is also used to evaluate the effect of changes in the system. Finally a control system can be developed for the real system based on the simulated system. Hence accurate models for the valve are required before it can be integrated into the system.

There are many approaches to modelling the flow out of a valve, all these methods require assumptions about the physical environment. Some approaches have attempted to correlate pressure-drop data for flow of powdered materials in an air stream by applying the Fanning equation [51]

$$P_1 - P_2 = f \frac{L}{D} \frac{v^2}{2g} \frac{\rho}{144} \qquad \textbf{Equation 5-1}$$

where $P_1 - P_2$ = pressure drop in conveying line, $N / m^2$

$f$ = a dimensionless friction factor

$L$ = total length of line, m

$D$ = pipe bore, m

$v$ = velocity of mixture, m / sec

$g$ = gravity, $m / sec^2$

$\rho$ = density of gas $kg / m^3$

The original Fanning equation was developed for the flow of homogeneous fluids in turbulent flow since then, the value of the friction factor for these fluids has been correlated and found to be a function of the Reynolds number.

$$N_R = \frac{\rho v D}{\mu}$$ **Equation 5-2**

where

$\mu$=viscosity, kg/m.s
$v$=velocity, m/sec
$\rho$=density, kg/m$^3$
$D$=diameter of the orifice, m

It is often convenient, particularly with control valves, to be able to express the relationship between pressure drop and flow rate through a valve by a flow coefficient. In many parts of the world, including the UK and the USA, the flow coefficient in most general use is $C_v$, while in parts of Europe the coefficient $K_v$ is often used. Another coefficient, $A_v$, is also available, which is associated with the SI units.

Each type and size of valve has a particular flow coefficient and the general formulae which follow indicate how a knowledge of this can be used to establish the pressure drop across a valve for a given flow rate or, alternatively, to determine the flow rate through a valve which will generate a given pressure drop.

Flow coefficient values are determined by testing and may not be valid for all conditions of flow. They require accurate information about the environment they are to be used in.

**Flow coefficient $C_v$**

This is defined as the rate of flow of water in US gallons per minute, at 60°F (15.6°C), that will generate a pressure drop of one pound-force per square inch across the valve.

*Liquid flow*

The basic formula is

$$C_v = \frac{Q\sqrt{G}}{\sqrt{(\Delta P)}}$$ **Equation 5-3**

where

$Q$ = flow rate in US gal / min;

$G$ = specific gravity of liquid (water = 1);

$\Delta P$ = pressure drop across valve lbf / in$^2$.

This assumes the flow to be neither viscous, cavitating, nor flashing.

*Gaseous Flow*

*Volume flow*

$$C_v = \frac{Q}{\sqrt{\frac{289}{GT} C_1 C_2 P_1 \sin\sqrt{\left\{\frac{\Delta P}{P_1}\right\}\vartheta}}}$$ **Equation 5-4**

*Weight flow*

$$C_v = \frac{4.32W\sqrt{T}}{C_1 C_2 P_1 \sqrt{M \sin\left\{\frac{3417}{C_1 C_2}\sqrt{\frac{\Delta P}{P_1}}\right\}\vartheta}}$$ **Equation 5-5**

*where*

$G$ = specific gravity of gas (air = 1);

$T$ = temperature of gas in $K$ (=° C + 273);

$C_1$ = gas flow factor (type of valve constant);

$C_2$ = correction factor for ratio of specific heats;

$\Delta P$ = pressure drop across valve in lbf / in$^2$;

$P_1$ = valve inlet pressure in lbf / in$^2$;

$\vartheta$ = angular degrees;

$M$ = molecular weight of gas;

$W$ = gas flow rate in lb / h.

**Flow coefficient $K_v$**

This may be defined as the rate of flow of water in cubic metres per hour that will generate a pressure drop of one bar across the valve.

The basic equation is

$$K_v = \frac{Q\sqrt{G}}{\sqrt{(\Delta P)}}$$ **Equation 5-6**

*where*

$Q$ = flow rate in $m^3$ / h;

$G$ = specific gravity of liquid (water = 1);

$\Delta P$ = pressure drop across valve in bar.

which again assumes the flow to be neither viscous, cavitating, or flashing.

**Flow coefficient $A_v$**

As already stated, this coefficient is associated with SI units. Methods of evaluating control valve capacity using flow coefficient $A_v$ are described in a British Standard prepared under the authority of the Instrumentation Industry Standards Committee and deals with incompressible fluids, gases, and vapours. All units used are in accordance with the International System (SI).

*Liquid flow*

The basic formula is

$$A_v = \frac{Q\sqrt{\rho}}{\sqrt{\Delta P}}$$ **Equation 5-7**

*where*

$Q$ = flow rate in $m^3$ / s;

$\Delta P$ = pressure loss in pascals;

$\rho$ = density of liquid in kg / $m^3$.

*Gaseous flow*

The recommended working formula is

$$A_v = \frac{W}{1.67 \times 10^{-2} \times C_1 C_2 Y \sqrt{(\rho_1 P_1)}} \quad \text{Equation 5-8}$$

*where*

$W$ = flow rate in kg / s;

$C_1$ = gas flow factor (type - of - valve constant);

$C_2$ = factor for variation in specific heats;

$\rho_1$ = density of fluid at inlet in kg / m$^3$;

$P_1$ = pressure of fluid at inlet in pascals;

$Y$ = subcritical flow factor, being given by

$$Y = \sin\left\{\frac{3417}{C_1 C_2}\sqrt{\frac{(\Delta P)}{P_1}}\right\} \text{ degrees}$$

where $\Delta P$ = pressure drop in pascals.

If the $\{\ \}$ expression equals 90°, then the flow is turbulent and, in this case, $Y$ is unity.

## 5.2 The Need for a Double Acting Valve

The use of the pneumatic muscle as the actuation device necessitated a pressure regulation device to inflate/ deflate the muscle. This posed an interesting problem in itself. The solution to the problem would have to achieve a number of objectives;

1. Control of the quantity of air entering the pneumatic muscle.

2. Control of the quantity of air leaving the system.

3. Ability to alternate between states of high pressure and low pressure.

4. Ability to achieve (1) and (2) in real time.

5. Ability to achieve (1) and (2) without excessive overshoot, that is, the requirement of a stable system.

The physical system had the following attributes which the design solution would have to take into account;

1. Low damping, that is, little air was lost from the system when the system was closed.

2. The small volume of the system meant that very little air was required for inflation/deflation.

3. The combined effects of (1) and (2) meant that the system had a very quick response to small changes in air supplied to the system.

The low damping meant that the major loss of air in the system was by air leaving the entry/exit orifice as seen in Figure 5-1.

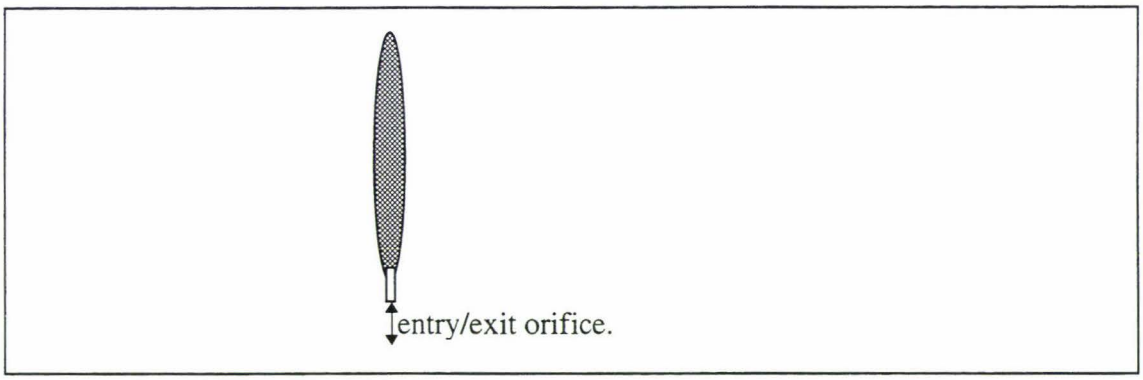


**Figure 5-1 Single orifice of a pneumatic muscle.**

The design solutions considered to accomplish the system's objectives were;

1. Single acting proportional pneumatic servo-control valve.

2. Double acting proportional pneumatic servo-control valve.

3. Manual proportional pneumatic valve.

4. Controlling the rate at which air entered the system ie. controlling the air compressor.

5. Single acting solenoid pneumatic servo-control valve.

6. Double acting solenoid pneumatic servo-control valve.

The double acting solenoid valve was chosen for the following reasons;

1. The double acting concept could control the quantity of air which entered the system, through the inlet valve.
2. The double acting concept could control the quantity of air which left the system through the outlet valve.
3. The department in which this research was conducted had already developed a single acting solenoid valve. This is a commercial product now in use [49].
4. It was expected that the solenoid valve already available within the Production Technology Department could be further developed to achieve the systems objectives.
5. Solenoid valves are cheap to manufacture, as relatively few working components are required.

## 5.3 Design for a Double Acting Valve

The double acting solenoid valve has two single acting valves connected together in a series configuration. One valve is an inlet into the system to increase the pressure of the system. The other acts as an air outlet for the system so that the pressure of the muscle can be decreased. Figure 5-2 gives the basic diagram showing the two valves in series.

**Diagram of double acting valve concept**

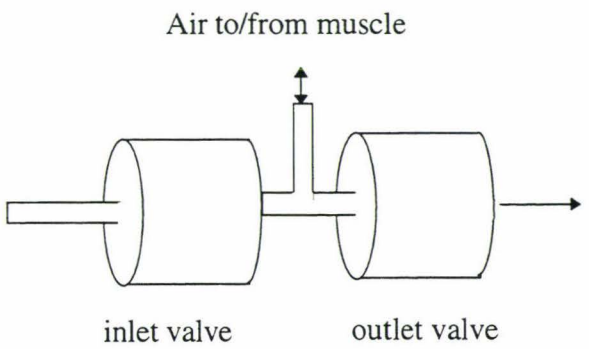

**Figure 5-2 Double acting valve concept.**

The double acting valve was a single compact block. The advantages of this initial design are it is transportable, durable, simple to construct and keeps costs to a minimum.

A pressure transducer is incorporated in the unit to determine the pressure for feedback to the valves. This transducer is required so that the system will know what pressure it is operating at so that the system may adjust itself when its operation deviates from that which is desired. In order to gain the optimal performance the location of the transducer should be close to the muscle as this provides the best measure of the pressure at which the muscle is operating as shown in Figure 5-3.

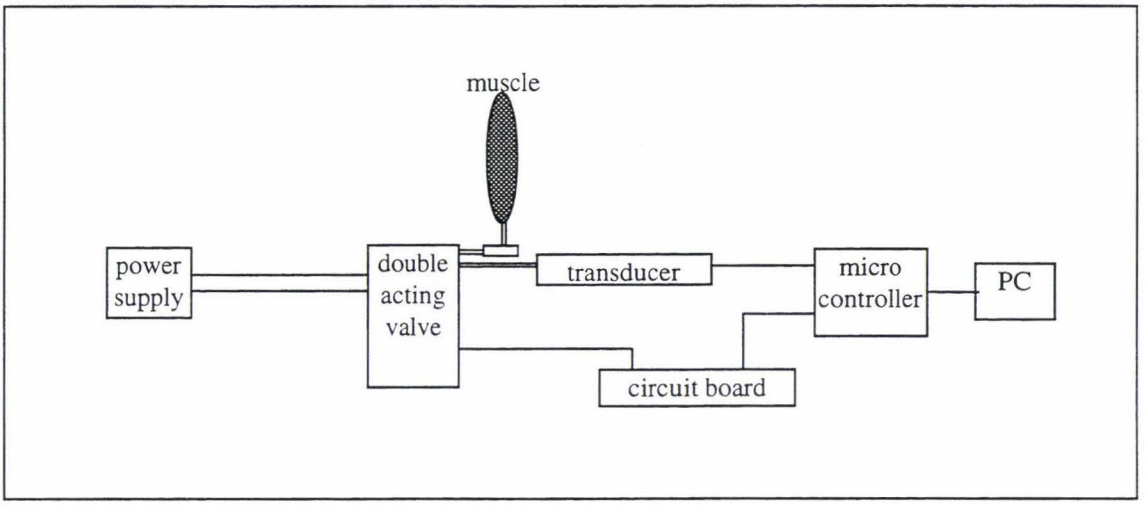


**Figure 5-3 System layout.**

In the prototype system this is not possible as the physical constraints of a real world system require the weight carried by the robotic end effector to be minimised. This means that many of the components must be located away from the muscle to reduce weight. In the design used here, the transducer was located close to the valve, as was the micro-controller for the analogue to digital conversion. This is shown in Figure 5-4.

Power connections for each valve are situated on a circuit board which is located at the side of the valve unit. The power connections are kept separate from the valve unit because the operation of the valve produces heat and considerable vibration. Having the circuitry separate from the valve ensures that the circuitry will not be adversely affected by the operation of the valve.

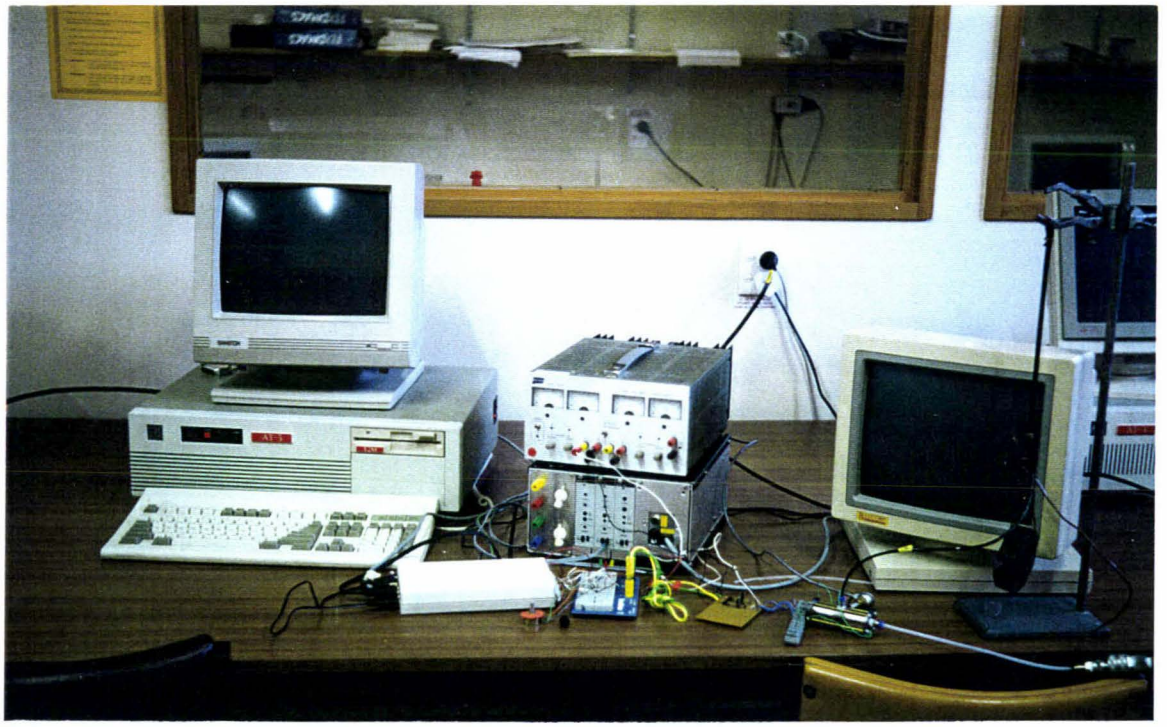

**Figure 5-4 Picture of the system.**

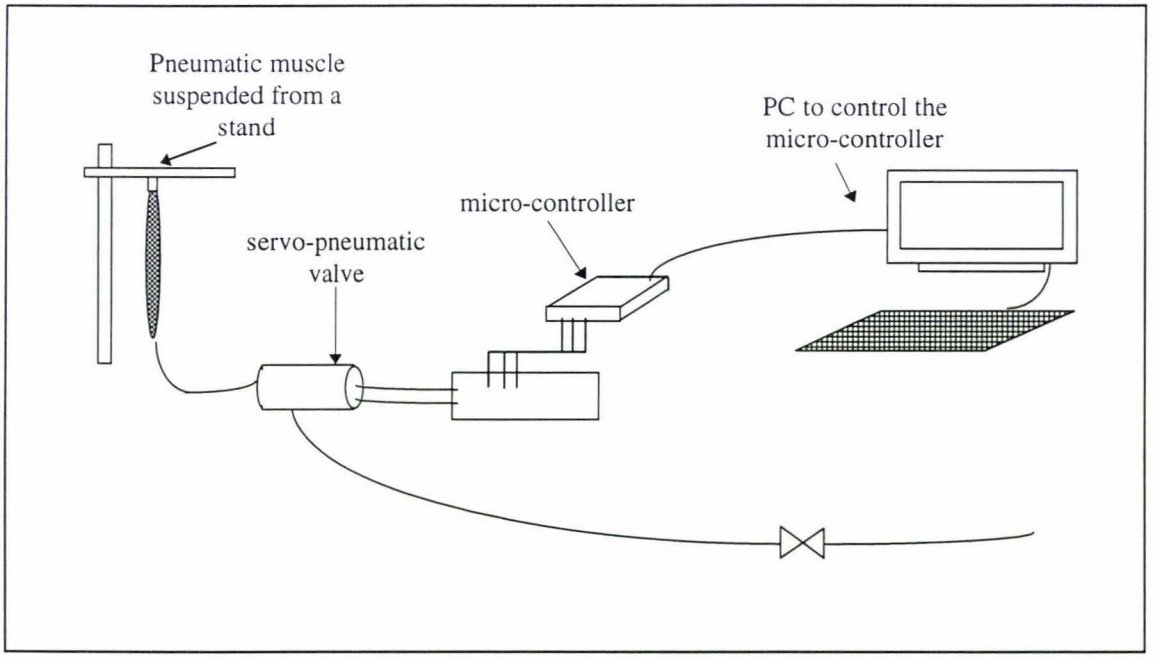


**Figure 5-5 Diagram of the system.**

## 5.4 Physical Alterations to the Valve

It was observed that when the valve was used to control the muscle using the two position control algorithm of Spellman's [49], the muscle pulsed and oscillated wildly. The movement of the muscle was very rapid and large movements were observed. In a robotics application this is clearly undesirable as the position of a robotic manipulator would move very sharply without much control or co-ordination in its movement. This uncontrollability of the valve in tracking a set point when using the muscle was attributed to;

- Too much air entering the system when the valve was opened for short periods of time.
- The valves not sealing properly and air leaking into the muscle.

This was causing the pressure to exhibit large oscillations and large overshoot. The inlet to the muscle was initially 1.5 mm in diameter. The first alteration to the system was to reduce this diameter. A restriction was inserted into the valve inlet to reduce the inlet orifice diameter to 1 mm, which decreased the amount of air entering the system.

The second alteration dealt with the problem of the valve not sealing. A nylon seat was built on the valve orifice to reduce the amount of air leaking into muscle as shown in Figure 5-6 and Appendix D-4.

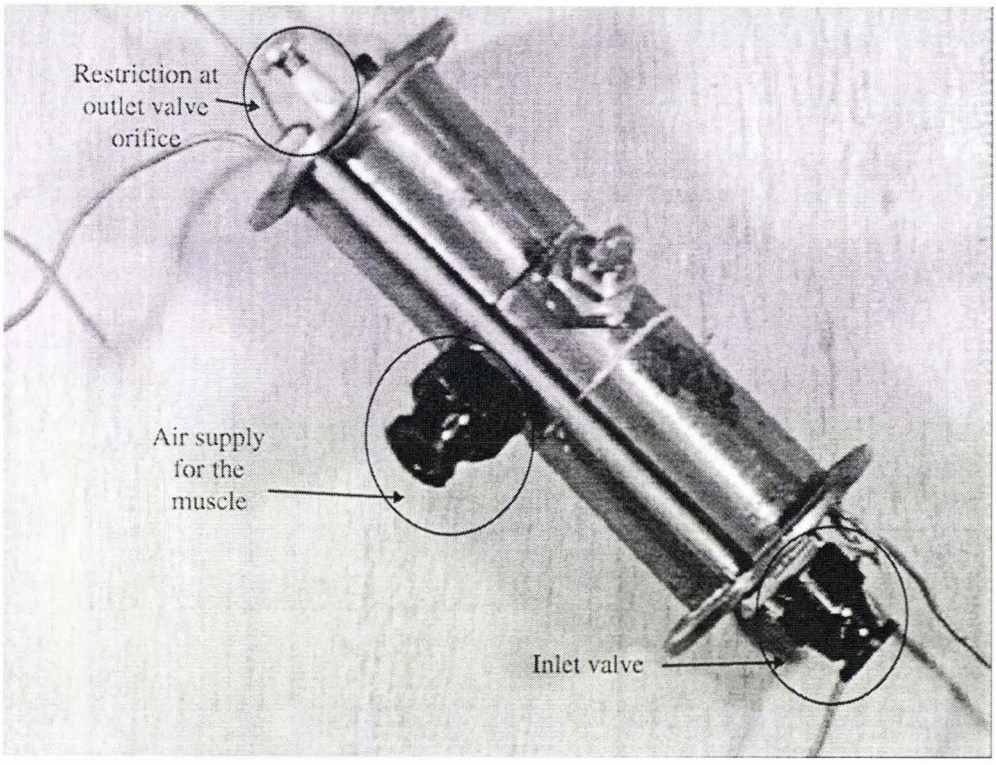


**Figure 5-6 Picture of the valve.**

## 5.5 Open Loop Control

As part of the development process, a driver was written to control the valve from a 286 PC. With the use of a driver to run the valve directly from the PC, differing pulsing schemes could be implemented and quickly trialled. The effect of pulsing the inlet and outlet at the same time could be investigated, the driver coding is shown in Appendix D-3.

## 5.6 Rebuilding of the Circuit Board

The work on the valve was based on the findings of Spellman [49]. The valve's circuitry had to be rebuilt using a basic design which closely followed Spellman's design, Figure 5-7 and Appendix D-4 contain diagrams of the new circuit. The drivers were removed from the bread board and relocated on a separate piece of circuit board and the opto-couplers were also wired into a piece of circuit board. The diodes were left on the bread-board and a strain gauge transducer was added.

The design of the circuitry is in four sections, as shown in Figure 5-7.

Section 1. Contains the driver for valve one. This uses an opto-coupler to provide an isolated switching device. For turning the supply voltage on and off.

Section 2. Is the driving circuitry for valve two and is identical to section one.

Section 3. Is the feedback circuitry from the strain gauges. These produce a signal to indicate the pressure the system is operating at.

Section 4. Is the feedback circuitry from the potentiometer. This provides a setpoint for the valve to track

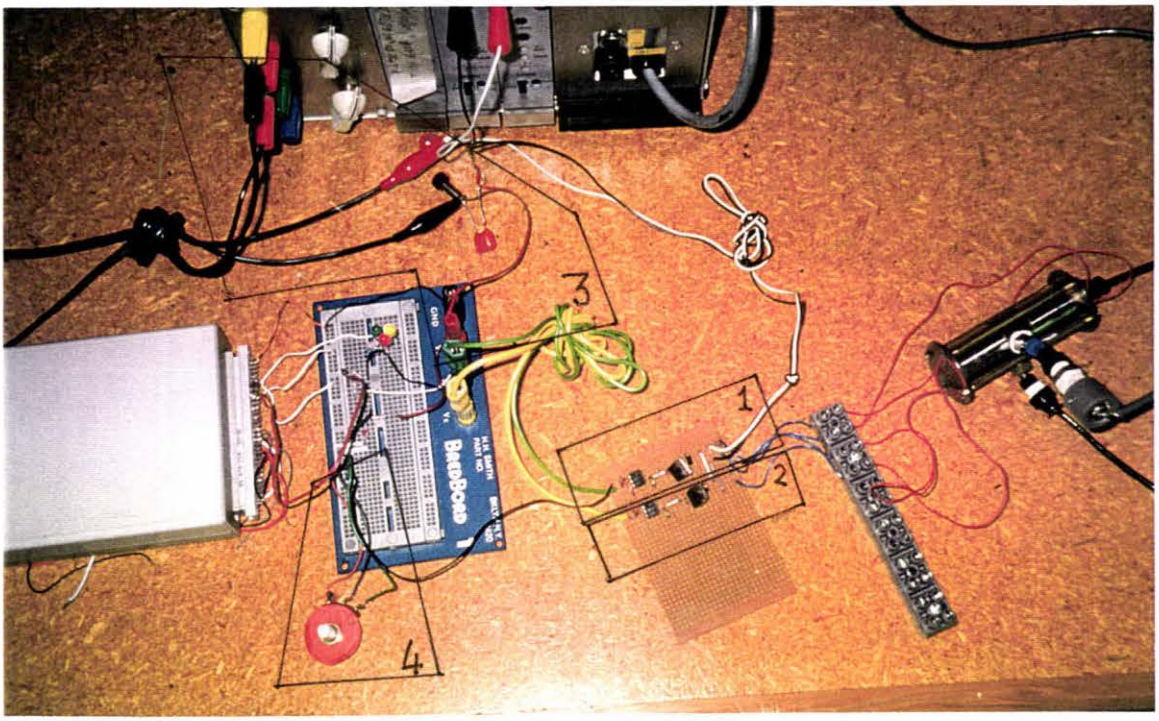


**Figure 5-7 Valve circuitry.**

## 5.7 Algorithm Development

### 5.7.1 Two Position Controller

A controller medium was required to control the servo-pneumatic valve. The Phillip's 80C552 single-chip 8-bit micro-controller was chosen for the job. It incorporates features such as 10 bit analogue to digital conversion with 8 multiplexed analogue inputs, in addition to the standard features of the 80C552 family to which it belongs.

The initial algorithm developed by Spellmen [49] was tested on this platform. The initial algorithm worked on the principle of dividing the valve into two modes of operation, a scheme known as two position control. The error signal in Spellmans algorithm is used to change between the two modes.

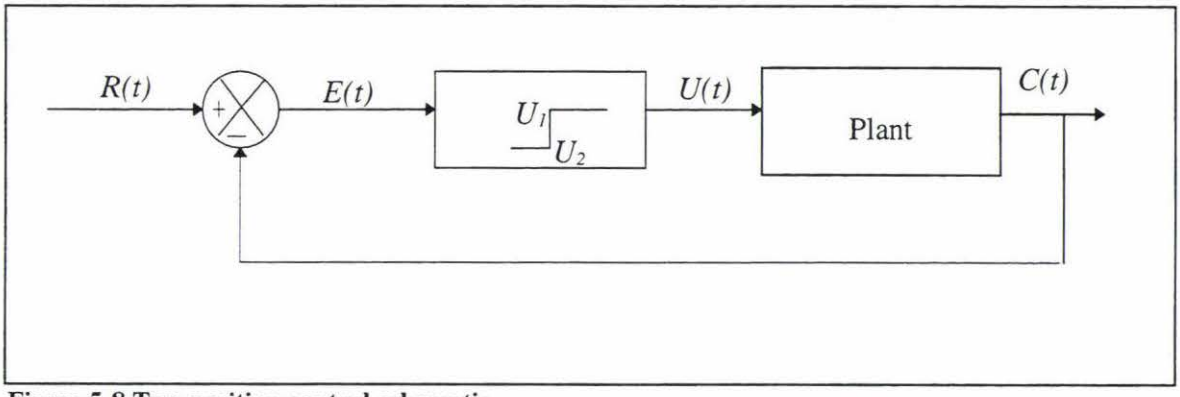


**Figure 5-8 Two position control schematic.**
*U(t)* is the output signal from the controller.
*R(t)* is the reference inputs.
*C(t)* is the system outputs.
*E(t)* is the actuating error.

The rational behind this sort of algorithm is that if the switching is fast enough, then the amount of air added will be in small enough increments to closely follow the set-point.

In two-position control, the signal remains at either a maximum or minimum value, depending on whether the actuating error signal is positive or negative, so that

$$U(t)=U_1 \quad \text{for } E(t)>0$$
$$=U_2 \quad \text{for } E(t)<0$$

where $U_1$ and $U_2$ are constant amounts of voltage. The minimum value is usually either zero or $-U_1$. Two position controllers are generally used in electrical devices and widely used as controllers for electric solenoid-operated valves.

The range through which the actuating error signal must move before the switching occurs is called the differential gap. A graphical representation of the differential gap is presented in Figure 5-9. The micro-controller algorithm used is shown in Figure 5-10 and the program coding Appendix D-3.

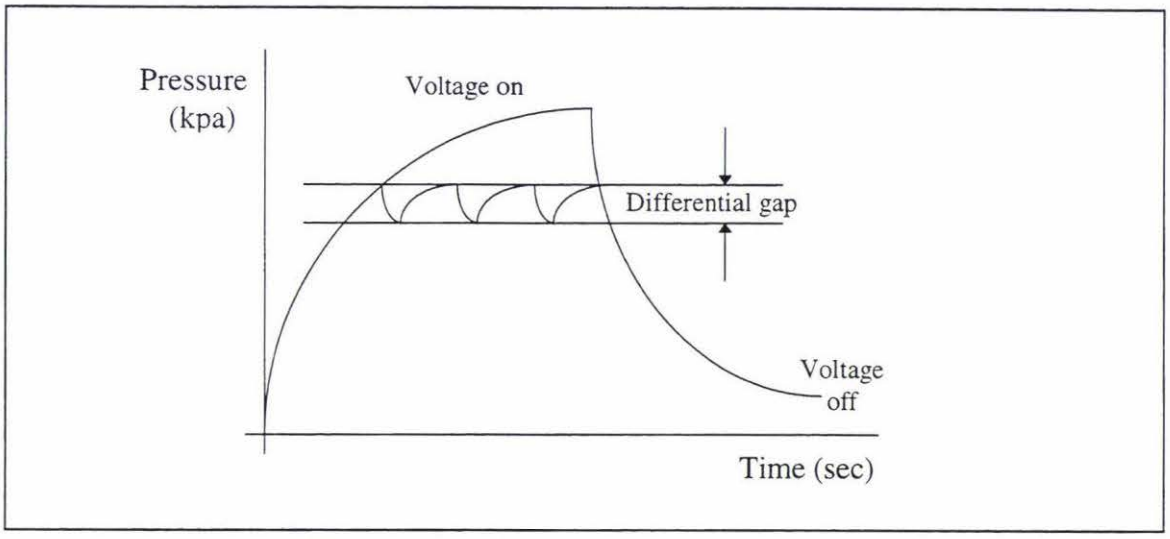


**Figure 5-9 Graph of two position control action.**

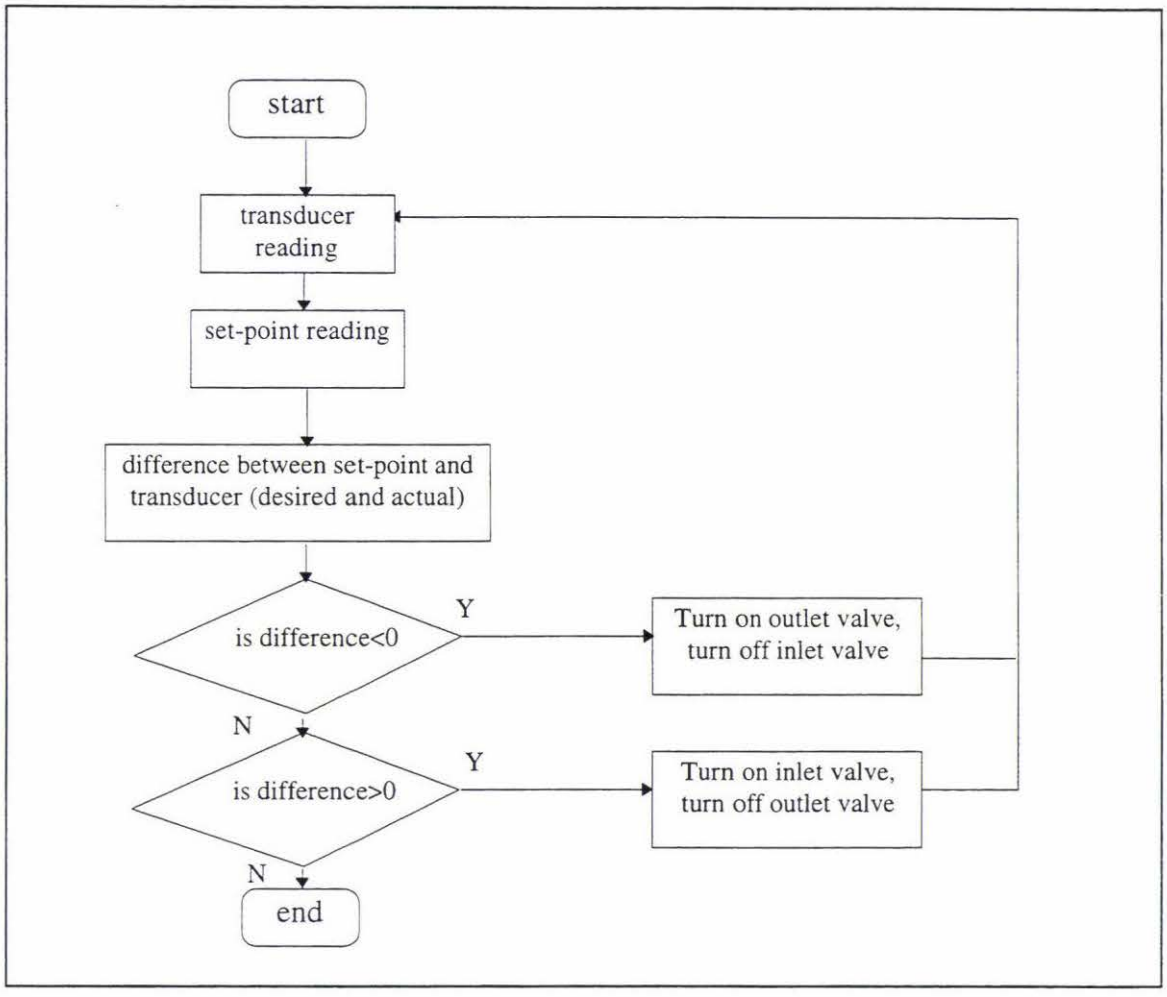


**Figure 5-10 Flow chart for micro controller implementation of a two position controller.**

### 5.7.2 Pulse Width Modulation of the Inlet Only

A pulse width modulation algorithm was implemented in accordance with the recommendations made by Spellman [49]. This technique gradually inflates the muscle by applying air in short bursts over long periods of time.

Proportional control of the pulse width modulation algorithm was then investigated. The combination of pulse width modulation and proportional control was expected to provide greater accuracy than just pulse width modulation on its own. The proportional controller decreases the period of the bursts of air as the desired pressure is approached. This was expected to cause the desired pressure to be achieved gradually.

The pulse width modulation algorithm utilises three parameters, $t_{on}$, the period the air bursts the muscle for; $t_{off}$, the period of time during which air is not applied to the muscle and $t_{fill}$ is the time required to inflate the muscle to its maximum capacity. The flow chart for the micro-controller implementation of the inlet only pulse width modulation algorithm is shown in Figure 5-11 with the program coding appendix D-3.

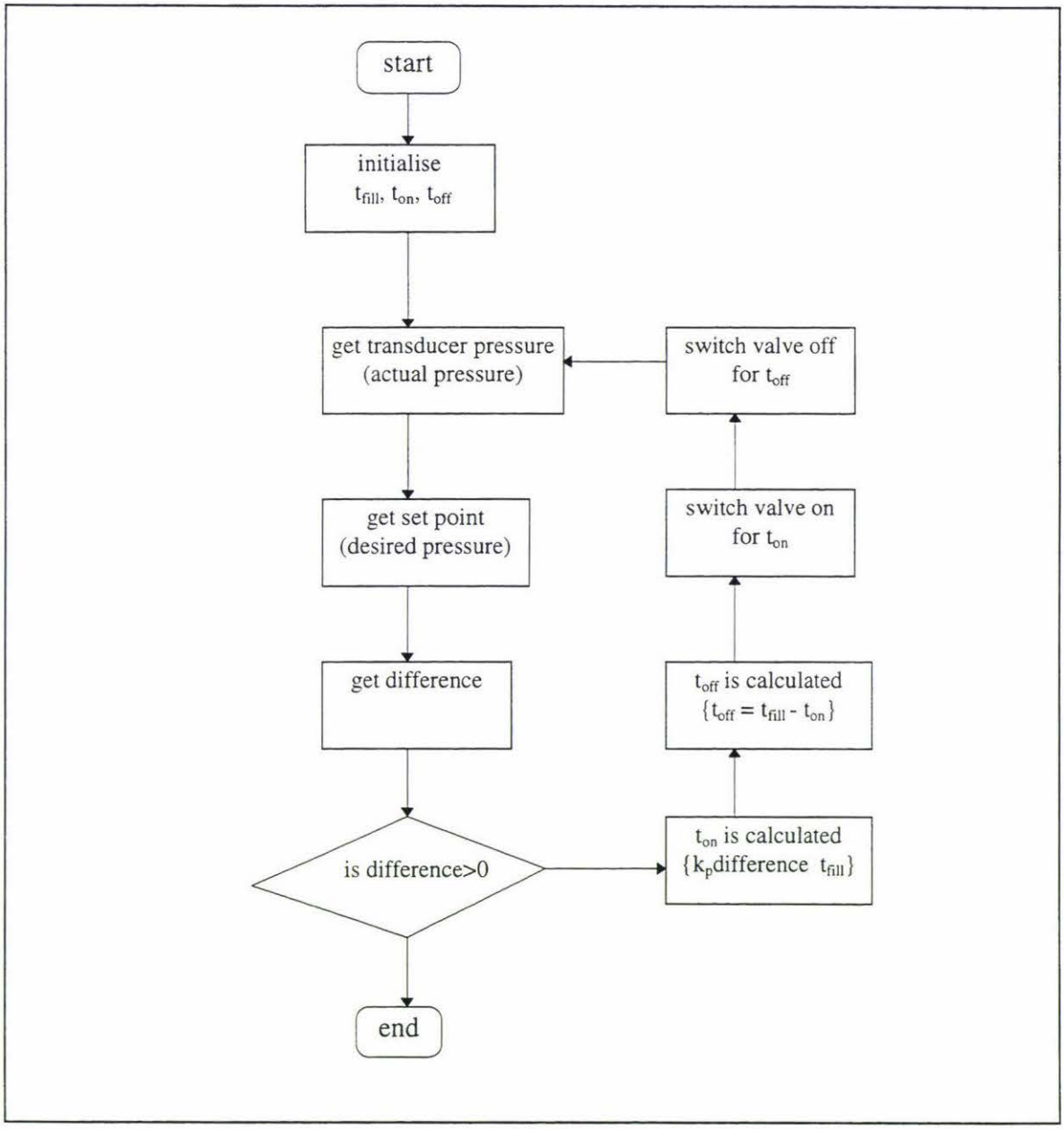


**Figure 5-11 Pulse width modulation of the inlet only.**

### 5.7.3 Hybrid Pulse Width Modulation of the Inlet and the Outlet

The initial pulse width modulation algorithm controlled only the inlet valve. This was because of the assumption that the system had a certain amount of natural damping. This natural damping of the system could be used to remove any excess of air from the system. An alternative algorithm that increased the rate of air loss was developed which used pulse width modulation of both the inlet and outlet. The flow chart for this algorithm is shown in Figure 5-12 with the program coding appendix D-3.

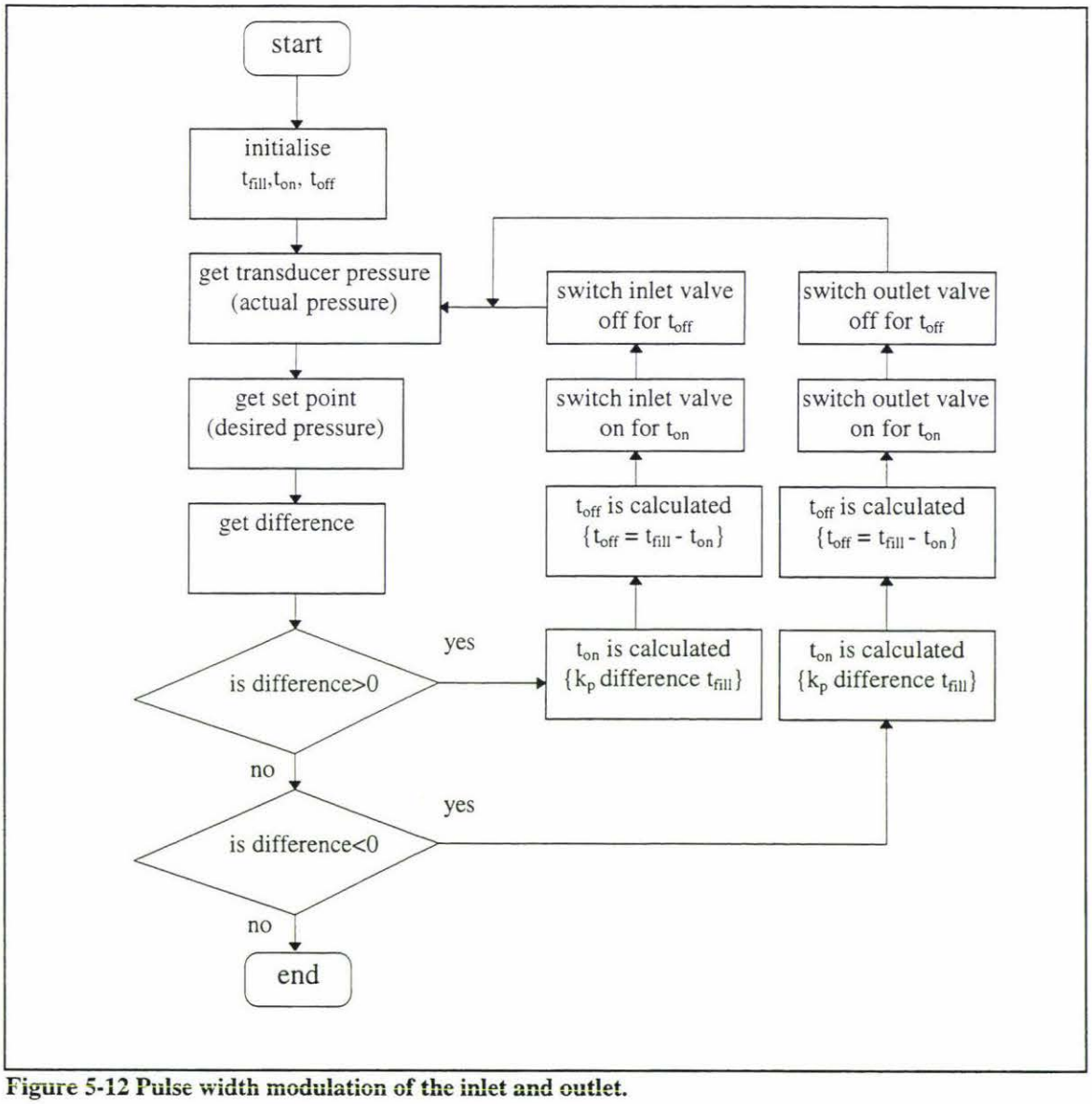


**Figure 5-12 Pulse width modulation of the inlet and outlet.**

### 5.7.4 Sliding Mode Control

In sliding mode control, the error (e) and the rate of change of the error ($e^{\bullet}$) between the set point and the actual pressure are used to determine what kind of control scheme should be used.

The parameters e and $e^{\bullet}$ identify the boundary between control regions; in each region the controllers response is defined by a particular set of piece wise equations.

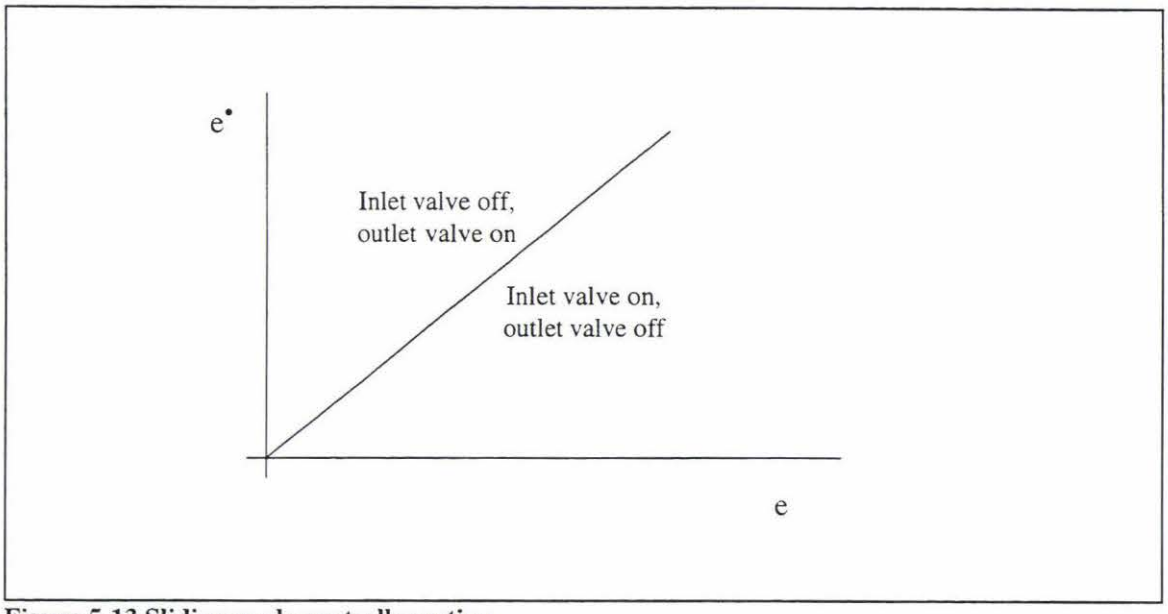


**Figure 5-13 Sliding mode controller action.**

This control scheme provides both the ability to track a set point and the ability to control the rate at which it approaches the set point. This is known as position and velocity control. This provides the ability to control the movement speed of the actuator and hence the speed of the link mechanism. The flow chart is shown in Figure 5-14 with the program coding Appendix D-3.

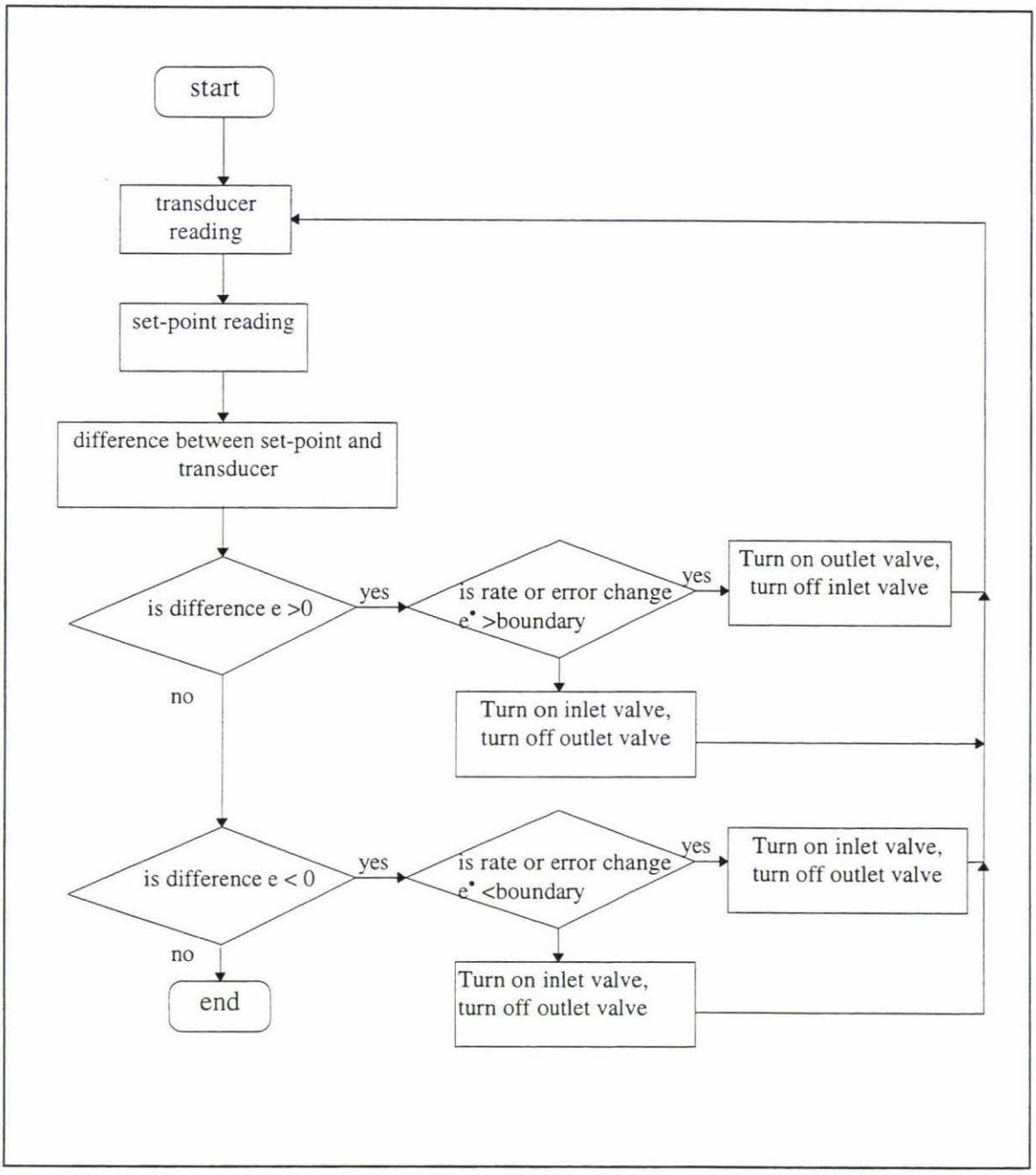


**Figure 5-14 Sliding mode controller flow chart.**

## 5.8 Comparison of Control Schemes

The two positional controller was tested on the muscle first. The muscle was observed to move wildly and it exhibited considerable overshoot, as also observed by Spellman. This indicated that the algorithm was not accurately controlling the muscle.

The second algorithm which used pulse width modulation on the inlet only (section 5.8) caused the muscle to oscillate even more wildly than the two-position controller. This was attributed to too much air entering the system causing excessive overshoot. This also suggests that the response of the system is too great.

The next algorithm used pulse width modulation of both the inlet and outlet, section 5.9. The algorithm was still showing large oscillations but the response was quicker. The oscillations were still too great to be of any use for a robotics application.

The sliding mode controller (section 5.10) proved to be the most stable of the control schemes trialled. However this scheme, while being better than the others tested, did not completely prevent the muscle from oscillating about its set point. The oscillations were too great for high precision robotics but the performance of the controller was good enough to prove the feasibility of the concept.

The oscillation in all the schemes used so far is thought to be the result of excessive amounts of air entering the system. This is due to the resolution of the system being inadequate and could be rectified by reducing the amount of the air bursts entering the system.

## 5.9 Pneumatic Ram

When a pneumatic ram was used instead of a muscle, the valve appeared to control the length of the ram very well. Proximity sensors were set up and a short micro-controller program was written to move the ram until the proximity sensors were triggered. It then held its position there.

## 5.10 Discussion on the Functionality of the System

The valve did not control the pressure of the muscle accurately for all cases (sections 5.7). A number of control schemes were trialled but all produced similar results.

The most significant limitation of the system are that the amount of air coming into the muscle was too large; the minimum air burst filled quarter of the muscle's volume which meant that the maximum resolution available to the system was a quarter of its length. This resulted in large oscillations about the set point.

The other problem was the slow switching time. If the valve could be switched at a faster rate then less air would come through. This would require the solenoid to be operated at a faster rate which could be achieved by modifying the system in terms of producing more magnetic force. This could be achieved by a larger stator, smaller armature and lighter weight of the armature. Unfortunately, faster switching time means more wear and tear, and ultimately a shorter product life.

## 5.11 Properties of the Valve

### 5.11.1 Switching times

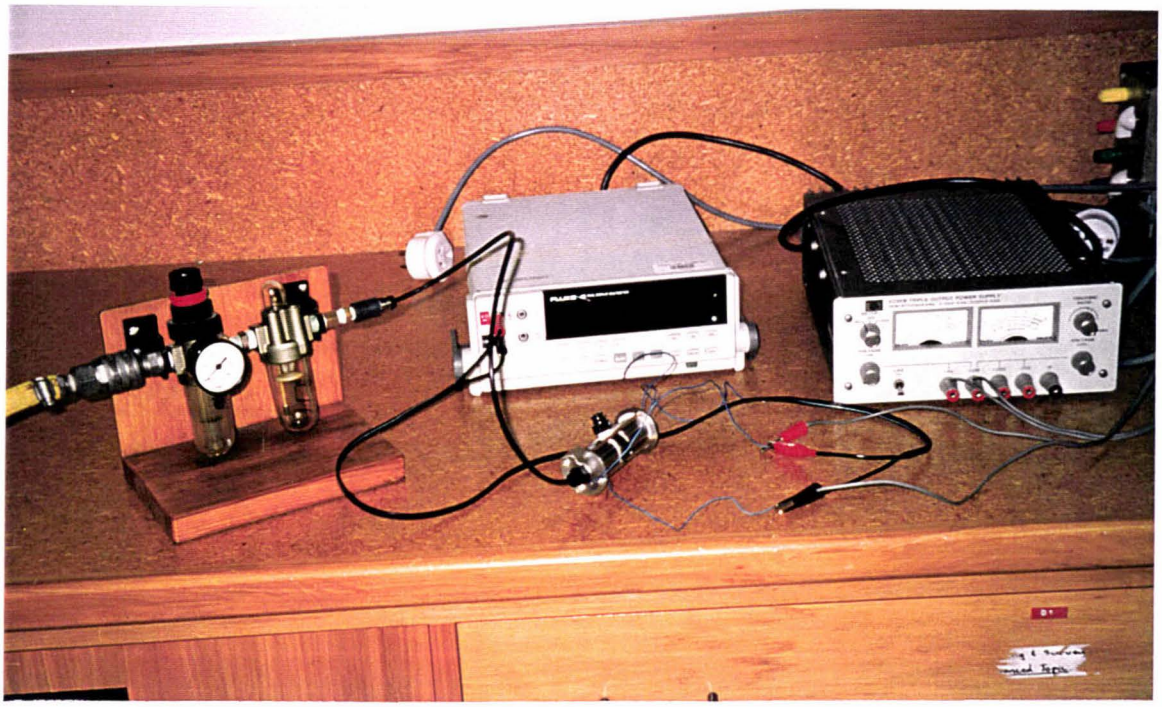

Figure 5-15 Testing of the voltage to switch the inlet on/off.

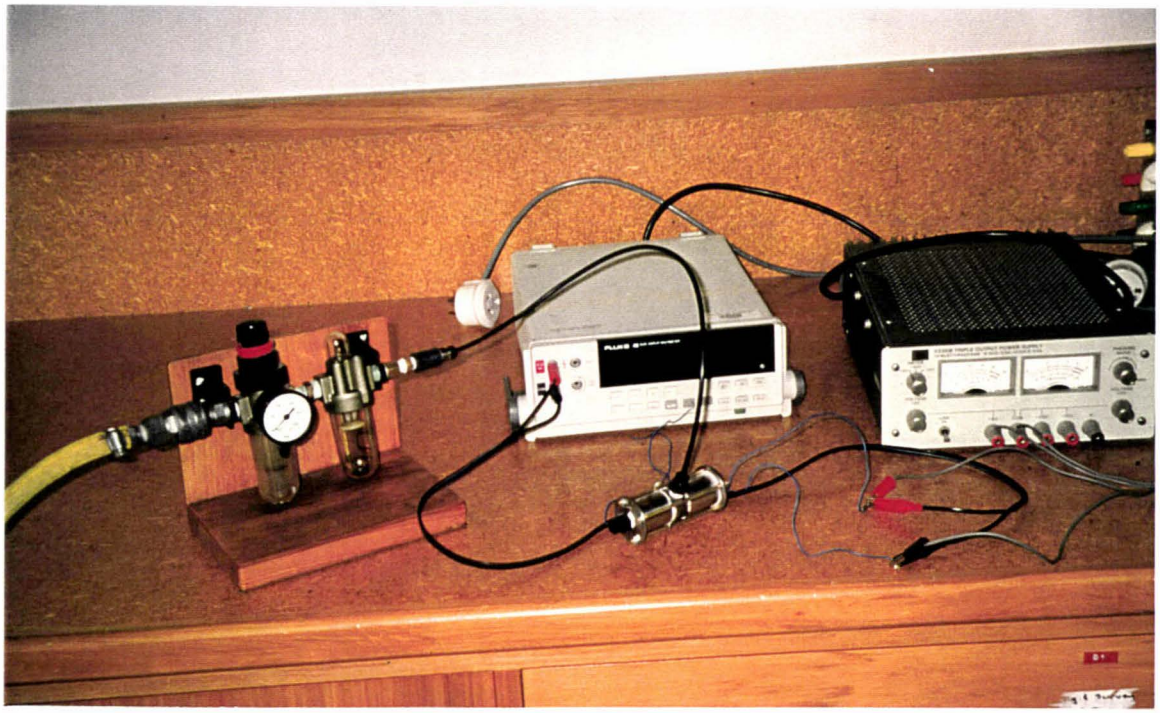

Figure 5-16 Testing of the voltage to switch the outlet on/off.

Following on from Spellman's experiments, tests were conducted to examine the properties of the modified valve. The air supply came from a compressed air source and was controlled by a pressure regulator with an analogue read-out range of 0-1000kpa in 50kpa increments. At atmospheric pressure the inlet valve required 3.5 volts to turn on and 0.8 volts to turn off. The outlet valve was similarly tested and required 2.8 volts to turn on and 0.75 volts to turn off. These experiments were conducted under ambient temperatures.

From the results shown in Figure 5-17 and Appendix D-1, table D-4, it can be seen that as the pressure in the muscle is increased, the voltage required to turn the valve on increased. This is because more force is required to open the valve against the high air pressure in the muscle.

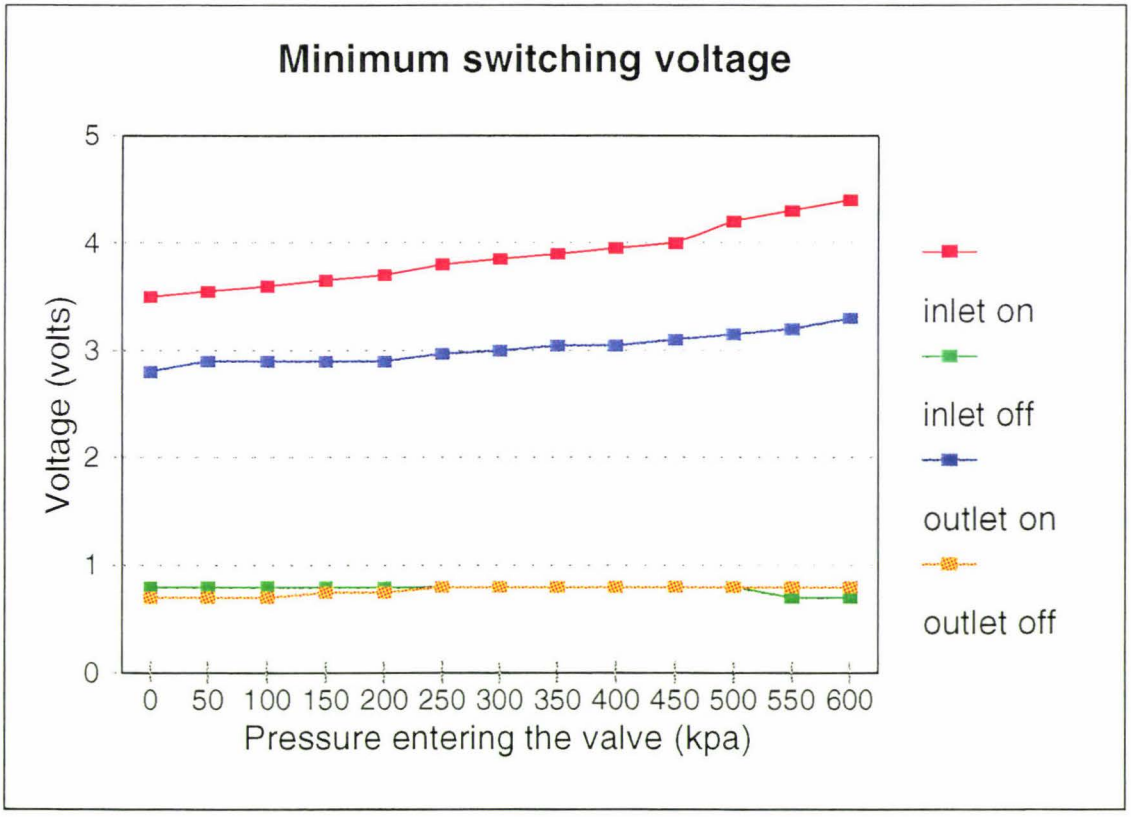


**Figure 5-17 Graph of voltages required to switch the inlet and outlet valves.**

## 5.12 Response Times

The time delay characteristic of the two valves were then investigated. A strain gauge sensor was used to measure the time delay, other devices considered were a capacitive sensor or a resistance measuring device. In prior experiments conducted by Spellman [49] a microphone was used to detect a noise signal from the air released when the valve opening. This was considered to be accurate enough to determine the properties of the valves.

Each valve was tested individually by connecting it to the pressure regulator which was run off the compressed air supply. The power supply was set at a constant 10V and connected to channel 1 of a digital oscilloscope, a Hewlett Packard 54502A, 400Mhz as shown in Figure 5-18 and Figure 5-19.

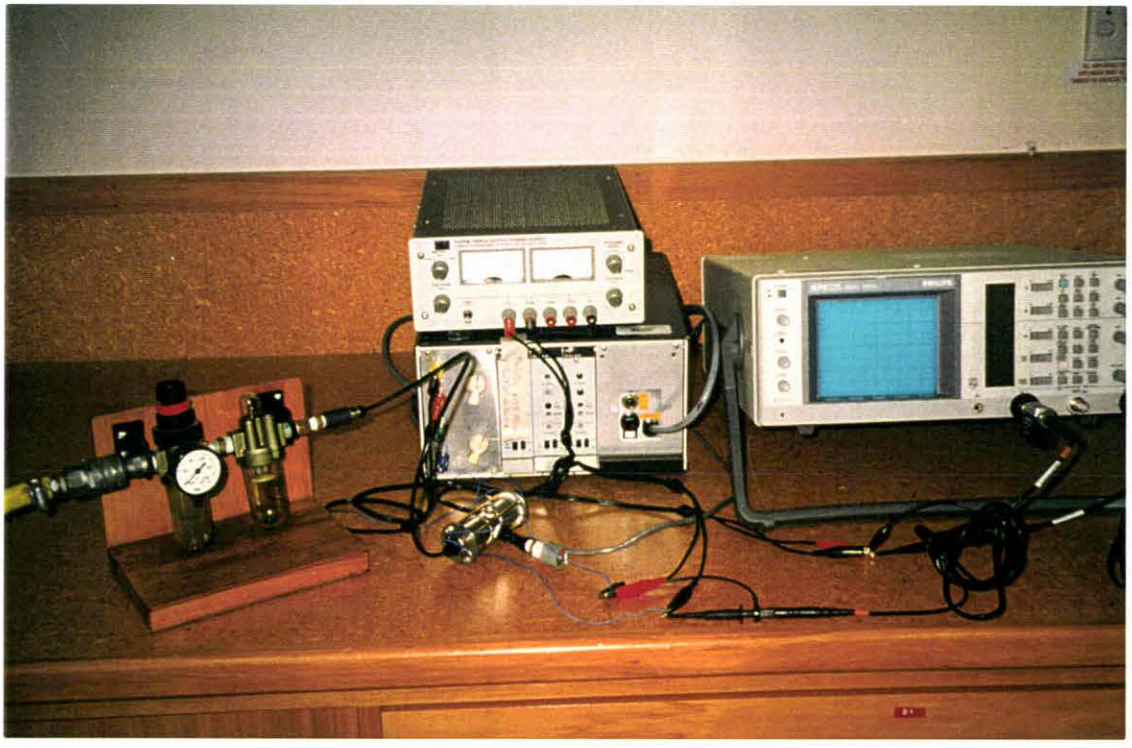

**Figure 5-18 Experimental setup to test the inlet response times.**

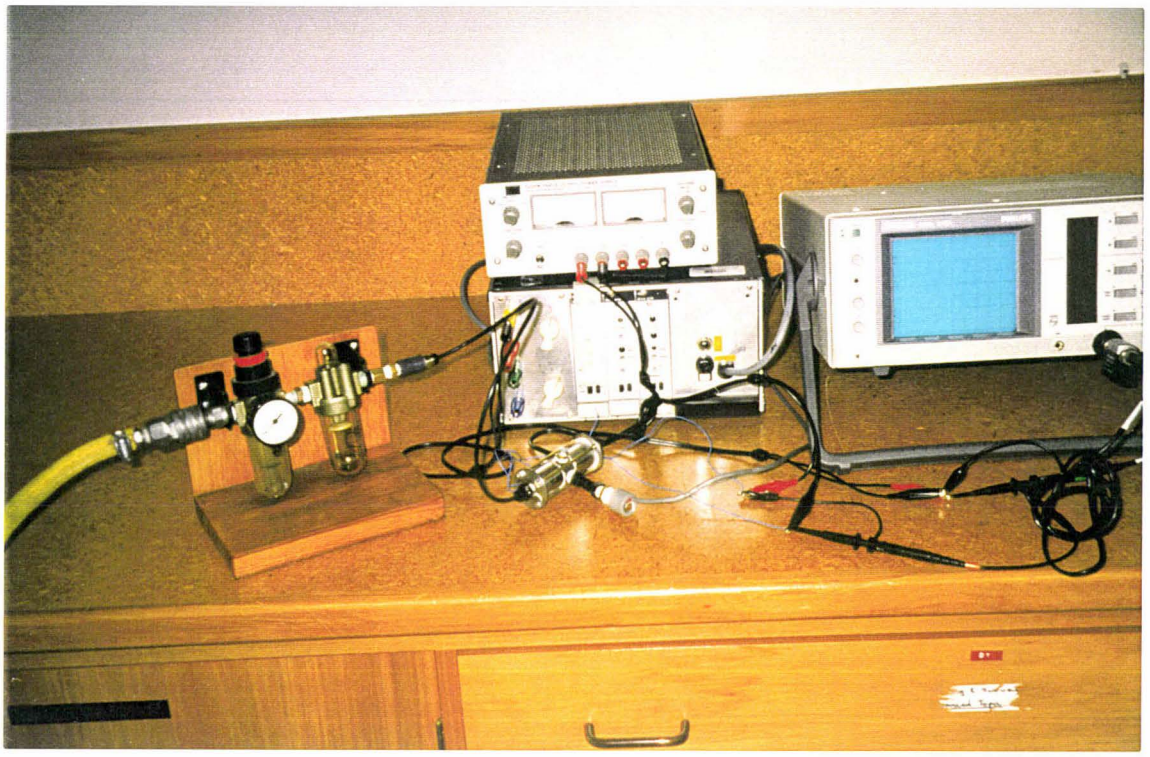

**Figure 5-19 Experimental setup to test the outlet response times.**

The valve was set in held at a stationary location. The strain gauge was placed on the outlet line 62mm from the exit valve. The velocity of air coming out was measured as 65 m/s for inlet valve, so there is a time delay of 1.02 milliseconds for the air to reach the strain gauge sensor.

The strain gauge's electrical connections were placed onto channel 2 of the oscilloscope which was arranged to detect the responses of the incoming signals. When the power was activated, the output from channel one was recorded as being high and this was nominated as the time the valve turned on.

The strain gauge system became active when the air reached it and its output could be seen on the oscilloscope display. The time delay between the power turning on and the air supply reaching the strain gauge sensor could be found from the time divisions on the oscilloscope screen as shown in Figure 5-20.

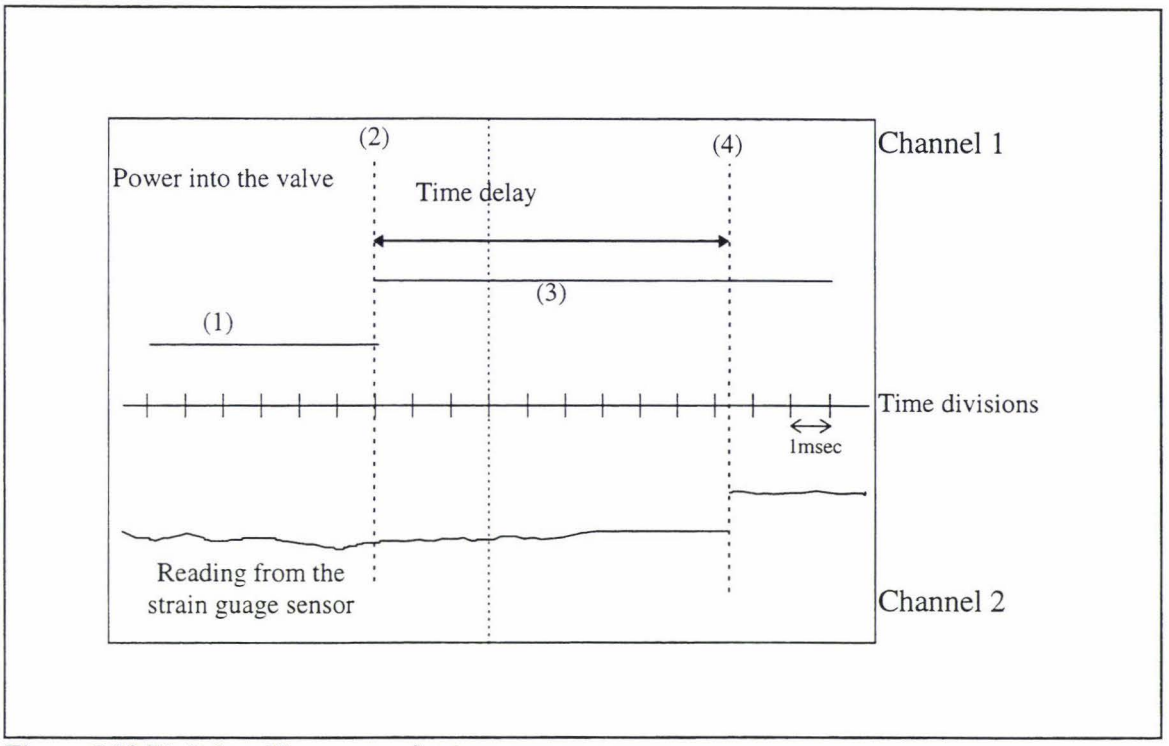


**Figure 5-20 Digital oscilloscope readout.**

(1) This is the voltage level when the valve is off.
(2) This is the time when the voltage is increases and the valve starts to turn on.
(3) This is the voltage level when the valve is turned off.
(4) This is the time when the valve has turned on.

The time delay was measured for a range of entry air pressures as shown in Figure 5-21. The voltage was held at a constant 10 volts for the experiments.

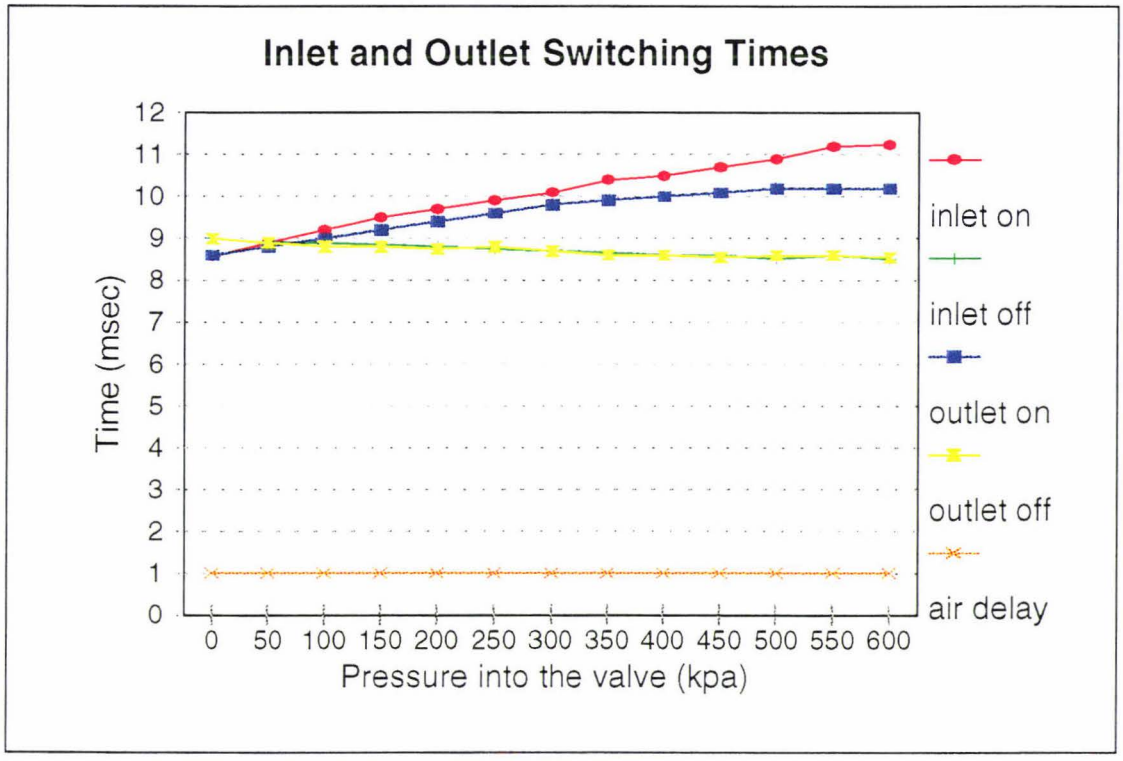


**Figure 5-21 Switching times for the valve.**

## *5.13 Results*

As can be seen from Figure 5-21, the two valves displayed quite different characteristic time delays. Both valves were able to turn on faster if a high initial value is applied, say 10 volts rather than 5 volts. The reason for this initial high voltage demand is that a larger force is required in opening the valve to overcome the inertia of the armature then less voltage is needed to hold it open. This force compared with the voltage necessary to hold the valve open is larger. Therefore, to open the valve at a higher voltage is required.

To close the valve the power supply is simply removed, and the delay time then depends upon the spring force and the force of the air, which are constant. This explains the smaller deviations in the delay times for closing the valves. Results from these experiments are shown in Appendix D-1, Tables D-1 to D-3.

Other results from the experiments showed the inlet valve had much less deviation in its delay values with 10 V than the outlet valve. However, the outlet valve showed faster response times. It is desirable in this system that the delay times be minimised and the deviation between turning on the valve and turning it off also be kept to a minimum.

The response times of these valves were, considerably better than servo-pneumatic valves on the market today [55]. These commercial valves have typical delay times around 20 milliseconds and greater. This is approximately twice as slow as the valves tested here.

Another result is the decrease in delay times that can be seen when the pressure entering the valve is decreased. For the inlet valve the air pressure going into the valve will be at a constant value of 550 +/- 50kpa, that of the air supply, but for the outlet valve the pressures will vary according to the pressure values in the air muscle.

Overall, the response times of these valves was superb and with modern manufacturing techniques the variation between valves could be reduced.

## 5.14 Modelling the Valve

It was decided to use the fanning equation to develop a model of the valve. The speed at which the air left the valve was measured using a flow meter. The pressure into the valve was varied and the air out of the valve was recorded. This is shown in Figure 5-22, with the experimental data in Appendix D-2, Table D-5 and Full-regression D-1.

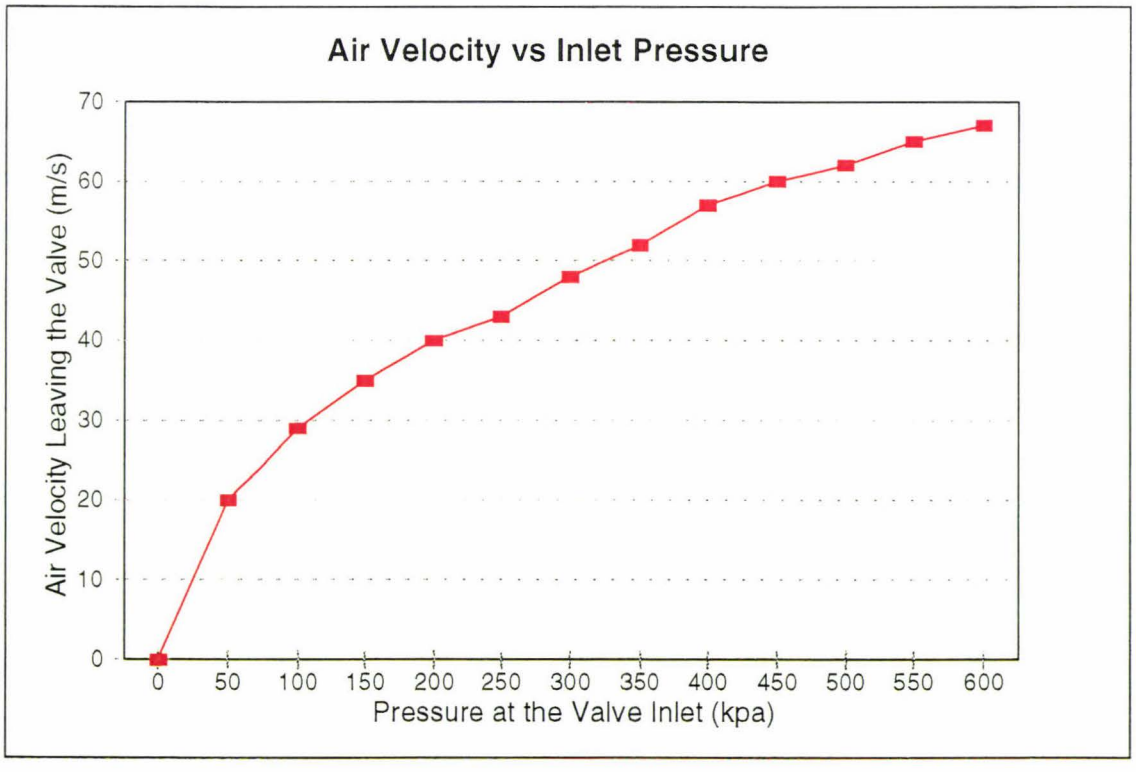


**Figure 5-22 Graph of air velocity vs Pressure.**

A regression was done using pressure as a predictor to optimise the Fanning equation. The optimised equation was found to be

**Equation Describing the Valves Behaviour**

$$P = -5.29 + 0.131\,V^2 \qquad \textbf{Equation 5-9}$$

*where* $P$ is the pressure into the valve
$V$ is the velocity of air out of the valve.

## 5.15 Summary and Conclusions

A prototype valve built by the Production Technology Department at Massey University. This valve was built to supply air to pneumatic actuators. The initial prototype had the problem of leaking air and passing too much air to be useful for controlling the pneumatic muscle.

Modifications were made to the valve to overcome these problems. A restriction was placed in the orifice to reduce the diameter of air flowing through the valve and a nylon seat was made for the armature to reduce the air leaks within the valve. The modifications on the valve resulted in the sealing of air leaks from the valve and reducing the air flow through the valve. This improved the valves performance.

Tests were then conducted on the valve to characterise the valves operation. A preliminary model describing the valve was then formed from these test results. This model can be used in a simulation of the valves operation in a robot system and in the design of a controller for the robot system.

A variety of control schemes were trialled on the valve system. These schemes were two-position control, sliding model control and a proportionally controlled pulse width modulation scheme. All of these schemes proved to be successful in controlling the pressure of a large commercial ram, but unsuccessful in controlling the pneumatic muscle. This has been attributed to too much air entering the valve, and then the pneumatic muscle. This can be overcome by making further modifications to the valve to reduce the orifice size, which would reduce the flow of air in the valve and into muscle and making the valve switch at a faster rate.

# 6. Conclusions and Further work

## 6.1 Research Content

The main thrust of my research has been on the design of models for use in a controller for the robotic system under investigation. The models for the system are in three parts.

- Models of the robot structure.
- Models of the pneumatic muscle applying force to the link structure.
- Models of the valve supplying air to the pneumatic muscles.

In addition the modelling development work on the prototype valve was under taken. A variety of controllers were then applied to the valve muscle system and tested. A novel pneumatic actuator which provides a rotary action was developed and tested. A model was then developed for this.

## 6.2 Conclusions

Preliminary models for the link structure have been developed. These describe the forces and torque's required to bring about changes in position, velocity and the acceleration of the link members. Two implementations of models for the link structure were developed.

The Lagrange-Euler algorithm was implemented in Maple, a mathematical manipulation package, this provides an explicit set of equations of the robot structure. The equations are in a form where they can be algebraically manipulated, partially differentiated and then arranged into state space form without the use of a numerical technique.

The other implementation of the Lagrange-Euler algorithm was in Matlab, a mathematical package, this implementation provided a set of equations which could not be partially differentiated and arranged into state space form for use in controller design without the use of a numerical technique.

The equations generated by the Maple implementation had a significant advantage, as numerical techniques can have robustness and computation efficiency problems. These equations can then be used for controller design purposes and for a simulation of the system.

Models of the pneumatic muscles were investigated. Two analytical models were obtained from available literature, they were based on the work of Caldwell et al and the Chow and Hannaford. Statistical models based on tests on the pneumatic muscle were developed. These were a black box model, where regression was used to optimise a set of predictors to the test results, and a quasi-static model, where observations and assumptions were made to determine model predictors which were optimise using regression of the test results.

The analytical models were compared against experimental results obtained from the muscle and it was found that these models do not adequately describe the muscles behaviour. This was concluded to be due to these models not taking into account dead space within the system and temperature effects. The quasi static model was designed to take into account dead space within the system and provided better performance than the analytical models. The black box regression model took into account dead space and temperature effects and provided the most accurate description of the system.

Hysteresis was investigated in the system, it was found that hysteresis was small enough to be excluded from the models of the muscle. The small hysteresis present is due to the design of the muscles being used. These muscles have been made of materials which produces less hysteresis than in other designs of pneumatic muscles.

A set of models for the pneumatic muscle are now available which are in a form where they can be implemented in a simulation of the system and for the design of a controller.

A prototype valve built by the Production Technology Department at Massey University was modified, tested and then modelled. The modifications on the valve resulted in the sealing of air leaks from the valve and reducing the air flow through the valve. This improved the valves performance. Data was then collected on the valve and the Fanning equation used to model the valves flow characteristics. A preliminary model of the valve was formed. This model can be used in a simulation of the system and in the design of a controller for the system.

A variety of control schemes were trialled on the valve muscle system. These schemes were two-position control, sliding model control and a proportionally controlled pulse width modulation scheme. All of these schemes proved to be effective in controlling the pressure of a large commercial ram, but ineffective in controlling the pneumatic muscle. This is due to the valve letting too much air into the pneumatic muscle in each burst caused by the switching time being too slow for the pneumatic muscle system and the orifice size being too large.

A novel pneumatic muscle was designed and built as part of an investigation into alternative actuation systems. This muscle provides a rotary action. An analytical model of the muscle was developed. This pneumatic muscle can be used in future robotic devices and has the advantage of being able to be used as a joint in a robotic device.

## 6.3 Future work

Further work on the robot system modelling includes-

Further development of models for the link structure. Preliminary models for the link structure have been developed. These describe the forces and torques required to bring about changes in position, velocity and the acceleration of the link members. These models are unvalidated and further work needs to be done on these;

1. Measurement of the moments of inertia for each member which are required to make the models of the link structure functional.
2. Experimental data on the link structure needs to be collected.
3. A comparison of results from the experimental data and the analytical model for the link structure.
4. Possible development of black box models if the analytical models prove to be an unreliable predictor of the links structure's behaviour.

These models need to be integrated with the models for the pneumatic muscle. Further work on the models includes;

1. Obtaining dynamic models of the pneumatic muscles response.
2. Verifying these models of the muscles response.
3. Integration of the models with this of the robot structure.

Further work on the valve requires the development of more prototype valves with modifications intended to;

1. Reduce the amount of air entering the muscle.
2. Increase the speed at which the valve switches.
3. Reduce the weight of the valve and cost of components.

4. Increase the robustness and reliability of the valve.

Once the valve is fully operational, models of the valve's response must be made which will involve;

1. Development of a static analytical model of the valves behaviour based on the orifice size, air flow properties, magnetic properties of the solenoid.
2. Conducting experiments to test this model.
3. A comparison of results to validate the accuracy of the analytical model.
4. Possible development of black box models.
5. Analytical models then need to be developed to describe the valves dynamic response. They can be formulated from the static models.
6. Conducting experiments to test the dynamic model.

The last phase of the modelling of the system is to integrate the model for the link structure and the combined models of the valve/muscle actuation system. This requires-

1. Combining the model for the valve, muscle and link structure to form a new model for the whole system.
2. Obtaining experimental data for the whole system which considers the static and dynamic properties of the whole system.
3. This experimental data obtained from the system then needs to be compared with the models describing how system performs.
4. Analysis on how well the models perform then needs to be undertaken and a decision on the models accuracy needs to be made.
5. If the models of the full system prove to be inaccurate then corrections to these models need to be initiated, this may incorporate a black box approach.

Controller strategies then need to be investigated. To date the work on the controller aspect of the project includes the development of two postition controller, a proportionally controlled pulse width modulation algorithm and a sliding model controller for the valve/muscle system. All of these controllers are untuned at this stage.

In order to obtain a fully functional system with a tuned controller, there needs to be a fully simulated system. The settling times need to be determined for the whole system and controller values developed based on this. The steps are;

1. Develop a simulation of the whole system.
2. Obtain the settling time and response times of the full system.
3. Generate controller values which will tune the system based on these response times.
4. Implement the system with the tuned controller.

This will conclude development of a primitive lower level controller. The nature of the system indicated that the system is coupled and as a result the tuned classical controller may be insufficient to make the system fully functional. It may prove an unsatisfactory solution to the control problem. Further analysis may be required which may involve-

1. Implementation of neural network control based on the simulated system.
2. Implementation of fuzzy logic based control.
3. Implementation of an adaptive controller.

This will involve looking at multiple-input multiple-output controller strategies.

Future work on the rotary pneumatic muscle will include;

1. Replacing the nylon fibres constraining the rotary pneumatic muscle with non-stretching fibres. Steel filament wire with a nylon coating has been purchased and these should be trialled in the rotary pneumatic actuator to see if they improve the actuator's performance.

2. Experiments should then be conducted on the rotary actuator to verify the analytical models developed for the muscle. If these models do not adequately describe the actuator's behaviour, then quasi-static models and black box models should be investigated and developed.

## 6.4 Contribution of Research

The work from the research requirements of the Masters degree has contributed to the furtherment of scientific knowledge in the following areas;

1. New implementations of models of the dynamic interactions of robot structures are available in Maple.

2. New models of the behaviour of the pneumatic muscle are available, this has lead to an increased understanding of the behaviour of the pneumatic muscle.

3. Valves have been developed to actuate the muscle and models for them are available. This has increased the understanding of the valve system for the robot structure under development.

4. A novel pneumatic muscle has been developed. An analysical model has been developed for the rotary pneumatic muscle. This provides an alternative form of robot actuation and can be used in further development of robotic devices.

# References


[1] M. T. Harris and S. Nahavandi, 31st August and 1st September 1995, *The design and development of an intelligent robotic hand*, Proceedings of the Second New Zealand Postgraduate Conference for Engineering and Technology Students. pp.119-124.

[2] Kumpati. S. Narendra, 1986, *Adaptive learning systems, theory and applications*, Plenum Press, New York, London. pp.175-194.

[3] Mikell P. Groover, 1980, *Automation, production systems and computer aided manufacturing*, Prentice Hall inc, Englewood Cliffs, New Jersey 07632, part 3.

[4] Peter Harriott, 1964, *Process control*, McGraw-Hill Book Company, New York, London. pp.194-359.

[5] Katsuhiko Ogata, 1990, *Modern Control Engineering*, Second Edition, Prentice Hall, Englewood Cliffs, New Jersey 07632.

[6] Yoram Koren,1985, *Robotics for engineers*, McGraw-Hill Book Company, New York, London. pp.2-10.

[7] D J. Todd, 1986, *Fundamentals of robot technology*, Kogan Page, Pentonville Road, London. pp.205-213.

[8] Y. Xu, J. M. Hollerbach and D. Ma, Feburary 1995, *A non-linear PD controller for force and contact transient control*, IEEE Control Systems 0272-1708/95.

[9] L S. Wilfing, J. T. Wen and S H. Murphy, 1994, *Integral force control with robustness enhancement*, IEEE Control Systems 02072-1708/94.

[10] Dale A. Lawrence and Jim D. Chapel, 1994, *Quantitative control of manipulator/task interaction*, IEEE Control Systems 0272-1708/94.

[11] Shagun Ma, Shigeo Hirose and Hiroshi Yoshinada, 1993, Design and experiments for a coupled tendon driven manipulator, IEEE Control Systems 02721708/93.

[12] T. J. Tarn, A. K. Bejczy, G. T. Marth and A. K. Ramodarai, 1993, Performance comparison of four manipulator servo schemes, IEEE Control Systems 02721708/93.

[13] Harry Berghuis and Henk Nijmeijer, 1993, A passivity approach to controller-observer design for robots, IEEE Control Systems 1042296-95.

[14] Katsuhiko Ogata, 1990, *Modern Control Engineering*, Second Edition, Prentice Hall, Englewood Cliffs, New Jersey 07632. pp.608-610.

[15] James M. Hyde and Mark R. Crutkosky, 1994, *Controlling contact transitions*, IEEE Control Systems 02072-1708.

[16] C H. An, C H. Atkeson and J M. Hollerbach, 1986, *Experimental determination of the effects of feedforwatd control on trajectory tracking errors*, Proc. IEEE Conf, on Robotics and Automation, San Francisco. pp.55-60.

[17] Harry Berghuis, Romeo Ortega, and Henk Nijmeijer December, 1993, *A robust adaptive robot controller*, IEEE trans Robotics and Automation, vol 9 no6.

[18] Louis L. Whitcome, Alfred A. Rizza, Daniel E. Kodischek, 1993, *Comparative experiments with a new adaptive controller for robot arms*, IEEE Robotics and Automation, 1042-296x/93.

[19] Young-Tae-Lee, Hyouk-Ryeol Choi, Wan-Kyun Chung and Youngil Youm, 1994, *Stiffness control of a coupled Tendon-Driven Robot hand*, IEEE Control Systems, 0272-1708/94.

[20] Chae H. An, Christopher C. Atkeson and John M. Hollerbach, 1988, *Model based control of a robot mainipulator*, The MIT Press Cambridge, Massachuetsetts London, England.

[21] K. S. Fu, R C. Gonzalez and C S. G. Lee, 1987, *Robotics, Control, Sensing, Vision and intelligence*, McGraw-Hill Book Company, New York, London. pp.7-11.

[22] Albert Y. Zomaya, 1992, *Modelling and simulation of Robot Manipulators*, World Scientific Publishing Company, Singapore, New Jersey, Hong Kong. pp.131-169.

[23] Robert E. Parkin, 1991, *Applied Robotics Analysis*, Prentice Hall, Englewood Cliffs, New Jersey 07632. pp.285-289.

[24] Phillippe Colffet and Michel Chirouze, 1983, An introduction to robot technology, Kogan Page Ltd, London. pp.185-189.

[25] K. S. Fu, R C. Gonzalez and C S. G. Lee, 1987, *Robotics, Control, Sensing, Vision and intelligence*, McGraw-Hill Book Company, New York, London. pp.82-106.

[26] Francis N-Nagy and Andras Siegler, 1987, *Engineering Foundations of Robotics*, Prentice Hall, Englewood Cliffs, New Jersey, London, pp.222-234.

[27] Michael Brady, John M. Hollerbach, Timothy L. Johnson, Tomas Lozano-Perez and Mathew T. Masson, 1982, *Robot Motion, Planning and Control*, The MIT Press, Cambridge Massachusetts, London England. pp.51-66.

[28] Tsuneo Yoshikawa, 1988, *Foundations of robotics, analysis and control*, Corona Publishing Co, Japan. pp.83-123.

[29] Robert J Schilling, 1990, *Fundamentals of robotics*, Prentice-Hall, Englewood Cliffs, New Jersey, 07632. pp.205-227.

[30] Anthony C. McDonald, 1988, *Robot Technology*, Prentice Hall, Englewood Cliffs, New Jersey, 07632. pp.288-290.

[31] Gerry B. Andeen, 1988, *The Robot Design Hand Book*, McGraw-Hill Book Company, New York.

[32] John F. Young, 1973, *Robotics*, The Butterworth Group, London. pp.42-54

[33] P. Dario, M. Bermasco, L Bernardi, and A Bicchi, 1987, *Shape Memory Alloy Actuating Module for Fine Manipulation*, IEEE Micro-robots and teleoperators workshop, Hyannis, Massachusetts.

[34] Dynalloy 1989, *Biometal Guide Book*, Dynalloy Inc, Irvine, Cal. USA.

[35] A, McKerrow, 1991, *Introduction to Robotics*, Addison-Wesley.

[36] D G. Caldwell, 1992, *Polymeric Gels: Pseudo Muscular Actuators for Variable Compliance Tendons*, IEEE/RSJ IROS '92 Conf, pp950-57, Raleigh, USA.

[37] A. Wasserman, 1990, *Size and shape changes of contractile polymers*, Pergarion Press, London.

[38] Darwin G. Caldwell, A. Razak and M. Goodwin, 1993, *Braided pneumatic muscle actuators*, IFAC Intelligent Autonomous Vehicles, Southampton, UK.

[39] Darwin G Caldwell, Gustavo A. Medrano-Cerda and Mike Goodwin, 1995, *Control of Pneumatic Actuators*, IEEE Control Systems.

[40] Ching Ping Chow and Blake Hannaford, 1994, *Static and Dyanamic properties of the McKibben Pneumatic Artificial Muscles*, IEEE Robotics and Automation 1050-4729/94.

[41] Ching Ping Chow and Blake Hannaford, Feburary 1996, *Measurement and modelling of McKibben Pneumatic Artificial Muscles*, IEEE Robotics and Automation vol 12, no 1.

[42] Ted Hasselroth, Kakali Saekar, P. Patrick van der Smagt, and Klaus Schulten, January 1994, *Neural network control of a pneumatic robot arm*, IEEE Systems on Man, Cybernetics vol 24, no 1.

[43] John F. Young, 1973, *Robotics*, The Butterworth Group, London. pp.77-88.

[44] M M. Gavrilovic and M R. Maric, 1969, *Positional servo-mechanisms activated by artificial muscles*, Medicine and Biological Engineering, 7:7-82.

[45] H F. Jr Schulte, 1961, *The characteristics of the McKibben artificial muscle, In: The Application of exturnal power in prosthetics and orthotics*, National Academy of Sciences-National Research Council, Washington D.C.

[46] K Inoue ,1988, *Rubberatuators and applications for robots*, Robotics Research, The 4th International Symposium, Bolles R, Roth B (eds). MIT Pres Cambridge, Massachusetts.

[47] Bruce W. Char, Keith O. Geddes, Gaston H. Monagan and Stephen M. Watt, 1990, *Maple-A Tutorial Introduction to Maple*, 3rd edition, Waterloo Maple Publishing.

[48] J M. Winters, 1990, *Hill-Based muscle models: a system design perspective, In: Multiple muscle systems*, Winters J, Woo S (eds) Springer-Verlag, New York.

[49] A M. E. Spellman, 1995, *A servo pneumatic valve to control air muscles*, Department of Production Technology, Massey University, Palmerston North, New Zealand.

[50] R C. Whitehouse, *The valve and actuator's manual*, Eur. Ing., published by Mechanical Engineering Publications Limited, London.

[51] F. A. Holland, 1973, *Fluid flow*, Edward Arnold (publishers) Ltd.

[52] William Edward Honey, 1993, *Robo-sim Users Guide*, Sun Teq Engineering, inc. Albuquerue, NM 87108-3204.

[53] Clive Moler, John Little, Steve Bangert, 1988, *Pro-Matlab*, The Mathworks, Inc.

[54] *Shadow Robot Project*, INL 357 Liverpool Road London, Technology enhancement programme, Design and Technology. pp.20-21.

[55] Master Pneumatic-Detroit Inc, *Product Information*, 6701-18 Mile Road, Stering Heights, Ph 313 254 1000.

[56] Mark Vivino, 12/22/93, *NIH user guide*, NIH image Devision of computer research, 310 496 9344.

[57] Mini-tab Inc, July 1994, *Mini-tab reference manual*, 3081 Enterprise Drive, State College, P.A. 16801-3008 USA, Ph 814 238 3280, ISBN 0-925636-22-3, Printed in USA.

# Appendix

This page has been printed in a different colour to differentiate the appendix from the main document to allow for easier appendix identification.

# Appendix A Dynamic kinematic modelling of the structure

## A-1. Maple programs to produce the dynamic interactions of the link structure

**Maple program to produce the gravity components**
These programs were implemented in Maple, a mathematical modelling package.

```
• with(linalg):#program by Nigel Yee this program produces the interactions of
#the link structures gravity components
chnge:=array([[0,-1,0,0],[1,0,0,0],[0,0,0,0],[0,0,0,0]]);

h(1):=array([[m(1)*((l1)^2)/3,0,0,-m(1)*(l1)/2],[0,0,0,0],[0,0,0,0],[-0.5*m(1)*l1,0,0,m(1)]]);

h(2):=array([[m(2)*((l2)^2)/3,0,0,-m(2)*l2*1/2],[0,0,0,0],[0,0,0,0],[-0.5*m(2)*l2,0,0,m(2)]]);

h(3):=array([[m(3)*((l3)^2)/3,0,0,-m(3)*l3*1/2],[0,0,0,0],[0,0,0,0],[-0.5*m(3)*l3,0,0,m(3)]]);

t(1):=array([[cos(a),-sin(a),0,l1*cos(a)],[sin(a),cos(a),0,l1*sin(a)],[0,0,1,0],[0,0,0,1]]);

t(2):=array([[cos(b),-sin(b),0,l2*cos(b)],[sin(b),cos(b),0,l2*sin(b)],[0,0,1,0],[0,0,0,1]]);

t(3):=array([[cos(c),-sin(c),0,l3*cos(c)],[sin(c),cos(c),0,l3*sin(c)],[0,0,1,0],[0,0,0,1]]);

g:=array([[0,-g,0,0]]);

r(1):=array([[-(l1)/2],[0],[0],[1]]);
r(2):=array([[-(l2)/2],[0],[0],[1]]);
r(3):=array([[-(l3)/2],[0],[0],[1]]);

#m11 term 3 link manipulator

• n:= 3;
ii:=1;j:=1;#in the gravity term because the term is transposed for the first row the i term varies to change the
column the j term indicates the row term the i term indicates the column

for i from ii by 1 to n do
old(i):=0;

k:=i;tr_sum:=0;

for loop_sum from k by 1 to n do #k loop to check how many trace terms to have


t_totj:=array([[1,0,0,0],[0,1,0,0],[0,0,1,0],[0,0,0,1]]);

t_toti:=array([[1,0,0,0],[0,1,0,0],[0,0,1,0],[0,0,0,1]]);

for first_part from 1 by 1 to (i-1) do # first u term is j----------

t_tot1:=evalm(t_totj &* t(first_part)); #first part of the a matrix
t_totj:=t_tot1;#dummy summer

od;

t_tot1:=evalm(t_totj &* chnge);
t_totj:=t_tot1;#dummy summer
```

```
for last_part from i by 1 to loop_sum do

t_tot1:=evalm(t_totj &* t(last_part)); #last part of the a matrix
t_totj:=t_tot1;#dummy summer

od;
# end of the first U j term----------------------------------------------
tra:=evalm(g &* t_totj);
tra1:=evalm(tra &* r(loop_sum));
trac1:=trace(tra1);
tra:=-m(loop_sum)*trac1;
trac:=tra+tr_sum;tr_sum:=trac;od;
term(i):=trac+old(i);old(i):=term(i);od;
```

**Maple Program to produce the inertial terms**

```
• with(linalg):# program to produce the inertial components.
chnge:=array([[0,-1,0,0],[1,0,0,0],[0,0,0,0],[0,0,0,0]]);

• h(1):=array([[m(1)*((l1)^2)/3,0,0,-m(1)*(l1)*1/2],[0,0,0,0],[0,0,0,0],[-(1/2)*m(1)*l1,0,0,m(1)]]);

h(2):=array([[m(2)*((l2)^2)/3,0,0,-m(2)*l2*1/2],[0,0,0,0],[0,0,0,0],[-(1/2)*m(2)*l2,0,0,m(2)]]);

h(3):=array([[m(3)*((l3)^2)/3,0,0,-m(3)*l3*1/2],[0,0,0,0],[0,0,0,0],[-(1/2)*m(3)*l3,0,0,m(3)]]);

t(1):=array([[cos(a),-sin(a),0,l1*cos(a)],[sin(a),cos(a),0,l1*sin(a)],[0,0,1,0],[0,0,0,1]]);

t(2):=array([[cos(b),-sin(b),0,l2*cos(b)],[sin(b),cos(b),0,l2*sin(b)],[0,0,1,0],[0,0,0,1]]);

t(3):=array([[cos(c),-sin(c),0,l3*cos(c)],[sin(c),cos(c),0,l3*sin(c)],[0,0,1,0],[0,0,0,1]]);


#m11 term 3 link manipulator

• n:= 3;
#n=no of degrees in the system
ii:=1;


jj:=1;

for i from ii by 1 to n do
jj:=1;old(i):=0;
term(i):=0;
for j from jj by 1 to n do
tr_sum:=0;
k:=max(i,j);
for loop_sum from k by 1 to n do   #k loop to check how many trace terms to have

t_totj:=array([[1,0,0,0],[0,1,0,0],[0,0,1,0],[0,0,0,1]]);

t_toti:=array([[1,0,0,0],[0,1,0,0],[0,0,1,0],[0,0,0,1]]);

for first_part from 1 by 1 to (j-1) do # first u term is j-------------------------

t_tot1:=evalm(t_totj &* t(first_part)); #first part of the a matrix
t_totj:=t_tot1;#dummy summer

od;

t_tot1:=evalm(t_totj &* chnge);
t_totj:=t_tot1;#dummy summer

for last_part from j by 1 to loop_sum do

t_tot1:=evalm(t_totj &* t(last_part)); #last part of the a matrix
t_totj:=t_tot1;#dummy summer

od;
# end of the first U j term-----------------------------------------------------
for first_part from 1 by 1 to (i-1) do# second u term is i
```

```
t_tot2:=evalm(t_toti &* t(first_part)); #first part of the a matrix
t_toti:=t_tot2;#dummy summer
od;

t_tot2:=evalm(t_toti &* chnge);
t_toti:=t_tot2;#dummy summer

for last_part from i by 1 to loop_sum do

t_tot2:=evalm(t_toti &* t(last_part)); #last part of the a matrix
t_toti:=t_tot2;#dummy summer

od;

tra:=evalm(t_totj &* h(loop_sum));
tra1:=evalm(tra &* transpose(t_toti));
trac1:=trace(tra1);
trac:=trac1+tr_sum;tr_sum:=trac;od;
term(i):=trac*o((j)*kkk)+old(i);
old(i):=term(i);
od;
old(i):=term(i);
od;
```

**Maple program to produce the coriolis components**

```
• with(linalg):#program by Nigel yee this produces the coriolis interactions.
chnge:=array([[0,-1,0,0],[1,0,0,0],[0,0,0,0],[0,0,0,0]]);

• h(1):=array([[m(1)*((l1)^2)/3,0,0,-m(1)*(l1)/2],[0,0,0,0],[0,0,0,0],[-0.5*m(1)*l1,0,0,m(1)]]);

h(2):=array([[m(2)*((l2)^2)/3,0,0,-m(2)*l2*1/2],[0,0,0,0],[0,0,0,0],[-0.5*m(2)*l2,0,0,m(2)]]);

h(3):=array([[m(3)*((l3)^2)/3,0,0,-m(3)*l3*1/2],[0,0,0,0],[0,0,0,0],[-0.5*m(3)*l3,0,0,m(3)]]);

h(4):=array([[m(4)*((l4)^2)/3,0,0,-m(4)*l4*1/2],[0,0,0,0],[0,0,0,0],[-0.5*m(4)*l4,0,0,m(4)]]);

t(1):=array([[cos(a),-sin(a),0,l1*cos(a)],[sin(a),cos(a),0,l1*sin(a)],[0,0,1,0],[0,0,0,1]]);

t(2):=array([[cos(b),-sin(b),0,l2*cos(b)],[sin(b),cos(b),0,l2*sin(b)],[0,0,1,0],[0,0,0,1]]);

t(3):=array([[cos(c),-sin(c),0,l3*cos(c)],[sin(c),cos(c),0,l3*sin(c)],[0,0,1,0],[0,0,0,1]]);

t(4):=array([[cos(d),-sin(d),0,l4*cos(d)],[sin(d),cos(d),0,ld*sin(d)],[0,0,1,0],[0,0,0,1]]);
#m11 term 3 link manipulator

• n:= 3;
ii:=1;kk:=1;mm_term:=1;
for i from ii by 1 to n do #row increment counter
old(i):=0;
for k from kk by 1 to n do
for m_term from mm_term by 1 to n do #column increment counter
j1:=max(i,m_term);
j:=max(j1,k);
tr_sum:=0; #summer is set to 0 for each unique row, column term
for j_count from j by 1 to n do #main loop for individual pseudo, coriolis ter Ujkm term

t_totj:=array([[1,0,0,0],[0,1,0,0],[0,0,1,0],[0,0,0,1]]);
t_toti:=array([[1,0,0,0],[0,1,0,0],[0,0,1,0],[0,0,0,1]]);

if k > m_term # check to see if k is larger than m then identify the Ujkm scheme

then

for first_part from 1 by 1 to ((m_term)-1) do# first part of Ujkm ie 0Am-1

t_tot1:=evalm(t_totj &* t(first_part)); #first part of the a matrix
t_totj:=t_tot1;#dummy summer

od;

t_tot1:=evalm(t_totj &* chnge);# multiplies by change, this is specified by the joint type
t_totj:=t_tot1;#dummy summer

for second_part from m_term by 1 to (k-1) do #sums second part Ujkm ie  mAk-1

t_tot1:=evalm(t_totj &* t(second_part)); #mAk-1 part loop engine
t_totj:=t_tot1;#dummy summer

od;

t_tot1:=evalm(t_totj &* chnge);# multiplies by change, this is specified by the joint type
```

```
t_totj:=t_tot1;#dummy summer

for last_part from k by 1 to j_count do #sums last part Ujkm ie  kAj

t_tot1:=evalm(t_totj &* t(last_part)); #last part of the a matrix
t_totj:=t_tot1;#dummy summer

od;
else #alternative scheme for Ujmk type equation

for first_part from 1 by 1 to (k-1) do# sums first part Ujmk ie  0Ak-1

t_tot1:=evalm(t_totj &* t(first_part)); #first part of the a matrix
t_totj:=t_tot1;#dummy summer

od;

t_tot1:=evalm(t_totj &* chnge);# change matrix specified by the joint type
t_totj:=t_tot1;#dummy summer

for second_part from k by 1 to (m_term-1) do #sums second part Ujmk ie  kAm-1

t_tot1:=evalm(t_totj &* t(second_part)); #kAm-1 part loop engine
t_totj:=t_tot1;#dummy summer

od;

t_tot1:=evalm(t_totj &* chnge); # change matrix specified by the joint type
t_totj:=t_tot1;#dummy summer

for last_part from m_term by 1 to j_count do #sums last part Ujmk ie mAj

t_tot1:=evalm(t_totj &* t(last_part)); #mAj part loop engine
t_totj:=t_tot1;#dummy summer

od;
fi;#END OF THE FIRST BIG Ujkm TERM----------------------------------
# START OF THE Uji TERM-------------------------------------------
for first_part from 1 by 1 to (i-1) do #sums Uji term for 0Ai

t_tot2:=evalm(t_toti &* t(first_part)); #0Ai part of loop engine
t_toti:=t_tot2;#dummy summer
od;
t_tot2:=evalm(t_toti &* chnge); #change matrix specified by the joint type
t_toti:=t_tot2;#dummy summer

for last_part from i by 1 to j_count do #second part of Uji term ie iAj

t_tot2:=evalm(t_toti &* t(last_part)); #iAj part of loop engine
t_toti:=t_tot2;#dummy summer
#END OF Uij (second U term)-------------------------------------
od;

tra:=evalm(t_totj &* h(j_count));#Ujkm*J(mat) multiplication
tra1:=evalm(tra &* transpose(t_toti));#Ujkm*J(mat)*Uji(trans) multiplic
trac1:=trace(tra1);#does a trace
trac:=trac1+tr_sum;tr_sum:=trac;od;#sums the individual trace terms
term(i):=trac*o((k)*kkk)*o((m_term)*mmm)+old(i);old(i):=term(i);od;od;od;
```

## A-2. Equations for a two link manipulator used in testing the algorithm

$$\tau_1=[m_1 l_{g1}^2+I_1 + m_1 l_1^2 ]\vartheta''_1+[ m_2 l_1 l_{g2}^2 cos(\vartheta_2-\vartheta_1)] ]\vartheta''_1- m_2 l_1 l_{g2} cos(\vartheta_2-\vartheta_1)] \vartheta'^2_2+( m_1 l_{g1}+ m_2 l_1) g cos(\vartheta_1)$$

$$\tau_2=[m_2 l_1 l_{g2} cos(\vartheta_2-\vartheta_1)]\vartheta''_1+ [m_2 l_{g2}^2 + I_2] ]\vartheta''_2 + m_2 l_1 l_{g2} sin(\vartheta_2-\vartheta_1)] \vartheta'^2_2 + m_2 l_{g2} g cos(\vartheta_2).$$

# Appendix B Matlab implementation of the dynamic interactions of a link structure

## B-1. Matlab programs to produce the dynamic interactions of the link structure

Matlab functions, the first program produces the Coriolis interactions of the link structure. This program was written by Nigel Yee.

```
function [old]=coriolis(m,l1,l2,l3,a,b,c,g)

%works out the gravity terms input requirements are m(1), m(2)...m(n), l(1), (l(2)...l(n),a,b,c,....,n,

chnge=[0,-1,0,0;1,0,0,0;0,0,0,0;0,0,0,0];
h(1:4,1:4)=[m(1)*((l1)^2)/3,0,0,-m(1)*((l1)/2);0,0,0,0;0,0,0,0;-0.5*m(1)*l1,0,0,m(1)];

h(5:8,1:4)=[m(2)*((l2)^2)/3,0,0,-m(2)*l2*1/2;0,0,0,0;0,0,0,0;-0.5*m(2)*l2,0,0,m(2)];

h(9:12,1:4)=[m(3)*((l3)^2)/3,0,0,-m(3)*l3*1/2;0,0,0,0;0,0,0,0;-0.5*m(3)*l3,0,0,m(3)];

t(1:4,1:4)=[cos(a),-sin(a),0,l1*cos(a);sin(a),cos(a),0,l1*sin(a);0,0,1,0;0,0,0,1];

t(5:8,1:4)=[cos(b),-sin(b),0,l2*cos(b);sin(b),cos(b),0,l2*sin(b);0,0,1,0;0,0,0,1];

t(9:12,1:4)=[cos(c),-sin(c),0,l3*cos(c);sin(c),cos(c),0,l3*sin(c);0,0,1,0;0,0,0,1];


%m11 term 3 link manipulator
n= 3;
ii=1;kk=1;mm_term=1;%basic initialisation of the loop i and j parameters
old=zeros(size(n,n));

for i = ii : n        %row increment counter

for k = kk : n


for m_term =mm_term: n                    %column increment counter
j1=max(i,m_term);
j=max(j1,k);
tr_sum=0;                                 %summer is set to 0 for each unique row, column
term
        for j_count = j : n               %main loop for individual pseudo, coriolis ter Ujkm
term


        t_totj=[1,0,0,0;0,1,0,0;0,0,1,0;0,0,0,1];

        t_toti=[1,0,0,0;0,1,0,0;0,0,1,0;0,0,0,1];

                if k > m_term
                        %check to see if k is larger than m then identify the Ujkm scheme
```

```
                    for first_part =1 : ((m_term)-1) % first part of Ujkm ie 0Am-1

                    t_tot1(1:4,1:4)=t_totj *t(first_part*4-3:first_part*4,1:4);        %first part of
the a matrix
                    t_totj=t_tot1  ;                    %dummy summer
                    end

          t_tot1(1:4,1:4)=t_totj*chnge;       %multiplies by change, this is specified by the joint
type
          t_totj=t_tot1;                                        %dummy summer
          disp('middel part')

                    for second_part = m_term :(k-1)                    %sums second part Ujkm
ie  mAk-1



                    t_tot1(1:4,1:4)=t_totj * t(second_part*4-3:second_part*4,1:4);
     %mAk-1 part loop engine
                    t_totj=t_tot1;                                        %dummy summer

                    end

          t_tot1(1:4,1:4)=t_totj * chnge; % multiplies by change, this is specified by the joint type
          t_totj=t_tot1;  %dummy summer

                    for last_part = k : j_count          %sums last part Ujkm ie  kAj

                    t_tot1(1:4,1:4)=t_totj * t(last_part*4-3:last_part*4,1:4);                %last
part of the a matrix
                    t_totj=t_tot1;                                %dummy summer
                    disp('last part')

                    end
          else %alternative scheme for Ujmk type equation

                    for first_part = 1 : (k-1) % sums first part Ujmk ie  0Ak-1

                    t_tot1(1:4,1:4)=t_totj *t(first_part*4-3:first_part*4,1:4);        %first part of
the a matrix
                    t_totj=t_tot1  ;                    %dummy summer
                    end

          t_tot1(1:4,1:4)=t_totj*chnge;       %multiplies by change, this is specified by the joint
type
          t_totj=t_tot1;                                        %dummy summer

                    for second_part = k : (m_term-1)          %sums second part Ujmk ie  kAm-
1


                    t_tot1(1:4,1:4)=t_totj * t(second_part*4-3:second_part*4,1:4);
     %mAk-1 part loop engine
```

```
                t_totj=t_tot1;                                          %dummy summer


                end
            t_tot1(1:4,1:4)=t_totj * chnge; % multiplies by change, this is specified by the joint type
            t_totj=t_tot1 ;  %dummy summer

                for last_part= m_term : j_count              %sums last part Ujmk ie mAj

                t_tot1(1:4,1:4)=t_totj * t(last_part*4-3:last_part*4,1:4);              %last
part of the a matrix
                t_totj=t_tot1;                                  %dummy summer
                disp('last part')
                end
            end  %END OF THE FIRST BIG Ujkm TERM---------------------------------
            %START OF THE Uji TERM-----------------------------------------


            for first_part = 1 : (i-1) % second u term is i

                t_tot2=t_toti* t(first_part*4-3:first_part*4,1:4);       %first part of the a
matrix
                t_toti=t_tot2;                                  %dummy summer
                end

            t_tot2(1:4,1:4)=t_toti* chnge;
            t_toti=t_tot2;                  %dummy summer


                for last_part = i : j_count %second part of Uji term ie iAj
                t_tot2(1:4,1:4)=t_toti * t(last_part*4-3:last_part*4,1:4); %last part of the a
matrix
                t_toti=t_tot2;                          %dummy summer

                end


            tra(1:4,1:4)= t_totj * h(j_count*4-3:j_count*4,1:4);   %Ujkm*J(mat) multiplication
            tra1=tra * ((t_toti)');

            trac1=trace(tra1);      %does a trace

            trac=trac1+tr_sum;
            tr_sum=trac;                end%     sums the individual trace terms
old(i:i,((m_term-1)*3+k):((m_term-1)*3+k))=trac;
end
end
end
```

```
%This program produces the inertial interactions of the link structure. This program was written by Nigel Yee.
function [old]=inertial(m,l1,l2,l3,a,b,c,g)

%works out the gravity terms input requirements are m(1), m(2)...m(n), l(1), (l(2)...l(n),a,b,c,....,n,

chnge=[0,-1,0,0;1,0,0,0;0,0,0,0;0,0,0,0];
h(1:4,1:4)=[m(1)*((l1)^2)/3,0,0,-m(1)*((l1)/2);0,0,0,0;0,0,0,0;-0.5*m(1)*l1,0,0,m(1)];

h(5:8,1:4)=[m(2)*((l2)^2)/3,0,0,-m(2)*l2*1/2;0,0,0,0;0,0,0,0;-0.5*m(2)*l2,0,0,m(2)];

h(9:12,1:4)=[m(3)*((l3)^2)/3,0,0,-m(3)*l3*1/2;0,0,0,0;0,0,0,0;-0.5*m(3)*l3,0,0,m(3)];

t(1:4,1:4)=[cos(a),-sin(a),0,l1*cos(a);sin(a),cos(a),0,l1*sin(a);0,0,1,0;0,0,0,1];

t(5:8,1:4)=[cos(b),-sin(b),0,l2*cos(b);sin(b),cos(b),0,l2*sin(b);0,0,1,0;0,0,0,1];

t(9:12,1:4)=[cos(c),-sin(c),0,l3*cos(c);sin(c),cos(c),0,l3*sin(c);0,0,1,0;0,0,0,1];


%m11 term 3 link manipulator
n= 3;
ii=1;jj=1; %in the gravity term because the term is transposed for the first row the i term varies to change the column the  term indicates the row term the i term indicates the column

old=zeros(size(n,n));

for i = ii : n

jj=1;

        for j = jj:n % j represents the velocity vector the result is in the form of int=[a theta1,b theta2,c theta3;d theta 1,e theta2,f theta 3,g theta 1,h theta 2,j theta 3] where theta is an angular acceleration.

        tr_sum=0;
        k=max(i,j);
                for loop_sum = k : n    %k loop to check how many trace terms to have


                t_totj=[1,0,0,0;0,1,0,0;0,0,1,0;0,0,0,1];

                t_toti=[1,0,0,0;0,1,0,0;0,0,1,0;0,0,0,1];


                        for first_part = 1: (j-1) % first u term is j----------------------

                        t_tot1(1:4,1:4)=t_totj *t(first_part*4-3:first_part*4,1:4);          %first part of the a matrix

                        t_totj=t_tot1  ;                        %dummy summer
                        end
```

```
                t_tot1(1:4,1:4)=t_totj*chnge;
                t_totj=t_tot1;                                  %dummy summer
                disp('middel part')


                        for last_part=j : loop_sum


                        t_tot1(1:4,1:4)=t_totj * t(last_part*4-3:last_part*4,1:4);              %last
part of the a matrix
                        t_totj=t_tot1;                          %dummy summer
                        disp('last part')

                        end
                % end of the first U j term----------------------------------------------------
                        for first_part = 1 : (i-1) % second u term is i

                        t_tot2=t_toti* t(first_part*4-3:first_part*4,1:4);       %first part of the a
matrix
                        t_toti=t_tot2;                          %dummy summer
                        end

                t_tot2(1:4,1:4)=t_toti* chnge;
                t_toti=t_tot2;                  %dummy summer

                        for last_part = i : loop_sum
                        t_tot2(1:4,1:4)=t_toti * t(last_part*4-3:last_part*4,1:4); %last part of the a
matrix
                        t_toti=t_tot2;                  %dummy summer

                        end

                tra= t_totj * h(loop_sum*4-3:loop_sum*4,1:4);
                tra1=tra * ((t_toti)');
                trac1=trace(tra1);
                trac=trac1+tr_sum;
                tr_sum=trac;
                end
        term(i:i,j:j)=trac;
        old(i)=term(i);
        end
old(i:i,n)=term(i:i,n);
end


disp(old)
```

%This program produces the gravitational forces of the link structure. This program was written by Nigel Yee.

```
function [old]=gravity1(m,l1,l2,l3,a,b,c,g)

%works out the gravity terms input requirements are m(1), m(2)...m(n), l(1), (l(2)...l(n),a,b,c,....,n,

chnge=[0,-1,0,0;1,0,0,0;0,0,0,0;0,0,0,0];
h(1:4,1:4)=[m(1)*((l1)^2)/3,0,0,-m(1)*((l1)/2);0,0,0,0;0,0,0,0;-0.5*m(1)*l1,0,0,m(1)];

h(5:8,1:4)=[m(2)*((l2)^2)/3,0,0,-m(2)*l2*1/2;0,0,0,0;0,0,0,0;-0.5*m(2)*l2,0,0,m(2)];

h(9:12,1:4)=[m(3)*((l3)^2)/3,0,0,-m(3)*l3*1/2;0,0,0,0;0,0,0,0;-0.5*m(3)*l3,0,0,m(3)];

t(1:4,1:4)=[cos(a),-sin(a),0,l1*cos(a);sin(a),cos(a),0,l1*sin(a);0,0,1,0;0,0,0,1];

t(5:8,1:4)=[cos(b),-sin(b),0,l2*cos(b);sin(b),cos(b),0,l2*sin(b);0,0,1,0;0,0,0,1];

t(9:12,1:4)=[cos(c),-sin(c),0,l3*cos(c);sin(c),cos(c),0,l3*sin(c);0,0,1,0;0,0,0,1];

g=[0,-g,0,0];

r(1:4,1:1)=[-(l1)/2;0;0;1];
r(5:8,1:1)=[-(l2)/2;0;0;1];
r(9:12,1:1)=[-(l3)/2;0;0;1];

%m11 term 3 link manipulator
n= 3;
ii=1;j=1; %in the gravity term because the term is transposed for the first row the i term varies to change the column the j term indicates the row term the i term indicates the column

old=zeros(size(1:n,1:1));

for i = ii : n


k=i;tr_sum=0;

        for loop_sum = k : n  %k loop to check how many trace terms to have


                t_totj=[1,0,0,0;0,1,0,0;0,0,1,0;0,0,0,1];

                t_toti=[1,0,0,0;0,1,0,0;0,0,1,0;0,0,0,1];

                for first_part =1 : (i-1) % first u term is j----------------

                        t_tot1(1:4,1:4)=t_totj *t(first_part*4-3:first_part*4,1:4);        %first part of
the a matrix
                        t_totj=t_tot1 ;                  %dummy summer
                        disp('first part')
                end
```

```
                t_tot1(1:4,1:4)=t_totj * chnge;
                t_totj=t_tot1;                                  %dummy summer
                disp('middel part')

                for last_part =i : loop_sum

                        t_tot1(1:4,1:4)=t_totj * t(last_part*4-3:last_part*4,1:4);          %last
part of the a matrix
                        t_totj=t_tot1;                          %dummy summer
                        disp('last part')
                end
                %end of the first U j term-----------------------------------------------
                tra=g * t_totj;
                tra1=tra* r(loop_sum*4-3:loop_sum*4,1:1);
                trac1=trace(tra1);
                tra=-m(loop_sum)*trac1;
                trac=tra+tr_sum;
                tr_sum=trac;
            disp('term')
                end
old(i:i,1:1)=trac(1,1);

end
disp(old)
```

# Appendix C Muscle characterisation data

## C-1. Raw data for the muscle

Raw data from the isometric tests conducted on the muscle.

| Pressure (kpa) | Force results (Newton) at temperature 21deg C. | Force results (Newton) at temperature 24deg C. | Force results (Newton) at temperature 27deg C. | Force results (Newton) at temperature 30deg C. | Force results (Newton) at temperature 33deg C. | Force results (Newton) at temperature 36deg C. | Force results (Newton) at temperature 39deg C. | Length of the muscle (mm) |
|---|---|---|---|---|---|---|---|---|
| 0 | -0.046 | -0.032 | -0.031 | -0.022 | -0.021 | -0.015 | -0.010 | 51 |
| 50 | -0.060 | -0.043 | -0.042 | -0.030 | -0.029 | -0.021 | -0.015 | 51 |
| 75 | -0.111 | -0.081 | -0.079 | -0.058 | -0.057 | -0.042 | -0.031 | 51 |
| 100 | -0.276 | -0.206 | -0.201 | -0.152 | -0.148 | -0.112 | -0.084 | 51 |
| 125 | -0.422 | -0.320 | -0.312 | -0.239 | -0.234 | -0.179 | -0.137 | 51 |
| 150 | -3.202 | -2.448 | -2.390 | -1.845 | -1.805 | -1.393 | -1.076 | 51 |
| 175 | -3.750 | -2.890 | -2.821 | -2.195 | -2.148 | -1.671 | -1.300 | 51 |
| 200 | -3.264 | -2.556 | -2.495 | -1.973 | -1.930 | -1.526 | -1.207 | 51 |
| 250 | -1.645 | -1.309 | -1.278 | -1.027 | -1.005 | -0.808 | -0.649 | 51 |
| 300 | -0.393 | -0.318 | -0.310 | -0.254 | -0.248 | -0.203 | -0.166 | 51 |
| 350 | 0.532 | 0.647 | 0.662 | 0.797 | 0.815 | 0.981 | 1.180 | 51 |
| 400 | 1.481 | 1.769 | 1.812 | 2.144 | 2.192 | 2.593 | 3.068 | 51 |
| 450 | 2.769 | 3.251 | 3.330 | 3.872 | 3.958 | 4.602 | 5.351 | 51 |
| 500 | 4.003 | 4.618 | 4.730 | 5.403 | 5.522 | 6.309 | 7.207 | 51 |
| 550 | 5.437 | 6.160 | 6.310 | 7.079 | 7.235 | 8.118 | 9.108 | 51 |
| 600 | 6.507 | 7.238 | 7.414 | 8.167 | 8.347 | 9.195 | 10.129 | 51 |
| 0 | -0.084 | -0.060 | -0.059 | -0.042 | -0.041 | -0.030 | -0.021 | 53 |
| 50 | -0.096 | -0.070 | -0.068 | -0.050 | -0.049 | -0.036 | -0.027 | 53 |
| 75 | -0.182 | -0.136 | -0.133 | -0.100 | -0.098 | -0.074 | -0.056 | 53 |
| 100 | -0.247 | -0.187 | -0.183 | -0.140 | -0.137 | -0.105 | -0.080 | 53 |
| 125 | -0.610 | -0.466 | -0.455 | -0.351 | -0.344 | -0.265 | -0.205 | 53 |
| 150 | -0.873 | -0.673 | -0.657 | -0.511 | -0.500 | -0.389 | -0.303 | 53 |
| 175 | -0.679 | -0.532 | -0.519 | -0.410 | -0.402 | -0.317 | -0.251 | 53 |
| 200 | -0.669 | -0.532 | -0.520 | -0.418 | -0.409 | -0.328 | -0.264 | 53 |
| 250 | -0.387 | -0.313 | -0.306 | -0.250 | -0.244 | -0.200 | -0.163 | 53 |
| 300 | 0.738 | 0.897 | 0.919 | 1.106 | 1.130 | 1.360 | 1.637 | 53 |
| 350 | 2.113 | 2.525 | 2.586 | 3.060 | 3.127 | 3.700 | 4.378 | 53 |
| 400 | 3.689 | 4.332 | 4.437 | 5.159 | 5.273 | 6.131 | 7.129 | 53 |
| 450 | 5.647 | 6.514 | 6.672 | 7.623 | 7.790 | 8.900 | 10.167 | 53 |
| 500 | 7.216 | 8.176 | 8.374 | 9.396 | 9.603 | 10.774 | 12.088 | 53 |
| 550 | 8.797 | 9.876 | 10.116 | 11.247 | 11.495 | 12.780 | 14.208 | 53 |
| 600 | 10.413 | 11.476 | 11.755 | 12.829 | 13.111 | 14.310 | 15.618 | 53 |
| 0 | 0.954 | 1.307 | 1.339 | 1.816 | 1.856 | 2.518 | 3.416 | 55 |
| 50 | 0.904 | 1.210 | 1.240 | 1.644 | 1.680 | 2.228 | 2.954 | 55 |
| 75 | 0.820 | 1.081 | 1.107 | 1.446 | 1.478 | 1.929 | 2.519 | 55 |
| 100 | 0.646 | 0.845 | 0.866 | 1.121 | 1.146 | 1.484 | 1.923 | 55 |
| 125 | 0.145 | 0.188 | 0.193 | 0.248 | 0.253 | 0.325 | 0.418 | 55 |
| 150 | -0.932 | -0.730 | -0.712 | -0.563 | -0.551 | -0.436 | -0.345 | 55 |

| | | | | | | | | |
|---|---|---|---|---|---|---|---|---|
| 175 | -0.699 | -0.556 | -0.543 | -0.436 | -0.427 | -0.343 | -0.276 | 55 |
| 200 | 0.177 | 0.221 | 0.226 | 0.279 | 0.285 | 0.352 | 0.434 | 55 |
| 250 | 2.776 | 3.431 | 3.514 | 4.302 | 4.396 | 5.381 | 6.586 | 55 |
| 300 | 4.965 | 5.932 | 6.076 | 7.189 | 7.347 | 8.694 | 10.286 | 55 |
| 350 | 7.485 | 8.789 | 9.002 | 10.468 | 10.698 | 12.440 | 14.465 | 55 |
| 400 | 10.173 | 11.736 | 12.020 | 13.732 | 14.034 | 16.033 | 18.316 | 55 |
| 450 | 12.442 | 14.097 | 14.439 | 16.200 | 16.557 | 18.577 | 20.843 | 55 |
| 500 | 14.631 | 16.426 | 16.825 | 18.706 | 19.117 | 21.255 | 23.631 | 55 |
| 550 | 16.822 | 18.540 | 18.990 | 20.725 | 21.181 | 23.117 | 25.230 | 55 |
| 600 | 19.265 | 21.034 | 21.544 | 23.293 | 23.806 | 25.739 | 27.829 | 55 |
| 0 | 2.324 | 3.112 | 3.187 | 4.226 | 4.319 | 5.728 | 7.595 | 57.4 |
| 50 | 2.246 | 2.961 | 3.033 | 3.960 | 4.047 | 5.284 | 6.898 | 57.4 |
| 75 | 2.301 | 3.010 | 3.083 | 3.994 | 4.082 | 5.287 | 6.849 | 57.4 |
| 100 | 2.270 | 2.946 | 3.018 | 3.878 | 3.963 | 5.094 | 6.547 | 57.4 |
| 125 | 1.297 | 1.670 | 1.710 | 2.181 | 2.229 | 2.842 | 3.623 | 57.4 |
| 150 | 0.177 | 0.226 | 0.232 | 0.293 | 0.299 | 0.379 | 0.479 | 57.4 |
| 175 | 1.999 | 2.533 | 2.594 | 3.254 | 3.326 | 4.173 | 5.235 | 57.4 |
| 200 | 3.707 | 4.658 | 4.771 | 5.937 | 6.068 | 7.551 | 9.396 | 57.4 |
| 250 | 8.420 | 10.407 | 10.660 | 13.047 | 13.335 | 16.321 | 19.977 | 57.4 |
| 300 | 12.464 | 15.149 | 15.516 | 18.676 | 19.086 | 22.972 | 27.650 | 57.4 |
| 350 | 15.926 | 19.028 | 19.490 | 23.061 | 23.568 | 27.886 | 32.995 | 57.4 |
| 400 | 19.808 | 23.259 | 23.823 | 27.701 | 28.311 | 32.920 | 38.279 | 57.4 |
| 450 | 23.496 | 27.105 | 27.763 | 31.716 | 32.414 | 37.030 | 42.303 | 57.4 |
| 500 | 28.264 | 32.023 | 32.800 | 36.802 | 37.612 | 42.200 | 47.349 | 57.4 |
| 550 | 31.528 | 34.747 | 35.590 | 38.843 | 39.698 | 43.326 | 47.286 | 57.4 |
| 600 | 35.980 | 38.542 | 39.477 | 41.877 | 42.799 | 45.401 | 48.161 | 57.4 |
| 0 | 2.639 | 3.479 | 3.564 | 4.653 | 4.755 | 6.208 | 8.106 | 58 |
| 50 | 2.576 | 3.370 | 3.451 | 4.471 | 4.569 | 5.919 | 7.668 | 58 |
| 75 | 2.436 | 3.161 | 3.238 | 4.162 | 4.253 | 5.466 | 7.025 | 58 |
| 100 | 2.200 | 2.833 | 2.901 | 3.699 | 3.780 | 4.820 | 6.146 | 58 |
| 125 | 1.490 | 1.903 | 1.949 | 2.465 | 2.520 | 3.187 | 4.031 | 58 |
| 150 | 0.826 | 1.038 | 1.063 | 1.323 | 1.352 | 1.683 | 2.094 | 58 |
| 175 | 2.546 | 3.173 | 3.250 | 4.011 | 4.100 | 5.060 | 6.245 | 58 |
| 200 | 5.110 | 6.316 | 6.469 | 7.918 | 8.093 | 9.905 | 12.124 | 58 |
| 250 | 8.799 | 10.694 | 10.954 | 13.184 | 13.474 | 16.217 | 19.519 | 58 |
| 300 | 13.159 | 15.722 | 16.104 | 19.054 | 19.473 | 23.041 | 27.262 | 58 |
| 350 | 16.639 | 19.538 | 20.012 | 23.270 | 23.782 | 27.653 | 32.155 | 58 |
| 400 | 20.519 | 23.671 | 24.245 | 27.698 | 28.307 | 32.338 | 36.943 | 58 |
| 450 | 24.279 | 27.508 | 28.176 | 31.613 | 32.309 | 36.250 | 40.673 | 58 |
| 500 | 27.844 | 31.260 | 32.019 | 35.599 | 36.382 | 40.450 | 44.972 | 58 |
| 550 | 31.673 | 34.254 | 35.086 | 37.577 | 38.404 | 41.130 | 44.050 | 58 |
| 600 | 37.099 | 39.358 | 40.314 | 42.353 | 43.285 | 45.476 | 47.777 | 58 |
| 0 | 3.711 | 4.854 | 4.972 | 6.441 | 6.583 | 8.527 | 11.046 | 59.39 |
| 50 | 3.630 | 4.711 | 4.825 | 6.202 | 6.338 | 8.146 | 10.469 | 59.39 |
| 75 | 3.492 | 4.460 | 4.568 | 5.778 | 5.905 | 7.469 | 9.446 | 59.39 |
| 100 | 3.277 | 4.152 | 4.252 | 5.335 | 5.452 | 6.841 | 8.582 | 59.39 |
| 125 | 2.631 | 3.306 | 3.386 | 4.214 | 4.307 | 5.359 | 6.669 | 59.39 |
| 150 | 2.663 | 3.319 | 3.399 | 4.196 | 4.288 | 5.292 | 6.532 | 59.39 |
| 175 | 4.749 | 5.870 | 6.012 | 7.359 | 7.521 | 9.206 | 11.268 | 59.39 |
| 200 | 7.326 | 8.904 | 9.120 | 10.977 | 11.218 | 13.503 | 16.252 | 59.39 |

| | | | | | | | | |
|---|---|---|---|---|---|---|---|---|
| 250 | 12.432 | 14.854 | 15.214 | 18.002 | 18.398 | 21.768 | 25.756 | 59.39 |
| 300 | 16.897 | 19.840 | 20.322 | 23.630 | 24.150 | 28.082 | 32.654 | 59.39 |
| 350 | 21.706 | 25.264 | 25.877 | 29.826 | 30.482 | 35.133 | 40.495 | 59.39 |
| 400 | 26.176 | 29.657 | 30.377 | 34.083 | 34.833 | 39.083 | 43.851 | 59.39 |
| 450 | 29.781 | 33.435 | 34.247 | 38.075 | 38.913 | 43.264 | 48.100 | 59.39 |
| 500 | 35.554 | 39.184 | 40.135 | 43.803 | 44.767 | 48.859 | 53.325 | 59.39 |
| 550 | 39.782 | 43.024 | 44.069 | 47.197 | 48.236 | 51.660 | 55.328 | 59.39 |
| 600 | 43.696 | 45.907 | 47.021 | 48.921 | 49.997 | 52.017 | 54.119 | 59.39 |
| 0 | 4.395 | 5.704 | 5.842 | 7.508 | 7.674 | 9.862 | 12.675 | 60.55 |
| 50 | 4.235 | 5.409 | 5.540 | 7.007 | 7.161 | 9.058 | 11.456 | 60.55 |
| 75 | 3.265 | 4.136 | 4.237 | 5.316 | 5.432 | 6.816 | 8.551 | 60.55 |
| 100 | 3.785 | 4.756 | 4.872 | 6.062 | 6.196 | 7.710 | 9.594 | 60.55 |
| 125 | 3.176 | 3.958 | 4.054 | 5.004 | 5.114 | 6.312 | 7.790 | 60.55 |
| 150 | 4.004 | 4.949 | 5.069 | 6.205 | 6.341 | 7.761 | 9.500 | 60.55 |
| 175 | 7.160 | 8.702 | 8.913 | 10.728 | 10.964 | 13.197 | 15.883 | 60.55 |
| 200 | 9.640 | 11.518 | 11.797 | 13.959 | 14.266 | 16.879 | 19.972 | 60.55 |
| 250 | 14.944 | 17.547 | 17.973 | 20.899 | 21.359 | 24.836 | 28.880 | 60.55 |
| 300 | 19.915 | 22.974 | 23.532 | 26.882 | 27.474 | 31.386 | 35.856 | 60.55 |
| 350 | 25.207 | 28.560 | 29.253 | 32.822 | 33.544 | 37.636 | 42.228 | 60.55 |
| 400 | 30.367 | 34.093 | 34.921 | 38.825 | 39.679 | 44.115 | 49.047 | 60.55 |
| 450 | 35.574 | 39.206 | 40.158 | 43.828 | 44.792 | 48.886 | 53.355 | 60.55 |
| 500 | 39.996 | 43.256 | 44.306 | 47.451 | 48.495 | 51.938 | 55.626 | 60.55 |
| 550 | 45.143 | 47.892 | 49.055 | 51.537 | 52.671 | 55.336 | 58.136 | 60.55 |
| 600 | 49.238 | 51.222 | 52.466 | 54.050 | 55.239 | 56.907 | 58.626 | 60.55 |
| 0 | 4.299 | 5.491 | 5.624 | 7.113 | 7.270 | 9.195 | 11.629 | 61 |
| 50 | 4.247 | 5.381 | 5.511 | 6.914 | 7.066 | 8.865 | 11.123 | 61 |
| 75 | 4.140 | 5.202 | 5.329 | 6.631 | 6.777 | 8.433 | 10.494 | 61 |
| 100 | 3.905 | 4.867 | 4.985 | 6.152 | 6.288 | 7.760 | 9.578 | 61 |
| 125 | 3.216 | 3.975 | 4.071 | 4.983 | 5.093 | 6.234 | 7.630 | 61 |
| 150 | 4.365 | 5.305 | 5.434 | 6.540 | 6.684 | 8.045 | 9.683 | 61 |
| 175 | 6.982 | 8.342 | 8.545 | 10.110 | 10.332 | 12.225 | 14.465 | 61 |
| 200 | 10.046 | 11.796 | 12.082 | 14.049 | 14.358 | 16.696 | 19.414 | 61 |
| 250 | 15.742 | 18.160 | 18.601 | 21.249 | 21.717 | 24.809 | 28.342 | 61 |
| 300 | 20.999 | 23.792 | 24.369 | 27.342 | 27.944 | 31.353 | 35.178 | 61 |
| 350 | 27.364 | 30.722 | 31.467 | 34.985 | 35.755 | 39.752 | 44.197 | 61 |
| 400 | 33.475 | 36.893 | 37.788 | 41.242 | 42.149 | 46.002 | 50.206 | 61 |
| 450 | 38.049 | 41.150 | 42.149 | 45.141 | 46.134 | 49.410 | 52.918 | 61 |
| 500 | 44.739 | 47.464 | 48.616 | 51.076 | 52.199 | 54.841 | 57.615 | 61 |
| 550 | 49.512 | 51.507 | 52.758 | 54.351 | 55.547 | 57.224 | 58.952 | 61 |
| 600 | 53.417 | 55.515 | 56.862 | 58.521 | 59.809 | 61.554 | 63.350 | 61 |
| 0 | 5.038 | 6.331 | 6.484 | 8.069 | 8.247 | 10.262 | 12.770 | 62 |
| 50 | 4.925 | 6.138 | 6.287 | 7.759 | 7.930 | 9.787 | 12.080 | 62 |
| 75 | 4.816 | 5.953 | 6.097 | 7.463 | 7.627 | 9.335 | 11.427 | 62 |
| 100 | 4.577 | 5.610 | 5.746 | 6.975 | 7.128 | 8.652 | 10.502 | 62 |
| 125 | 4.013 | 4.877 | 4.996 | 6.013 | 6.145 | 7.396 | 8.902 | 62 |
| 150 | 5.342 | 6.383 | 6.538 | 7.735 | 7.905 | 9.354 | 11.067 | 62 |
| 175 | 9.730 | 11.425 | 11.702 | 13.607 | 13.907 | 16.171 | 18.803 | 62 |
| 200 | 12.123 | 13.985 | 14.325 | 16.364 | 16.724 | 19.106 | 21.827 | 62 |
| 250 | 18.374 | 20.818 | 21.323 | 23.924 | 24.451 | 27.434 | 30.781 | 62 |
| 300 | 23.025 | 25.850 | 26.478 | 29.438 | 30.085 | 33.449 | 37.189 | 62 |

| | | | | | | | | |
|---|---|---|---|---|---|---|---|---|
| 350 | 28.695 | 31.625 | 32.392 | 35.353 | 36.131 | 39.433 | 43.037 | 62 |
| 400 | 34.867 | 37.709 | 38.624 | 41.366 | 42.276 | 45.278 | 48.493 | 62 |
| 450 | 40.279 | 42.732 | 43.769 | 45.984 | 46.996 | 49.374 | 51.872 | 62 |
| 500 | 45.186 | 47.007 | 48.148 | 49.602 | 50.693 | 52.224 | 53.801 | 62 |
| 550 | 53.402 | 55.499 | 56.846 | 58.505 | 59.792 | 61.537 | 63.332 | 62 |
| 600 | 57.506 | 59.705 | 61.154 | 62.876 | 64.260 | 66.069 | 67.930 | 62 |
| 0 | 5.306 | 6.558 | 6.717 | 8.222 | 8.403 | 10.285 | 12.589 | 63 |
| 50 | 5.231 | 6.412 | 6.567 | 7.971 | 8.147 | 9.888 | 12.003 | 63 |
| 75 | 5.170 | 6.284 | 6.436 | 7.747 | 7.917 | 9.529 | 11.469 | 63 |
| 100 | 4.861 | 5.858 | 6.000 | 7.161 | 7.318 | 8.733 | 10.423 | 63 |
| 125 | 4.763 | 5.691 | 5.829 | 6.897 | 7.049 | 8.340 | 9.868 | 63 |
| 150 | 6.389 | 7.502 | 7.684 | 8.935 | 9.132 | 10.618 | 12.347 | 63 |
| 175 | 10.780 | 12.547 | 12.851 | 14.812 | 15.138 | 17.448 | 20.111 | 63 |
| 200 | 14.058 | 16.217 | 16.611 | 18.976 | 19.394 | 22.155 | 25.310 | 63 |
| 250 | 20.567 | 23.514 | 24.085 | 27.269 | 27.869 | 31.553 | 35.725 | 63 |
| 300 | 28.459 | 31.951 | 32.726 | 36.385 | 37.186 | 41.343 | 45.965 | 63 |
| 350 | 33.433 | 36.847 | 37.741 | 41.190 | 42.097 | 45.944 | 50.143 | 63 |
| 400 | 40.398 | 43.274 | 44.325 | 47.020 | 48.054 | 50.976 | 54.075 | 63 |
| 450 | 46.353 | 48.698 | 49.880 | 51.896 | 53.037 | 55.180 | 57.409 | 63 |
| 500 | 52.146 | 54.194 | 55.509 | 57.129 | 58.386 | 60.089 | 61.843 | 63 |
| 550 | 57.135 | 59.320 | 60.760 | 62.471 | 63.845 | 65.643 | 67.491 | 63 |
| 600 | 63.402 | 65.761 | 67.357 | 69.185 | 70.707 | 72.626 | 74.598 | 63 |
| 0 | 5.381 | 6.540 | 6.699 | 8.063 | 8.240 | 9.918 | 11.937 | 63.87 |
| 50 | 5.284 | 6.368 | 6.522 | 7.784 | 7.955 | 9.493 | 11.329 | 63.87 |
| 75 | 5.150 | 6.153 | 6.303 | 7.457 | 7.621 | 9.017 | 10.669 | 63.87 |
| 100 | 4.848 | 5.742 | 5.882 | 6.899 | 7.051 | 8.271 | 9.702 | 63.87 |
| 125 | 4.696 | 5.514 | 5.648 | 6.567 | 6.712 | 7.805 | 9.075 | 63.87 |
| 150 | 8.139 | 9.473 | 9.703 | 11.184 | 11.430 | 13.174 | 15.184 | 63.87 |
| 175 | 10.292 | 11.873 | 12.161 | 13.893 | 14.198 | 16.220 | 18.530 | 63.87 |
| 200 | 13.349 | 15.262 | 15.632 | 17.699 | 18.088 | 20.480 | 23.187 | 63.87 |
| 250 | 20.320 | 23.023 | 23.581 | 26.458 | 27.040 | 30.339 | 34.041 | 63.87 |
| 300 | 26.545 | 29.802 | 30.525 | 33.938 | 34.685 | 38.563 | 42.874 | 63.87 |
| 350 | 33.944 | 37.410 | 38.318 | 41.820 | 42.740 | 46.646 | 50.910 | 63.87 |
| 400 | 39.858 | 42.696 | 43.732 | 46.391 | 47.412 | 50.294 | 53.352 | 63.87 |
| 450 | 46.138 | 47.997 | 49.162 | 50.647 | 51.761 | 53.324 | 54.935 | 63.87 |
| 500 | 52.393 | 54.450 | 55.772 | 57.400 | 58.662 | 60.374 | 62.136 | 63.87 |
| 550 | 57.206 | 59.394 | 60.835 | 62.548 | 63.924 | 65.724 | 67.575 | 63.87 |
| 600 | 60.480 | 62.668 | 64.189 | 65.866 | 67.315 | 69.073 | 70.877 | 63.87 |
| 0 | 3.716 | 4.440 | 4.548 | 5.381 | 5.499 | 6.507 | 7.699 | 65 |
| 50 | 3.575 | 4.235 | 4.337 | 5.088 | 5.200 | 6.099 | 7.154 | 65 |
| 75 | 3.417 | 4.012 | 4.110 | 4.779 | 4.884 | 5.679 | 6.603 | 65 |
| 100 | 3.258 | 3.792 | 3.884 | 4.477 | 4.575 | 5.273 | 6.078 | 65 |
| 125 | 4.710 | 5.433 | 5.565 | 6.358 | 6.498 | 7.423 | 8.480 | 65 |
| 150 | 7.681 | 8.782 | 8.995 | 10.184 | 10.408 | 11.784 | 13.342 | 65 |
| 175 | 11.657 | 13.207 | 13.528 | 15.178 | 15.512 | 17.405 | 19.528 | 65 |
| 200 | 15.156 | 17.016 | 17.429 | 19.377 | 19.803 | 22.017 | 24.479 | 65 |
| 250 | 22.740 | 25.296 | 25.910 | 28.542 | 29.170 | 32.134 | 35.399 | 65 |
| 300 | 29.712 | 32.746 | 33.540 | 36.606 | 37.411 | 40.831 | 44.563 | 65 |
| 350 | 37.587 | 41.037 | 42.034 | 45.447 | 46.446 | 50.218 | 54.296 | 65 |
| 400 | 46.398 | 50.179 | 51.397 | 55.047 | 56.258 | 60.252 | 64.530 | 65 |

| | | | | | | | | |
|---|---|---|---|---|---|---|---|---|
| 450 | 53.077 | 55.763 | 57.116 | 59.424 | 60.731 | 63.185 | 65.737 | 65 |
| 500 | 59.420 | 61.753 | 63.252 | 65.098 | 66.530 | 68.472 | 70.469 | 65 |
| 550 | 65.286 | 67.715 | 69.359 | 71.241 | 72.809 | 74.785 | 76.814 | 65 |
| 600 | 71.357 | 73.865 | 75.658 | 77.557 | 79.263 | 81.253 | 83.292 | 65 |
| 0 | 6.785 | 7.967 | 8.160 | 9.489 | 9.698 | 11.276 | 13.112 | 65.8 |
| 50 | 6.542 | 7.614 | 7.799 | 8.989 | 9.187 | 10.589 | 12.205 | 65.8 |
| 75 | 6.453 | 7.444 | 7.625 | 8.711 | 8.902 | 10.170 | 11.618 | 65.8 |
| 100 | 6.354 | 7.199 | 7.374 | 8.273 | 8.455 | 9.487 | 10.644 | 65.8 |
| 125 | 8.180 | 9.184 | 9.407 | 10.458 | 10.688 | 11.883 | 13.212 | 65.8 |
| 150 | 11.700 | 13.015 | 13.331 | 14.685 | 15.008 | 16.533 | 18.213 | 65.8 |
| 175 | 13.864 | 15.280 | 15.650 | 17.081 | 17.457 | 19.052 | 20.793 | 65.8 |
| 200 | 18.657 | 20.178 | 20.667 | 22.135 | 22.622 | 24.228 | 25.948 | 65.8 |
| 250 | 25.480 | 27.032 | 27.688 | 29.089 | 29.729 | 31.233 | 32.813 | 65.8 |
| 300 | 32.076 | 33.369 | 34.179 | 35.211 | 35.985 | 37.072 | 38.192 | 65.8 |
| 350 | 38.520 | 40.033 | 41.004 | 42.201 | 43.129 | 44.388 | 45.683 | 65.8 |
| 400 | 44.901 | 46.618 | 47.750 | 49.094 | 50.174 | 51.587 | 53.040 | 65.8 |
| 450 | 52.914 | 54.883 | 56.215 | 57.741 | 59.011 | 60.613 | 62.258 | 65.8 |
| 500 | 58.907 | 61.038 | 62.520 | 64.153 | 65.564 | 67.277 | 69.034 | 65.8 |
| 550 | 66.382 | 68.715 | 70.383 | 72.150 | 73.737 | 75.588 | 77.485 | 65.8 |
| 600 | 73.074 | 75.567 | 77.401 | 79.265 | 81.009 | 82.960 | 84.957 | 65.8 |
| 0 | 7.621 | 8.792 | 9.005 | 10.287 | 10.514 | 12.011 | 13.721 | 67 |
| 50 | 7.488 | 8.561 | 8.769 | 9.928 | 10.146 | 11.488 | 13.007 | 67 |
| 75 | 7.523 | 8.524 | 8.730 | 9.796 | 10.011 | 11.232 | 12.603 | 67 |
| 100 | 7.900 | 8.869 | 9.085 | 10.100 | 10.322 | 11.477 | 12.760 | 67 |
| 125 | 11.023 | 12.262 | 12.560 | 13.836 | 14.140 | 15.577 | 17.159 | 67 |
| 150 | 14.553 | 16.039 | 16.428 | 17.930 | 18.324 | 19.999 | 21.827 | 67 |
| 175 | 18.612 | 20.321 | 20.814 | 22.504 | 22.999 | 24.866 | 26.886 | 67 |
| 200 | 23.569 | 25.490 | 26.109 | 27.962 | 28.577 | 30.606 | 32.779 | 67 |
| 250 | 31.716 | 33.648 | 34.464 | 36.208 | 37.005 | 38.877 | 40.844 | 67 |
| 300 | 40.096 | 41.712 | 42.724 | 44.015 | 44.983 | 46.341 | 47.741 | 67 |
| 350 | 46.942 | 48.785 | 49.970 | 51.428 | 52.559 | 54.093 | 55.671 | 67 |
| 400 | 53.118 | 55.149 | 56.488 | 58.079 | 59.356 | 61.028 | 62.746 | 67 |
| 450 | 63.030 | 65.375 | 66.962 | 68.779 | 70.293 | 72.200 | 74.160 | 67 |
| 500 | 69.649 | 72.097 | 73.847 | 75.701 | 77.366 | 79.308 | 81.299 | 67 |
| 550 | 76.680 | 79.296 | 81.221 | 83.177 | 85.007 | 87.054 | 89.150 | 67 |
| 600 | 82.180 | 84.899 | 86.960 | 88.965 | 90.923 | 93.019 | 95.164 | 67 |

**Table C-1 Isometric data for temperatures 21-39deg.**

Raw data from the Isobaric tests conducted on the muscle.

| Length of the muscle (mm) | Force results (N) at press 0 kpa | Force results (N) at press 50 kpa | Force results (N) at press 75 kpa | Force results (N) at press 100 kpa | Force results (N) at press 125 kpa | Force results (N) at press 150 kpa | Force results (N) at press 175 kpa | Force results (N) at press 200 kpa | Force results (N) at press 250 kpa | Force results (N) at press 300 kpa | Force results (N) at press 350 kpa | Force results (N) at press 400 kpa | Force results (N) at press 450 kpa | Force results (N) at press 500 kpa | Force results (N) at press 550 kpa | Force results (N) at press 600 kpa | temp in deg C |
|---|---|---|---|---|---|---|---|---|---|---|---|---|---|---|---|---|---|
| 51.45 | -0.55 | 0.54 | 0.29 | 0.52 | -1.02 | -2.60 | -2.75 | -2.76 | -2.65 | -1.19 | 1.13 | 1.18 | 2.57 | 4.20 | 5.24 | 5.61 | 21 |
| 53.00 | 0.82 | -1.00 | 0.12 | -1.15 | -0.41 | -1.77 | -0.98 | -0.27 | -0.49 | 1.44 | 2.01 | 3.99 | 4.95 | 6.22 | 8.20 | 10.51 | 21 |
| 55.00 | 1.55 | 0.90 | 0.02 | 0.75 | 0.35 | 0.07 | -0.90 | 0.28 | 3.08 | 4.17 | 7.09 | 11.17 | 11.54 | 14.43 | 17.32 | 20.07 | 21 |
| 57.40 | 3.02 | 2.65 | 2.40 | 1.27 | 1.80 | 0.88 | 2.30 | 3.51 | 8.92 | 11.86 | 16.03 | 19.31 | 24.00 | 28.66 | 31.63 | 36.18 | 21 |
| 58.00 | 2.64 | 2.38 | 2.14 | 2.20 | 0.89 | 0.73 | 1.55 | 5.01 | 8.70 | 14.16 | 16.74 | 19.82 | 23.38 | 27.44 | 32.07 | 36.90 | 21 |
| 59.39 | 3.51 | 2.83 | 4.49 | 3.18 | 2.93 | 2.76 | 4.15 | 7.83 | 12.73 | 17.80 | 20.71 | 25.68 | 30.38 | 36.25 | 40.18 | 44.40 | 21 |
| 60.55 | 4.80 | 4.14 | 2.87 | 2.99 | 2.78 | 4.70 | 7.36 | 9.84 | 15.94 | 20.32 | 25.81 | 29.97 | 34.67 | 40.70 | 45.84 | 49.34 | 21 |
| 61.00 | 4.60 | 5.25 | 4.14 | 3.81 | 3.72 | 5.27 | 6.08 | 9.75 | 16.04 | 21.80 | 27.66 | 34.18 | 37.65 | 43.84 | 48.81 | 52.92 | 21 |
| 62.00 | 4.14 | 4.23 | 5.82 | 3.78 | 4.61 | 5.04 | 9.33 | 12.22 | 18.67 | 22.73 | 29.70 | 34.47 | 40.38 | 45.69 | 53.60 | 58.01 | 21 |
| 63.00 | 5.61 | 4.33 | 5.37 | 4.16 | 5.56 | 7.29 | 11.08 | 14.86 | 20.17 | 29.16 | 34.13 | 40.10 | 46.05 | 51.55 | 57.34 | 62.40 | 21 |
| 63.87 | 5.18 | 4.68 | 4.25 | 4.45 | 4.40 | 7.84 | 11.19 | 12.35 | 20.02 | 25.85 | 34.94 | 40.06 | 45.94 | 52.39 | 57.41 | 60.38 | 21 |
| 65.00 | 3.12 | 2.88 | 2.52 | 3.06 | 4.61 | 7.68 | 11.26 | 14.26 | 23.14 | 29.61 | 38.09 | 46.10 | 52.78 | 59.32 | 65.29 | 71.76 | 21 |
| 65.80 | 6.19 | 7.24 | 5.85 | 6.35 | 8.38 | 12.60 | 12.86 | 19.06 | 26.08 | 32.78 | 37.72 | 44.70 | 52.31 | 59.01 | 65.78 | 73.17 | 21 |
| 67.00 | 8.22 | 6.49 | 6.72 | 8.10 | 11.12 | 15.45 | 17.71 | 24.57 | 30.72 | 40.40 | 45.94 | 53.82 | 63.23 | 69.65 | 76.28 | 82.58 | 21 |
| 51.45 | -1.03 | -0.94 | 0.82 | 0.69 | -0.82 | -2.65 | -2.89 | -1.76 | -1.61 | 0.58 | 0.95 | 1.97 | 3.85 | 5.32 | 6.86 | 7.74 | 24 |
| 53.00 | -0.76 | 0.23 | -0.54 | -1.19 | -1.07 | -0.97 | -0.93 | -0.53 | 0.09 | 0.80 | 3.32 | 4.23 | 6.31 | 7.58 | 10.78 | 11.78 | 24 |
| 55.00 | 1.91 | 0.41 | 0.48 | 0.65 | -0.01 | -1.33 | -0.46 | 1.12 | 3.03 | 5.33 | 9.29 | 11.04 | 13.90 | 17.33 | 18.04 | 20.83 | 24 |
| 57.40 | 4.01 | 2.76 | 3.91 | 1.95 | 0.77 | -0.07 | 2.63 | 5.16 | 11.21 | 15.35 | 18.23 | 22.36 | 27.20 | 32.62 | 34.35 | 38.74 | 24 |
| 58.00 | 3.98 | 3.17 | 3.46 | 3.53 | 1.90 | 1.84 | 3.47 | 5.62 | 10.89 | 15.82 | 19.34 | 23.77 | 28.11 | 30.36 | 33.35 | 38.96 | 24 |
| 59.39 | 5.05 | 5.41 | 4.66 | 4.25 | 3.31 | 3.22 | 5.47 | 9.50 | 15.65 | 19.44 | 25.86 | 29.76 | 33.74 | 40.08 | 43.92 | 46.21 | 24 |
| 60.55 | 5.60 | 6.31 | 3.14 | 4.56 | 4.96 | 4.75 | 9.40 | 11.42 | 16.75 | 23.97 | 28.46 | 34.19 | 39.81 | 43.26 | 47.79 | 50.52 | 24 |
| 61.00 | 6.39 | 5.58 | 4.80 | 4.27 | 3.17 | 4.61 | 8.74 | 12.10 | 17.86 | 23.29 | 30.82 | 36.99 | 40.45 | 47.56 | 52.31 | 54.51 | 24 |
| 62.00 | 5.53 | 6.84 | 5.25 | 4.61 | 5.48 | 5.68 | 12.12 | 13.99 | 20.12 | 26.35 | 32.12 | 37.21 | 42.43 | 47.11 | 54.60 | 59.71 | 24 |
| 63.00 | 5.76 | 5.51 | 6.78 | 5.16 | 5.59 | 7.20 | 13.05 | 16.02 | 23.71 | 31.25 | 37.05 | 42.67 | 48.10 | 54.19 | 59.52 | 66.06 | 24 |
| 63.87 | 6.74 | 5.97 | 5.65 | 5.34 | 5.81 | 10.47 | 12.57 | 14.26 | 23.42 | 28.90 | 36.71 | 43.70 | 47.80 | 53.75 | 59.49 | 62.87 | 24 |
| 65.00 | 4.64 | 3.83 | 4.71 | 4.49 | 5.73 | 9.58 | 12.41 | 16.42 | 24.40 | 33.25 | 41.94 | 51.08 | 56.56 | 62.75 | 68.32 | 74.47 | 24 |
| 65.80 | 8.37 | 8.21 | 6.74 | 6.60 | 9.18 | 12.52 | 14.98 | 19.28 | 27.23 | 32.97 | 40.13 | 46.22 | 55.48 | 61.54 | 68.62 | 75.67 | 24 |
| 67.00 | 7.79 | 7.66 | 8.22 | 8.97 | 12.56 | 16.84 | 19.42 | 24.69 | 34.45 | 42.61 | 48.49 | 54.85 | 66.28 | 71.30 | 78.90 | 83.90 | 24 |
| 51.45 | 0.97 | -0.34 | -0.38 | -0.90 | 0.49 | -1.79 | -3.72 | -2.20 | -1.08 | -1.21 | -0.34 | 1.51 | 2.93 | 5.53 | 6.41 | 6.41 | 27 |
| 53.00 | -0.16 | -0.37 | -0.43 | -0.08 | -0.16 | -0.86 | -0.82 | 0.08 | -0.51 | 0.72 | 2.69 | 4.04 | 7.37 | 9.37 | 10.22 | 12.25 | 27 |
| 55.00 | 1.74 | 0.34 | 0.31 | 1.87 | 0.59 | -0.61 | -0.04 | 0.83 | 3.01 | 6.98 | 9.70 | 12.12 | 14.84 | 16.72 | 18.69 | 21.94 | 27 |
| 57.40 | 3.69 | 2.83 | 2.08 | 2.12 | 0.71 | 1.13 | 1.89 | 4.17 | 10.36 | 14.92 | 20.09 | 24.32 | 27.96 | 33.00 | 34.79 | 38.78 | 27 |
| 58.00 | 4.56 | 3.95 | 3.64 | 2.40 | 2.75 | 1.76 | 4.05 | 6.77 | 11.95 | 15.50 | 20.51 | 24.25 | 28.18 | 32.92 | 35.59 | 40.51 | 27 |
| 59.39 | 4.27 | 4.63 | 4.77 | 5.25 | 2.69 | 3.50 | 6.71 | 8.12 | 14.81 | 21.32 | 25.48 | 29.88 | 33.95 | 40.84 | 44.37 | 46.12 | 27 |
| 60.55 | 6.44 | 5.24 | 4.04 | 5.77 | 3.15 | 5.57 | 8.91 | 11.70 | 18.87 | 23.03 | 29.75 | 34.52 | 39.56 | 44.11 | 49.95 | 53.47 | 27 |
| 61.00 | 6.52 | 4.61 | 6.03 | 5.18 | 3.97 | 5.53 | 8.54 | 12.68 | 18.30 | 24.67 | 31.47 | 37.29 | 41.45 | 48.12 | 53.76 | 57.56 | 27 |
| 62.00 | 5.98 | 7.09 | 5.20 | 6.45 | 4.60 | 7.54 | 11.40 | 14.62 | 21.22 | 26.58 | 31.59 | 39.12 | 43.47 | 47.85 | 56.95 | 61.55 | 27 |
| 63.00 | 6.22 | 6.47 | 7.14 | 5.60 | 5.03 | 7.58 | 13.65 | 16.31 | 24.08 | 32.23 | 38.44 | 43.82 | 49.88 | 55.41 | 60.46 | 67.76 | 27 |
| 63.87 | 6.10 | 6.02 | 7.20 | 6.18 | 6.35 | 9.10 | 11.76 | 16.03 | 24.58 | 31.13 | 38.32 | 42.83 | 49.66 | 54.77 | 60.94 | 63.39 | 27 |
| 65.00 | 4.05 | 4.74 | 3.91 | 2.98 | 6.07 | 7.99 | 13.03 | 17.13 | 26.81 | 34.14 | 41.43 | 51.40 | 58.12 | 63.05 | 68.66 | 75.56 | 27 |
| 65.80 | 9.16 | 7.40 | 8.02 | 7.97 | 10.41 | 12.63 | 15.55 | 21.07 | 27.79 | 34.58 | 40.30 | 48.05 | 56.72 | 61.82 | 69.98 | 78.40 | 27 |

| | | | | | | | | | | | | | | | | | |
|---|---|---|---|---|---|---|---|---|---|---|---|---|---|---|---|---|---|
| 67.00 | 8.20 | 9.67 | 8.73 | 9.68 | 12.96 | 16.13 | 20.41 | 25.51 | 35.26 | 41.72 | 49.07 | 56.49 | 67.86 | 73.95 | 81.22 | 87.66 | 27 |
| 51.45 | -0.62 | 0.07 | -0.56 | -0.75 | 0.06 | -2.44 | -2.70 | -2.67 | -0.33 | -0.65 | 0.60 | 2.24 | 4.37 | 5.70 | 7.18 | 7.87 | 30 |
| 53.00 | -0.94 | -0.55 | -0.30 | 0.06 | 0.15 | -1.41 | -0.81 | -1.12 | -0.25 | 1.41 | 2.56 | 4.16 | 7.12 | 8.90 | 10.95 | 12.73 | 30 |
| 55.00 | 1.32 | 1.64 | 2.45 | 1.42 | 0.05 | 0.44 | -1.24 | 0.48 | 3.50 | 6.69 | 11.07 | 14.23 | 16.50 | 18.21 | 20.33 | 23.29 | 30 |
| 57.40 | 4.83 | 4.46 | 4.09 | 3.68 | 1.38 | 0.79 | 3.95 | 6.04 | 12.65 | 17.68 | 23.76 | 27.90 | 31.42 | 37.60 | 38.94 | 41.08 | 30 |
| 58.00 | 4.45 | 5.27 | 3.46 | 3.90 | 3.47 | 0.82 | 3.21 | 7.42 | 12.28 | 19.05 | 22.27 | 28.60 | 31.91 | 35.20 | 37.18 | 42.55 | 30 |
| 59.39 | 6.24 | 6.40 | 5.48 | 5.14 | 4.41 | 3.50 | 7.86 | 11.68 | 18.70 | 24.33 | 30.33 | 34.98 | 37.68 | 42.90 | 47.10 | 48.52 | 30 |
| 60.55 | 6.51 | 7.21 | 5.02 | 5.16 | 6.00 | 6.60 | 10.83 | 14.36 | 20.00 | 26.98 | 32.12 | 39.82 | 44.13 | 47.25 | 50.74 | 53.95 | 30 |
| 61.00 | 7.71 | 6.81 | 7.13 | 5.35 | 5.28 | 7.14 | 10.31 | 13.55 | 21.25 | 28.04 | 35.69 | 40.44 | 44.94 | 51.58 | 54.75 | 58.42 | 30 |
| 62.00 | 8.07 | 7.26 | 8.36 | 6.37 | 6.91 | 8.04 | 13.61 | 16.46 | 24.32 | 30.44 | 35.25 | 40.37 | 46.08 | 49.00 | 58.80 | 62.58 | 30 |
| 63.00 | 7.92 | 7.87 | 7.15 | 7.96 | 6.20 | 9.44 | 14.21 | 19.18 | 28.07 | 36.69 | 40.29 | 46.22 | 51.20 | 56.13 | 63.47 | 69.79 | 30 |
| 63.87 | 9.06 | 8.78 | 7.56 | 7.30 | 6.37 | 11.78 | 13.69 | 16.80 | 25.56 | 34.84 | 42.52 | 47.19 | 50.05 | 56.50 | 62.95 | 65.37 | 30 |
| 65.00 | 5.58 | 4.09 | 5.18 | 3.98 | 7.26 | 11.18 | 16.08 | 20.08 | 28.54 | 36.31 | 46.05 | 54.05 | 59.72 | 64.40 | 70.94 | 78.06 | 30 |
| 65.80 | 9.49 | 9.79 | 8.11 | 8.37 | 10.96 | 15.09 | 17.28 | 21.53 | 28.09 | 36.01 | 42.70 | 49.29 | 58.54 | 64.45 | 73.15 | 78.77 | 30 |
| 67.00 | 9.59 | 10.93 | 9.80 | 10.20 | 13.54 | 18.03 | 22.50 | 27.36 | 36.41 | 43.61 | 51.03 | 58.28 | 68.28 | 74.90 | 82.68 | 89.27 | 30 |
| 51.45 | 0.68 | 0.87 | -1.06 | -1.05 | -1.23 | -1.91 | -2.95 | -2.43 | -0.90 | 0.35 | 1.21 | 2.79 | 3.16 | 5.02 | 7.14 | 8.95 | 33 |
| 53.00 | 0.76 | 0.95 | 0.20 | -0.24 | -0.24 | -0.30 | -0.80 | 0.39 | 0.06 | 0.23 | 3.23 | 4.27 | 7.99 | 9.80 | 11.39 | 13.41 | 33 |
| 55.00 | 2.06 | 2.08 | 1.48 | 1.15 | -0.55 | -0.35 | 0.27 | 0.79 | 3.40 | 6.35 | 10.50 | 14.13 | 15.86 | 20.02 | 20.28 | 22.91 | 33 |
| 57.40 | 5.22 | 4.95 | 4.78 | 3.56 | 2.93 | 1.00 | 3.53 | 6.97 | 12.73 | 19.79 | 23.37 | 28.31 | 32.51 | 38.41 | 39.90 | 42.70 | 33 |
| 58.00 | 4.56 | 4.37 | 4.85 | 3.28 | 2.52 | 1.85 | 5.00 | 8.29 | 12.57 | 18.67 | 24.78 | 27.81 | 32.51 | 36.68 | 39.00 | 43.19 | 33 |
| 59.39 | 7.18 | 6.24 | 5.51 | 5.85 | 4.71 | 4.39 | 7.42 | 11.22 | 18.30 | 24.95 | 30.88 | 35.83 | 39.71 | 45.37 | 48.84 | 50.80 | 33 |
| 60.55 | 8.67 | 6.26 | 6.43 | 6.50 | 5.71 | 5.34 | 10.06 | 13.87 | 20.36 | 28.27 | 32.94 | 39.38 | 45.49 | 48.00 | 52.67 | 56.04 | 33 |
| 61.00 | 7.47 | 6.37 | 7.18 | 5.89 | 4.09 | 7.18 | 10.83 | 13.36 | 21.52 | 27.24 | 36.05 | 41.35 | 46.03 | 52.60 | 56.45 | 60.81 | 33 |
| 62.00 | 7.25 | 8.03 | 8.53 | 7.33 | 6.25 | 7.21 | 13.61 | 15.82 | 23.95 | 29.09 | 35.53 | 42.48 | 47.80 | 51.19 | 59.69 | 64.46 | 33 |
| 63.00 | 8.80 | 7.45 | 8.42 | 7.62 | 6.75 | 9.03 | 16.04 | 18.79 | 27.17 | 36.49 | 42.50 | 47.65 | 53.44 | 59.29 | 64.14 | 71.41 | 33 |
| 63.87 | 8.44 | 7.45 | 7.62 | 7.05 | 7.61 | 11.93 | 13.20 | 18.59 | 26.04 | 33.88 | 43.34 | 47.21 | 51.76 | 58.56 | 64.62 | 66.61 | 33 |
| 65.00 | 5.20 | 5.90 | 4.88 | 3.58 | 5.90 | 9.41 | 14.51 | 20.80 | 28.27 | 37.71 | 46.35 | 56.16 | 59.93 | 65.73 | 73.31 | 79.06 | 33 |
| 65.80 | 9.90 | 9.39 | 9.00 | 9.16 | 9.89 | 14.61 | 17.16 | 23.22 | 29.03 | 34.99 | 42.63 | 49.77 | 58.01 | 66.46 | 73.84 | 81.71 | 33 |
| 67.00 | 11.31 | 9.15 | 10.61 | 10.22 | 15.14 | 19.12 | 22.30 | 29.18 | 36.90 | 44.58 | 53.26 | 59.76 | 70.59 | 77.77 | 84.61 | 90.92 | 33 |
| 51.45 | 0.69 | 0.28 | -0.34 | -1.01 | -0.78 | -0.79 | -2.47 | -1.83 | -0.61 | -0.40 | 1.98 | 2.39 | 3.90 | 6.51 | 7.82 | 8.70 | 36 |
| 53.00 | -0.93 | 0.16 | -0.07 | -1.00 | -0.67 | -0.79 | 0.08 | -0.53 | 0.30 | 1.76 | 4.20 | 5.43 | 9.40 | 11.67 | 12.98 | 13.91 | 36 |
| 55.00 | 2.62 | 2.23 | 1.63 | 2.08 | -0.27 | -1.14 | 0.26 | 0.85 | 4.88 | 8.99 | 13.24 | 16.03 | 19.18 | 22.15 | 23.52 | 26.14 | 36 |
| 57.40 | 6.33 | 5.48 | 4.69 | 4.49 | 2.24 | 1.38 | 3.77 | 6.65 | 15.82 | 22.67 | 27.29 | 32.42 | 36.93 | 42.20 | 43.03 | 45.40 | 36 |
| 58.00 | 6.11 | 6.12 | 6.17 | 4.42 | 2.99 | 1.88 | 4.76 | 10.51 | 16.72 | 23.54 | 28.15 | 31.64 | 36.65 | 39.95 | 41.43 | 46.28 | 36 |
| 59.39 | 9.53 | 9.15 | 8.27 | 7.74 | 6.16 | 5.79 | 8.21 | 14.10 | 21.47 | 27.18 | 34.43 | 38.68 | 43.36 | 49.46 | 50.96 | 51.42 | 36 |
| 60.55 | 10.06 | 8.16 | 6.32 | 7.61 | 7.31 | 6.96 | 13.40 | 17.58 | 24.34 | 31.39 | 37.24 | 43.21 | 48.29 | 51.44 | 54.44 | 56.11 | 36 |
| 61.00 | 9.49 | 8.07 | 8.43 | 7.56 | 6.93 | 8.35 | 12.63 | 17.00 | 25.01 | 31.75 | 40.55 | 45.30 | 50.31 | 54.74 | 56.52 | 61.65 | 36 |
| 62.00 | 10.86 | 10.59 | 8.94 | 7.65 | 7.60 | 9.55 | 17.17 | 19.71 | 26.53 | 33.05 | 39.83 | 45.98 | 49.37 | 52.92 | 62.54 | 65.37 | 36 |
| 63.00 | 11.19 | 9.29 | 9.73 | 8.63 | 8.34 | 10.82 | 18.25 | 21.76 | 31.25 | 42.34 | 46.04 | 51.48 | 55.88 | 60.19 | 66.34 | 73.23 | 36 |
| 63.87 | 9.82 | 8.99 | 10.02 | 7.27 | 7.80 | 12.87 | 16.72 | 20.58 | 30.74 | 38.66 | 46.35 | 49.39 | 53.42 | 60.47 | 66.12 | 68.77 | 36 |
| 65.00 | 6.51 | 5.60 | 4.98 | 5.17 | 6.82 | 12.38 | 17.10 | 21.72 | 31.73 | 41.53 | 51.02 | 59.75 | 62.38 | 69.37 | 75.78 | 80.25 | 36 |
| 65.80 | 11.98 | 9.79 | 10.17 | 9.09 | 11.88 | 16.53 | 19.95 | 24.63 | 32.03 | 36.27 | 44.49 | 50.79 | 60.81 | 68.08 | 76.29 | 82.06 | 36 |
| 67.00 | 11.51 | 10.49 | 12.03 | 11.58 | 16.28 | 20.40 | 23.87 | 31.41 | 38.08 | 46.74 | 53.19 | 61.13 | 71.50 | 79.21 | 86.95 | 93.82 | 36 |
| 51.45 | 0.39 | 0.68 | 0.37 | -0.68 | -0.14 | -0.28 | -0.30 | -1.81 | -0.65 | -0.87 | 0.18 | 2.07 | 5.95 | 7.51 | 9.11 | 11.03 | 39 |
| 53.00 | 0.78 | -0.13 | 0.04 | 0.02 | 0.40 | -0.70 | 0.55 | -0.76 | -1.16 | 0.64 | 5.18 | 7.53 | 9.97 | 11.29 | 13.91 | 15.72 | 39 |
| 55.00 | 3.72 | 3.75 | 2.72 | 1.32 | 1.12 | 0.16 | -0.58 | 1.23 | 5.59 | 9.89 | 13.86 | 18.22 | 20.24 | 23.63 | 24.23 | 27.83 | 39 |
| 57.40 | 7.19 | 6.90 | 6.15 | 7.15 | 3.42 | 0.58 | 4.64 | 9.60 | 19.48 | 26.95 | 33.39 | 38.38 | 43.00 | 47.65 | 48.09 | 48.76 | 39 |
| 58.00 | 8.11 | 8.57 | 6.33 | 5.35 | 4.53 | 1.89 | 6.64 | 13.12 | 19.42 | 27.66 | 33.06 | 37.64 | 39.87 | 45.97 | 44.15 | 47.88 | 39 |
| 59.39 | 11.65 | 9.57 | 9.45 | 7.68 | 6.37 | 7.03 | 11.47 | 15.85 | 26.26 | 31.95 | 40.39 | 44.35 | 48.10 | 53.62 | 56.03 | 53.42 | 39 |
| 60.55 | 13.67 | 12.26 | 8.95 | 8.99 | 8.19 | 9.20 | 16.28 | 20.07 | 28.48 | 35.56 | 42.03 | 49.95 | 54.15 | 56.43 | 59.04 | 58.93 | 39 |

| | | | | | | | | | | | | | | | | |
|---|---|---|---|---|---|---|---|---|---|---|---|---|---|---|---|---|
| 61.00 | 11.43 | 11.02 | 10.09 | 10.38 | 7.63 | 10.68 | 13.76 | 20.41 | 27.34 | 34.38 | 44.20 | 49.21 | 53.62 | 57.32 | 59.45 | 63.25 | 39 |
| 62.00 | 13.77 | 11.98 | 10.43 | 11.40 | 8.60 | 11.07 | 18.10 | 21.13 | 31.68 | 37.69 | 42.24 | 47.59 | 52.77 | 54.80 | 63.63 | 68.23 | 39 |
| 63.00 | 12.99 | 12.30 | 12.37 | 9.52 | 9.47 | 11.75 | 20.01 | 24.61 | 35.52 | 44.97 | 49.64 | 53.48 | 56.51 | 62.44 | 68.49 | 75.40 | 39 |
| 63.87 | 12.84 | 11.23 | 11.67 | 9.10 | 9.48 | 15.08 | 18.93 | 23.59 | 33.84 | 42.37 | 50.21 | 53.05 | 54.53 | 62.14 | 67.98 | 71.38 | 39 |
| 65.00 | 8.60 | 6.85 | 7.50 | 6.78 | 7.78 | 14.24 | 19.13 | 24.88 | 36.10 | 44.76 | 54.50 | 64.33 | 64.84 | 69.47 | 76.51 | 84.19 | 39 |
| 65.80 | 12.91 | 11.40 | 11.52 | 10.04 | 12.31 | 18.41 | 21.79 | 26.35 | 33.21 | 37.39 | 46.18 | 52.74 | 62.86 | 69.93 | 76.69 | 85.06 | 39 |
| 67.00 | 13.32 | 13.01 | 12.50 | 12.26 | 16.76 | 20.93 | 26.09 | 33.08 | 40.74 | 47.94 | 55.17 | 63.45 | 74.06 | 82.30 | 89.45 | 94.66 | 39 |

**Table C-2 Isobaric test data, 0-600 kpa, 21-39deg C.**

Raw data from the isotonic tests conducted on the muscle.

| Pressure (kpa) | length recorded (mm) with a force of 5 N. | length recorded (mm) with a force of 7 N. | length recorded (mm) with a force of 10 N. | length recorded (mm) with a force of 13 N. | length recorded (mm) with a force of 15 N. | length recorded (mm) with a force of 17 N. | length recorded (mm) with a force of 20 N. |
|---|---|---|---|---|---|---|---|
| 0 | 62.7 | 66.0 | 69.0 | 70.6 | 71.5 | 72.0 | 72.5 |
| 50 | 61.5 | 67.3 | 68.8 | 69.9 | 71.2 | 71.7 | 72.0 |
| 100 | 61.8 | 67.2 | 67.6 | 68.8 | 69.8 | 71.0 | 71.5 |
| 125 | 62.5 | 65.0 | 66.0 | 67.5 | 68.6 | 69.5 | 70.6 |
| 150 | 60.7 | 63.1 | 64.0 | 66.5 | 67.7 | 68.4 | 69.2 |
| 175 | 58.9 | 61.3 | 62.4 | 64.5 | 65.8 | 67.1 | 68.5 |
| 200 | 57.0 | 59.5 | 60.5 | 62.6 | 63.6 | 65.3 | 66.5 |
| 225 | 55.5 | 57.7 | 58.7 | 60.2 | 61.8 | 63.7 | 64.7 |
| 250 | 54.0 | 55.9 | 56.9 | 58.0 | 60.1 | 62.2 | 63.3 |
| 275 | 52.7 | 54.8 | 55.6 | 56.6 | 58.6 | 60.8 | 61.9 |
| 300 | 52.1 | 53.7 | 54.7 | 55.5 | 57.4 | 59.4 | 60.6 |
| 325 | 50.7 | 52.9 | 53.9 | 54.5 | 56.2 | 58.0 | 59.3 |
| 350 | 49.5 | 52.1 | 53.3 | 53.6 | 55.1 | 56.8 | 58.1 |
| 375 | 49.2 | 51.5 | 52.7 | 52.7 | 54.3 | 56.0 | 57.2 |
| 400 | 48.7 | 50.9 | 52.2 | 51.9 | 53.9 | 55.3 | 56.4 |
| 425 | 48.2 | 50.3 | 51.5 | 51.3 | 53.0 | 54.8 | 55.7 |
| 450 | 47.7 | 49.9 | 51.0 | 50.9 | 52.4 | 54.3 | 55.1 |
| 475 | 47.6 | 49.5 | 50.6 | 50.5 | 52.1 | 53.9 | 54.4 |
| 500 | 47.5 | 49.1 | 50.2 | 50.2 | 51.8 | 53.5 | 53.9 |
| 525 | 47.3 | 48.7 | 49.9 | 50.0 | 51.5 | 52.9 | 53.4 |
| 550 | 47.2 | 48.4 | 49.6 | 49.8 | 51.3 | 52.4 | 53.0 |
| 575 | 47.1 | 48.2 | 49.2 | 49.8 | 51.1 | 52.0 | 52.6 |
| 600 | 46.6 | 48.1 | 49.0 | 49.7 | 51.0 | 51.7 | 52.4 |

**Table C-3 Isotonic test results.**

Raw data from the isometric hysteresis test results conducted on the muscle.

| press (kpa) | force up (N) at length 61.9 mm | force down (N) at length 61.9 mm | force up (N) at length 61.9 mm | force down (N) at length 61.9 mm | force up (N) at length 63.9 mm | force down (N) at length 63.9 mm | force up (N) at length 63.9 mm | force down (N) at length 63.9 mm | force up (N) at length 55.9 mm | force down (N) at length 55.9 mm | force up (N) at length 55.9 mm | force down (N) at length 55.9 mm | force up (N) at length 61 mm | force down (N) at length 61 mm | force up (N) at length 61 mm | force down (N) at length 61 mm |
|---|---|---|---|---|---|---|---|---|---|---|---|---|---|---|---|---|
| 0 | -2.82 | -2.88 | -2.82 | -2.99 | -0.72 | -1.07 | -0.69 | -1.04 | -4.84 | -4.87 | -4.64 | -4.71 | -2.01 | -2.32 | -2.03 | -2.25 |
| 50 | -2.90 | -3.02 | -2.87 | -3.05 | -0.82 | -1.12 | -0.83 | -1.09 | -4.91 | -4.91 | -4.74 | -4.77 | -2.02 | -2.37 | -2.13 | -2.29 |
| 100 | -3.17 | -3.38 | -3.21 | -3.35 | -1.20 | -1.47 | -1.21 | -1.43 | -5.16 | -5.24 | -5.01 | -5.08 | -2.38 | -2.73 | -2.48 | -2.64 |
| 150 | -4.82 | -4.82 | -4.44 | -4.89 | 1.20 | -0.21 | 0.88 | 0.74 | -7.21 | -7.20 | -6.85 | -6.54 | -2.65 | -3.21 | -1.80 | -2.89 |
| 200 | -0.24 | -0.58 | -0.20 | -0.32 | 7.41 | 6.07 | 7.65 | 7.17 | -5.13 | -5.67 | -5.63 | -5.47 | 3.15 | 2.10 | 2.63 | 1.73 |
| 250 | 4.67 | 3.90 | 5.33 | 4.54 | 13.41 | 12.34 | 13.37 | 13.57 | -2.44 | -2.48 | -2.03 | -2.14 | 8.32 | 7.33 | 8.65 | 7.52 |
| 300 | 9.20 | 8.78 | 8.95 | 8.96 | 20.96 | 18.49 | 20.81 | 20.47 | 0.54 | 0.22 | 0.92 | 0.60 | 13.56 | 12.33 | 13.46 | 12.67 |
| 350 | 13.00 | 12.60 | 13.55 | 12.64 | 27.27 | 24.73 | 27.60 | 27.18 | 3.49 | 3.11 | 3.81 | 3.50 | 17.96 | 18.45 | 17.77 | 18.12 |
| 400 | 17.67 | 16.94 | 17.81 |  | 32.19 | 30.90 | 33.83 |  | 6.14 | 6.09 | 6.55 |  | 22.71 | 23.36 | 22.57 |  |
| 450 | 21.98 | 19.79 |  |  | 39.06 | 38.29 |  |  | 8.64 | 8.62 |  |  | 29.08 | 28.32 |  |  |
| 500 | 25.60 | 24.48 |  |  | 44.80 | 43.43 |  |  | 11.18 | 11.23 |  |  | 33.01 | 32.61 |  |  |
| 550 | 30.79 | 30.43 |  |  | 51.75 | 51.39 |  |  | 13.64 | 13.61 |  |  | 38.76 | 36.96 |  |  |
| 600 | 34.27 |  |  |  | 53.99 |  |  |  | 16.06 |  |  |  | 41.46 |  |  |  |

**Table C-4 Isometric hysteresis test results.**

Raw data from the isometric hysteresis test results conducted on the muscle.

**Hysteresis isometric results analysis.**

| Press (kpa) | force difference (N) at length 61.9mm | force difference (N) at length 61.9mm | force difference (N) at length 63.9mm | force difference (N) at length 63.9mm | force difference (N) at length 55.9mm | force difference (N) at length 55.9mm | force difference (N) at length 61mm | force difference (N) at length 61mm |
|---|---|---|---|---|---|---|---|---|
| 0 | 0.06 | 0.17 | 0.35 | 0.35 | 0.03 | 0.06 | 0.31 | 0.22 |
| 50 | 0.13 | 0.19 | 0.30 | 0.27 | 0.01 | 0.03 | 0.35 | 0.16 |
| 100 | 0.21 | 0.14 | 0.27 | 0.22 | 0.08 | 0.06 | 0.35 | 0.17 |
| 150 | 0.00 | 0.44 | 1.41 | 0.15 | -0.01 | -0.31 | 0.56 | 1.10 |
| 200 | 0.34 | 0.13 | 1.35 | 0.49 | 0.54 | -0.16 | 1.05 | 0.90 |
| 250 | 0.77 | 0.78 | 1.07 | -0.20 | 0.04 | 0.11 | 0.99 | 1.13 |
| 300 | 0.42 | -0.00 | 2.47 | 0.34 | 0.32 | 0.32 | 1.24 | 0.79 |
| 350 | 0.40 | 0.91 | 2.54 | 0.42 | 0.39 | 0.31 | -0.50 | -0.35 |
| 400 | 0.73 | 0.00 | 1.29 | 0.00 | 0.06 | 0.00 | -0.65 | 0.00 |
| 450 | 2.19 |  | 0.77 |  | 0.02 |  | 0.76 |  |
| 500 | 1.12 |  | 1.37 |  | -0.05 |  | 0.40 |  |
| 550 | 0.36 |  | 0.36 |  | 0.03 |  | 1.80 |  |
| 600 | 0.00 |  | 0.00 |  | 0.00 |  | 0.00 |  |
| **mean (N)** | **0.79** | **0.46** | **1.40** | **0.26** | **0.17** | **0.14** | **0.64** | **0.62** |

**Table C-5 Isometric hysteresis results differences between up and down force results.**

Raw data from the isotonic hysteresis test results conducted on the muscle.

| press (kpa) | force up (N) at mass 1.154 Kg | force down (N) at mass 1.154 Kg | force up (N) at mass 1.154 Kg | force down (N) at mass 1.154 Kg | force up (N) at mass 0.751 Kg | force down (N) at mass 0.751 Kg | force up (N) at mass 0.751 Kg | force down (N) at mass 0.751 Kg | force up (N) at mass 1.751 Kg | force down (N) at mass 1.751 Kg | force up (N) at mass 1.751 Kg | force down (N) at mass 1.751 Kg | force up (N) at mass 1.339 Kg | force down (N) at mass 1.339 Kg | force up (N) at mass 1.339 Kg | force down (N) at mass 1.339 Kg |
|---|---|---|---|---|---|---|---|---|---|---|---|---|---|---|---|---|
| 0 | 69.00 | 68.78 | 68.78 | 68.67 | 66.00 | 66.11 | 66.00 | 66.11 | 72.00 | 72.11 | 72.11 | 72.00 | 70.00 | 70.33 | 70.33 | 70.33 |
| 50 | 68.34 | 68.12 | 68.12 | 68.12 | 66.11 | 66.11 | 66.11 | 66.11 | 71.56 | 71.67 | 71.78 | 71.78 | 69.67 | 69.78 | 69.89 | 69.89 |
| 100 | 66.91 | 66.69 | 66.91 | 66.69 | 65.23 | 64.90 | 65.12 | 64.90 | 70.90 | 70.79 | 71.01 | 71.01 | 68.68 | 68.79 | 68.90 | 69.01 |
| 150 | 64.49 | 64.38 | 64.16 | 64.27 | 61.93 | 61.71 | 61.93 | 61.82 | 69.69 | 69.58 | 69.80 | 70.02 | 67.25 | 67.58 | 67.47 | 67.36 |
| 200 | 60.98 | 60.87 | 60.98 | 60.76 | 58.42 | 58.09 | 58.31 | 58.20 | 67.60 | 67.71 | 67.82 | 67.38 | 64.40 | 64.84 | 64.73 | 64.51 |
| 250 | 58.23 | 57.90 | 58.34 | 58.23 | 56.11 | 55.67 | 56.00 | 55.89 | 65.08 | 64.75 | 65.19 | 64.75 | 61.76 | 61.43 | 62.09 | 61.76 |
| 300 | 56.47 | 56.47 | 56.36 | 56.25 | 54.57 | 54.35 | 54.57 | 54.46 | 62.66 | 62.77 | 62.99 | 63.10 | 59.78 | 59.56 | 59.78 | 59.78 |
| 350 | 55.04 | 54.93 | 55.04 | 55.04 | 53.47 | 53.36 | 53.47 | 53.47 | 60.90 | 60.68 | 60.90 | 61.01 | 58.13 | 57.69 | 58.24 | 58.24 |
| 400 | 54.16 | 54.16 | 53.95 | 53.95 | 52.70 | 52.59 | 52.70 | 52.70 | 59.58 | 59.36 | 59.58 | 59.58 | 56.70 | 56.70 | 57.03 | 57.03 |
| 450 | 53.40 | 53.29 | | | 52.04 | 51.93 | | | 58.59 | 58.37 | | | 55.82 | 55.82 | | |
| 500 | 52.85 | 52.74 | | | 51.60 | 51.49 | | | 57.71 | 57.60 | | | 55.05 | 55.05 | | |
| 550 | 52.41 | 52.30 | | | 51.16 | 51.16 | | | 56.95 | 57.05 | | | 54.51 | 54.51 | | |
| 600 | 51.86 | 51.86 | | | 50.73 | 50.73 | | | 56.51 | 56.51 | | | 53.96 | 53.96 | | |

**Table C-6 Isotonic hysteresis test results.**

Raw data from the isotonic hysteresis test results conducted on the muscle.

| Pressure (kpa) | force difference (N) at mass 1.154 Kg | force difference (N) at mass 1.154 Kg | force difference (N) at mass 0.751 Kg | force difference (N) at mass 0.751 Kg | force difference (N) at mass 1.751 Kg | force difference (N) at mass 1.751 Kg | force difference (N) at mass 1.339 Kg | force difference (N) at mass 1.339 Kg |
|---|---|---|---|---|---|---|---|---|
| 0 | 0.22 | 0.11 | -0.11 | -0.11 | -0.11 | 0.11 | -0.33 | 0.00 |
| 50 | 0.22 | 0.00 | 0.00 | 0.00 | -0.11 | 0.00 | -0.11 | 0.00 |
| 100 | 0.22 | 0.22 | 0.33 | 0.22 | 0.11 | 0.00 | -0.11 | -0.11 |
| 150 | 0.11 | -0.11 | 0.22 | 0.11 | 0.11 | -0.22 | -0.33 | 0.11 |
| 200 | 0.11 | 0.22 | 0.33 | 0.11 | -0.11 | 0.44 | -0.44 | 0.22 |
| 250 | 0.33 | 0.11 | 0.44 | 0.11 | 0.33 | 0.44 | 0.33 | 0.33 |
| 300 | 0.00 | 0.11 | 0.22 | 0.11 | -0.11 | -0.11 | 0.22 | 0.00 |
| 350 | 0.11 | 0.00 | 0.11 | 0.00 | 0.22 | -0.11 | 0.44 | 0.00 |
| 400 | 0.00 | 0.00 | 0.11 | 0.00 | 0.22 | 0.00 | 0.00 | 0.00 |
| 450 | 0.11 | | 0.11 | | 0.22 | | 0.00 | |
| 500 | 0.11 | | 0.11 | | 0.11 | | 0.00 | |
| 550 | 0.11 | | 0.00 | | -0.11 | | 0.00 | |
| 600 | 0.00 | | 0.00 | | 0.00 | | 0.00 | |
| **mean** | **0.13** | **0.07** | **0.14** | **0.06** | **0.06** | **0.06** | **-0.03** | **0.06** |

**Table C-7 Isotonic hysteresis results differences between up and down length measurements.**

## C-2. Regression analysis of the isometric data collected from the muscle

Regression analysis of the isometric data in the 150 to 600kpa region.

Best fit regression summary using only a single term predictor .

Temperature 21deg C

| length (mm) | P | $P^2$ | $P^3$ | cos(P) | sin(P) |
|---|---|---|---|---|---|
| 51.45 | 1 | 2 | 4 | 3 | 5 |
| 53 | 1 | 2 | 4 | 3 | 5 |
| 55 | 1 | 2 | 4 | 3 | 5 |
| 57.4 | 1 | 2 | 4 | 3 | 5 |
| 58 | 1 | 2 | 4 | 3 | 5 |
| 59.39 | 1 | 3 | 4 | 2 | 5 |
| 60.55 | 1 | 3 | 4 | 2 | 5 |
| 61 | 1 | 3 | 4 | 2 | 5 |
| 62 | 1 | 2 | 4 | 3 | 5 |
| 63 | 1 | 3 | 4 | 2 | 5 |
| 63.87 | 1 | 3 | 4 | 2 | 5 |
| 65 | 1 | 3 | 4 | 2 | 5 |
| 65.8 | 1 | 2 | 4 | 3 | 5 |
| 67 | 1 | 3 | 4 | 2 | 5 |

**Table C-8 Summarised best fits results 21deg.**

The best fits regression indicates that pressure is the most likely predictor.
Regression results using pressure to predict force.
Pressure gradient and intercept coefficients.

Temperature 21deg C

| length (mm) | pressure gradient coeffient | intercept coefficient |
|---|---|---|
| 51.45 | 0.0230 | -7.43 |
| 53 | 0.0261 | -6.06 |
| 55 | 0.0465 | -8.69 |
| 57.4 | 0.0793 | -11.8 |
| 58 | 0.0785 | -10.9 |
| 59.39 | 0.0919 | -10.9 |
| 60.55 | 0.101 | -10.5 |
| 61 | 0.112 | -12.2 |
| 62 | 0.115 | -11.0 |
| 63 | 0.126 | -10.9 |
| 63.87 | 0.123 | -10.2 |
| 65 | 0.144 | -13.2 |
| 65.8 | 0.137 | -9.19 |
| 67 | 0.152 | -6.93 |

**Table C-9 Pressure gradient and intercept coefficients 21deg C,150-600kpa.**

Temperature 24deg C

| muscle length (mm) | pressure gradient coefficient | intercept coefficient |
|---|---|---|
| 51.45 | 0.0242577 | -7.93 |
| 53 | 0.027701 | -6.5256 |
| 55 | 0.048068 | -8.9149 |
| 57.4 | 0.0827333 | -12.2910 |
| 58 | 0.081478 | -11.2888 |
| 59.39 | 0.0961821 | -11.5717 |
| 60.55 | 0.104927 | -10.9130 |
| 61 | 0.116393 | -12.6702 |
| 62 | 0.118294 | -11.1376 |
| 63 | 0.129981 | -11.1489 |
| 63.87 | 0.127252 | -10.589 |
| 65 | 0.149250 | -13.557 |
| 65.8 | 0.141909 | -9.3035 |
| 67 | 0.157952 | -7.146 |

**Table C-10 Pressure gradient and intercept coefficients 24deg C, 150-600kpa.**

Temperature 27deg C

| muscle length (mm) | pressure gradient coefficient | intercept coefficient |
|---|---|---|
| 51.45 | 0.023882 | -7.6855 |
| 53 | 0.028189 | -6.4978 |
| 55 | 0.049868 | -9.2910 |
| 57.4 | 0.0859644 | -12.8043 |
| 58 | 0.084235 | -11.5426 |
| 59.39 | 0.099533 | -11.8010 |
| 60.55 | 0.109115 | -11.2804 |
| 61 | 0.121391 | -13.2784 |
| 62 | 0.123363 | -11.7072 |
| 63 | 0.135353 | -11.7217 |
| 63.87 | 0.131991 | -10.854 |
| 65 | 0.155519 | -14.232 |
| 65.8 | 0.147464 | -9.7497 |
| 67 | 0.164069 | -7.394 |

**Table C-11 Pressure gradient and intercept coefficients 27deg.**

Temperature 30deg C

| muscle length (mm) | pressure gradient coefficient | intercept coefficient |
|---|---|---|
| 51.45 | 0.025550 | -8.2881 |
| 53 | 0.029448 | -6.7312 |
| 55 | 0.052147 | -9.733 |
| 57.4 | 0.0891487 | -13.2639 |
| 58 | 0.087795 | -12.0231 |

| | | |
|---|---|---|
| 59.39 | 0.103357 | -11.9773 |
| 60.55 | 0.125341 | -13.5662 |
| 61 | 0.128115 | -12.1497 |
| 62 | 0.146071 | -12.616 |
| 63 | 0.137442 | -11.358 |
| 63.87 | 0.167728 | -15.403 |
| 65 | 0.161424 | -14.711 |
| 65.8 | 0.153667 | -10.3676 |
| 67 | 0.170057 | -7.621 |

**Table C-12 Pressure gradient and intercept coefficients 30deg C, 150-600kpa.**

Temperature 33deg C

| muscle length (mm) | pressure gradient coefficient | intercept coefficient |
|---|---|---|
| 51.45 | 0.02663 | -8.6211 |
| 53 | 0.030880 | -7.2390 |
| 55 | 0.05388 | -10.0568 |
| 57.4 | 0.0922487 | -13.702 |
| 58 | 0.091005 | -12.5921 |
| 59.39 | 0.106901 | -12.6588 |
| 60.55 | 0.117875 | -12.2177 |
| 61 | 0.129955 | -14.1908 |
| 62 | 0.133028 | -12.6808 |
| 63 | 0.146071 | -12.616 |
| 63.87 | 0.142414 | -11.814 |
| 65 | 0.167728 | -15.403 |
| 65.8 | 0.159356 | -10.6516 |
| 67 | 0.176208 | -7.886 |

**Table C-13 Pressure gradient and intercept coefficients 33deg C, 150-600kpa.**

Temperature 36deg C

| muscle length (mm) | pressure gradient coefficient | intercept coefficient |
|---|---|---|
| 51.45 | 0.0275240 | -8.9645 |
| 53 | 0.031496 | -7.3051 |
| 55 | 0.055629 | -10.2811 |
| 57.4 | 0.095264 | -14.1185 |
| 58 | 0.094358 | -13.0157 |
| 59.39 | 0.111352 | -13.3519 |
| 60.55 | 0.121792 | -12.5989 |
| 61 | 0.135085 | -14.7804 |
| 62 | 0.137882 | -13.1766 |
| 63 | 0.150934 | -15.0934 |
| 63.87 | 0.147003 | -12.073 |
| 65 | 0.173385 | -15.890 |
| 65.8 | 0.165080 | -11.0701 |
| 67 | 0.183077 | -8.342 |

**Table C-14 Pressure gradient and intercept coefficients 36deg C,150-600kpa.**

Temperature 39 deg C

| muscle length (mm) | pressure gradient coefficient | intercept coefficient |
|---|---|---|
| 51.45 | 0.0285 | -9.2269 |
| 53 | 0.033014 | -7.7700 |
| 55 | 0.057862 | -10.7549 |
| 57.4 | 0.098889 | -14.6699 |
| 58 | 0.097150 | -13.2707 |
| 59.39 | 0.114689 | -13.6557 |
| 60.55 | 0.126050 | -13.0937 |
| 61 | 0.139578 | -15.1968 |
| 62 | 0.146524 | -14.743 |
| 63 | 0.156346 | -13.546 |
| 63.87 | 0.152666 | -12.701 |
| 65 | 0.179488 | -16.426 |
| 65.8 | 0.170694 | -11.4349 |
| 67 | 0.189455 | -8.649 |

**Table C-15 Pressure gradient and intercept coefficients 39deg C, 150-600kpa.**

Summarised best fits regression results are shown. These results were used to identify the relationship between muscle length, pressure gradient and intercept coefficients in tables C-9 to C-15.

| Pressure gradient coefficient | Length | Length^3 | cos(L) | sin(L) |
|---|---|---|---|---|
| 21 | 1 | 2 | 4 | 3 |
| 24 | 1 | 2 | 4 | 3 |
| 27 | 1 | 2 | 4 | 3 |
| 30 | 1 | 2 | 3 | 4 |
| 33 | 1 | 2 | 3 | 4 |
| 36 | 1 | 2 | 3 | 4 |
| 39 | 1 | 2 | 3 | 4 |

**Table C-16 Summarised best fits results of the gradient coefficients.**

| Pressure intercept coefficient | Length | Length^3 | cos(L) | sin(L) |
|---|---|---|---|---|
| 21 | 1 | 2 | 4 | 3 |
| 24 | 1 | 2 | 4 | 3 |
| 27 | 1 | 2 | 4 | 3 |
| 30 | 1 | 2 | 4 | 4 |
| 33 | 1 | 2 | 4 | 4 |
| 36 | 1 | 2 | 4 | 4 |
| 39 | 1 | 2 | 4 | 4 |

**Table C-17 Summarised best fits results of the intercept coefficients 150-600kpa, 21-39deg C.**

Regression results of the muscle length, intercept and gradient coefficients tables C-9 to C-15 are listed below.

| Temp\Coefficient type | muscle length pressure gradient ($K_1$) | muscle length gradient ($K_2$) | pressure gradient ($K_3$) | intercept (c) |
|---|---|---|---|---|
| 21 | 0.00869 | -0.159 | -0.426 | -0.43 |
| 24 | 0.00897 | -0.143 | -0.439 | -1.78 |
| 27 | 0.00939 | -0.176 | -0.461 | -0.09 |
| 30 | 0.0102 | -0.221 | -0.501 | 1.86 |
| 33 | 0.0101 | -0.177 | -0.494 | -0.95 |
| 36 | 0.0105 | -0.211 | -0.513 | 0.54 |
| 39 | 0.0108 | -0.203 | -0.531 | -0.29 |

**Table C-18 Summarised full regressions of the intercept and gradient coefficients, Table C-9 to C-15.**

Best Subsets Regression of muscle length pressure gradient coefficient and temperature.

| Vars | R-sq | Adj. R-sq | C-p | s | Temp | log(t) | sin(t) | cos(t) |
|---|---|---|---|---|---|---|---|---|
| 1 | 99.6 | 99.5 | 23.9 | 0.0000541 | X | | | |
| 1 | 98.0 | 97.6 | 122.4 | 0.0001168 | | X | | |
| 2 | 99.9 | 99.8 | 7.8 | 0.0000346 | X | | | X |
| 2 | 99.8 | 99.6 | 13.7 | 0.0000447 | X | X | | |
| 3 | 100.0 | 99.9 | 3.0 | 0.0000190 | X | X | | X |
| 3 | 99.9 | 99.7 | 9.4 | 0.0000391 | X | | X | X |
| 4 | 100.0 | 99.9 | 5.0 | 0.0000233 | X | X | X | X |

**Best-fit C-1 Best fits regression analysis of the muscle length pressure gradient in Table C18 and temperature, 150-600kpa 21-39degC.**

This indicates that the temperature is a good predictor of the pressure distance gradient coefficient

Best Subsets Regression of muscle length gradient coefficient and temperature

| Vars | R-sq | Adj. R-sq | C-p | s | t e m p | l o g ( t ) | s i n ( t ) | c o s ( t ) |
|---|---|---|---|---|---|---|---|---|
| 1 | 56.3 | 47.5 | 5.4 | 0.021231 | | | | X |
| 1 | 20.9 | 5.1 | 12.3 | 0.028549 | | | X | |
| 2 | 61.0 | 41.5 | 6.5 | 0.022410 | X | | | X |
| 2 | 59.0 | 38.6 | 6.9 | 0.022970 | | X | | X |
| 3 | 89.6 | 79.2 | 3.0 | 0.013380 | X | X | | X |
| 3 | 62.1 | 24.1 | 8.3 | 0.025527 | X | | X | X |
| 4 | 89.6 | 68.9 | 5.0 | 0.016334 | X | X | X | X |

**Best-fit C-2 Best fits regression analysis of the muscle length gradient in Table C18 and temperature, 150-600kpa 21-39degC.**

This indicates that temperature is not well related to the muscle length gradient coefficient

Best Subsets Regression of pressure gradient coefficient and temperature

| Vars | R-sq | Adj. R-sq | C-p | s | t e m p | l o g ( t ) | s i n ( t ) | c o s ( t ) |
|---|---|---|---|---|---|---|---|---|
| 1 | 99.9 | 99.9 | 10.2 | 0.0014361 | X | | | |
| 1 | 98.9 | 98.7 | 118.2 | 0.0043452 | | X | | |
| 2 | 100.0 | 100.0 | 1.2 | 0.0006485 | X | | | X |
| 2 | 99.9 | 99.9 | 8.7 | 0.0013731 | X | | X | |
| 3 | 100.0 | 100.0 | 3.0 | 0.0007275 | X | | X | X |
| 3 | 100.0 | 100.0 | 3.1 | 0.0007359 | X | X | | X |
| 4 | 100.0 | 99.9 | 5.0 | 0.0008827 | X | X | X | X |

**Best-fit C-3 Best fits regression analysis of the pressure gradient in Table C18 and temperature, 150-600kpa 21-39degC.**

This indicates that temperature is linearly related to the pressure gradient coefficient

Best Subsets Regression of intercept coefficient and temperature

| Vars | R-sq | Adj. R-sq | C-p | s | t e m p | l o g ( t ) | s i n ( t ) | c o s ( t ) |
|---|---|---|---|---|---|---|---|---|
| 1 | 53.4 | 44.1 | 0.8 | 0.40671 | | | | X |
| 1 | 17.6 | 1.2 | 3.7 | 0.54070 | | | X | |
| 2 | 74.8 | 62.2 | 1.0 | 0.33436 | | X | | X |
| 2 | 74.1 | 61.1 | 1.1 | 0.33914 | X | | | X |
| 3 | 75.2 | 50.4 | 3.0 | 0.38312 | X | X | | X |
| 3 | 74.9 | 49.7 | 3.0 | 0.38557 | | X | X | X |
| 4 | 75.4 | 26.1 | 5.0 | 0.46744 | X | X | X | X |

**Best-fit C-4 Best fits regression analysis of the intercept coefficient in Table C18 and temperature, 150-600kpa 21-39degC.**

This indicates that temperature is not well related to the intercept coefficient

Full regressions of temperature, gradient and intercept coefficients were undertaken, the data that was used was the isometric data 150-600kpa, 21-39deg C.

Regression of muscle length pressure gradient and temperature

*The regression equation is*

$K_1 = 0.00620 + 0.000120\ temp$

| Predictor | Coef | Stdev | t-ratio | p |
|---|---|---|---|---|
| Constant | 0.0062000 | 0.0003712 | 16.70 | 0.000 |
| temp | 0.00012024 | 0.00001213 | 9.91 | 0.000 |

*s = 0.0001926  R-sq = 95.2%  R-sq(adj) = 94.2%*

*Analysis of Variance*

| SOURCE | DF | SS | MS | F | p |
|---|---|---|---|---|---|
| Regression | 1 | 3.64322E-06 | 3.64322E-06 | 98.18 | 0.000 |
| Error | 5 | 1.85529E-07 | 3.71058E-08 | | |
| Total | 6 | 3.82874E-06 | | | |

**Full-regression C-1 Full regression of muscle length pressure gradient and temperature, 150-600kpa 21-39degC.**

Regression of pressure gradient and temperature.

*The regression equation is*
$K_3$ = - 0.304 - 0.00590 temp

| Predictor | Coef | Stdev | t-ratio | p |
|---|---|---|---|---|
| Constant | -0.30357 | 0.01918 | -15.83 | 0.000 |
| temp | -0.0059048 | 0.0006269 | -9.42 | 0.000 |

s = 0.009951 R-sq = 94.7% R-sq(adj) = 93.6%

*Analysis of Variance*

| SOURCE | DF | SS | MS | F | p |
|---|---|---|---|---|---|
| Regression | 1 | 0.0087863 | 0.0087863 | 88.72 | 0.000 |
| Error | 5 | 0.0004951 | 0.0000990 | | |
| Total | 6 | 0.0092814 | | | |

**Full-regression C-2 Full regression of pressure gradient and temperature, 150-600kpa 21-39degC.**

## Isometric analysis 0-125kpa region.

Regression coefficients for the isometric experiments, Regression was done on force with pressure for a predictor.

Summary of the best fits regression for the pressure force relationship.

Temperature 21deg C.

| length (l) (mm) | P | $P^2$ | $P^3$ | cos(P) | sin(P) |
|---|---|---|---|---|---|
| 51.45 | 2 | 1 | 3 | 4 | 5 |
| 53 | 2 | 1 | 3 | 4 | 5 |
| 55 | 2 | 1 | 3 | 4 | 5 |
| 57.4 | 2 | 1 | 3 | 4 | 5 |
| 58 | 2 | 1 | 3 | 4 | 5 |
| 59.39 | 1 | 3 | 4 | 2 | 5 |
| 60.55 | 1 | 3 | 4 | 2 | 5 |
| 61 | 1 | 3 | 4 | 2 | 5 |
| 62 | 1 | 2 | 4 | 3 | 5 |
| 63 | 1 | 3 | 4 | 2 | 5 |
| 63.87 | 1 | 3 | 4 | 2 | 5 |
| 65 | 1 | 3 | 4 | 2 | 5 |
| 65.8 | 1 | 2 | 4 | 3 | 5 |
| 67 | 1 | 3 | 4 | 2 | 5 |

**Table C-19 Summarised best fits isometric data 0-125kpa region 21deg C.**

Temperature 24deg C.

| length (l) (mm) | P | $P^2$ | $P^3$ | cos(P) | sin(P) |
|---|---|---|---|---|---|
| 51.45 | 3 | 4 | 5 | 2 | 1 |
| 53 | 3 | 5 | 1 | 4 | 2 |
| 55 | 2 | 3 | 1 | 4 | 5 |
| 57.4 | 2 | 4 | 5 | 1 | 3 |
| 58 | 2 | 4 | 5 | 1 | 3 |
| 59.39 | 3 | 3 | 5 | 1 | 4 |
| 60.55 | 2 | 3 | 1 | 5 | 4 |
| 61 | 2 | 3 | 1 | 4 | 5 |
| 62 | 1 | 2 | 4 | 3 | 5 |
| 63 | 1 | 3 | 4 | 2 | 5 |
| 63.87 | 1 | 3 | 4 | 2 | 5 |
| 65 | 1 | 3 | 4 | 2 | 5 |
| 65.8 | 1 | 2 | 4 | 3 | 5 |
| 67 | 1 | 3 | 4 | 2 | 5 |

**Table C-20 Summarised best fits isometric data 0-125kpa region 24deg C.**

Temperature 27deg C.

| length (l) (mm) | P | $P^2$ | $P^3$ | cos(P) | sin(P) |
|---|---|---|---|---|---|
| 51.45 | 2 | 4 | 1 | 3 | 5 |
| 53 | 2 | 4 | 1 | 3 | 5 |
| 55 | 4 | 2 | 1 | 3 | 5 |
| 57.4 | 3 | 2 | 4 | 1 | 5 |
| 58 | 1 | 2 | 4 | 3 | 5 |
| 59.39 | 1 | 3 | 4 | 2 | 5 |
| 60.55 | 1 | 3 | 4 | 2 | 5 |
| 61 | 1 | 3 | 4 | 2 | 5 |
| 62 | 1 | 2 | 4 | 3 | 5 |
| 63 | 1 | 3 | 4 | 2 | 5 |
| 63.87 | 2 | 1 | 4 | 3 | 5 |
| 65 | 2 | 1 | 4 | 3 | 5 |
| 65.8 | 2 | 4 | 1 | 3 | 5 |
| 67 | 2 | 3 | 1 | 4 | 5 |

**Table C-21 Summarised best fits isometric data 0-125kpa region 27deg C.**

Temperature 30deg C.

| length (l) (mm) | P | $P^2$ | $P^3$ | cos(P) | sin(P) |
|---|---|---|---|---|---|
| 51.45 | 2 | 4 | 1 | 3 | 5 |
| 53 | 2 | 4 | 1 | 3 | 5 |
| 55 | 2 | 4 | 1 | 3 | 5 |
| 57.4 | 3 | 4 | 2 | 1 | 5 |
| 58 | 3 | 2 | 4 | 1 | 5 |
| 59.39 | 2 | 3 | 4 | 1 | 5 |
| 60.55 | 1 | 3 | 4 | 2 | 5 |
| 61 | 1 | 3 | 4 | 2 | 5 |

| | | | | | |
|---|---|---|---|---|---|
| 62 | 1 | 2 | 4 | 3 | 5 |
| 63 | 1 | 3 | 4 | 2 | 5 |
| 63.87 | 1 | 3 | 4 | 2 | 5 |
| 65 | 2 | 4 | 1 | 2 | 5 |
| 65.8 | 2 | 4 | 1 | 3 | 5 |
| 67 | 2 | 3 | 1 | 4 | 5 |

**Table C-22 Summarised best fits isometric data 0-125kpa region 30deg C.**

Temperature 33deg C.

| length (l) (mm) | P | $P^2$ | $P^3$ | cos(P) | sin(P) |
|---|---|---|---|---|---|
| 51.45 | 3 | 4 | 1 | 2 | 5 |
| 53 | 2 | 4 | 1 | 3 | 5 |
| 55 | 2 | 3 | 4 | 1 | 5 |
| 57.4 | 2 | 1 | 4 | 3 | 5 |
| 58 | 1 | 2 | 3 | 4 | 5 |
| 59.39 | 1 | 3 | 4 | 2 | 5 |
| 60.55 | 1 | 3 | 4 | 2 | 5 |
| 61 | 2 | 3 | 4 | 2 | 5 |
| 62 | 1 | 2 | 4 | 3 | 5 |
| 63 | 1 | 3 | 4 | 2 | 5 |
| 63.87 | 1 | 3 | 4 | 2 | 5 |
| 65 | 2 | 3 | 4 | 2 | 5 |
| 65.8 | 3 | 2 | 1 | 4 | 5 |
| 67 | 3 | 1 | 4 | 2 | 5 |

**Table C-23 Summarised best fits isometric data 0-125kpa region 33deg C.**

Temperature 36deg C.

| length (l) (mm) | P | $P^2$ | $P^3$ | cos(P) | sin(P) |
|---|---|---|---|---|---|
| 51.45 | 2 | 4 | 3 | 1 | 5 |
| 53 | 2 | 3 | 4 | 1 | 5 |
| 55 | 3 | 2 | 1 | 4 | 5 |
| 57.4 | 3 | 1 | 1 | 4 | 5 |
| 58 | 2 | 1 | 4 | 3 | 5 |
| 59.39 | 1 | 3 | 4 | 2 | 5 |
| 60.55 | 1 | 3 | 4 | 2 | 5 |
| 61 | 1 | 3 | 2 | 4 | 5 |
| 62 | 1 | 2 | 4 | 3 | 5 |
| 63 | 1 | 3 | 4 | 2 | 5 |
| 63.87 | 1 | 3 | 4 | 2 | 5 |
| 65 | 2 | 3 | 1 | 4 | 5 |
| 65.8 | 3 | 4 | 1 | 2 | 5 |
| 67 | 4 | 3 | 1 | 2 | 5 |

**Table C-24 Summarised best fits isometric data 0-125kpa region 36deg C.**

Temperature 39deg C.

| length (l) (mm) | P | $P^2$ | $P^3$ | cos(P) | sin(P) |
|---|---|---|---|---|---|
| 51.45 | 4 | 2 | 1 | 3 | 5 |
| 53 | 4 | 2 | 1 | 3 | 5 |
| 55 | 3 | 4 | 1 | 2 | 5 |
| 57.4 | 3 | 4 | 2 | 1 | 5 |
| 58 | 2 | 4 | 3 | 1 | 5 |
| 59.39 | 1 | 3 | 4 | 2 | 5 |
| 60.55 | 1 | 3 | 4 | 2 | 5 |
| 61 | 1 | 3 | 4 | 2 | 5 |
| 62 | 1 | 2 | 4 | 3 | 5 |
| 63 | 1 | 3 | 4 | 2 | 5 |
| 63.87 | 1 | 3 | 4 | 2 | 5 |
| 65 | 2 | 4 | 1 | 3 | 5 |
| 65.8 | 2 | 4 | 1 | 3 | 5 |
| 67 | 3 | 4 | 1 | 2 | 5 |

**Table C-25 Summarised best fits isometric data 0-125kpa region 39deg C.**

From the best fits it was observed that most of the distance curves had pressure as the best predictor of force. Pressure was then regressed against force. The pressure gradient and intercept coefficients obtained from these regressions are listed in tables below.

Temperature 21deg C.

| muscle length (mm) | pressure gradient coefficient | intercept coefficient |
|---|---|---|
| 51.45 | -0.00299 | 0.261 |
| 53 | -0.00360 | 0.014 |
| 55 | -0.00577 | 1.10 |
| 57.4 | -0.00613 | 2.52 |
| 58 | -0.00823 | 2.84 |
| 59.39 | -0.00777 | 3.89 |
| 60.55 | -0.00949 | 4.44 |
| 61 | -0.00769 | 4.5 |
| 62 | -0.00747 | 5.2 |
| 63 | -0.00450 | 5.39 |
| 63.87 | -0.00572 | 5.47 |
| 65 | 0.00657 | 3.42 |
| 65.8 | 0.00724 | 6.36 |
| 67 | 0.0214 | 5.82 |

**Table C-26 Pressure gradient and intercept coefficients for the isometric data 0-125kpa, 21deg C.**

Temperature 24deg C.

| muscle length (mm) | pressure gradient coefficient | intercept coefficient |
|---|---|---|
| 51.45 | -0.0018161 | -0.0855 |
| 53 | -0.002161 | -0.0463 |
| 55 | -0.004994 | 1.0516 |

| | | |
|---|---|---|
| 57.4 | -0.006261 | 2.5256 |
| 58 | -0.007620 | 2.8576 |
| 59.39 | -0.009203 | 4.1203 |
| 60.55 | -0.011503 | 4.6585 |
| 61 | -0.0065 | 4.6645 |
| 62 | -0.005822 | 5.3461 |
| 63 | -0.006792 | 5.7490 |
| 63.87 | -0.006175 | 5.7120 |
| 65 | 0.000611 | 3.8776 |
| 65.8 | 0.0011032 | 6.3803 |
| 67 | 0.02122 | 7.251 |

**Table C-27 Pressure gradient and intercept coefficients for the isometric data 0-125kpa, 24deg C.**

Temperature 27deg C.

| muscle length (mm) | pressure gradient coefficient | intercept coefficient |
|---|---|---|
| 51.45 | -0.002118 | -0.0096 |
| 53 | -0.003995 | -0.0060 |
| 55 | -0.004931 | 0.9693 |
| 57.4 | -0.008110 | 3.0316 |
| 58 | -0.005282 | 2.7120 |
| 59.39 | -0.006990 | 4.2625 |
| 60.55 | -0.007652 | 4.700 |
| 61 | -0.008536 | 4.8981 |
| 62 | -0.009788 | 5.7032 |
| 63 | -0.005383 | 5.8556 |
| 63.87 | -0.006080 | 5.9324 |
| 65 | 0.004347 | 3.8355 |
| 65.8 | 0.007008 | 6.8939 |
| 67 | 0.02033 | 7.589 |

**Table C-28 Pressure gradient and intercept coefficients for the isometric data 0-125kpa, 27deg C.**

Temperature 30deg C.

| muscle length (mm) | pressure gradient coefficient | intercept coefficient |
|---|---|---|
| 51.45 | -0.001137 | -0.1423 |
| 53 | -0.005761 | 0.1483 |
| 55 | -0.005746 | 1.0297 |
| 57.4 | -0.005838 | 2.8679 |
| 58 | -0.010579 | 3.1821 |
| 59.39 | -0.007411 | 4.2079 |
| 60.55 | -0.012516 | 5.0328 |
| 61 | -0.009424 | 5.0701 |
| 62 | -0.006524 | 5.6355 |
| 63 | -0.002825 | 5.9006 |
| 63.87 | -0.001999 | 5.7551 |
| 65 | 0.002204 | 4.1236 |
| 65.8 | 0.011295 | 6.8071 |
| 67 | 0.02465 | 7.581 |

**Table C-29 Pressure gradient and intercept coefficients for the isometric data 0-125kpa, 30deg C.**

Temperature 33deg C.

| muscle length (mm) | pressure gradient coefficient | intercept coefficient |
|---|---|---|
| 51.45 | -0.001304 | -0.2133 |
| 53 | -0.005027 | 0.1463 |
| 55 | -0.007440 | 1.2329 |
| 57.4 | -0.007822 | 3.0209 |
| 58 | -0.006213 | 2.9571 |
| 59.39 | -0.009927 | 4.6187 |
| 60.55 | -0.012313 | 5.2921 |
| 61 | -0.011595 | 5.4507 |
| 62 | -0.007111 | 5.8185 |
| 63 | -0.004794 | 6.1812 |
| 63.87 | -0.006635 | 6.3691 |
| 65 | 0.00391 | 4.1608 |
| 65.8 | 0.009568 | 7.3224 |
| 67 | 0.02363 | 8.066 |

**Table C-30 Pressure gradient and intercept coefficients for the isometric data 0-125kpa, 33deg C.**

Temperature 36deg C.

| muscle length (mm) | pressure gradient coefficient | intercept coefficient |
|---|---|---|
| 51.45 | -0.002691 | -.2227 |
| 53 | -0.002619 | 0.1098 |
| 55 | -0.003526 | 1.0247 |
| 57.4 | -0.008658 | 3.1123 |
| 58 | -0.006510 | 3.2397 |
| 59.39 | -0.010214 | 4.7921 |
| 60.55 | -0.010015 | 5.0861 |
| 61 | -0.008834 | 5.4048 |
| 62 | -0.008577 | 6.1444 |
| 63 | -0.005344 | 6.4812 |
| 63.87 | -0.007284 | 6.5853 |
| 65 | 0.004367 | 4.3256 |
| 65.8 | 0.011828 | 7.4400 |
| 67 | 0.02620 | 8.220 |

**Table C-31 Pressure gradient and intercept coefficients for the isometric data 0-125kpa, 36deg C.**

Temperature 39deg C.

| muscle length (mm) | pressure gradient coefficient | intercept coefficient |
|---|---|---|
| 51.45 | -0.001841 | -0.1974 |
| 53 | -0.007681 | 0.1872 |
| 55 | -0.005084 | 1.0809 |
| 57.4 | -0.006994 | 3.0474 |
| 58 | -0.008496 | 3.4218 |
| 59.39 | -0.009622 | 4.8228 |
| 60.55 | -0.010488 | 5.4552 |
| 61 | -0.007627 | 5.4864 |
| 62 | -0.009840 | 6.4373 |
| 63 | -0.007449 | 6.9088 |
| 63.87 | -0.009081 | 6.8632 |
| 65 | 0.002668 | 4.6179 |
| 65.8 | 0.011318 | 7.6327 |
| 67 | 0.02585 | 8.595 |

**Table C-32 Pressure gradient and intercept coefficients for the isometric data 0-125kpa, 39deg C.**

Best subsets regression was undertaken to indentify the relationship type between the pressure gradient and intercept coefficient.

| Pressure gradient coeffienent | length | length$^3$ | cos(L) | sin(L) | length and length$^3$ |
|---|---|---|---|---|---|
| 21 | 3 | 2 | 4 | 5 | 1 |
| 24 | 3 | 2 | 4 | 5 | 1 |
| 27 | 3 | 2 | 4 | 5 | 1 |
| 30 | 3 | 2 | 4 | 5 | 1 |
| 33 | 3 | 2 | 4 | 5 | 1 |
| 36 | 3 | 2 | 4 | 5 | 1 |
| 39 | 3 | 2 | 4 | 5 | 1 |

**Table C-33 Summarised best fit results for the isometric data, pressure gradient coefficients, 0-125kpa 21-39deg C.**

The gradient coefficients from the best fits were found to be best approximated by distance by a combination of length$^3$ and length.

| Pressure intercept coeffienent | length | length$^2$ | cos(d) | sin(d) |
|---|---|---|---|---|
| 21 | 1 | 2 | 3 | 4 |
| 24 | 1 | 2 | 3 | 4 |
| 27 | 1 | 2 | 3 | 4 |
| 30 | 1 | 2 | 3 | 4 |
| 33 | 1 | 2 | 3 | 4 |
| 36 | 1 | 2 | 3 | 4 |
| 39 | 1 | 2 | 3 | 4 |

**Table C-34 Best fit results for the isometric data of the intercept coefficients**

The intercept coefficients from the best fits were found to be best approximated by length.

Regressions of the gradient and intercept coefficients were undertaken against the most likely predictor identified on the best fits regression are shown in tabel C-35.

full regression relating the gradient and intercept terms to temperature.

| Temp\ Coefficient type | Pressure muscle length cubed gradient coefficient ($K_1$) | Pressure muscle length gradient coefficient ($K_2$) | Pressure gradient coefficient ($K_3$) | Muscle length gradient coefficient ($K_4$) | intercept coefficient ($c$) |
|---|---|---|---|---|---|
| 21 | 0.00000164 | -0.016488 | 0.6250 | 0.40029 | -20.429 |
| 24 | 0.00000158 | -0.016100 | 0.6151 | 0.46120 | -23.891 |
| 27 | 0.00000161 | -0.016175 | 0.6147 | 0.47898 | -24.797 |
| 30 | 0.00000193 | -0.019331 | 0.7331 | 0.47788 | -24.671 |
| 33 | 0.00000196 | -0.019707 | 0.7492 | 0.51017 | -26.384 |
| 36 | 0.00000203 | -0.020492 | 0.7804 | 0.52730 | -27.321 |
| 39 | 0.00000197 | -0.019754 | 0.7499 | 0.55010 | -28.506 |

**Table C-35 Gradient and intercept coefficients isometric data 0-125kpa 21-39deg C.**

Best Subsets Regression of muscle length cubed pressure gradient coefficient ($K_1$).

| Vars | R-sq | Adj. R-sq | C-p | s | cos(t) | sin(t) | t^2 |
|---|---|---|---|---|---|---|---|
| 1 | 77.1 | 72.6 | -0.1 | 0.0000001 | X | | |
| 1 | 75.3 | 70.3 | 0.2 | 0.0000001 | | | X |
| 2 | 79.5 | 69.2 | 1.6 | 0.0000001 | X | X | |
| 2 | 78.5 | 67.8 | 1.7 | 0.0000001 | X | X | |
| 3 | 84.2 | 68.4 | 3.0 | 0.0000001 | X | X | X |
| 3 | 82.8 | 65.7 | 3.2 | 0.0000001 | | X | X X |
| 4 | 84.4 | 53.1 | 5.0 | 0.0000001 | X | X | X X |

**Best-fit C-5 Best fits regression analysis of the muscle length cubed pressure gradient coefficient in Table C-35 and temperature, 0-125kpa 21-39degC.**

Best Subsets Regression of muscle length pressure gradient coefficient($K_2$).

| Vars | R-sq | Adj. R-sq | C-p | s | cos(t) | sin(t) | t^2 |
|---|---|---|---|---|---|---|---|
| 1 | 77.3 | 72.7 | 0.0 | 0.0010134 | X | | |
| 1 | 75.4 | 70.5 | 0.3 | 0.0010544 | | | X |
| 2 | 80.5 | 70.8 | 1.6 | 0.0010491 | X | X | |
| 2 | 79.5 | 69.3 | 1.7 | 0.0010753 | | X | X |
| 3 | 84.8 | 69.6 | 3.0 | 0.0010697 | X | X | X |
| 3 | 83.6 | 67.2 | 3.2 | 0.0011111 | | X | X X |
| 4 | 84.9 | 54.8 | 5.0 | 0.0013048 | X | X | X X |

**Best-fit C-6 Best fits regression analysis of the muscle length pressure gradient coefficient in Table C-35 and temperature, 0-125kpa 21-39degC.**

Best Subsets Regression of pressure gradient coefficient($K_3$).

| Vars | R-sq | Adj. R-sq | C-p | s | cos(t) | sin(t) | t^2 |
|---|---|---|---|---|---|---|---|
| 1 | 77.7 | 73.2 | 0.1 | 0.038052 | X | | |
| 1 | 75.7 | 70.9 | 0.3 | 0.039675 | | | X |
| 2 | 81.4 | 72.0 | 1.6 | 0.038878 | X | X | |
| 2 | 80.4 | 70.5 | 1.7 | 0.039908 | | X | X |
| 3 | 85.4 | 70.7 | 3.0 | 0.039772 | X | X | X |
| 3 | 84.2 | 68.3 | 3.2 | 0.041382 | | X | X X |
| 4 | 85.5 | 56.5 | 5.0 | 0.048501 | X | X | X X |

**Best-fit C-7 Best fits regression analysis of the pressure gradient coefficient in Table C-35 and temperature, 0-125kpa 21-39degC.**

Best Subsets Regression of muscle length gradient($K_4$).

| Vars | R-sq | Adj. R-sq | C-p | s | t | cos(t) | sin(t) | t2 |
|---|---|---|---|---|---|---|---|---|
| 1 | 92.7 | 91.2 | 0.9 | 0.014564 | X | | | |
| 1 | 90.1 | 88.1 | 2.2 | 0.016940 | | | | X |
| 2 | 94.8 | 92.2 | 1.7 | 0.013712 | X | X | | |
| 2 | 94.0 | 91.0 | 2.2 | 0.014735 | X | | | X |
| 3 | 95.7 | 91.3 | 3.3 | 0.014448 | X | X | | X |
| 3 | 95.0 | 90.0 | 3.6 | 0.015526 | X | X | X | |
| 4 | 96.2 | 88.6 | 5.0 | 0.016582 | X | X | X | X |

**Best-fit C-8 Best fits regression analysis of the muscle length gradient coefficient in Table C-35 and temperature, 0-125kpa 21-39degC.**

Best Subsets Regression of intercept coefficient($K_5$).

| Vars | R-sq | Adj. R-sq | C-p | s | t | cos(t) | sin(t) | t2 |
|---|---|---|---|---|---|---|---|---|
| 1 | 91.4 | 89.7 | 0.9 | 0.84709 | X | | | |
| 1 | 88.6 | 86.4 | 2.1 | 0.97380 | | | | X |
| 2 | 94.0 | 91.0 | 1.7 | 0.79143 | X | X | | |
| 2 | 93.0 | 89.5 | 2.2 | 0.85276 | X | | | X |
| 3 | 95.1 | 90.1 | 3.2 | 0.82859 | X | X | | X |
| 3 | 94.2 | 88.3 | 3.6 | 0.90088 | X | X | X | |
| 4 | 95.6 | 86.7 | 5.0 | 0.96041 | X | X | X | X |

**Best-fit C-9 Best fits regression analysis of the intercept coefficient in Table C-35 and temperature, 0-125kpa 21-39degC.**

The gradient and intercept coefficients of table C-35 were the fully regressed with temperature.

Full regression of pressure muscle length cubed gradient coefficient ($K_1$) and temperature.

```
The regression equation is
k1 =0.000001 +0.000000 temperature

Predictor          Coef        Stdev    t-ratio        p
Constant     0.00000102   0.00000020       5.12    0.004
temperature  0.00000003   0.00000001       4.11    0.009

s = 0.000000103 R-sq = 77.1%     R-sq(adj) = 72.6%
```

```
Analysis of Variance

SOURCE       DF          SS          MS          F       p
Regression    1 1.79200E-13 1.79200E-13      16.86   0.009
Error         5 5.31428E-14 1.06286E-14
Total         6 2.32343E-13
```

**Full-regression C-3 Full regression of muscle length cubed pressure gradient and temperature, 0-125kpa 21-39degC.**

Full regression of pressure muscle length gradient coefficient ($K_2$) and temperature.

```
The regression equation is
k2 = - 0.0104 -0.000263 temperature

Predictor          Coef       Stdev    t-ratio       p
Constant      -0.010395    0.001953      -5.32   0.003
temperature -0.00026326  0.00006384      -4.12   0.009

s = 0.001013    R-sq = 77.3%     R-sq(adj) = 72.7%

Analysis of Variance

SOURCE       DF          SS          MS          F       p
Regression    1 0.000017465 0.000017465      17.01   0.009
Error         5 0.000005135 0.000001027
Total         6 0.000022600
```

**Full-regression C-4 Full regression of muscle length pressure gradient and temperature, 0-125kpa 21-39degC.**

Full regression of pressure gradient coefficient ($K_3$) and temperature.

```
The regression equation is
k3 = 0.395 + 0.0100 temperature

Predictor        Coef       Stdev    t-ratio       p
Constant      0.39541     0.07334       5.39   0.003
temperature 0.009998    0.002397       4.17   0.009

s = 0.03805     R-sq = 77.7%     R-sq(adj) = 73.2%

Analysis of Variance

SOURCE       DF          SS          MS          F       p
Regression    1    0.025188    0.025188      17.40   0.009
Error         5    0.007240    0.001448
Total         6    0.032428
```

**Full-regression C-5 Full regression of pressure gradient and temperature, 0-125kpa 21-39degC.**

Full regression of muscle length gradient coefficient ($K_4$) and temperature.

```
The regression equation is
k4 = 0.268 + 0.00730 temperature

Predictor        Coef       Stdev    t-ratio       p
Constant      0.26770     0.02807       9.54   0.000
temperature 0.0072955   0.0009174       7.95   0.001

s = 0.01456     R-sq = 92.7%     R-sq(adj) = 91.2%
```

```
Analysis of Variance

SOURCE       DF          SS          MS          F          p
Regression    1    0.013412    0.013412      63.24      0.001
Error         5    0.001061    0.000212
Total         6    0.014473
```

**Full-regression C-6 Full regression of muscle length gradient and temperature, 0-125kpa 21-39degC.**

Full regression of the intercept coefficient ($c$) and temperature.

```
The regression equation is
c = - 13.5 - 0.389 temperature

Predictor        Coef        Stdev    t-ratio          p
Constant      -13.472        1.633      -8.25      0.000
temperature -0.38902      0.05336      -7.29      0.001

s = 0.8471      R-sq = 91.4%      R-sq(adj) = 89.7%

Analysis of Variance

SOURCE       DF          SS          MS          F          p
Regression    1      38.138      38.138      53.15      0.001
Error         5       3.588       0.718
Total         6      41.725
```

**Full-regression C-7 Full regression of intercept coefficient and temperature, 0-125kpa 21-39degC.**

## C-3. Regression analysis of the isobaric data collected from the muscle

Regression analysis of the isobaric data in the 150 to 600kpa region.

Best fit regression summary using only a single term predictor.

Temperature 21deg C.

| Pressure (kpa) | d | $d^2$ | cos(d) | sin(d) | log(d) |
|---|---|---|---|---|---|
| 150 | 2 | 1 | 5 | 4 | 3 |
| 175 | 2 | 1 | 5 | 4 | 3 |
| 200 | 2 | 1 | 5 | 4 | 3 |
| 250 | 2 | 1 | 4 | 5 | 3 |
| 300 | 2 | 1 | 4 | 5 | 3 |
| 350 | 2 | 1 | 4 | 5 | 3 |
| 400 | 1 | 2 | 5 | 4 | 3 |
| 450 | 1 | 2 | 5 | 4 | 3 |
| 500 | 1 | 2 | 5 | 4 | 3 |
| 550 | 1 | 2 | 4 | 5 | 3 |
| 600 | 1 | 3 | 4 | 5 | 2 |

**Table C-36 Summarised best fits Isobaric data 21deg C.**

Temperature 21deg C.

| Pressure (kpa) | muscle length gradient coefficient | intercept coefficient |
|---|---|---|
| 150 | 1.01714 | -56.862 |
| 175 | 1.29706 | -71.391 |
| 200 | 1.58494 | -86.162 |
| 250 | 2.05337 | -109.257 |
| 300 | 2.05079 | -131.598 |
| 350 | 2.9399 | -152.909 |
| 400 | 3.36092 | -173.301 |
| 450 | 3.84361 | -197.447 |
| 500 | 4.2039 | -214.405 |
| 550 | 4.5946 | -233.281 |
| 600 | 4.8853 | -246.572 |

**Table C-37 Muscle length gradient and intercept coefficients 21deg C.**

Best fits regression of pressureand the muscle length gradient coefficients at temperature 21deg C.

| Vars | R-sq | Adj. R-sq | C-p | s | log(pres) | Pres | P^3 | P^2 |
|---|---|---|---|---|---|---|---|---|
| 1 | 99.0 | 98.8 | 1.5 | 0.14758 | | X | | |
| 1 | 96.4 | 96.0 | 22.1 | 0.27379 | X | | | |
| 1 | 95.5 | 95.0 | 28.8 | 0.30787 | | | | X |
| 1 | 88.6 | 87.3 | 86.0 | 0.48944 | | | X | |
| 1 | 95.5 | 95.0 | 28.8 | 0.30787 | | | X | |

**Best-fit C-10 Best fits analysis of the muscle length gradient coefficients and pressure at temperature 21deg C.**

Best fits regression of pressure and the intercept coefficients at temperature 21deg C.

| Vars | R-sq | Adj. R-sq | C-p | s | Pres | log(P) | P^2 | sin(P) |
|---|---|---|---|---|---|---|---|---|
| 1 | 99.4 | 99.3 | 126.8 | 5.6441 | X | | | |
| 1 | 98.8 | 98.7 | 257.6 | 7.9372 | | X | | |
| 2 | 99.9 | 99.9 | 6.5 | 1.7561 | X | | X | |
| 2 | 99.9 | 99.9 | 9.2 | 1.9528 | X | | | X |
| 3 | 99.9 | 99.9 | 8.0 | 1.8353 | X | X | X | |
| 3 | 99.9 | 99.9 | 8.1 | 1.8391 | X | | X | X |
| 4 | 100.0 | 100.0 | 5.0 | 1.4637 | X | X | X | X |

**Best-fit C-11 Best fits analysis of the muscle length intercept coefficients and pressure at temperature 21deg C.**

Looking at the results of the single term predictors it is evident that pressure is linearly related to the muscle length gradient coefficient and intercept coefficient.
The regression results using pressure to predict these coefficients is listed below in Table C-38.

| temp | pressure muscle length gradient coefficient | muscle length gradient | pressure gradient | intercept coefficient |
|---|---|---|---|---|
| 21 | 0.00878 | -0.2391 | -0.42523 | -0.379 |

**Table C-38 Pressure muscle length gradient and intercept coefficients, 125-600kpa, 21-39deg C.**

## C-4. Quasi-static model development and comparison of different models

Quasi-static model parameter optimization.

Linear region pressure from 0-125kpa temperature 21deg C.

```
The regression equation is
real for = - 26.1 + 0.495 d - 0.00260 P

Predictor        Coef        Stdev    t-ratio        p
Constant      -26.093        1.464     -17.82    0.000
d             0.49531      0.02407      20.58    0.000
P          -0.002596     0.002568      -1.01    0.316

R-sq = 86.4%     R-sq(adj) = 86.0%

Analysis of Variance

SOURCE        DF          SS          MS          F        p
Regression     2      362.39      181.20     212.19    0.000
Error         67       57.21        0.85
Total         69      419.61

SOURCE        DF      SEQ SS
d              1      361.52
P              1        0.87
```

**Full-regression C-8 Quasi static model for the 0-125kpa region developed using the isometric data 0-125kpa with temperature 21deg C.**

Descriptive statistics on the residuals of various model examined are listed below. This data refers to how well the models operate in the 0-125kpa region with temperature at 21deg C.

| Model type | Number of samples used. | MEAN | MEDIAN | TRMEAN | STDEV | SEMEAN |
|---|---|---|---|---|---|---|
| determin | 70 | -1.349 | -1.777 | -1.512 | 3.414 | 0.408 |
| black box temp 21°C 0-125kpa | 70 | 0.041 | -0.053 | 0.002 | 1.012 | 0.121 |
| black box temp 21-39°C 0-125kpa | 70 | -0.722 | -0.584 | -0.642 | 0.986 | 0.118 |
| Caldwell | 70 | -2.130 | -2.376 | -2.258 | 3.899 | 0.466 |
| quasi 0-125kpa | 70 | 0.000 | 0.058 | 0.030 | 2.891 | 0.109 |

**Table C-39 Results of the models used to predict the isobaric data 0-125kpa with temperature 21deg C.**

Quasi-static optimization 150-600kpa region with the temperature at 21deg C..

```
The regression equation is
real for = - 60.3 + 0.00829 p*d - 0.402 (p-125)

Predictor        Coef        Stdev    t-ratio        p
Constant     -60.2732       0.6232     -96.72    0.000
p*d       0.00829195   0.00007591     109.23    0.000
(p-125)    -0.402270    0.004657     -86.37    0.000

R-sq = 99.4%     R-sq(adj) = 99.3%

Analysis of Variance

SOURCE        DF          SS          MS          F        p
Regression     2       65060       32530   11655.89    0.000
Error        151         421           3
Total        153       65481

SOURCE        DF      SEQ SS
p*d            1       44239
(p-125)        1       20821
```

**Full-regression C-9 Quasi static model for the 150-600kpa region developed using the isometric data 150-600kpa with temperature 21deg C.**

Descriptive statistics on the residuals of various model examined are listed below. This data refers to how well the models operate in the 150-600kpa region with temperature at 21deg C.

| Model type | Number of samples used. | MEAN | MEDIAN | TRMEAN | STDEV | SEMEAN |
|---|---|---|---|---|---|---|
| determin | 154 | -0.354 | -1.375 | -0.724 | 7.047 | 0.568 |
| black box temp 21°C 150-600kpa | 154 | 2.403 | 2.464 | 2.416 | 1.922 | 0.155 |
| black box temp 21-39°C 150-600kpa | 154 | 0.837 | 0.779 | 0.839 | 1.693 | 0.136 |
| caldwell | 154 | -4.309 | -4.927 | -4.506 | 4.262 | 0.343 |
| quasi 150-600kpa | 154 | -0.000 | -0.139 | -0.013 | 2.455 | 0.134 |

**Table C-40 Results of the models used to predict the isobaric data 150-600kpa with temperature 21deg C.**

Descriptive statistics on the residuals of various model examined are listed below. This data refers to how well the models operate in the 0-600kpa region with temperature at 21deg C.

| Model type | Number of samples used. | MEAN | MEDIAN | TRMEAN | STDEV | SEMEAN |
|---|---|---|---|---|---|---|
| determin | 224 | -0.665 | -1.568 | -0.997 | 6.156 | 0.411 |
| black box temp 21°C 0-600kpa | 224 | 1.664 | 1.761 | 1.619 | 2.014 | 0.135 |
| black box temp 21-39°C 0-600kpa | 224 | 0.350 | 0.160 | 0.332 | 1.671 | 0.112 |
| Caldwell | 224 | -3.628 | -4.010 | -3.793 | 4.265 | 0.285 |
| quasi 0-600kpa | 154 | -0.000 | -0.139 | -0.013 | 2.532 | 0.134 |

**Table C-41 Results of the models used to predict the isobaric data 0-600kpa with temperature 21deg C.**

Descriptive statistics on the residuals of various model examined are listed below. This data refers to how well the models operate in the 0-125kpa region with temperature at 21-39deg C.

| Model type | Number of samples used. | MEAN | MEDIAN | TRMEAN | STDEV | SEMEAN |
|---|---|---|---|---|---|---|
| determin | 490 | 0.455 | -0.321 | 0.230 | 4.213 | 0.190 |
| black box temp 21°C 0-125kpa | 490 | 1.844 | 1.463 | 1.692 | 2.321 | 0.105 |
| black box temp 21-39°C 0-125kpa | 490 | 0.1093 | -0.1428 | 0.0463 | 2.0071 | 0.0907 |
| Caldwell | 490 | -0.326 | -1.180 | -0.536 | 3.892 | 0.206 |
| quasi 0-125kpa | 490 | 1.8032 | 1.2870 | 1.6776 | 3.769 | 0.0966 |

**Table C-42 Results of the models used to predict the isobaric data 0-125kpa with temperature 21-39deg C.**

Descriptive statistics on the residuals of various model examined are listed below. This data refers to how well the models operate in the 150-600kpa region with temperature at 21-39deg C.

| Model type | Number of samples used. | MEAN | MEDIAN | TRMEAN | STDEV | SEMEAN |
|---|---|---|---|---|---|---|
| determin | 1078 | 4.136 | 3.255 | 3.796 | 9.352 | 0.285 |
| black box temp 21°C 150-600kpa | 1078 | 6.892 | 5.881 | 6.644 | 4.490 | 0.137 |
| black box temp 21-39°C 150-600kpa | 1078 | 1.825 | 1.709 | 1.817 | 3.292 | 0.100 |
| caldwell | 1078 | 0.181 | -0.454 | -0.086 | 8.265 | 0.209 |
| quasi 150-600kpa | 1078 | -0.0000 | -0.1395 | -0.0123 | 5.951 | 0.0504 |

**Table C-43 Results of the models used to predict the isobaric data 150-600kpa with temperature 21-39deg C.**

Descriptive statistics on the residuals of various model examined are listed below. This data refers to how well the models operate in the 0-600kpa region with temperature at 21-39deg C.

| Model type | Number of samples used. | MEAN | MEDIAN | TRMEAN | STDEV | SEMEAN |
|---|---|---|---|---|---|---|
| determin | 1568 | 2.985 | 1.299 | 2.576 | 8.280 | 0.209 |
| black box temp 21°C 0-600kpa | 1568 | 5.314 | 4.424 | 5.005 | 4.584 | 0.116 |
| black box temp 21-39°C 0-600kpa | 1568 | 1.2889 | 0.9409 | 1.2375 | 3.0561 | 0.0772 |
| Caldwell | 1568 | 0.022 | -0.749 | -0.225 | 7.549 | 0.157 |
| quasi 0-600kpa | 1568 | 3.650 | 2.570 | 3.315 | 5.696 | 0.104 |

**Table C-44 Results of the models used to predict the isobaric data 0-600kpa with temperature 21-39deg C.**

## C-5. Muscle measurement algorithm

Macro used to measure the length of the muscle with the use of a CCD camera.

macro 'test'

```
var
 count,min,max:integer;
 ppv,i,row,:real;
begin
ResetCounter;
        for i:= 1 to nSlices do begin
 SelectSlice(i);
FlipHorizontal;
        SetThreshold(130);

        MakeBinary;
        MakeRoi(10,300,500,70);
        GetPlotData(count,ppv,min,max);
        row:=0;
                while PlotData[row] = 0 do begin
                                row :=row+1;
                                end;
 rUser1[i]:=row;
        KillRoi;
        Measure;
        ShowResults;

end;
        MakeRoi(10,300,500,70);
end;
```

# Appendix D Valve characterisation

## D-1. Switching time data

Times recorded for the valve to switch on and off.

| pressure | inlet on | inlet off | outlet on | outlet off | air delay |
|---|---|---|---|---|---|
| 0 | 8.573 | 9 | 8.6 | 9 | 1.016 |
| 50 | 8.9 | 8.9 | 8.8 | 8.9 | 1.016 |
| 100 | 9.2 | 8.9 | 9 | 8.8 | 1.016 |
| 150 | 9.5 | 8.85 | 9.2 | 8.8 | 1.016 |
| 200 | 9.7 | 8.8 | 9.4 | 8.75 | 1.016 |
| 250 | 9.9 | 8.75 | 9.6 | 8.8 | 1.016 |
| 300 | 10.1 | 8.7 | 9.8 | 8.7 | 1.016 |
| 350 | 10.4 | 8.65 | 9.9 | 8.6 | 1.016 |
| 400 | 10.5 | 8.6 | 10 | 8.6 | 1.016 |
| 450 | 10.7 | 8.6 | 10.1 | 8.55 | 1.016 |
| 500 | 10.9 | 8.5 | 10.2 | 8.6 | 1.016 |
| 550 | 11.2 | 8.6 | 10.2 | 8.6 | 1.016 |
| 600 | 11.235 | 8.5 | 10.2 | 8.55 | 1.016 |

**Table D-1 Switching time test results one.**

| pressure | inlet on | inlet off | outlet on | outlet off | air delay |
|---|---|---|---|---|---|
| 0 | 8.5 | 9 | 10 | 8.8 | 1.016 |
| 50 | 8.8 | 8.9 | 9.9 | 8.8 | 1.016 |
| 100 | 9 | 8.8 | 10.2 | 8.7 | 1.016 |
| 150 | 9.3 | 8.8 | 10.5 | 8.7 | 1.016 |
| 200 | 9.5 | 8.7 | 10 | 8.6 | 1.016 |
| 250 | 9.8 | 8.8 | 10 | 8.6 | 1.016 |
| 300 | 10 | 8.7 | 10.1 | 8.55 | 1.016 |
| 350 | 10.2 | 8.6 | 10.3 | 8.55 | 1.016 |
| 400 | 10.4 | 8.6 | 9.95 | 8.55 | 1.016 |
| 450 | 10.6 | 8.6 | 10.1 | 8.5 | 1.016 |
| 500 | 10.8 | 8.5 | 10.2 | 8.5 | 1.016 |
| 550 | 11 | 8.5 | 9.8 | 8.5 | 1.016 |
| 600 | 11 | 8.5 | 10 | 8.5 | 1.016 |

**Table D-2 Switching time test results two.**

| pressure | inlet on | inlet off | outlet on | outlet off | air delay |
|---|---|---|---|---|---|
| 0 | 8.8 | 9 | 9 | 8.8 | 1.016 |
| 50 | 8.8 | 8.9 | 9.2 | 8.8 | 1.016 |
| 100 | 9 | 8.8 | 9.2 | 8.7 | 1.016 |
| 150 | 9 | 8.8 | 9.5 | 8.7 | 1.016 |
| 200 | 9.2 | 8.7 | 9.2 | 8.6 | 1.016 |
| 250 | 9.7 | 8.8 | 9.5 | 8.6 | 1.016 |
| 300 | 10 | 8.7 | 9.7 | 8.55 | 1.016 |
| 350 | 10 | 8.6 | 9.7 | 8.55 | 1.016 |
| 400 | 10.2 | 8.6 | 10 | 8.55 | 1.016 |
| 450 | 10.2 | 8.6 | 10.2 | 8.5 | 1.016 |
| 500 | 10 | 8.5 | 10.2 | 8.5 | 1.016 |
| 550 | 10.5 | 8.5 | 10.5 | 8.5 | 1.016 |
| 600 | 10.5 | 8.5 | 10.5 | 8.5 | 1.016 |
| std | 0.773 | 0.155 | 0.479 | 0.128 | 0 |

**Table D-3 Switching time test results three.**

Minimum voltages required to make the valve to switch on or off.

| pressure | inlet on | inlet off | outlet on | outlet off |
|---|---|---|---|---|
| 0 | 3.5 | 0.8 | 2.8 | 0.7 |
| 50 | 3.55 | 0.8 | 2.9 | 0.7 |
| 100 | 3.6 | 0.8 | 2.9 | 0.7 |
| 150 | 3.65 | 0.8 | 2.9 | 0.75 |
| 200 | 3.7 | 0.8 | 2.9 | 0.75 |
| 250 | 3.8 | 0.8 | 2.97 | 0.8 |
| 300 | 3.85 | 0.8 | 3 | 0.8 |
| 350 | 3.9 | 0.8 | 3.05 | 0.8 |
| 400 | 3.95 | 0.8 | 3.05 | 0.8 |
| 450 | 4 | 0.8 | 3.1 | 0.8 |
| 500 | 4.2 | 0.8 | 3.15 | 0.8 |
| 550 | 4.3 | 0.7 | 3.2 | 0.8 |
| 600 | 4.4 | 0.7 | 3.3 | 0.8 |

**Table D-4 Minimum switching voltages.**

## D-2. Valve modelling results

Air velocity at the outlet data.

| Pressure | Air velocity |
|---|---|
| 0 | 0 |
| 50 | 20 |
| 100 | 29 |
| 150 | 35 |
| 200 | 40 |
| 250 | 43 |
| 300 | 48 |
| 350 | 52 |
| 400 | 57 |
| 450 | 60 |
| 500 | 62 |
| 550 | 65 |
| 600 | 67 |

**Table D-5 Air velocity data.**

Full regression of the air velocity data.

Pressure = - 5.29 + 0.131 $V^2$

| Predictor | Coef | Stdev | t-ratio | p |
|---|---|---|---|---|
| Constant | -5.293 | 5.709 | -0.93 | 0.374 |
| $V^2$ | 0.130854 | 0.002087 | 62.69 | 0.000 |

s = 10.74 R-sq = 99.7% R-sq(adj) = 99.7%

Analysis of Variance

| SOURCE | DF | SS | MS | F | p |
|---|---|---|---|---|---|
| Regression | 1 | 453730 | 453730 | 3929.97 | 0.000 |
| Error | 11 | 1270 | 115 | | |
| Total | 12 | 455000 | | | |

**Full-regression D-1 Relationship between air velocity and pressure in the valve.**

## D-3. Valve controller programs

Program listing for the driver interface for the open loop controller.

RS-232 pinout 25 pin 9 pin
see dos help interlnk notes

| | | | |
|---|---|---|---|
| Transmit | 2 | 3 | |
| Receive | 3 | 2 | |
| Request to send | 4 | 7 | o/p |
| Clear to send | 5 | 8 | i/p |
| Data set ready | 6 | 6 | i/p |
| Common | 7 | 5 | |
| Data Carrier detect | 8 | 1 | i/p |
| Data terminal ready | 20 | 4 | o/p |
| Ring indicator | 22 | 9 | i/p |

inputs cts dsr ri rlsd

Simple I/O system
outputs:
DTR 20 red
RTS 4 black
inputs:
CTS 5 green
DSR 6 yellow

MOUSE info

Agiler 25 (meas) 9 (calc)

| | | | |
|---|---|---|---|
| orange purple | 2 | 3 | Tx |
| red black | 3 | 2 | Rx |
| black yellow | 4 | 7 | RTS 11.3V |
| grey | 5 | 8 | |
| white | 6 | 6 | |
| green green | 7 | 5 | ground |
| brown | 8 | 1 | |
| yellow red | 20 | 4 | DTR 11.6V |
| blue | 22 | | |

white NC

MCR bits 0, 1, 3 set -> DTR, RTS, OUT2

RS232 Null cable
pins 25 9 25 pin

| | | | |
|---|---|---|---|
| 2 | 3 | 3 | Tx - Rx |
| 3 | 2 | 2 | |
| 4 | 8 | 5 | Request To Send - Clear To Send |
| 5 | 7 | 4 | |
| 7 | 5 | 7 | Gnd |
| 8 | 20 | 20 | Data Carrier Detect - Data Terminal Ready |
| 20 | 8 | 8 | |

Parallel port cable for fast lynx

| | |
|---|---|
| 2 | 15 |
| 3 | 13 |
| 4 | 12 |
| 5 | 10 |
| 6 | 11 |
| | |
| 10 | 5 |
| 11 | 6 |
| 12 | 4 |
| 13 | 3 |
| 15 | 2 |

Info on com port control

Line Control Register LCR
sets format of data communications, also DLAB

Modem Status Register MSR

bit0 DCTS 5 Clear to send input changed
bit1 DDSR 6 data set ready input changed
bit2 TERI 22 trailing edge of ring indicator - RI changed 1->0
bit3 DRLSD 8 RLSD (DCD - Data carrier detect) changed
bit4 CTS 5 clear to send input
bit5 DSR 6 data set ready input
bit6 RI 22 ring indicator input
bit7 RSLD 8 DCD input

Line Status Register LSR
bit0 receiver data ready
bit1 overrun error - bits 1->4 generate prioity1 interrupt
bit2 parity error
bit3 framing error
bit4 break interrupt indicator
bit5 transmitter holding reg empty
bit6 transmitter shift reg empty
bit7 0

Interrupt Enable Register IER
selects what will generate an interrupt

bit0 Received Data Available
bit1 Tx holding register empty
bit2 Receive line status - error in received data (parity etc)
bit3 Modem status - change in CTS, DSR, RI, DCD (RL Sig Detect?)
bit4, 5, 6, 7 = 0

CTS 5
DSR 6
RI 22
DCD (RLSD) 8

Interrupt Identification Register IIR
flags which interrupt to service

bit0 0 if interrupt pending - read LSR to reset
bit1, 2
11 Receive line status - error in received data
10 Reveived data available
01 Transmitter holding reg empty
00 Modem status change - CTS, DSR, RI, DCD

bit3, 4, 5, 6, 7 0

Modem Control Register MCR
controls o/p lines

| | pin nos |
|---|---|
| bit0 DTR | 20 |
| bit1 RTS | 4 |
| bit2 OUT1 | ?? |
| bit3 OUT2 | ?? gate for interrupts?? |
| bit4 loop back mode | |

bit5, 6, 7 = 0

Set bit3 of IER - modem status interrupt \
set bit3 of MCR - OUT2 / enable interrupt
enter waiting loop

The Interrupt service routine should:
set bit3 of IER off to prevent further interrupts
read IIR and find bit0 = 0, bit1 = 0, bit2 = 0 (which will reset IIR)
inc a counter so I know where it's been

Writing to DTR (MCR bit0 = ??
read MSR modem status register

Currently using {don't know about this - delete it }
(Null Modem) -> (pc end)

| | | |
|---|---|---|
| b4 | 4 | 5 |
| b5 | NC | 6 |
| b6 | NC | 22 |
| b7 | 20 | 8 |

**Micro controller program for the two position controller.**

```
{$C- Version 4  Program: Nigel Yee simplified two position control algorithm}


PROGRAM  version4;

Var
     difference:integer;
     detect:boolean;
     actual_strain,x,y,l,m,desired_strain:word;

Procedure Start_ADC_for_transducer;
      begin
       ADCON:=$01;                {clears the ADC register}
       ADCON:=ADCON or $08;           {starts ADC on port 0}
       while not ((ADCON and $10)=$10) do;       {waits until conversion is completed}
       x:=ADCH;                                  {gets the higher bit}
       y:=ADCON;                                 {gets lower 2 bits}
       actual_strain:=((x*$04)+(y DIV $20));     {computes into 10 bit form}
       writeln(actual_strain);
       ADCON:=ADCON and $EF;
      end;

Procedure Start_ADC_for_potentiometer;
      begin
       ADCON:=$03;
       ADCON:=ADCON or $08;
       while not ((ADCON and $10)=$10) do;
       l:=ADCH;
       m:=ADCON;
       desired_strain:=((l*$04)+(m DIV $20));
       writeln('  ',desired_strain);
       ADCON:=ADCON and $EF;
      end;

Procedure compare_actual_with_desired;
      begin

       difference:=desired_strain-(actual_strain); {gets the error between the desired and actual strain}
       writeln('  ',difference);  {writes the error strain value}
      end;




Procedure operate_valve;
      begin
      p1.3:=true;
      p1.5:=true;
      p1.7:=true;
      p1.2:=true;
      p1.4:=true;
```

```
    if(difference > 5) then
    begin
      p1.2:=false;                    {turn on inlet valve}
      p1.3:=false;              {turns on inlet Led}

    end


    else
      if(difference <- 5) then
    begin
      p1.7:=false;          {turn on outlet valve}
      p1.4:=false;              {turns on outlet Led}


    end
      else
      if (difference <= 5) and (difference >= -5) then
      p1.5:=false;              {indicate no further operation required through red LED}
        {UNTIL??????????????????????????????}

   end;



{Main Program}
begin

    reset(serial);
    writeln;
    writeln;


    repeat
        Start_ADC_for_transducer;
        Start_ADC_for_potentiometer;
        compare_actual_with_desired;

        operate_valve;

    until false;
    p1.2:=false;
    p1.5:=false;
    p1.4:=false;

end.
```

**Micro controller program for the control of the pneumatic ram.**

{$C- Version 7 Program: Nigel Yee - This program is designed to be used on a large pneumatic ram, It controls the rams operation to stop at a proximity sensor}

```
PROGRAM version7;

Var
    difference:integer;
    loopy:integer;
    a:integer;
    detect:boolean;
    actual_strain,x,y,l,m,desired_strain:word;

Procedure Start_ADC_for_transducer;
    begin
     ADCON:=$01;                {clears the ADC register}
     ADCON:=ADCON or $08;       {starts ADC on port 0}
     while not ((ADCON and $10)=$10) do;    {waits until conversion is completed}
     x:=ADCH;                               {gets the higher bit}
     y:=ADCON;                              {gets lower 2 bits}
     actual_strain:=((x*$04)+(y DIV $20));  {computes into 10 bit form}
     writeln(700-actual_strain);
     ADCON:=ADCON and $EF;
    end;

Procedure Start_ADC_for_potentiometer;
    begin
     ADCON:=$03;
     ADCON:=ADCON or $08;
     while not ((ADCON and $10)=$10) do;
     l:=ADCH;
     m:=ADCON;
     desired_strain:=((l*$04)+(m DIV $20));
     writeln('  ',desired_strain);
     ADCON:=ADCON and $EF;
    end;

Procedure compare_actual_with_desired;
    begin

     difference:=desired_strain-(actual_strain);  {gets the error value of the strain}
     writeln('  ',difference);
    end;

Procedure operate_valve;
    begin
    p1.3:=true;
    p1.5:=true;
    p1.7:=true;
    p1.2:=true;
    p1.4:=true;
```

```
      if(difference > 5)then
      begin
       p1.2:=false;                    {turn on inlet valve}
       p1.3:=false;


      end
       else
       if(difference <- 5)then
      begin
       p1.7:=false;          {turn on outlet valve}
       p1.4:=false;


      end
       else
      if (difference <= 5) and (difference >= -5) then
       p1.5:=false;              {indicate no further operation required through red LED}
         {UNTIL??????????????????????????????}



     end;

Procedure  check_posn;
      begin
      if (p1.1 = true) or (p1.0 = true) then
      begin
      writeln('sensor on');
      difference:=0;  {if the proximity sensor is true then the valve is at its desired position and the}
                      {pressure needs not be increased any further}
      end
      end;


{Main Program}
begin

      reset(serial);
      writeln;
      writeln;


      repeat
            p1.1:=false;
            p1.0:=false;
            Start_ADC_for_transducer;
            Start_ADC_for_potentiometer;
            compare_actual_with_desired;
            check_posn;
            operate_valve;
```

```
    until false;
    p1.2:=false;
    p1.5:=false;
    p1.4:=false;

end.
```

**Micro controller program for proportional pulse width modulation control of the inlet valve only.**

```
{$C- version 8  Program: Nigel Yee, this program uses pulse width modulation of the input valve only}


PROGRAM  version8;


Var
    difference:integer;
    loopy:integer;
    pwm_on:integer;
    pwm_off:integer;
    detect:boolean;
    actual_strain,x,y,l,m,desired_strain:word;

Procedure Start_ADC_for_transducer;
    begin

     ADCON:=$01;                {clears the ADC register}
     ADCON:=ADCON or $08;               {starts ADC on port 0}
     while not ((ADCON and $10)=$10) do;        {waits until conversion is completed}
     x:=ADCH;                                   {gets the higher bit}
     y:=ADCON;                                  {gets lower 2 bits}
     actual_strain:=((x*$04)+(y DIV $20));      {computes into 10 bit form}
     writeln(actual_strain);
     ADCON:=ADCON and $EF;
    end;

Procedure Start_ADC_for_potentiometer;
    begin
     ADCON:=$03;
     ADCON:=ADCON or $08;
     while not ((ADCON and $10)=$10) do;
     l:=ADCH;
     m:=ADCON;
     desired_strain:=((l*$04)+(m DIV $20));
     writeln('  ',desired_strain);
     ADCON:=ADCON and $EF;
    end;

Procedure compare_actual_with_desired;
    begin

     difference:=desired_strain-(actual_strain);{actual strain reading gets smaller as strain gets larger}
     writeln('  ',difference);
    end;

Procedure operate_valve;
    begin
    p1.0:=true;  {turns off inlet valve}
    p1.5:=true;
    p1.1:=true;   {outlet off outler valve}
    p1.2:=true;   {turns on inlet valve LED}
    p1.4:=true;     {turns off outlet LED)
```

```
    end;

Procedure valve_on;
    begin                {turns on the inlet valve for the length of pwm_on}
     p1.2:=false;        {turns on inlet valve LED}
     p1.0:=false;        {turns on inlet valve}
     writeln('on',pwm_on);
     for loopy:= 1 to pwm_on do
     p1.0:=true;

    end;

Procedure off;
     begin               {turns off the inlet valve for the length of pwm_off}
     p1.2:=false;        {turns on inlet valve LED}
     p1.0:=true;         {turns off inlet valve}

     for loopy := 1 to pwm_off do;
    end;


Procedure on_outlet;
     begin
     p1.1:=false;        {turns on outlet valve}
     p1.4:=false;        {turns on outlet valve LED}
     end;

Procedure start_pwm;

   begin
     if (difference > 2) and (difference < 700) then
     begin
       pwm_on:=difference * 100 DIV 700;  {1/500 is the proportional control value}
                                          {100 is the time on, sets the time the valve is }
                                          {to be turned on, pwm_on}

      pwm_off:=101-pwm_on;   {sets the time the valve is to be turned off, pwm_off}
      valve_on;
      off;
      writeln('up',pwm_on);
     end
     else
     if (difference >=700) then      {anti derivative saturation term clause}
     begin
      pwm_on:=101;
      pwm_off:=1;
      valve_on;
      off;
     end
   end;


Procedure outlet_valve;
```

```
    begin
     if (difference < -2)  then
     begin
       on_outlet;
     end
     else
     if (difference <=1) and (difference >= -1) then
     begin
      p1.5:=false;
     end
   end;



{Main Program}
begin

     reset(serial);
     writeln;
     writeln;

     repeat

          Start_ADC_for_transducer;
          Start_ADC_for_potentiometer;
          compare_actual_with_desired;
          operate_valve;
          start_pwm;        {operates the pwm on the inlet valve}
          outlet_valve;        {operates the pwm on the outlet valve}
     until false;
     p1.2:=false;
     p1.5:=false;
     p1.4:=false;


end.
```

**Micro controller program for proportional pulse width modulation control of the inlet valve and outlet valves.**

```
{$C- version 9  Program: Nigel Yee, this program uses pulse width modulation of both input and output valves}


PROGRAM  version9;


Var
     difference:integer;
     loopy:integer;
     pwm_on:integer;
     pwm_off:integer;
     detect:boolean;
     actual_strain,x,y,l,m,desired_strain:word;

Procedure Start_ADC_for_transducer;
      begin

        ADCON:=$01;                  {clears the ADC register}
        ADCON:=ADCON or $08;              {starts ADC on port 0}
        while not ((ADCON and $10)=$10) do;        {waits until conversion is completed}
        x:=ADCH;                                   {gets the higher bit}
        y:=ADCON;                                  {gets lower 2 bits}
        actual_strain:=((x*$04)+(y DIV $20));      {computes into 10 bit form}
        writeln(actual_strain);
        ADCON:=ADCON and $EF;
      end;

Procedure Start_ADC_for_potentiometer;
      begin
        ADCON:=$03;
        ADCON:=ADCON or $08;
        while not ((ADCON and $10)=$10) do;
        l:=ADCH;
        m:=ADCON;
        desired_strain:=((l*$04)+(m DIV $20));
        writeln('  ',desired_strain);
        ADCON:=ADCON and $EF;
      end;

Procedure compare_actual_with_desired;
      begin

        difference:=desired_strain-(actual_strain);{actual strain reading gets smaller as strain gets larger}
        writeln('  ',difference);
      end;

Procedure operate_valve;
      begin
      p1.0:=true;  {turns off inlet valve}
      p1.5:=true;
      p1.1:=true;   {outlet off outler valve}
```

```
    p1.2:=true;  {turns on inlet valve LED}
    p1.4:=true;   {turns off outlet LED)
    end;

Procedure valve_on;
    begin                {turns on the inlet valve for the length of pwm_on}
     p1.2:=false;        {turns on inlet valve LED}
     p1.0:=false;        {turns on inlet valve}
     writeln('on',pwm_on);
     for loopy:= 1 to pwm_on do
     p1.0:=true;

    end;

Procedure off;
     begin               {turns off the inlet valve for the length of pwm_off}
     p1.2:=false;        {turns on inlet valve LED}
     p1.0:=true;         {turns off inlet valve}

     for loopy := 1 to pwm_off do;
    end;

Procedure on_outlet;
     begin               {turns on the outlet valve for the length of pwm_on}
     p1.1:=false;        {turns on outlet valve}
     p1.4:=false;        {turns on outlet valve LED}
     for loopy := 1 to pwm_on do
     p1.1:=true;
     writeln('outlet');
    end;

Procedure outlet_off;
     begin               {turns off the outlet valve for the length of pwm_off}
     p1.1:=true;         {turns off outlet valve}
     p1.4:=false;        {turns on outlet valve LED}
     for loopy:= 1 to pwm_off do;
    end;

Procedure start_pwm;

   begin
    if (difference > 2) and (difference < 700) then
    begin
     pwm_on:=difference * 100 DIV 700;  {1/500 is the proportional control value}
                                        {100 is the time on, sets the time the valve is }
                                        {to be turned on, pwm_on}

     pwm_off:=101-pwm_on;   {sets the time the valve is to be turned off, pwm_off}
     valve_on;
     off;
     writeln('up',pwm_on);
    end
    else
    if (difference >=700) then      {anti derivative saturation term clause}
```

```
      begin
       pwm_on:=101;
       pwm_off:=1;
       valve_on;
       off;
      end
    end;

Procedure end_pwm;

    begin
     if (difference < -2) and (difference > -700) then
     begin
      pwm_on:=0 - (difference * 100 DIV 700);  {second valve actuation based on difference}
                                               {sets the time the valve is to be turned on,}
                                                {pwm_on}
      pwm_off:=101-pwm_on;                    {sets the time the valve is to be turned off,}
                                                {pwm_off}
      on_outlet;
      outlet_off;
     end
     else
     if difference <= -700 then    {anti derivative saturation term}
     begin
      pwm_on:=101;
      pwm_off:=1;
      on_outlet;
      outlet_off;
     end
     else
     if (difference <=1) and (difference >= -1) then
     begin
     p1.5:=false;
     end
    end;



{Main Program}
begin

     reset(serial);
     writeln;
     writeln;

     repeat

          Start_ADC_for_transducer;
          Start_ADC_for_potentiometer;
          compare_actual_with_desired;
          operate_valve;
          start_pwm;        {operates the pwm on the inlet valve}
```

```
        end_pwm;        {operates the pwm on the outlet valve}
    until false;
    p1.2:=false;
    p1.5:=false;
    p1.4:=false;


end.
```

**Micro controller program for sliding mode control.**

```
{$C- Version 10  Program: Nigel Yee Sliding mode controller }


PROGRAM  version10;

Var
    difference:integer;
    loopy:integer;
    a:integer;
    height:integer;
    derivative:integer;
    boundry:integer;
    actual_strn_old:integer;
    detect:boolean;
    timer:word;
    actual_strain,x,y,l,m,desired_strain:word;

Procedure Start_ADC_for_transducer;
        begin
         ADCON:=$01;        {clears the ADC register}
         ADCON:=ADCON or $08;        {starts ADC on port 0}
         while not ((ADCON and $10)=$10) do;  {waits until conversion is completed}
         x:=ADCH;                          {gets the higher bit}
         y:=ADCON;                        {gets lower 2 bits}
         actual_strain:=((x*$04)+(y DIV $20)); {computes into 10 bit form}
         writeln(actual_strain);
         ADCON:=ADCON and $EF;
        end;

Procedure Start_ADC_for_potentiometer;
        begin
         ADCON:=$03;
         ADCON:=ADCON or $08;
         while not ((ADCON and $10)=$10) do;
         l:=ADCH;
         m:=ADCON;
         desired_strain:=((l*$04)+(m DIV $20));
         writeln('  ',desired_strain);
         ADCON:=ADCON and $EF;
        end;

Procedure compare_actual_with_desired;
        begin

         difference:=desired_strain-(actual_strain);  {works out the difference between desired and}
                                                      {actual strain}
         writeln('  ',difference);
        end;


Procedure derivative_term;
        begin
         writeln('actual strain',actual_strn_old);        {writes the actual strain}
```

```
  writeln('difference of error term',difference); {writes the error term}
  tr0:=false;                                     {turns the timer off}
  timer:=th0;                                     {timer dummy variable is given the timer valve}
  timer:=timer shl 8;
  timer:=timer + tl0;
  height:=difference-actual_strn_old;             {calculates the change in error values}
  writeln('height',height);                       {writes the change in error values}
  writeln('tim',timer);                           {writes the timer value}
  derivative:=(100000 * height) DIV timer;        {calculation for the rate of change of error}
  actual_strn_old:=difference;                    {initialises the error value}
  tl0:=0;                                         {re initialises timer}
  th0:=0;
  tr0:=true;                                      {starts timer}
  writeln('  ',actual_strn_old);
  writeln('  ',derivative);
  writeln('deriv',derivative);
 end;

Procedure boundry_condition;
        begin
         boundry:=50;
        end;



Procedure operate_valve;
        begin
        p1.1:=true;
        p1.5:=true;
        p1.0:=true;
        p1.2:=true;
        p1.4:=true;




        if(difference > 5) and (derivative < boundry) then
        begin
         p1.2:=false;        {turn on inlet valve if error value is larger than zero region and derivative}
                             {term is less than the boundary value}
         p1.0:=false;        {turns the inlet Led on}

        end

        else
         if (derivative >= boundry) then
        begin
         p1.1:=false;        {turn on outlet valve if  derivative term is larger than the boundary value}
         p1.4:=false;        {turn on outlet Led}

        end
        else
         if(difference <- 5) then
```

```
        begin
         p1.1:=false;              {if difference is less than zero region then the outlet valve is}
                                   { turned on}
         p1.4:=false;              {turn on outlet Led}


        end
         else
         if (difference <= 5) and (difference >= -5) then
         p1.5:=false;     {indicate no further operation required through red LED}
           {UNTIL??????????????????????????????}

    end;



{Main Program}
begin

        reset(serial);
        writeln;
        writeln;
        tmod:=tmod and %11110000;
        tmod:=tmod or %00000001;
        tl0:=0; {initialises the timer counter}
        th0:=0;
        tr0:=true; {starts the timer counter}
        actual_strn_old:=0; {sets the initial error reading to zero}

        repeat
                Start_ADC_for_transducer;
                Start_ADC_for_potentiometer;
                compare_actual_with_desired;
                derivative_term;
                boundry_condition;
                operate_valve;

        until false;
        p1.2:=false;
        p1.5:=false;
        p1.4:=false;

end.
```

## D-4. Circuitry and technical drawings of the valve

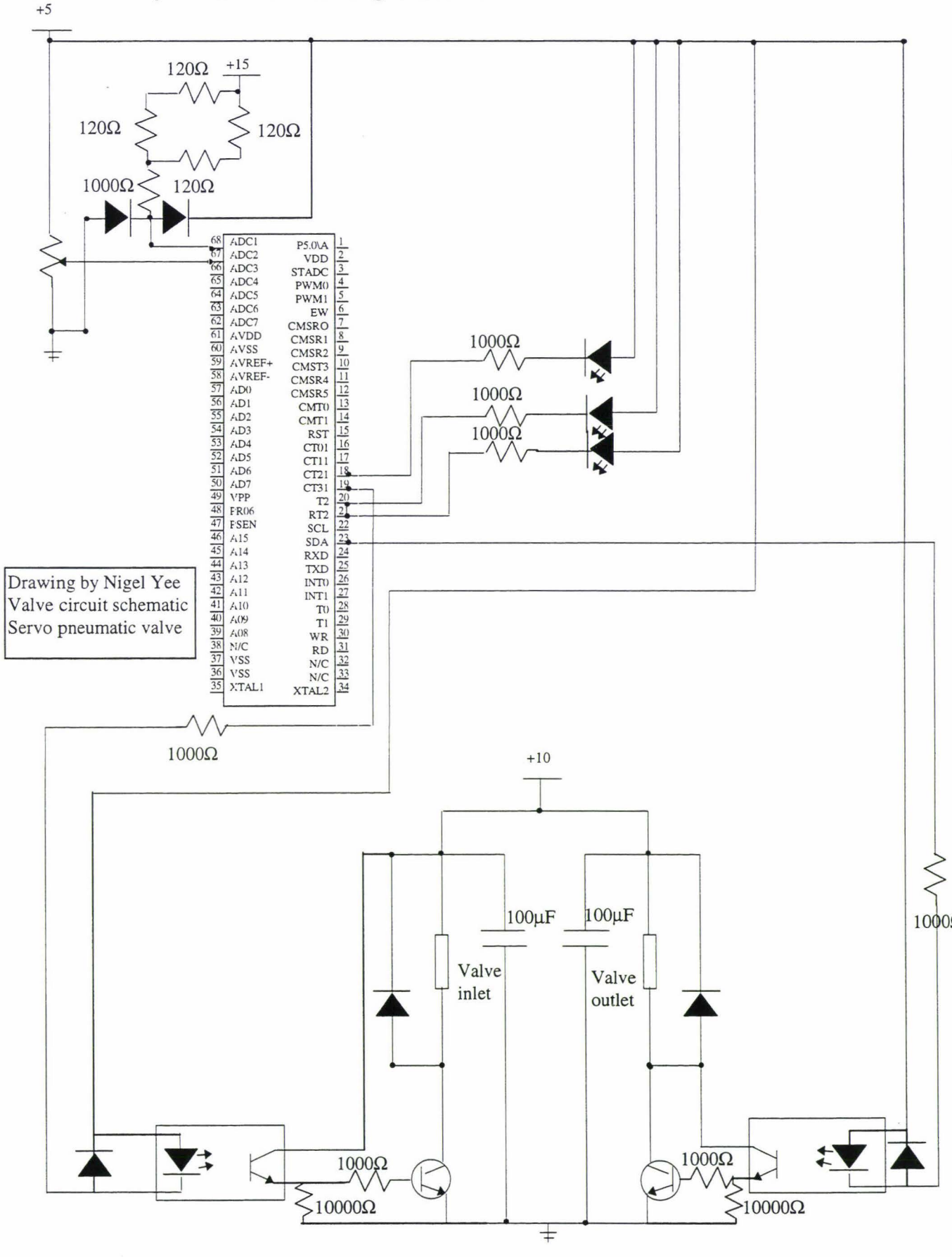

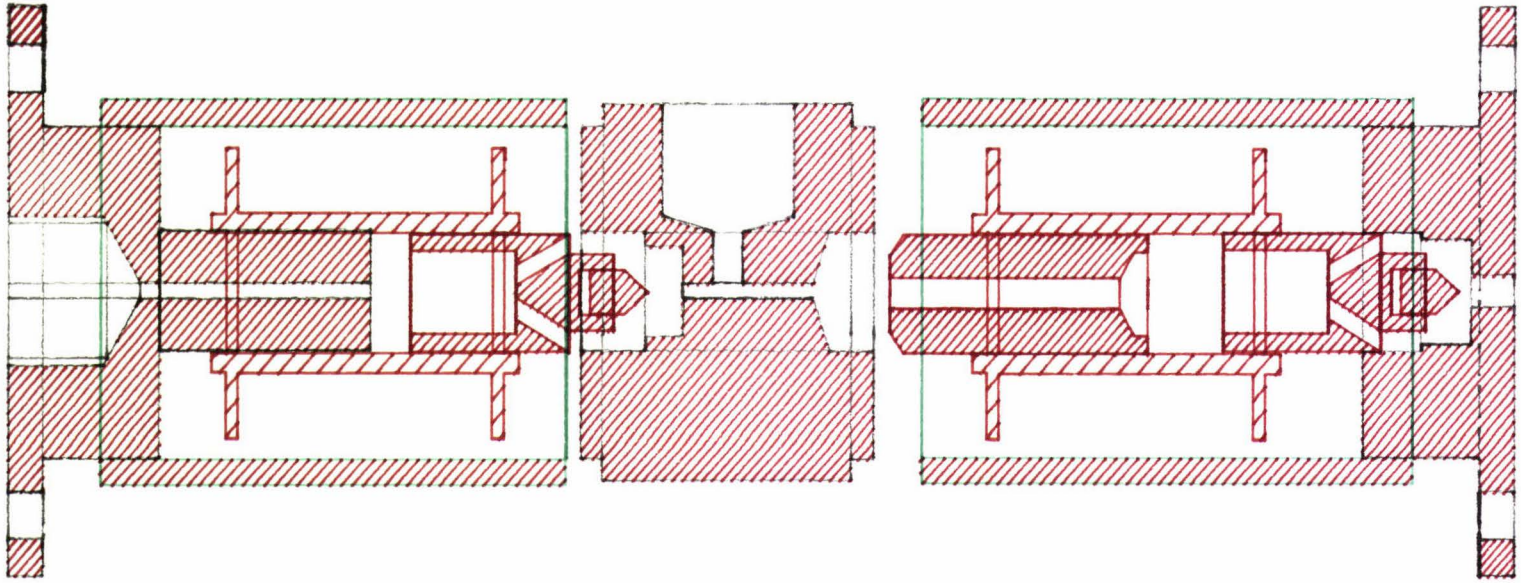

X section

| | | |
|---|---|---|
| Drawing not to scale | | Drawing by Nigel Yee |
| Date :28/6/96 | Drawing of the assembled valve | Drawing no 1 |
| | | |

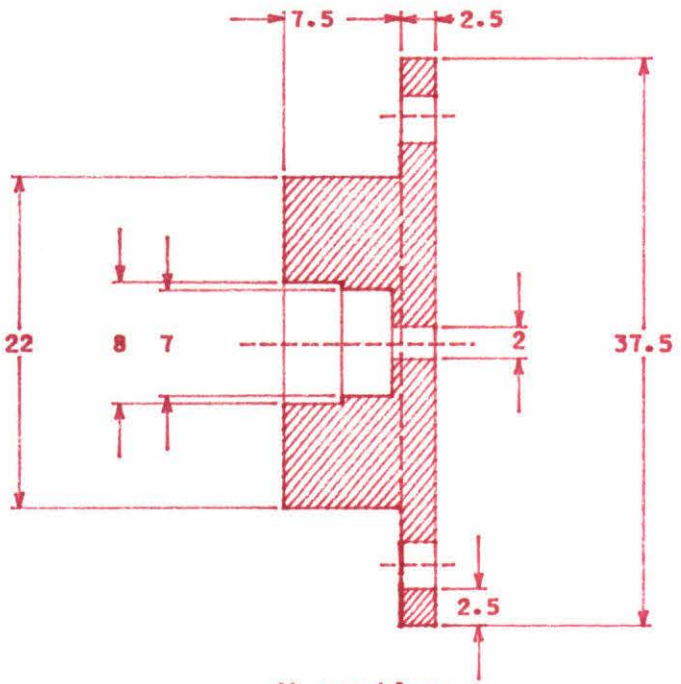


X section

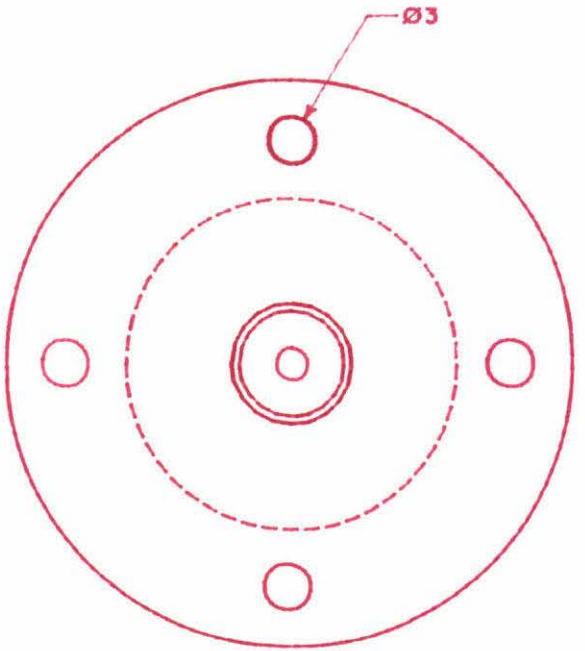


side

| | | |
|---|---|---|
| Drawing by Nigel Yee | | Material: Mild steel |
| Date: 26/6/96 | | Dimensions: mm |
| Drawing no 2 | | Scale 2:1 |

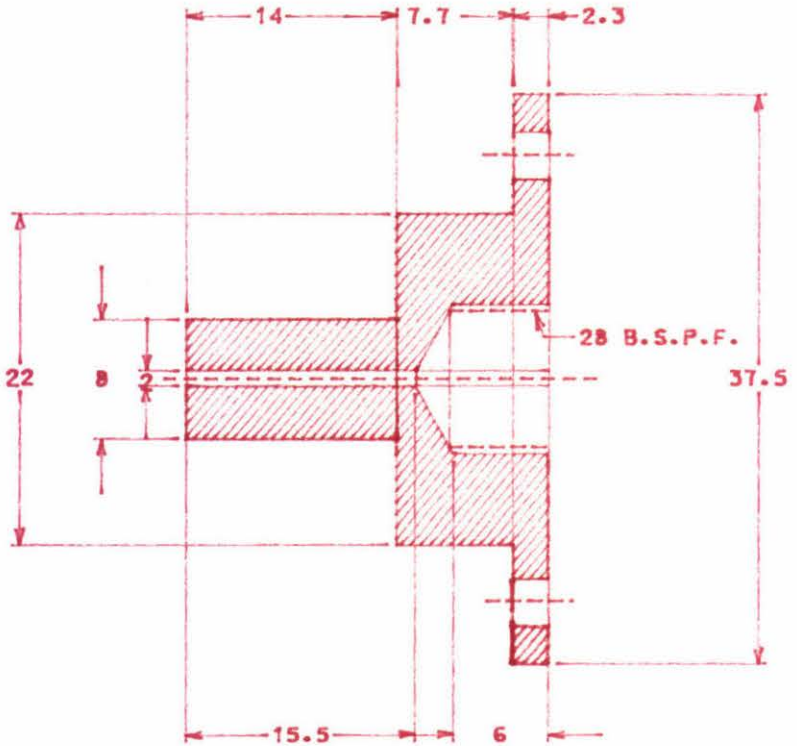


X section

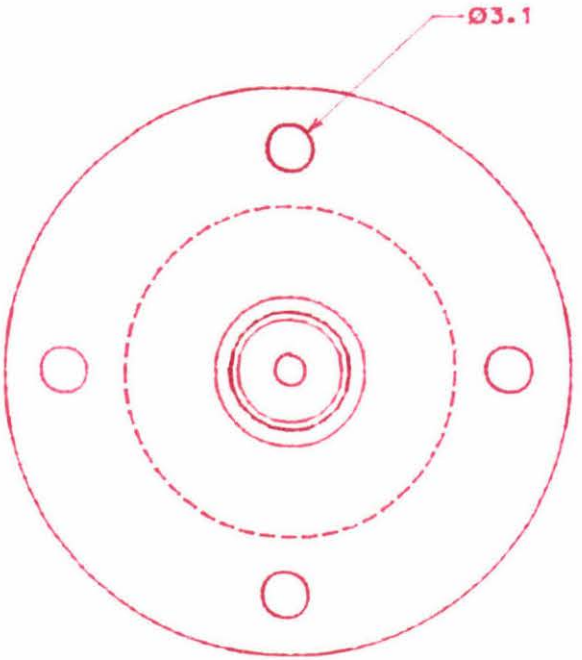


Side

| | | |
|---|---|---|
| Drawing by Nigel Yee | Inlet valve end | Material: mild steel |
| Date: 29/6/96 | for the double acting valve | Dimensions: mm |
| Drawing no 3 | | Scale: 2:1 |

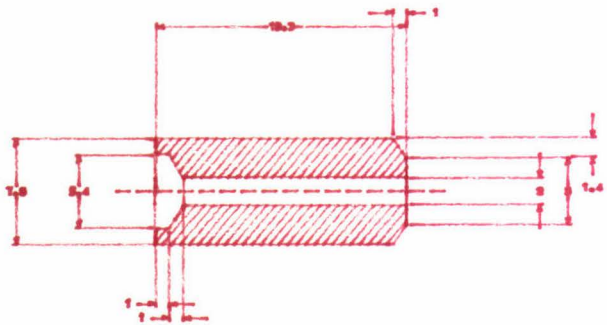

X-sectio n

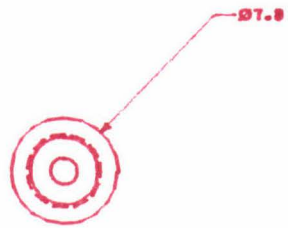


end

| | | |
|---|---|---|
| Date: 30/6/96 | Dimensioned drawings | Drawing by Nigel Yee |
| Dimensions : mm | of the valve stator | Material : mild steel |
| Drawing no 4 | | Scale 2:1 |

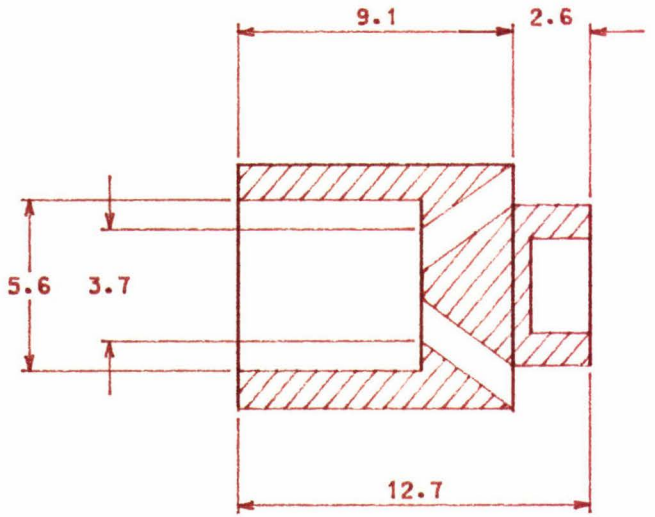


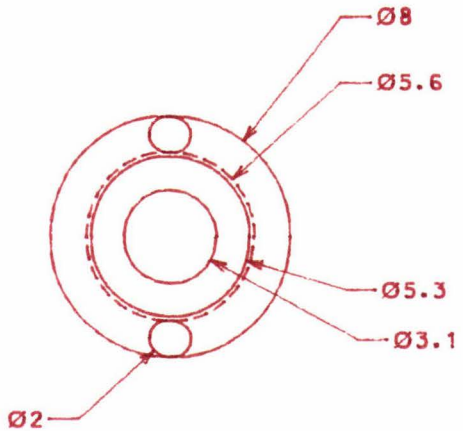


| | | |
|---|---|---|
| Drawing by Nigel Yee | Armature For Double Acting | Material : Mild steel |
| Date 24/6/96 | Pneumatic Valve | Dimensions : mm |
| Drawing No 5 | | Scale 3:1 |

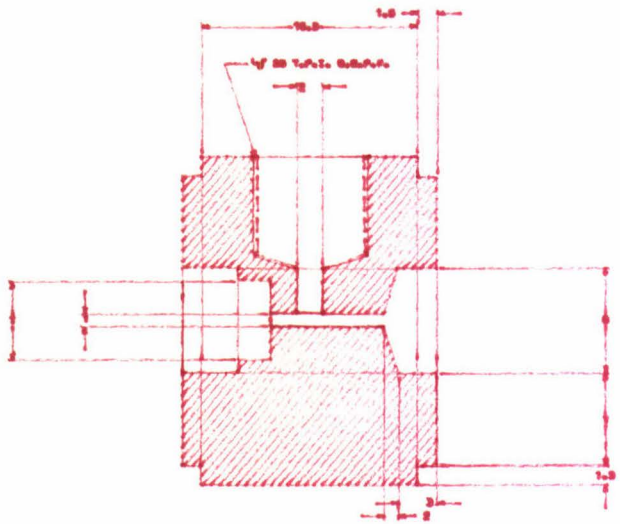

X section

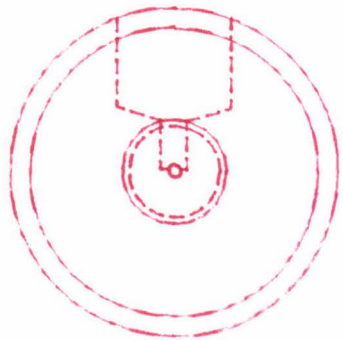

side

| | | |
|---|---|---|
| Drawing by Nigel Yee | Centre piece | Material: Mild steel |
| Date: 24/6/96 | Double acting valve | Dimensions : mm |
| Drawing no 6 | | Scale 1:2 |

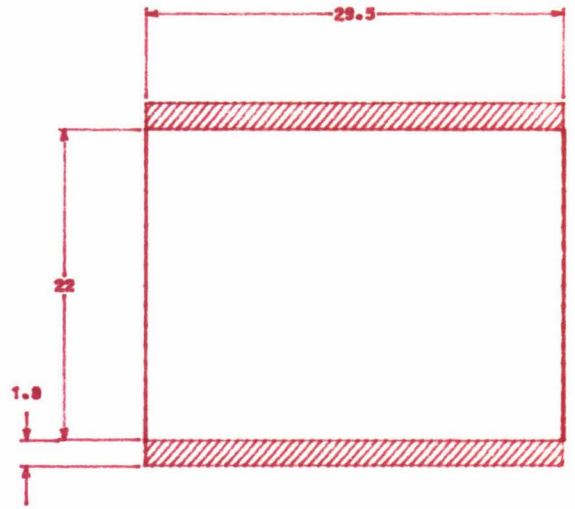


X Section

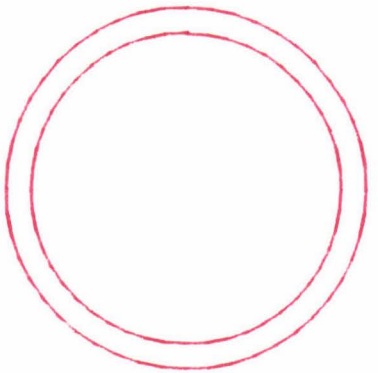

Side

| | | |
|---|---|---|
| Drawing by Nigel Yee | Outer case | Material: Mild steel |
| Date: 28/6/96 | for a double acting valve | Dimensions: mm |
| Drawing no 7 | | Scale: 2:1 |

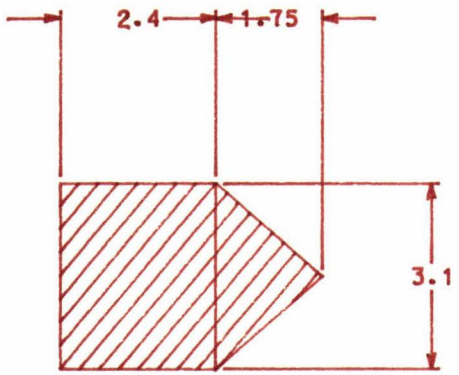


X-section

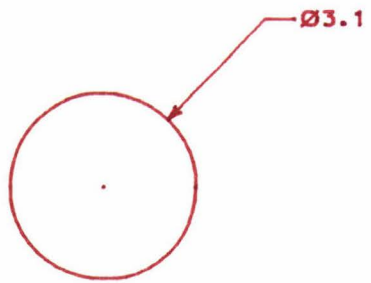


side

| | | |
|---|---|---|
| Drawing by Nigel Yee | Armature Tip | Material : Nylon |
| Date: 26/6/96 | for a double acting valve | Dimensions : mm |
| Drawing no 8 | | Scale 8:1 |

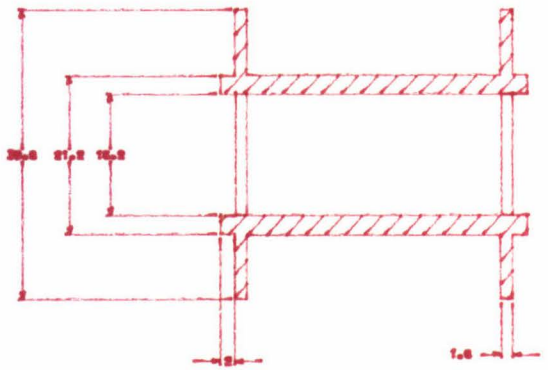

X section

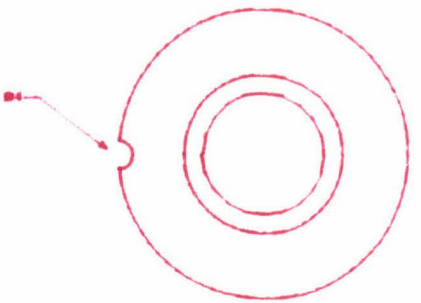

End

| | | |
|---|---|---|
| Drawing by Nigel Yee | Solenoid wire spool holder | Material: acetal |
| Date: 26/6/96 | | Dimensions: mm |
| Drawing 9 | | Scale 2:1 |

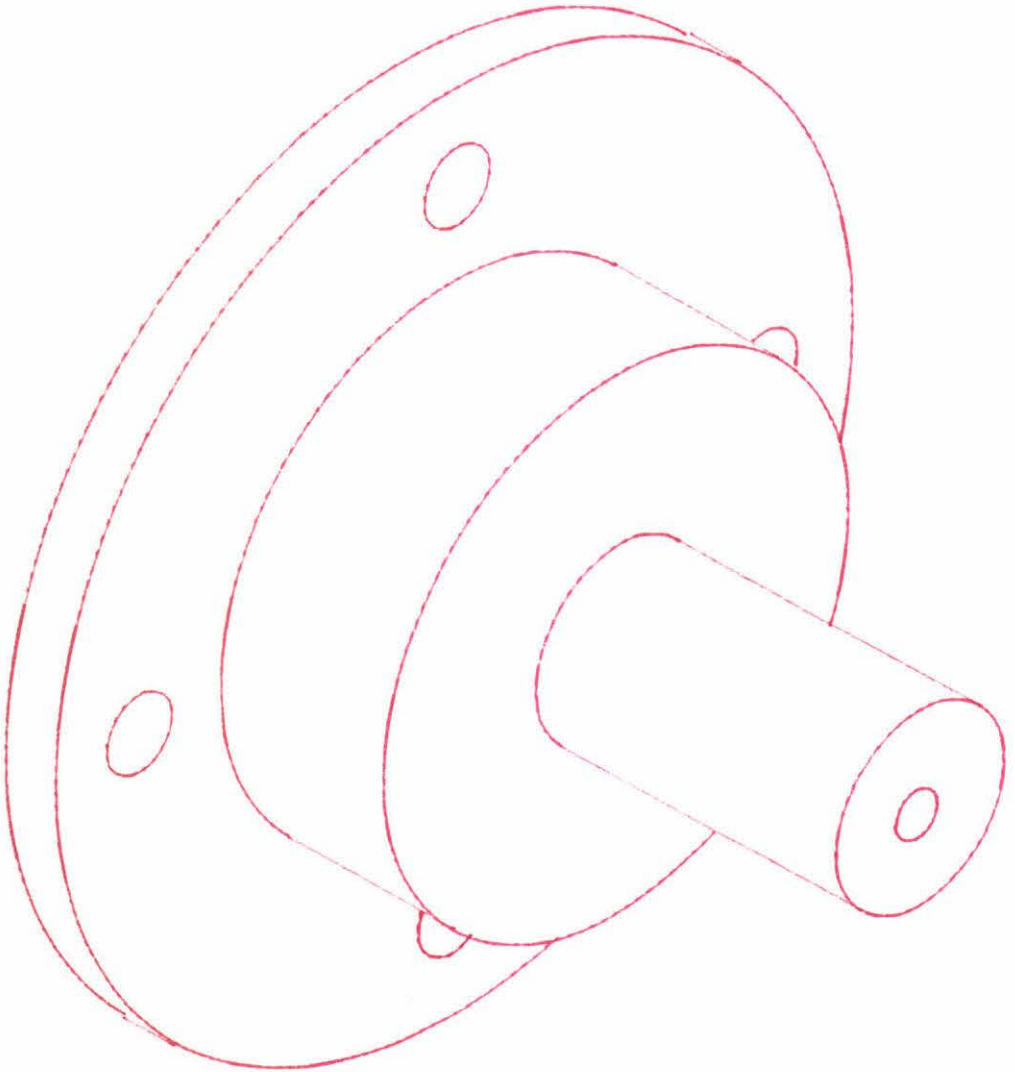

| | | |
|---|---|---|
| Drawing by Nigel Yee | Iso metric of the inlet piece of the double acting valve | Material: Steel |
| Date 10/1/96 | | Not to scale |
| Drawing no 10 | | |

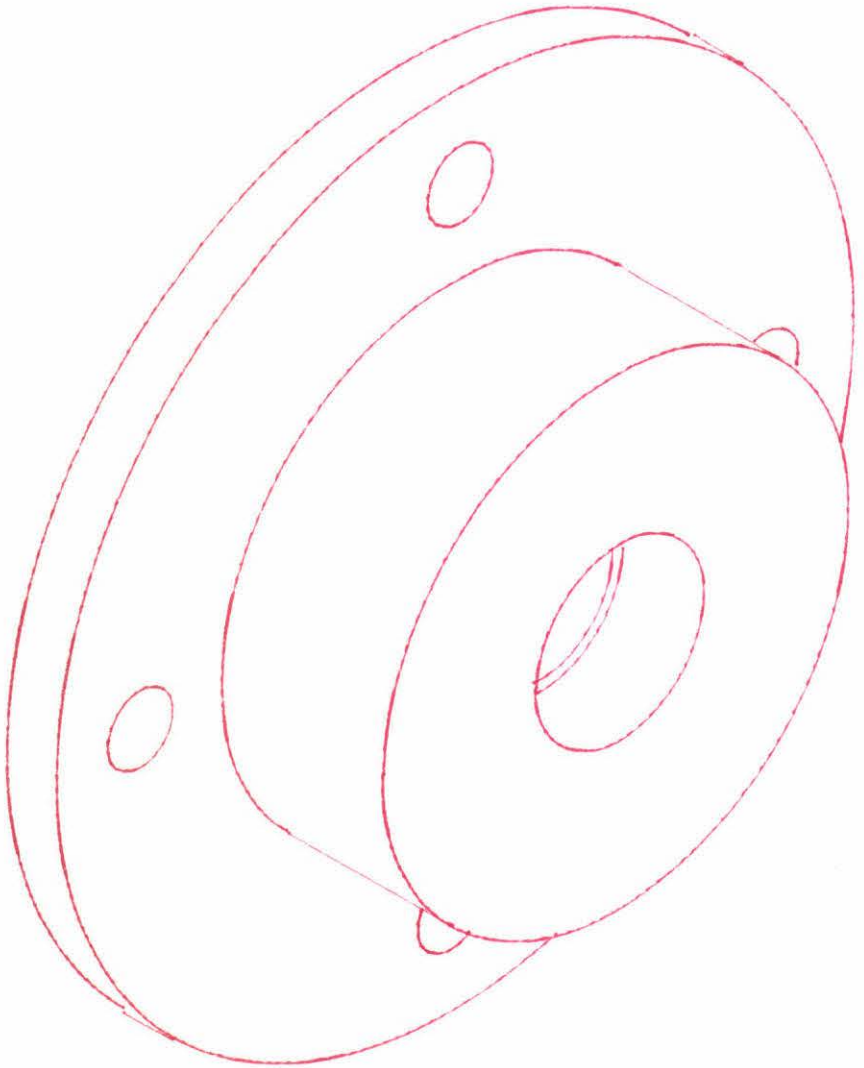

| | | |
|---|---|---|
| Drawing by Nigel Yee | Iso metric of the outlet piece of the double acting valve | Material: Steel |
| Date 10/1/96 | | Not to scale |
| Drawing no 11 | | |

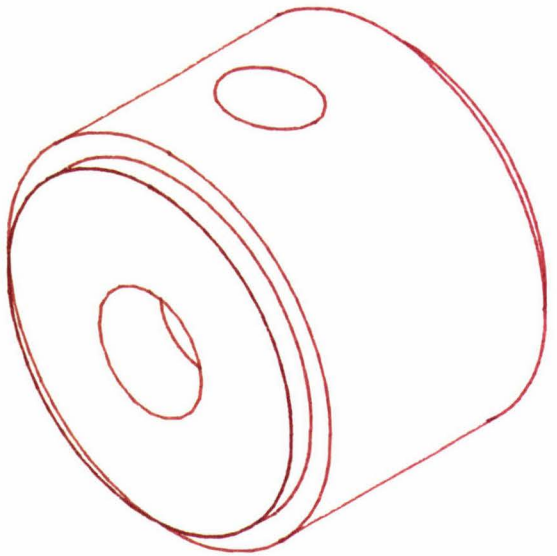

| | | |
|---|---|---|
| Drawing by Nigel Yee | Isometric of middle section of the valve | Material: Mild steel |
| Date: 1/2/96 | | Not to scale |
| Drawing no 12 | | |

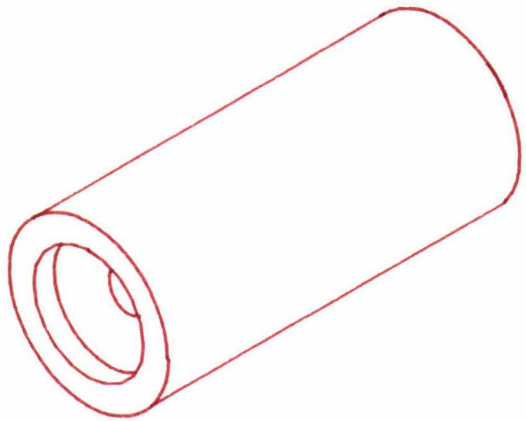

| | | |
|---|---|---|
| Drawing by Nigel Yee | Stator outlet end<br>Single valve unit | Material: Steel |
| Date 10/1/96 | | Not to scale |
| Drawing no 13 | | |

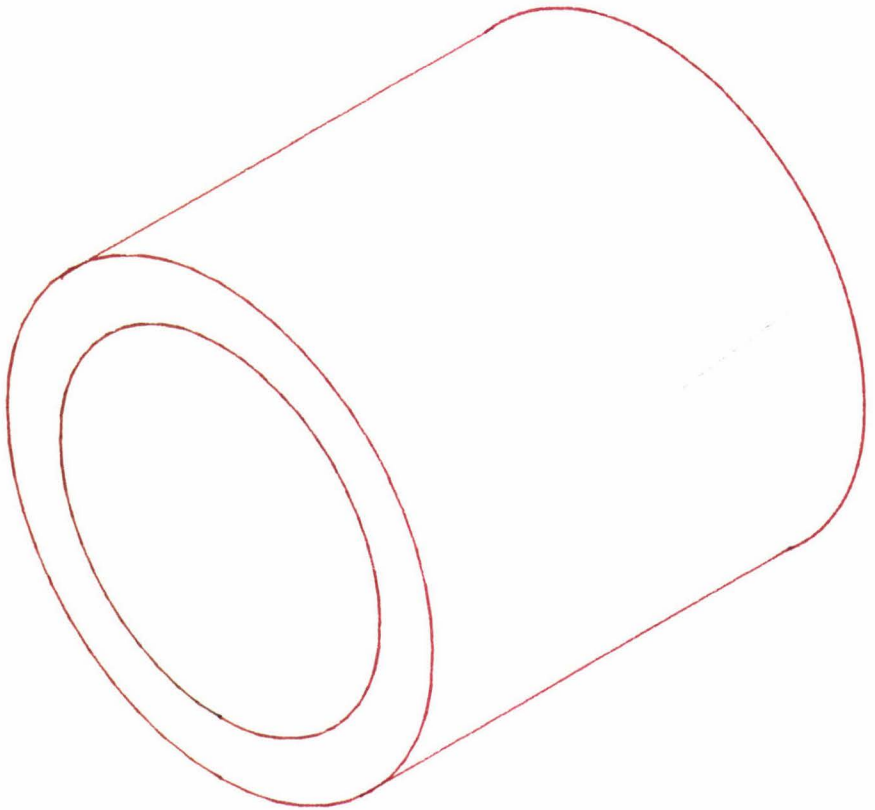

| | | |
|---|---|---|
| Drawing by Nigel Yee | Iso metric of the outter case of the double acting valve | Material: mild steel |
| Date 10/1/96 | | Not to scale |
| Drawing no 14 | | |

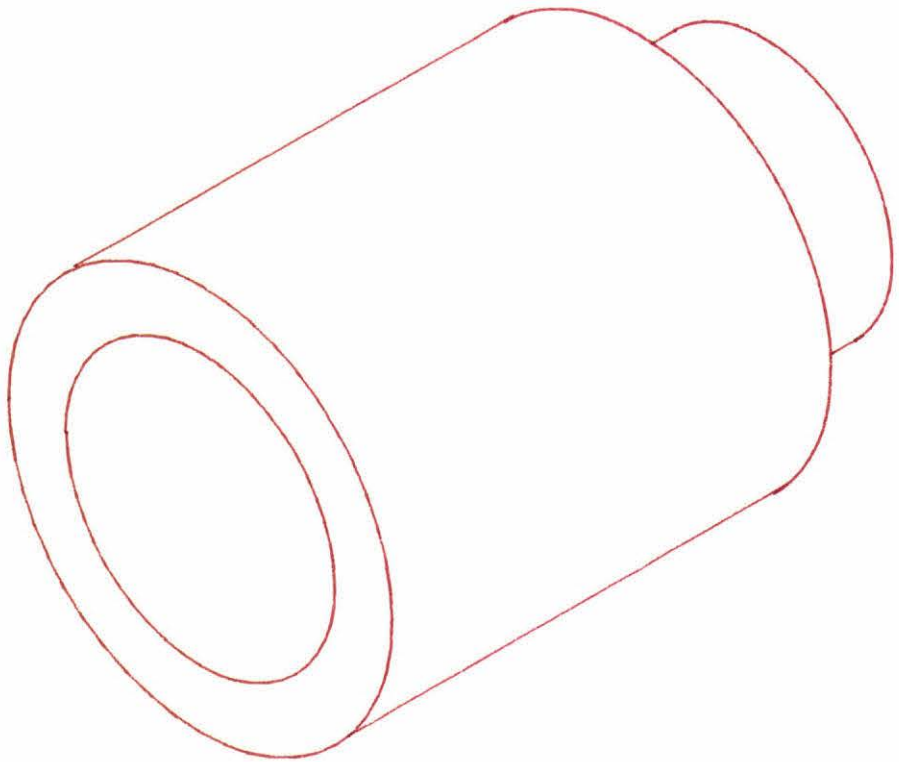

| | | |
|---|---|---|
| Drawing by Nigel Yee | Iso metric of the armature piece of the double acting valve | Material: mild steel |
| Date 10/1/96 | | Not ot scale |
| Drawing no 15 | | |

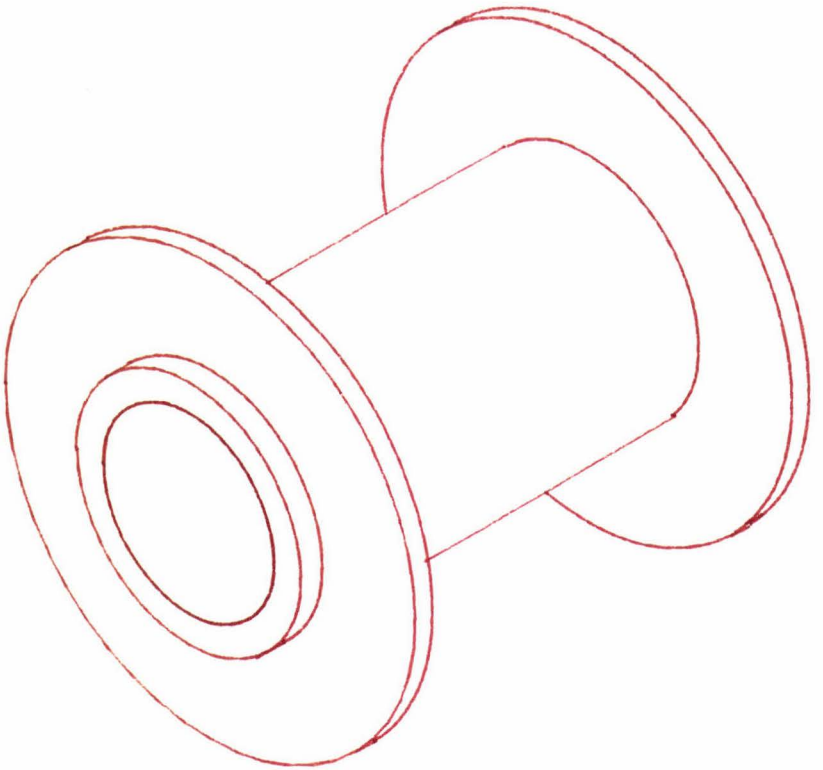

| | | |
|---|---|---|
| Drawing by Nigel Yee | Isometric of the bobbin unit for a double acting valve | Material: Acetal |
| Date 10/1/96 | | Dimensions: mm |
| Drawing no 16 | | |

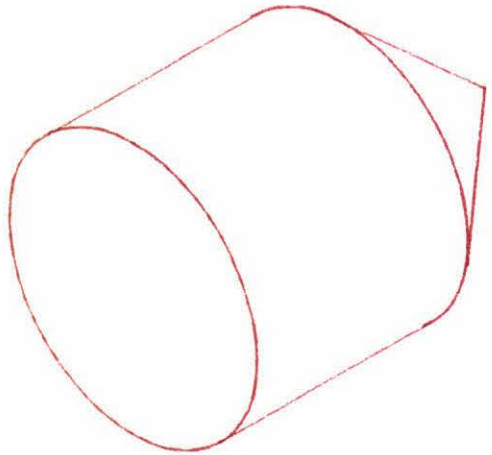

| | | |
|---|---|---|
| Drawing by Nigel Yee | Tip of the armature of the double acting valve | Material: Nylon |
| Date 10/1/96 | | Not to scale |
| Drawing no 17 | | |